Narendra B. Dahotre · Sameehan S. Joshi

Machining of Bone and Hard Tissues

Springer

Machining of Bone and Hard Tissues

Narendra B. Dahotre · Sameehan S. Joshi

Machining of Bone and Hard Tissues

Springer

Narendra B. Dahotre
University of North Texas
Denton, TX
USA

Sameehan S. Joshi
University of North Texas
Denton, TX
USA

ISBN 978-3-319-39157-1 ISBN 978-3-319-39158-8 (eBook)
DOI 10.1007/978-3-319-39158-8

Library of Congress Control Number: 2016940130

Printed on acid-free paper

This Springer imprint is published by Springer Nature
The registered company is Springer International Publishing AG Switzerland

Preface

Today, although the orthopedic surgery has come a long way through adaptation/integration of modern tools such as sensors and computer aided drawing (CAD) based generation of patient specific defined joint design and bone machining parameters, it is still largely conducted by the surgeon using conventional tools such as saw, ultrasonic cutter, hammer, drill, etc. Such mostly conventional way of orthopedic surgery is associated with human and tool attributes and hence leaves tremendous room for further development of operating tools and techniques. The further developments are likely to address adverse effects of orthopedic surgery such as but not limited to: severe damage of tissues within and surrounding repaired/operated regions, low precision in final dimensional tolerance on repaired/operated bone, relatively slow surgical processes, post-surgery tissue trauma, rigorous pain, and in some cases post-surgery and related addition of cost.

In light of this, this is the first book that provides a comprehensive review of the machining of bones and hard tissues for orthopedic surgery through points of view of engineering and biology. The book begins with a description on the types of orthopedic surgeries and their societal and economic impact. Such description was intended to underscore the growing importance of the field of orthopedic operations and the need and scope for further research and development in the field. The complexity of orthopedic surgery can be realized from the complex nature of bone in terms of its chemical and physical components and their properties. These aspects are covered in the following sections on bone characteristics and physical and biological effects of orthopedic surgery. The success of an orthopedic surgery for precision and minimal damage to the bone and surrounding tissues depends on the understanding and control of basic mechanical operations of the surgery. The fundamental physical principles and the interactions of process parameters associated with the mechanical operations such drilling, sawing, grinding, and milling along with thermal machining and associated machinability and resultant surface quality are the topics of the next chapter. Although the procedures in current orthopedic surgeries are mostly founded on the above mentioned mechanical operations, several non-conventional techniques such as laser, microwave, ion beam, ultrasonic,

waterjet, pneumatic, and hydraulic machining are being researched as potential replacements for conventional mechanical operations in bone machining. Description of these unconventional machining techniques is the topic of the subsequent chapter.

The book further extends the discussion on physical aspects of the machining in view of material (bone) and process parameters followed by a discussion on temperature analysis. Often, temperature rise is unintentional consequence of the conventional mechanical operations as well as that of some of the non-conventional methods whereas it is one of the inherent processing parameters of non-conventional machining techniques such as laser/ion beam machining. Hence, development, measurement, and control of temperature during these processes are elucidated in the following chapter. In depth understanding and predictive effects of mechanical and thermal loading during machining operations on the basis of computational modeling is the topic of the next chapter. Such description on the computational approach is intended to assist in planning and optimization of the process/procedure and system development for orthopedic surgery in clinical environment. Finally, the potential of fully integrated automated machining operation in clinical environment is presented in the last chapter. The comprehensive discussion of this book expected to lay the foundation for efforts toward future development of improved orthopedic surgery with semi- or full automation, high precision, rapid procedure, minimal invasive tissue-damage, no blood transfusion, improved implant integration, and reduced cost.

As per authors' knowledge, currently this is the only book on the present topic available in the body of open source literature. Especially, the uniqueness of this book lies in multidisciplinary nature of the subject matter which in turn likely to remain a valuable source of literature to scientists, engineers and academicians working in the area of bioengineering, biomedical engineering, manufacturing science and engineering, application engineers and scientists/researchers working in the manufacturing, orthopedic, and medical industry, and senior and graduate level students in biomedical/bioengineering, mechanical, manufacturing, and materials science and engineering. The authors are grateful to all researchers working in the area whose literature in various sources remained the basis of content of this book. Finally, the authors also thank Anurag Roy for conducting extensive literature search related to the subject matter that provided the initial path for the content discussed in this book.

Denton, TX, USA
March 2016

Narendra B. Dahotre
Sameehan S. Joshi

Contents

Chapter 1
Introduction

1.1 Orthopedic Surgery

Orthopedic surgery is the operational procedure employed for dealing with problems associated with bones, joints. Orthopedic surgeries are becoming important part of the human life. As a result of advances in medical field, the number of people seeking orthopedic treatments has been increasing. Some of the major contributors towards increasing number of orthopedic surgeries are old age, injuries related to sports, and military. The field of orthopedics has become very important in day to day life.

Even though treatments related to bone healing and joint repair date back to 100 BC, the word orthopedia was coined by Nicholas Andry, Professor of Medicine at the University of Paris in 1741 [1]. It is the combination of two Greek words, *Orthos* meaning free of deformity and *Paidios* means a child. The illustration used by Prof. Andry to explain orthopedia is shown in Fig. 1.1 indicating that the deformity (bend) in the trunk of a tree is analogous to the deformity in the back bone of human being or any other structural bone that can be rectified to make it straight (orthopedia) by orthopedic surgery. This description makes it clear that earlier focus was mainly on joint and limb problem in children but eventually the treatment has spread across people of all ages. In addition, there are many types of orthopedic surgeries evolved with the progress in medical field. The current era is described as the limb salvage era where orthopedic surgeries are not only confined to replacement of joints and removing the bend in the bone but they are also performed to replace or fix sections of bones of any limb in the body. On the contrary, earlier the common approach was to cut off the limb itself to cure and save the patient's life. Taking above discussion into consideration, there are various types of orthopedic surgeries evolved as a result of advancement in the medical field. Following subsection briefly discusses various types of orthopedic surgery.

N.B. Dahotre and S.S. Joshi, *Machining of Bone and Hard Tissues*,
DOI 10.1007/978-3-319-39158-8_1

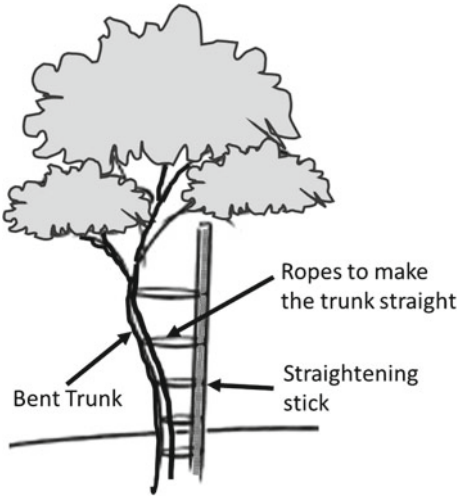

Fig. 1.1 Illustration of orthopedia similar to what published in Prof. Andry's book

1.1.1 Types of Orthopedic Surgery

There are various types of orthopedic surgeries. Basically they can be divided into surgeries related to the bone and surgeries related to the joints [2]. The brief classification and description of each type has been presented below.

Orthopedic Surgeries of Bone

- **Autograft (bone grafting)**: It is a surgical procedure wherein a healthy tissue is transplanted into damaged or missing region so as to repair complex bone fractures.
- **Laminectomy**: It is a surgical procedure which separates and segregates a portion of the vertebral bone named Lamina. This surgical procedure is aimed at reliving the pressure.
- **Osteotomy**: It is a surgical operation wherein aim is to decrease or increase the length of the bone using cutting exercises. It also involves changing the alignment in some cases. This procedure is adopted to check hallux valgus, introduce course-correction or in post-fracture situation whereby an attempt is made to straighten a healing bone, which maybe fanning out crookedly.
- **Reduction**: It is a medical exercise used for effective restoration of a fracture or any dislocation so as to ensure proper alignment. It is always an attempt on part of the orthopedic surgeons to reproduce the anatomy of a normal human being, especially that of the fractured bone using the reduction process.
- **Resection**: This primarily utilizes surgery to separate out abnormal tissues, for example mediastinal, neurogenic, germ cell tumors or thymoma. A very common case of resection is removal of the large intestine.
- **Limb Salvage**: Surgery is practiced whenever the need to rid the body of cancer arises and simultaneously concerns pertaining to avoiding amputation exist. In

light of this, the patient's appearance needs to be preserved uniquely and ensure that the affected limb has the maximum number of functional degrees.

Orthopedic Surgeries of Joints

- **Arthrodesis (fusion)**: It is the artificial induction of joint ossification for two or more bones using the surgical methods. It is most commonly performed on joints located in the spine, foot, ankle, and hand.
- **Arthroplasty**: It is a type of orthopedic surgery in which the articular surface of a musculoskeletal joint undergoes replacement, remodeling or realignment using osteotomy or similar procedures. For relieving pain and restoration of proper functioning of the joint post-damage by arthritis or other traumatic experiences, it is considered to be a very efficient methodology.
- **Revision**: It is the procedure adapted to replace old implants by modern advanced components. The requirements are planning during the pre-operative stage, sophisticated tools, proper implants, and expertise in challenging surgical procedures.
- **Synovectomy**: It is the removal of a portion of the synovial membrane belonging to the synovial joint using surgical methods. It has been extensively adopted for the treatment of rheumatoid arthritis, Synovial osteochondromatosis, and Synovial chondromatosis.

Thus in the advent of advances in surgical tools, monitoring instruments, and medicines orthopedic surgeries have become very common and frequent in improving the quality and span of human life. Following section provides an overview of the scocioeconomical aspects related to orthopedic surgeries.

1.2 Societal and Economic Impact

Since initial efforts dating as back as 100 BC, the main aim of orthopedic treatments has been to cure the pain and make the patients life as normal as possible. Orthopedic surgeries have helped people to live near normal life and with technical advances the results are improving. This has further resulted in development of a huge market for orthopedic surgery and related auxiliary fields. The situation can be realized by considering example of the field of bio materials. Orthopedics as a whole has a major share in the field of surgery (Fig. 1.2). The market is ever growing in terms of economics as well as absolute numbers. The major share as of 2009 came from the United States (Fig. 1.3). However, the numbers are also increasing in other countries. The reason could be attributed to spread of technical expertise and relatively inexpensive facilities available in other countries. As an example, the number of replacement surgeries has been growing steadily in Australia (Fig. 1.4, source from reference [3]). This trend shows that more and more people are leaning towards orthopedic surgeries than ever before. Orthopedic treatments are helping people to abate the pain in the joints as well as bones and they are making life more comfortable. The independence of a person in day to day activities is sustained by not requiring the assistance as a result of disappearance of pain after orthopedic treatment.

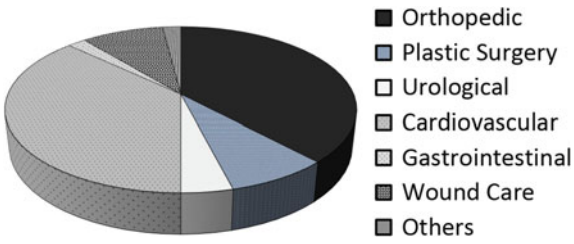

Fig. 1.2 Share of orthopedics related biomaterials in the year 2009 (*Data source* MarketsandMarkets—Market Research Reports)

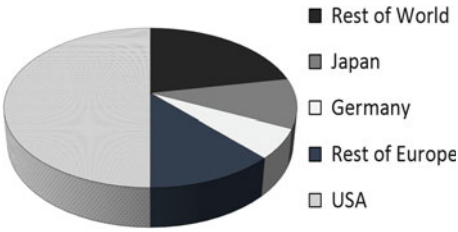

Fig. 1.3 Country-wise share of biomaterials in 2009 (*Data source* MedMarket Diligence)

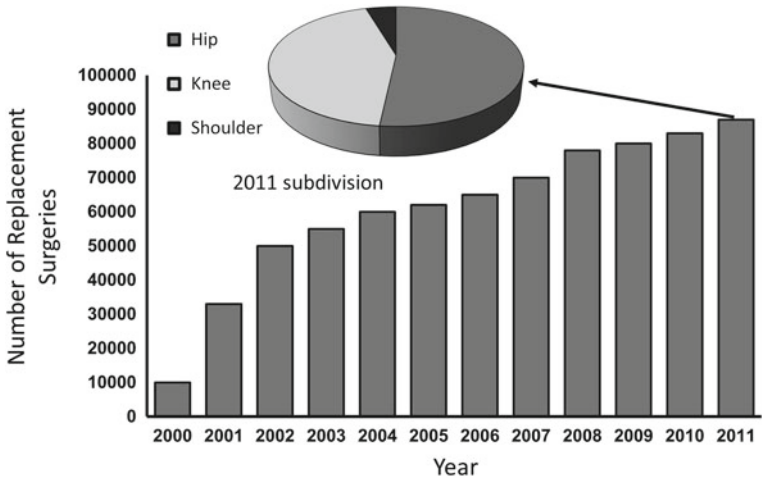

Fig. 1.4 Bar chart showing number of replacement surgeries per year in Australia (*Data source* Australian Orthopedic Association 2011)

Apart from influencing human life in positive manner, the other important factor related to orthopedic surgery is economic aspects. As a result of increasing numbers and demand, a huge amount of money is being invested in the orthopedics and related fields. The spread of orthopedic surgeries along with other treatments to many countries has created the field of medical tourism. A brief overview of costs

Table 1.1 Cost of orthopedic replacement surgery

Orthopedic surgery	Country-wise cost (USD)					
	USA	India	UK	Singapore	Mexico	Malaysia
Hip replacement	47,000	9000	12,000	11,000	17,300	10,000
Knee replacement	48,000	8500	10,160	13,000	14,650	8000
Hip resurfacing	47,000	8250	20,000	12,000	12,500	12,500

associated with some of the replacement surgeries is presented in Table 1.1 (source of data in Ref. [4]). Even though some countries like India offer significantly less cost than others, the ever increasing numbers described before make the market very big for orthopedic surgery. In addition, orthopedic surgeons are one of the highest earners amongst various kind of surgeons motivating medical students to pursue specialization in this field. Therefore, a lot of money is being invested by people in the field of orthopedics not only as the means of treatments but also in getting education in this field.

Orthopedic surgery has been an important part of human life. It wields huge economical impact making a large market related to the field of surgery itself and other auxiliary branches like biomaterials. Bone machining is an integral part and a foundation of the orthopedic surgery. Bone machining facilitates various orthopedic procedures. In view of this, the following section provides a brief overview of the role of the bone machining.

1.3 Bone Machining: Overview

Bone machining is a fundamental operation of the orthopedic procedure. Until lately, the field of machining was not considered from technical point of view. The main aim was to just perform the machining operation by intuitively controlling the parameters for minimal or no damage to the bone without any understanding of the fundamentals of the machining process. In addition, traditionally the techniques have been mainly based on contact machining employing mechanical tools like cutting saws and drills. However, the specialized tools of various metallic materials were also designed and investigative efforts on the interaction of bone with these metallic materials were initiated in the past century [5]. With further advances, a lot of investigations were conducted related to the tool materials, mechanical aspects of machining and their biological and cellular impact on the bone. As a result, the number of publications related to bone machining are ever increasing in each decade (Fig. 1.5). Furthermore, novel techniques are being developed which could potentially serve as minimally invasive for the patient. One of such minimally invasive techniques is laser based machining. The increasing trend of publications per year on laser based machining

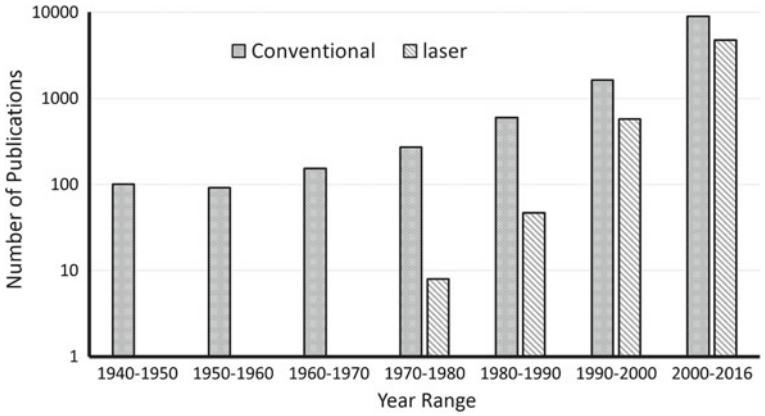

Fig. 1.5 Number of papers published over the period of time in the field of conventional and laser based bone machining. (*Data source* a literature search on Sciencedirect^{TM} and Google Scholar^{TM} engines)

since 1970 is an indication of the ever increasing amount of research efforts in the field (Fig. 1.5).

The field of bone machining can now be considered to have two major branches, namely conventional and non conventional methods of machining. Conventional methods are contact based techniques involving mechanical tools. Often, the methods bare the same name as that of the fundamental operation these methods carry out such as drilling and cutting. Non conventional methods on the other hand involve novel techniques such as high energy density radiation based techniques or integration of the existing advanced machining into hybrid techniques such as ultrasonic. The field of non conventional techniques is relatively new and efforts are being made to actually adopt these techniques in the clinical environment.

The research involving bone machining, whether conventional or non conventional mainly focuses on the following key aspects:

- Effect of machining parameters
- Tool design
- Development of new methods and setups
- Automation and robotics
- Biological impact

These studies involve both experimental and simulation approaches. All these efforts are clearly influenced by the complex chemical and physical nature of bones and their thermophysical properties. The inherent and undesired damaging effects of machining operations also find origin in the complex nature of bone. In light of this, the forthcoming section is dedicated to the description on the nature of bone, its types, and thermophysical properties.

1.4 Bone Characteristics

Bones are rigid organs that constitute part of the endoskeleton of vertebrates [7]. The underlying composite structure and chemical composition are responsible for functionality of the bone. The main functions of bone are enlisted below [8].

- **Structure**: To provide a structural stability to the body.
- **Protection**: To protect various organs by forming a skeleton.
- **Movements**: To facilitate the various movements of the body along with joints, ligaments, and muscles.
- **Cell production**: Bone marrow plays a key role in production of red and white blood cells.
- **Storage of components**: Bone stores many important constituents needed for biological processes within the body such as minerals (mainly phosphors and calcium), fatty acids and growth factors. In addition, bone also helps in body pH control via release of the stored components. Furthermore, bones act as a sink for harmful toxins such as heavy metals and help in excretion of these harmful chemicals.

Furthermore, both structure and properties of bone play a decisive role in determining its response towards machining operation by contributing to thermophysical properties of the bone. The structure and properties of the bone may vary depending on many variables such as type of bone, age, gender, dietary habits, and geographic location. As an example, the dependence of Young's modulus of bone on calcium content is shown in Fig. 1.6 [6]. It clearly points out the huge variation in Young's modulus with slight changes in Ca content. However, most of the times, the general nature of the structure and average values of the properties are considered in the literature for calculations related to machining process. Presently, the technological advances have made it possible to extract patient specific information about the bone tissue before the surgical operations itself. Therefore, it is important to understand the structure, chemistry, and in turn the thermophysical properties of the bone in

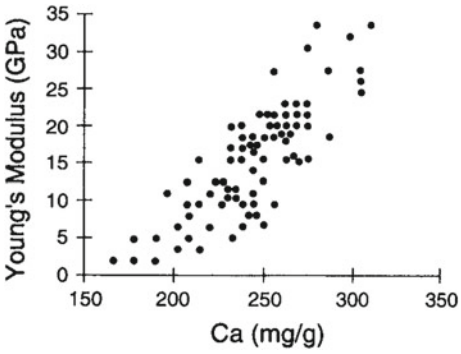

Fig. 1.6 Modulus versus calcium content (in mg/gm of dehydrated bone tissue) for cortical bone taken from 18 different species (reprinted from Currey [6] with permission. © Elsevier)

order to get an insight into material removal in this case. In light of this, the current chapter explores the basics about bone structure, its types, and general properties.

1.4.1 Bone Structure

Bone structure forms basis of the functions that these organs perform. It is composite in nature and hierarchical in terms of length scales. The blend of inorganic and organic materials contribute to this structure. The bone structure is discussed here from chemical as well as physical length scale point of view.

1.4.1.1 Chemistry

Biologically, osseous tissue forms the building block of the mineral bone matrix [8, 9]. These osseous tissues form osteotons which has a combination of various materials (Figs. 1.7 and 1.8). The in vivo (living) bone consists of 60–70 % mineral, 10–20 % water, and the rest is collagen. The mineral is composed primarily of hydroxyapatite ($Ca_{10}(PO)_6(OH)_2$) crystals and provides the compressive strength to the bone. The organic matter consists of type I collagen as the major component which provides bone its tensile strength. Proteoglycans (a type of protein) helps in preventing mineralization of the organic matter. The other compounds present apart from collagen are osteocalcin, adhesive proteins, growth factors, cytokines, and matricellular proteins [8]. Majority of the water is alongside the organic matter. The chemistry of the bone is summarized in Table 1.2. In addition to osseous tissues, the other types present are marrow, blood vessels, cartilage, endosteum, and periosteum nerves. They integrate with the bone to perform the function of the organ.

1.4.1.2 Length Scales

The chemical constituents of a bone described before are distributed in various length scales. On a macro level, femoral heads are connected to the middle section (technical details about which are given in the next subsection) giving a typical "bone shape" (Fig. 1.9 [10]). In cross section, on a micrometer length scale, an arrangement of osteons described earlier exists with osteocytes (bone cells) embedded within their pits (lucunae). A human body typically has billions of osteocytes [11]. Secretion by osteoblast (cells responsible for formation of bones) traps them in turn forming an osteocyte (Fig. 1.9). The blood vessels run through the cross section carrying essential supplies of necessary materials presenting an excellent example of natures own micro scaled fluid mechanics (Fig. 1.9). Going further on smaller scales, a network of collagen fibers is present (Fig. 1.9). The fibers are arranged in lamellar or woven fashion. The lamellar type consists of orthogonal and twisted types of fiber arrangement [12]. Further magnifying this fiber arrangement on microscale to nano scale,

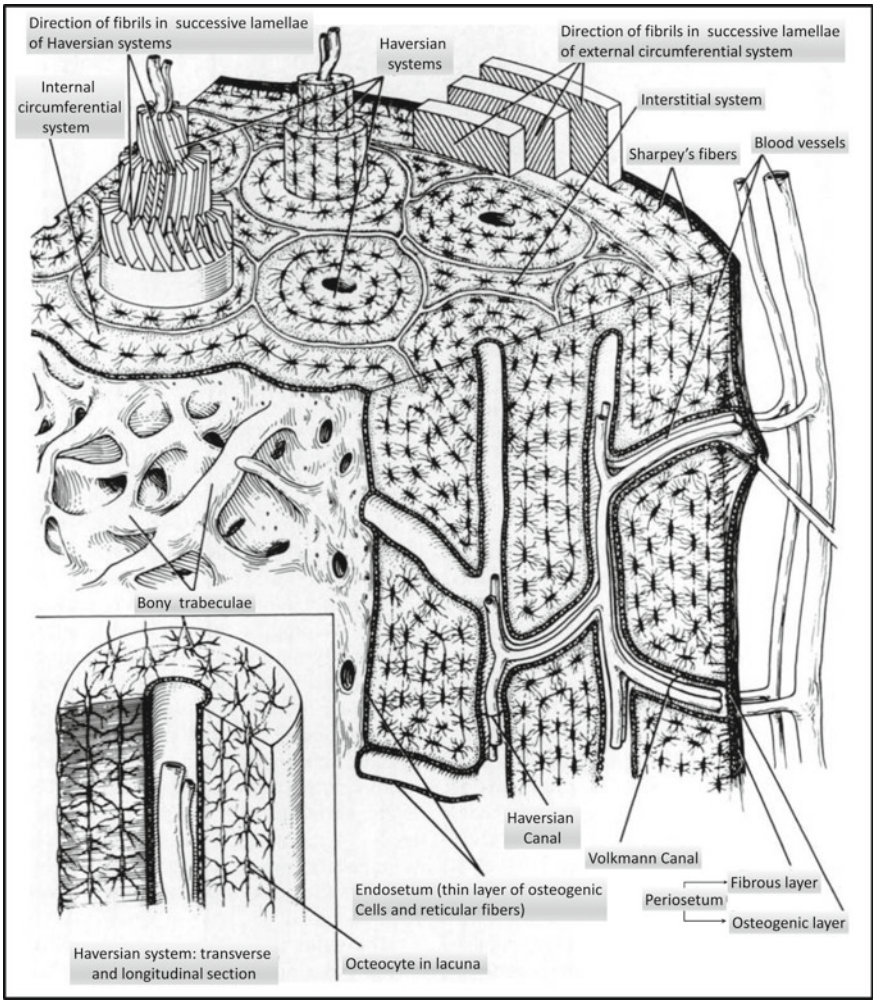

Fig. 1.7 Schematic of an osteon showing various structural features (reprinted from Buckwalter et al. [9] with permission. © Wolters Kluwer)

collagen molecules enclosing the mineral crystals are present (Fig. 1.9). This forms the basic ingredient of the bone as a body organ. The usual dimension of these crystals are $50 \times 25 \times 3\,\text{nm}^3$ (Fig. 1.10) [10]. Collagen fibers are fomred as a result of secretion by osteoblasts. A tertiary arrangements with periodicity of 67 and 40 nm hole zone between the end of the molecules is self assembled into collagen fibrils (Fig. 1.10). An overlap of 27 nm together with the hole zone results in the periodicity.

Thus, it is clear that, in general every bone consists of chemically complex and structurally intricate arrangement distributed at various length scales. However, the complexity of the matter does not end here. The bones have various types based on

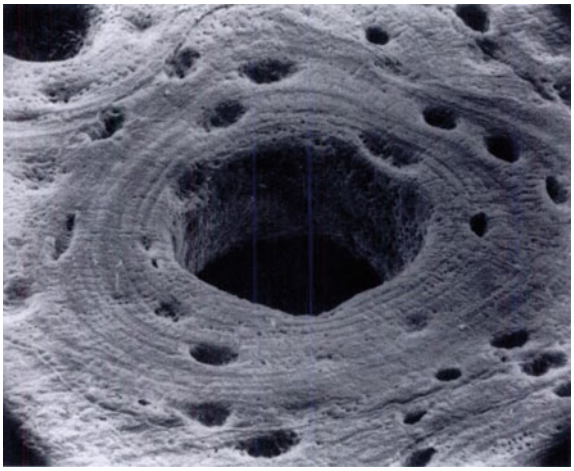

Fig. 1.8 Scanning electron microscope image of osteon (reprinted from Buckwalter et al. [9] with permission. © Wolters Kluwer)

Table 1.2 Chemistry of human bone

Constituent	Volume %	Notes
Mineral	60–70	Majority hydroxyapatite crystals, provides compressive strength
Water	10–20	Water molecules are associated mostly with organic matrix
Organic matter	10–30	Organic matter has type I collagen as the major component. It provides tensile strength to the bone

location within the body as well as the shape. Such a classification is presented in the next subsection.

1.4.2 Types of Bone

Bones have been broadly classified into various categories based on histology and anatomy. These classifications help in understanding the function of various bone types. A brief classification is presented in the current section. Even though the discussion doesn't cover the in-depth biological aspects, the information presented is adequate and essential from the machining point of view. In addition, references have been suggested which explore the in depth biology of the bones.

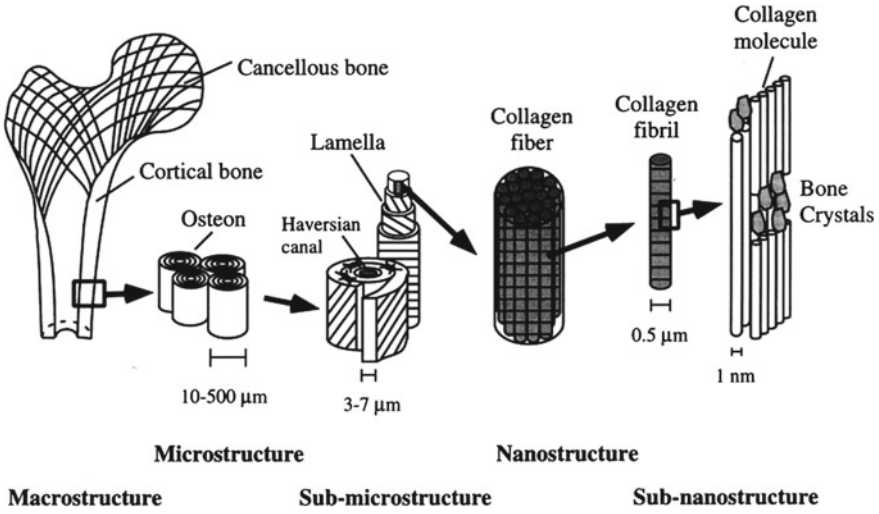

Fig. 1.9 Length scale distribution of the bone structure (reprinted from Rho et al. [10] with permission. © Elsevier)

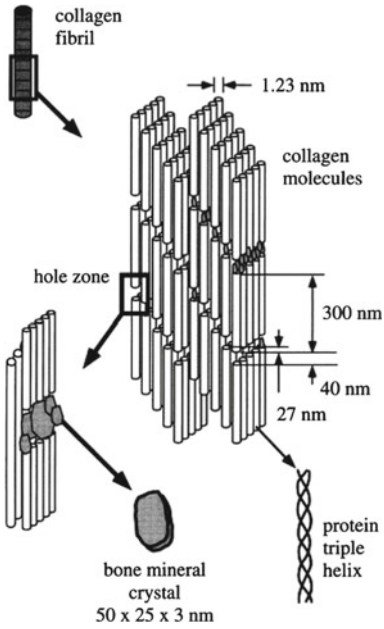

Fig. 1.10 Detailed features of nano level structure of bone (reprinted from Rho et al. [10] with permission. © Elsevier)

1.4.2.1 Histological Classification

Histology is basically the study of various tissue types and anatomy associated with a body structure. According to histology the bones are classified as woven and lamellar

bones. The woven bone is pathologic and has not reached full maturity. It is weak and possesses flexibility. It also has high turnover rate meaning a high volume of woven bone gets resorbed to release minerals in to the blood and forms again frequently [13]. Lamellar bones on the other hand are structural bones and makeup for large portion of the skeleton. These are further sub classified as cortical and cancellous bones. Cortical bones also called compact bones, are characterized by low turnover rate, minor amount of porosity, and compactness. They form 80 % of the skeleton [14].

The rest 20 % of the skeleton comprises of cancellous bones also termed as trabecular bones. These are comparatively much softer and porous and consist of loose network of bony struts. The space in between is filled with bone marrow. The soft and opens structure of cancellous bones helps in damping of physical shocks and load transmission with the help of joints.

1.4.2.2 Anatomical Classification

Anatomically bones are classified as long, short, flat, and irregular. Diaphysis, metaphysis, and epiphysis form the main components of long bones and do various structural functions. This is schematically illustrated in Fig. 1.11 [15]. Thick tube of cortical bone with thin canal of cancellous bone and marrow elements forms the shaft shaped diaphysis. The ends of long bone are formed by epiphysis consisting of thin layer of cortical bone enclosed in tracebular bone. The metaphysis functions as a transition zone from the diaphysis to the epiphysis. Examples of long bone include femur and humerus.

Short bones assist in shock absorption by spreading the load. Their width and length are comparable. The examples of short bones are carpals and tarsal. Flat bones on the other hand form a protective enclosure for body organs. These are mainly present in parts such as skull and rib cage. Irregular bones as the name suggests do not have a particular shape characteristic to be classified as long or short or flat. These bones serve a purpose of protection (for example protecting the spine) and serve as anchor points. The examples include vertebrae and face bones. Other peculiar types of bone which only occur in specific locations within the body are sutural/wormian bones (present in back portion of the skull) and sesamoid (present in knee joints). This classification is schematically shown in Fig. 1.12 [15].

1.4.3 Thermophysical Properties of Bone

A composite nature and various types of the bone described earlier heavily influence the thermophysical properties of the bone. These properties as described earlier determine the response of bone to the action of tools. Another aspect is knowledge about these properties is extremely important for process modeling. Considering wide variety of materials and structural features, the bone properties are highly variable

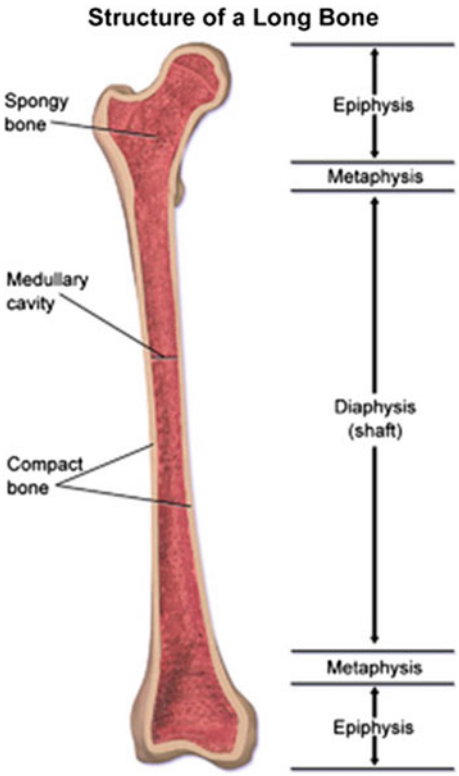

Fig. 1.11 The schematic of a long bone along with its structural components. © Blausen.com staff [15]

(Fig. 1.13 [16]) which makes it difficult to accurately determine them. Many factors including gender, age, and diet influence the bone structure and in turn the properties. Each constituent contributes to the overall properties of the bone composite. The composite nature of the bone can be realized during mechanical loading where fibers transmit the load to fibrils (Fig. 1.14 [17]). These fibrils absorb majority of the strain thus protecting the brittle mineral crystals. Thus the properties measured for the bone as a whole are a result of various materials and the way they have been arranged.

Usual practice of reporting the bone properties is the average in case of the type of bone under consideration. The important mechanical properties are strength, moduli of elasticity, shear, and flexure. These material properties determine the mechanical response of the bone towards various machining operations. The stress distribution within the material ultimately leads to its removal by fracture thus generating machining action. During such an action, the secondary effect that is thermal effect also comes into play giving rise to temperature rise. This effect is critical from bone damage point of view and can result in permanent death of bone tissues. The properties governing thermal effects during machining of the bone are specific heat capacity and thermal conductivity. Thermal properties are also very important in high energy density radiation based bone machining processes such as laser based techniques wherein thermal effects are primary in nature and are, in fact, employed for material

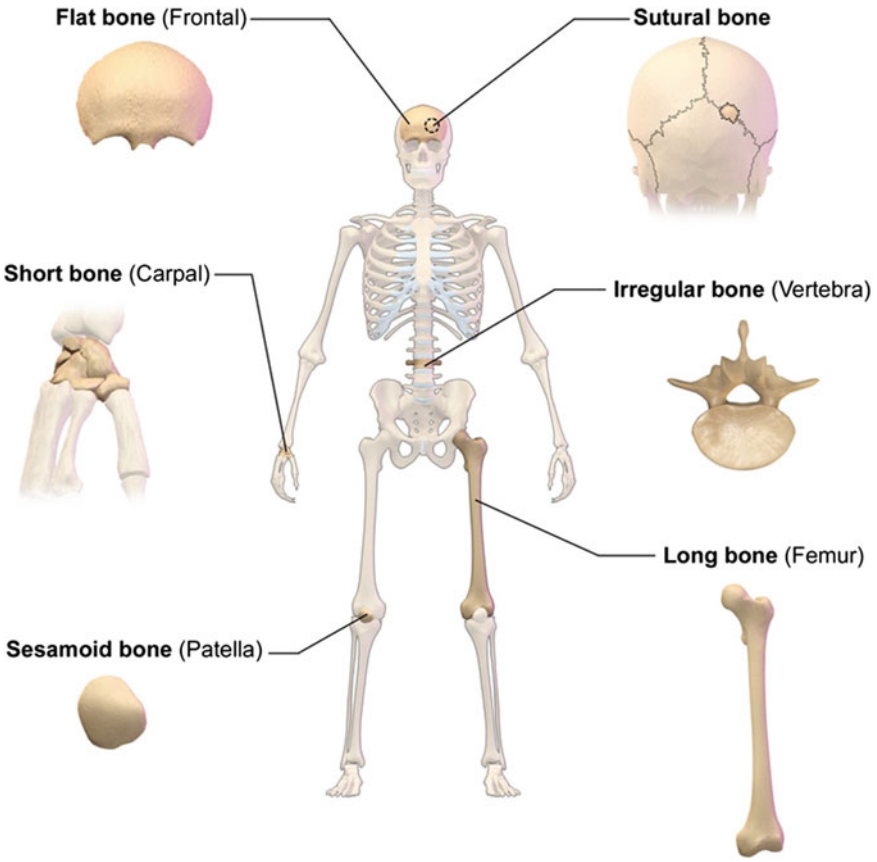

Fig. 1.12 Types of bone according to anatomy. © Blausen.com staff [15]

removal. Thus, its is important to have an idea about the properties described above for deciding the machining parameters or predict the response of bone to the machining by computer simulations. In light of this, important thermophysical properties of bone have been tabulated in Table 1.3. In some cases, however, individual thermophysical properties of the each chemical component might be required to predict the overall machining behavior on various length scales. The response of each component is expected to be different and one of those could play a deciding role. For example, during laser irradiation of bone using Er:YAG laser, water absorbs the Er:YAG wavelength and causes the bone to ablate. In light of this, some of the thermophysical properties of each component of the bone enlisted in Table 1.4 are compiled from various investigations [18–20].

Apart from the mechanical and thermal properties described above, in case of radiation based techniques and their modeling, optical properties of the bone also

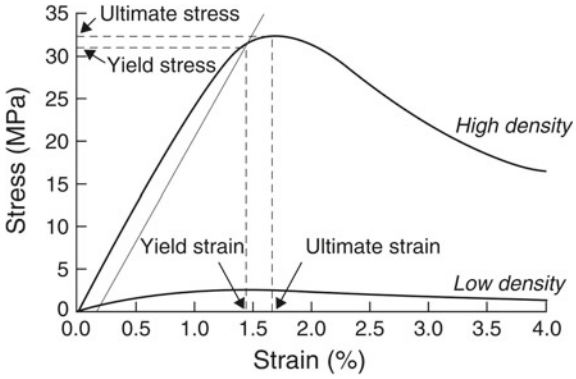

Fig. 1.13 Dependence of compressive stress-strain curve on bone density (reprinted from Morgan and Bouxsein [16] with permission. © Elsevier)

play a critical role. However these properties have been discussed in detail in the chapter on non conventional machining techniques.

Thus, it is clear that bones have various sizes and shapes and form an integral and vital part of the body system. Any damage to the bones may lead to impaired functionality of the organs. There is always an inherent damage to the bones during orthopedic surgery or any surgery which requires cutting through the bones to access the internal organs. Although technological advances have allowed in some cases to have minimally invasive surgeries, it is not possible to eliminate such a damage totally. The following section provides information about various damages that may occur to the bone during surgical machining operations.

1.5 Physical and Biological Effects of Orthopedic Surgery

A machining operation leads to damaging effects within the hard tissue apart from the material removal. Theses undesirable effects can be broadly classified as physical and biological damages. Improvements are constantly underway within the conventional bone machining methods and new techniques are being developed to minimize the damages. However, it is extremely difficult to achieve total damage elimination. Such damages may cause pain, longer healing times, and permanent impairment within the hard tissues. Current section briefly explores the physical and biological damages caused by bone machining operation in general. Detailed reasons behind origin of such damages will be explored in the forthcoming Chaps. 4 and 5.

1.5.1 Physical Damage

Machining operation inherently causes physical damages to the bone. These damages can occur in the form of cracking, surface roughness, and volumetric changes.

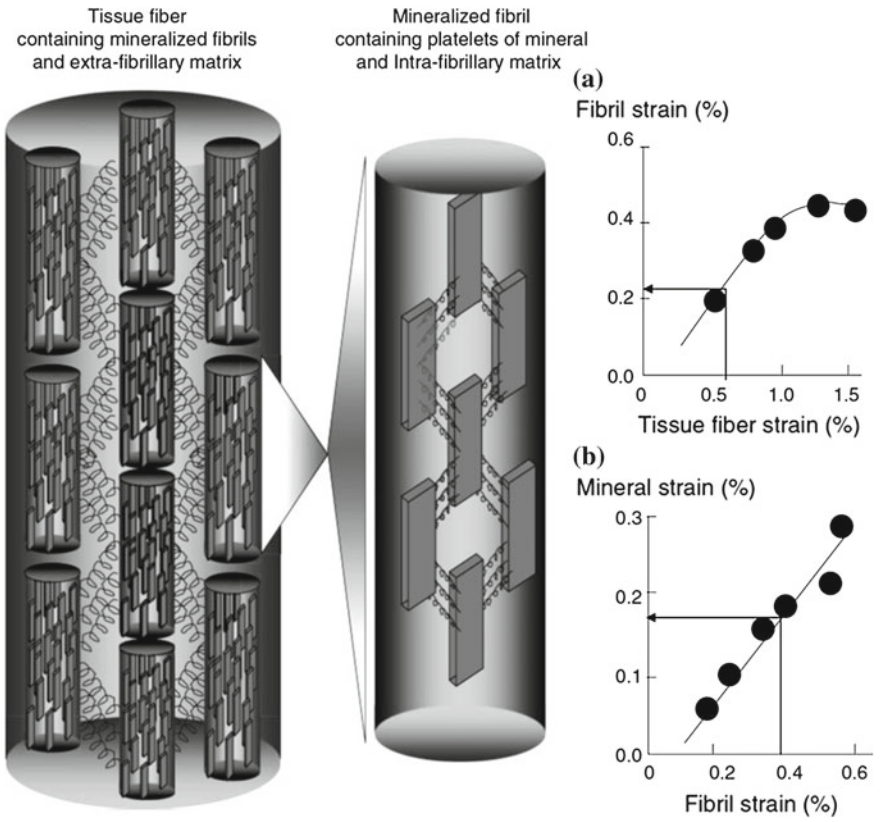

Fig. 1.14 Schematic of a bone fiber tissue and corresponding graphs, **a** indicating the load transmission from fibers to fibrils and **b** showing that majority of strain is absorbed by the fibrils to protect the mineral crystals (reprinted from Seeman [17] with permission. © Elsevier)

In case of contact based techniques these effects are induced by forces generated by movement of the tool. As soon as bone comes under the action of moving tool, the stress starts to buildup (similar to what shown in Fig. 1.13). After loading more than the ultimate tensile strength, bone fails. This failure might initiate with formation of cracks. Considering the brittle nature of the mineral, crack formation is easily facilitated. These cracks can propagate through the cross section and damage the tissues. In addition, based on tool geometry, the machining action can produce differential surface finish on the bone. Surface roughness, has influence on bone healing process [21] as well as the mechanical properties of the bone [22]. Thus, although the volume removal is the necessary action, other secondary effects act as harmful.

In case of high energy density radiation based techniques, even though there is not a direct mechanical stress generation, bone does experience generation of thermal stress. However, unlike mechanical machining, the high energy density radiation based technique is a non-contact machining technique. During such a non contact

Table 1.3 Thermophysical and mechanical properties of bone

Bone type (Direction)	Property								
	Density (kg/m^3)	Elastic modulus (GPa)	Tensile strength (MPa)	Flexural modulus (GPa)	Flexural strength (MPa)	Shear modulus (GPa)	Shear strength (MPa)	Thermal conductivity (W/m.K)	Specific heat capacity (J/kg.K)
Cortical (along grain)	1800–2000	18–26	135–167	14–22.6	150–180	4.5–6.0	150–180	0.41–0.63	1100–1260
Cortical (across grain)	1800–2000	10–13	49–60	14–22.6	50–65	3.3–4	50–65	0.41–0.63	1100–1260
Cancellous (high density)	700–975	0.8–1.5	6–12	0.8–1.5	6–12	0.3–0.5	6–12	0.20–0.31	1100–1260
Cancellous (low density)	300–550	0.07–0.4	2–3	0.07–0.4	2–3	0.03–0.15	2–3	0.12–0.19	1100–1260

Table 1.4 Thermophysical properties of bone components

Property	Material		
	Water	Collagen	Mineral
Density (g/cm^3)	1	∼1	3.14–3.21
Thermal conductivity (W/m^2/K)	0.37–0.50	0.55	0.6
Specific heat (J/kg/K)	0.662	1.79	4.17
Emissivity	1.01	1.01	1.01

high energy density radiation based machining technique, rapid heating gives rise to phase changes in bone constituents and vaporization removes the material. These techniques also affect surface roughness. In addition, as there is a large variation in temperature for very short duration of time, thermal stresses are generated that may result in formation of cracks leading to tissue damage.

From above discussions, it is clear that machining processes result in various physical damages. In light of this, the choice of processing parameters becomes very critical. Apart from mechanical effects (cracking), due to mechanical and thermal stresses, the temperature rise as undesirable side effect in mechanical contact machining and as an inherent part of the high energy density radiation machining is associated with biological and cellular damage of the bone. Following subsection covers the essential details about temperature induced biological and cellular damage, technically termed thermal osteonecrosis.

1.5.2 Osteonecrosis

Accumulation of heat during bone machining leads to substantial rise in the bone temperature. Such a rise in temperature can lead to necrosis (irrecoverable damage) in the tissues subjected to heat. In clinical terms, necrosis is the cell death due to an irreversible external injury, which is recognizable microscopically by alterations in the nucleus [23]. Normally observed changes are swelling, pyknosis (irreversible condensation of chromatin), karyorrhexis (destructive fragmentation), and karyolysis (dissolution of a cell nucleus). In addition the cytoplasm, a cellular liquid, becomes eosinophilic (readily stained by eosin chemical). In case of bone death, the term osteonecrosis is used.

Osteonecrosis has been reported to cause the collapse of the architectural bony structure, leading to joint pain, bone destruction, and loss of function [23]. An example of osteonecrosis in case of femoral bone is presented in Fig. 1.15 [24]. The process starts with the damage (Stage I), followed by trauma and pain leading to limited range of motion, particularly internal rotation and abduction. The pain gets worsened in Stage II and III. Progressive loss of articular cartilage occurs in Stage IV finally leading to decreased joint space and collapse of the femoral head.

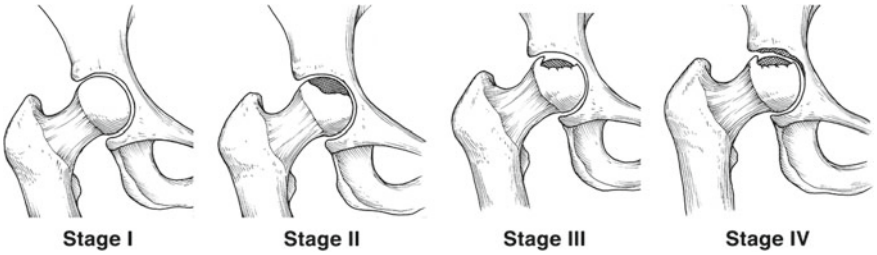

Fig. 1.15 Four radiographic stages of osteonecrosis. *Stage I* normal radiographic appearance. *Stage II* transition phase. *Stage III* sequestrum with subchondral collapse. Stage IV = decreased joint space and collapse of the femoral head (reprinted from Beaulé and Amstutz [24] with permission. © Wolters Kluwer)

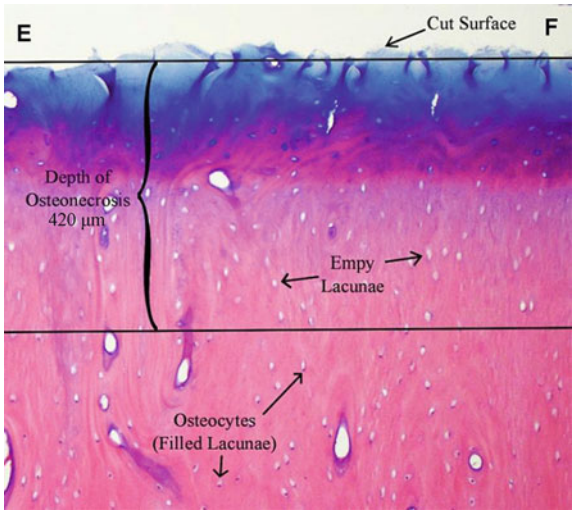

Fig. 1.16 Micrograph showing thermal damage in bone during cutting (reprinted from James et al. [25] with permission. © Elsevier)

Osteonecrosis can initiate because of several reasons such as accidents causing fracture, consumption of some medication, alcoholism, and heat exposure [23]. In case of bone machining, heat exposure becomes a significant factor leading to rise in temperature. This leads to thermal osteonecrosis causing damage to the bone structure. Origin of such damage arises from thermal instability of various constituents of the bone [26]. For example, the enzyme lysyl-tRNA-synthetase essential for cell functioning is prone to thermal damage. The process of denaturation (proteins experiencing structural damage) begins at 40 °C and half life reduces to less than 5 min at 45 °C [27]. Collagen, on the other hand is characterized by denaturation temperature of 60 °C [28]. An example of thermal damage during cutting of the bones is shown in Fig. 1.16 [25]. The discoloration at the cut surface is clearly seen. Heat decreases the affinity of extracellular protein collagen for the pink eosin stain and promotes affinity for the blue hematoxylin stain. Thermal damage at the cut surface is clearly visible

in Fig. 1.16 as the blue hematoxylin stain penetrates deep within the bone. This is indicated by the absence of osteocytes from their lacunae. The dispersion of empty lacunae is clearly separated from the viable osteocytes, indicating the probable depth of osteonecrosis.

In one of the early studies, Moritz and Henriques investigated the effect of the time and temperature on thermal necrosis of the bone [29]. Time for thermal necrosis was measured over a large temperature range (40–100 °C). A temperature of 70 °C killed the epithelial cells instantly, at 50 °C however 30 s were required. Temperature of 45 °C had to be maintained for more than 5 h to harm the cells. The study found that as the temperature increased, the amount of time required to initiate thermal necrosis decreased.

On the other hand, Lundskog [30] described extensive necrosis in cortical bone at a temperature of 70 °C and measured a threshold temperature of 50 °C at 30 s exposure. Eriksson et al. [31] found that in case of rabbit bones subjected to 47 °C for 1 min resulted in necrosis. It is assumed that on average the threshold temperature, at which necrosis is most likely to appear is around 50–60 °C, but the time duration is dependent on the severity of temperature, according to the variety of published experimental results. Nonetheless, it is realized that the thermal damage starts at around 45 °C and a temperature of above 55 °C produces coagulation of cell structures. From the physiopathological point of view enzyme inactivation occurs by disrupting the cell metabolism. Further increase in the temperature vaporizes the cell water giving rise to excess pressure which eventually culminates in explosion and carbonization of the cell [32].

References

1. I.V. Ponseti, Lowa Orthop. J. **11**, 59 (1991)
2. S.W. Wiesel, N.D. John (eds.), *Essentials of Orthopedic Surgery*. (Springer, Berlin, 2010)
3. A.O. Association, National Bone and Joint Registry Annual Report (Adelaide 2011)
4. N. Lunt, *Medical Tourism: Treatments, Markets and Health System Implications: A Scoping Review* (OECD, Directorate for Employment, Labour and Social Affairs, Paris, 2011)
5. L. Jones, B.A. Lieberman, Arch. Surg. **32**(6), 990 (1936)
6. J.D. Currey, J. Biomech. **21**(2), 131 (1988)
7. M. Benjamin, *in Miller-Keane Encyclopedia and Dictionary of Medicine, Nursing and Allied Health* (Saunders, Philadelphia, 1997)
8. M. Rauner, N. Stein, L.C. Hofbauer, in *Principles of Osteoimmunology* (Springer, Berlin, 2012), pp. 1–26
9. J. Buckwalter, M. Glimcher, R. Cooper, R. Recker et al., J. Bone Joint Surg. Am. **77**(8), 1256 (1995)
10. J.Y. Rho, L. Kuhn-Spearing, P. Zioupos, Med. Eng. Phys. **20**(2), 92 (1998)
11. P.R. Buenzli, N.A. Sims, Bone **75**, 144 (2015)
12. M.M. Giraud-Guille, Calcif. Tissue Int. **42**(3), 167 (1988)
13. A.M. Parfitt, Bone **30**(6), 807 (2002)
14. K. Rogers, *Bone and Muscle: Structure, Force, and Motion* (The Rosen Publishing Group, New York, 2010)
15. Blausen.com staff. Blausen gallery 2014. Wikiversity J. Med. doi:10.15347/wjm/2014.010. ISSN20018762. Own work

16. E.F. Morgan, M. Bouxsein, Principles Bone Biol. **1**, 29 (2008)
17. E. Seeman, Principles Bone Biol. **1**, 3 (2008)
18. T. Coelho, E. Nogueira, W. Weinand, W. Lima, A. Steimacher, A. Medina, M. Baesso, A. Bento, J. Appl. Phys. **101**(8), 084701 (2007)
19. L.D. Stumme, T.H. Baldini, E.A. Jonassen, J.M. Bach, in *Summer Bioengineering Conference* (2003), pp. 25–29
20. F.A. Duck, *Physical Properties of Tissues: A Comprehensive Reference Book* (Academic Press, London, 2013)
21. B.D. Boyan, V.L. Sylvia, Y. Liu, R. Sagun, D.L. Cochran, C.H. Lohmann, D.D. Dean, Z. Schwartz, Biomaterials **20**(23), 2305 (1999)
22. E. Donnelly, S.P. Baker, A.L. Boskey, M.C. van der Meulen, J. Biomed. Mater. Res. Part A **77**(2), 426 (2006)
23. C. Fondi, A. Franchi, Clin. Cases Miner. Bone Metab. **4**(1), 21 (2007)
24. P.E. Beaulé, H.C. Amstutz, J. Am. Acad. Orthop. Surg. **12**(2), 96 (2004)
25. T.P. James, G. Chang, S. Micucci, A. Sagar, E.L. Smith, C. Cassidy, Med. Eng. Phys. **36**(3), 364 (2014)
26. S. Karmani, Current Orthop. **20**(1), 52 (2006). doi:10.1016/j.cuor.2005.09.011. http://www.sciencedirect.com/science/article/pii/S0268089005001672
27. L. Rymo, U. Lagerkvist, A. Wonacott, J. Biol. Chem. **245**(17), 4308 (1970)
28. A.R. Errikson, *Heat Induced Bone Tissue Injury*, PhD Thesis (University of Gothenberg, Sweden 1972)
29. A.R. Moritz, F. Henriques Jr., Am. J. Pathol. **23**(5), 695 (1947)
30. J. Lundskog, Scand. J. Plast. Reconstr. Surg. **9**, 1 (1971)
31. A. Eriksson, T. Albrektsson, J. Prosthet. Dentist. **50**(1), 101 (1983)
32. J.Y. Giraud, S. Villemin, R. Darmana, J.P. Cahuzac, A. Autefage, J.P. Morucci, Clin. Phys. Physiol. Meas. **12**(1), 1 (1991)

Chapter 2
Fundamental Operations of Bone Machining

Currently, the majority of conventional orthopedic surgeries adopted for shaping and forming bones involve the contact methods based on controlled mechanical fracturing (chipping) of the bones. The fundamental operations involved in mechanical fracturing of bone are drilling, sawing, grinding/abrasive machining, and milling. The various methods designed for mechanically shaping and forming bones during orthopedic surgeries in the clinical environment are either based on single or combinations of these fundamental operations. The examples of methods based on combinatorial fundamental operations are: ultrasonic, pneumatic, and hydraulic machining. In addition to these mechanical operations/methods, several non-contact thermal photon/electron energy based techniques are also being researched for their possible use in orthopedic surgeries. The thermal energy-(bone) material interaction raises its temperature to the melting or vaporization temperature depending upon the magnitude of the thermal energy and photon/electron energy-material interaction characteristics. Thus a bone can be shaped and formed by removal of the bone material through controlled melting and/or vaporization. The non-contact thermal machining techniques/methods based on photonic/electron energy that are being explored in bone machining include but not limited to laser, microwave, and ion beam machining. The purpose of this chapter is to present only the fundamental principles behind mechanical and thermal operations in removal (machining) of material in general. Whereas, the implementation of these fundamental operations and methods/techniques particularly for machining of bones are described in detail in Chaps. 3, 4, and 5.

2.1 Drilling

Drilling is a basic machining operation to cut a hole into solid material. It can be further extended to enlarge previously drilled holes and in that case the operation can be described as core drilling or counter drilling/boring . If the same drill is employed to cut a hole of two or more diameters, the operation is termed as step drilling. For

N.B. Dahotre and S.S. Joshi, *Machining of Bone and Hard Tissues*,
DOI 10.1007/978-3-319-39158-8_2

enlarging the hole with an intention to achieve more accuracy, a boring operation is adopted. On the contrary, if the intentions are not just to enlarge a hole but also produce hole of accurate size and good surface finish with minimal material removal, an operation of reaming is employed. Furthermore, operations of enlarging a hole to a limited depth, enlarging a hole with a shallow depth to just finish face around the original hole, and cutting of an angular opening into the end of a hole are termed as counterboring, spot facing, and countersinking respectively. Finally, center drilling is an operation used to drill a hole that will act as a center of rotation for many other above mentioned drilling operations. Center drilling is typically performed using a drill with a special shape, known as a center drill.

These various drilling operations and the types of drills employed during these operations are schematically presented in Fig. 2.1. The most common type of drill used in drilling operation is the standard-point twist drill. They possess helical groves or flutes as shown on the drill in Fig. 2.1. The geometric parameters (cutting lips and edges) that influence the drilling performance of a drill are a point angle, lip-relief angle, a chisel-edge angle, and a helix angle. These geometric parameters are schematically illustrated in Fig. 2.2 [1]. The helix angle varies from 18° to 40° for the drill used to drill hard materials and soft materials respectively. The cutting lip relief angle ranges between 12–15° at the outside diameter and decreases toward the axis of the drill whereas too much relief weakens the cutting edge and reduces drill life. Although the average point angle is 118° it can vary for specific purposes from 136° for hard materials (steels) to 60° for soft materials (wood). Maintaining equal length of the cutting edges or lips along with their orientation in equal angle with the axis of the drill are important for their accurate/precision performance over its long life time.

Typically drilling operation can be categorized in two major operating regimes as low speed and high speed operating conditions [2]. A low speed drilling involves tool wear largely by abrasion and interaction of surface asperities under high pressure leading to edge deterioration and formation and fracture of fusion zones. On the contrary, although at high speed drilling high temperature development contributes to drill wear, the material next to the drill face becomes weaker and shears more easily in friction while both the coefficient of friction and the friction force remain low. If

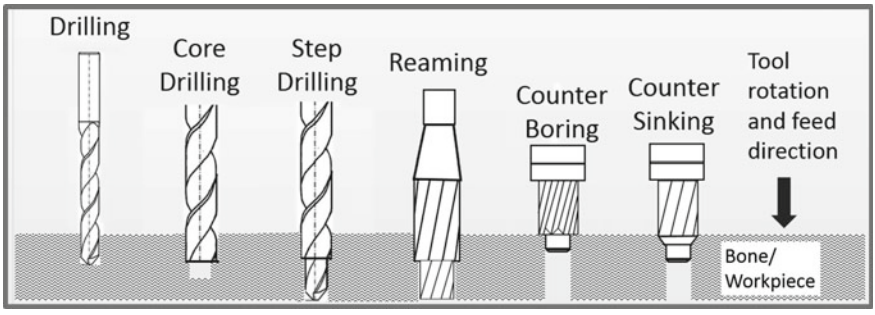

Fig. 2.1 Various drilling operations

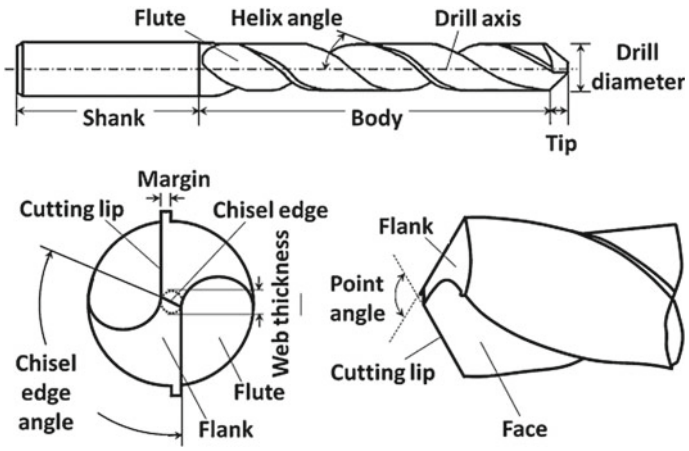

Fig. 2.2 Geometric features of twist drill (reprinted from Lee et al. [1] with permission. © Elsevier)

the drill of rotational velocity V_d exerts a force F (the force applied to the drill) on the chip being removed from the workpiece (assuming orthogonal machining) and its resolution (drilling force) in the direction of drill velocity is F_d then power, P required to drill is

$$P = F_d V_d \tag{2.1}$$

The power does not increase linearly with speed as the drilling force decrease at increased speed. During drilling the force that acts in the direction of the hole axis is defined as the thrust force [2]. The thrust force depends upon various factors such as feed, rotational speed, drill diameter, drill geometry, and the strength of the workpiece material. The power, P dissipated during drilling is the product of torque and rotational velocity, V_d. The measurement and direct correlation of these parameters with thrust force is complex and difficult. However, the material removal rate in drilling MRR_{drill} can be expressed in the following simplistic relationship.

$$MRR_{drill} = \frac{\pi D^2}{4} f_d R \tag{2.2}$$

where D is the drill diameter, f_d is the feed per rotation and R is the rotational velocity.

2.2 Sawing

In sawing the cutting tool is a blade (saw) with series of small teeth on its periphery (edge) that remove a small amount of material by reciprocating linear or unidirectional linear or circular motion. In sawing, due to a narrow width of cut (kerf) small volume of material is removed (wasted). The important parameters associated with

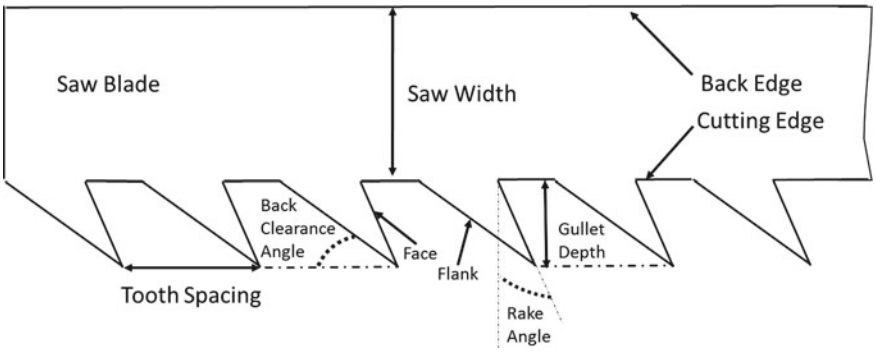

Fig. 2.3 Various geometric features of a saw

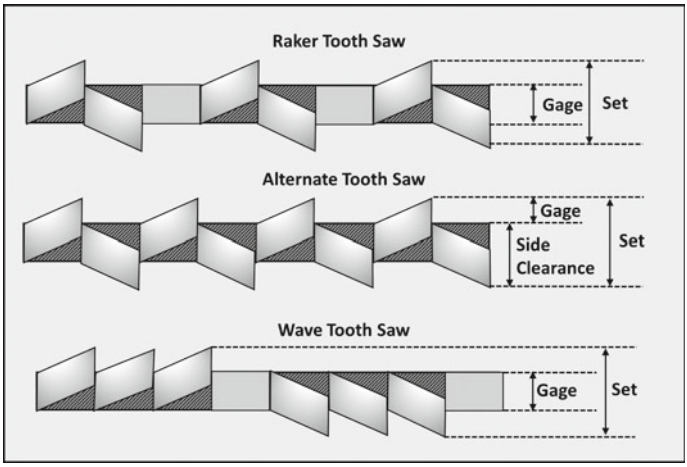

Fig. 2.4 Types of saw teeth

a saw are (1) material, (2) tooth spacing (pitch), (3) tooth size, (4) tooth form, and (5) tooth set and these are schematically illustrated in Fig. 2.3 [2]. Low alloy, high-carbon steel, special steel alloy including stainless steel, and high speed steel are the preferred materials for saw. Often, the saw teeth tips are welded/fused/inserted with diamond, ferrous or non-ferrous carbide, and high speed steels for better performance and longer lifetime of the saw. The performance of a saw in terms of rate of volume of material removal and depth of cut are highly influenced by the pitch. Coarse teeth are suitable for wider and faster cut whereas fine teeth are appropriate for narrow cut. The pitch of circular saw is usually in the range of 5–51 mm and typically the straight saws are available with the teeth in the range of 2 teeth/in. to 32 teeth/inch. The rake angle and clearance angle corresponding to single-point tool along with alternate offsetting of the teeth with respect to the saw plane (Fig. 2.4) provide anti-binding and anti-rubbing characteristics to the saw during cutting [2].

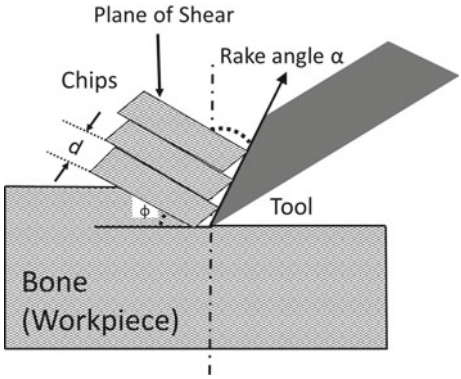

Fig. 2.5 Schematic of basic mechanism of chip formation during cutting

Even though the sawing blades have different shapes/forms (linear and circular) their series of cutting teeth operate in the same basic manner. Therefore, the principles of sawing (machining) operation can be explained on the basis of theory related to cutting by single-point cutting tool [2]. The basic mechanics of actual three dimensional sawing process can be simplistically explained by two dimensional orthogonal cutting model where the saw tooth edge is perpendicular to the movement of the saw (Fig. 2.5) [2].

As during sawing, the chips are generally produced by shearing process (Fig. 2.5) shearing occurs along a shear plane at the shear angle, Φ with the surface of the workpiece. The orthogonal cutting includes a configuration of a rake angle, α; a relief or clearance angle and tool angle that together add to 90° (Fig. 2.5).

For a saw set up at a cutting (sawing) speed, V_s to remove an unformed workpiece layer of thickness, h_o and a chip of thickness, h_c, then the cutting ratio, R_c and the shear angle, Φ are expressed as

$$R_c = \frac{h_o}{h_c} \; and \; \tan\Phi = \frac{R_c \cos\alpha}{1 - R_c \sin\alpha} \tag{2.3}$$

Since chip thickness, h_c, is greater than the depth of unformed workpiece layer of thickness, h_o, the velocity of the chip, V_c, has to be less than the sawing speed, V_s, thereby maintaining the continuity of mass expressed by the following relationships.

$$V_s h_o = V_c h_c \; or \; V_c = V_c R_c \; or \; V_c = V_s \frac{\sin\Phi}{\cos(\Phi - \alpha)} \tag{2.4}$$

Finally, assuming an ideal condition where all shear during sawing is concentrated in an infinitely thin shear layer, the shear strain, Γ can be expressed as

$$\Gamma = \frac{V_s}{\cos(\Phi - \alpha)} = \frac{V_{shear}}{\cos\alpha} = \frac{V_c}{sin\Phi} \tag{2.5}$$

where V_{shear} is the shearing velocity in shearing plane. For the sheared element (shear volume) of finite thickness, d, the shear strain, Γ can be expressed as

$$\Gamma = \frac{V_{shear}}{d} \tag{2.6}$$

The chip morphology significantly affects surface finish, integrity, and the overall sawing operation. The magnitude of the shear angle, Φ, for given undeformed chip thickness controls the sawing force and energy.

2.3 Grinding/Abrasive Machining

Abrasive/grinding machining is a process of material removal via accelerated wear/fracture of a surface by a multitude of hard, angular hard abrasive particles or grains (grits) bonded or not bonded to a tool of definite form. The material removal can be small (fine) or large scale. Typically abrasive/grinding machining is the last operation performed on the component as often it is employed to produce high quality surface finish (roughness) with a desirable residual stress distribution and without surface and sub-surface damage along with close dimensional tolerance.

The grits or abrasives commonly used during abrasive/grinding machining can be broadly categorized as conventional (aluminum oxide and silicon carbide) and super (cubic boron nitride and diamond) abrasives [1–3]. The life time and performance of these grits are function of their various physical and geometric properties such hardness, toughness, resistance to attrition and fracture, friability, shape, and size. Hardness is the ability of the grit to resist penetration while abrading/scratching the workpiece surface. The greater difference in hardness between a grit and the workpiece will result in more effective and efficient grinding process. Super abrasives are the hardest materials. Toughness is body strength of a grit to withstand the mechanical shocks. Attrition and friability are the abilities of a grit to dull or deteriorate by fragmentation in fine particles and break/fracture into large pieces during grinding operation. Friability provides self-sharpening ability while resistance to attrition maintains sharpness of the grit/abrasive. Both attrition and friability of the grit depends upon hardness and toughness of the grit material to sharpen and maintain the sharpness of the grit during abrasive machining. Furthermore, friability is also dependent on the shape and size of the grit. While blocky grits are less friable compared to plate-like (flat) grits, the finer grits due to smaller probability of defects in them are stronger and less friable than larger grits.

Typically abrasive/grinding machining operations are carried out with abrasive/grinding wheels or rotary tools bonded with grits of various shapes and sizes into disks, cylinders, and cones of various shapes and sizes. The basic types of grinding/abrasive machining are surface, cylindrical, internal, and center-less grinding/abrasive machining [4]. Grinding of a flat surface is surface grinding; in cylindrical grinding (center type grinding), the external cylindrical surface and shoulder of the

workpiece are ground; in external grinding, a small diameter wheel grinds the inside diameter of the workpiece; and when the workpiece is ground by a grinding wheel or tool without supporting by centers or chucks, the process is termed as center-less grinding. These grinding/abrasive machining operations are schematically illustrated in Fig. 2.6.

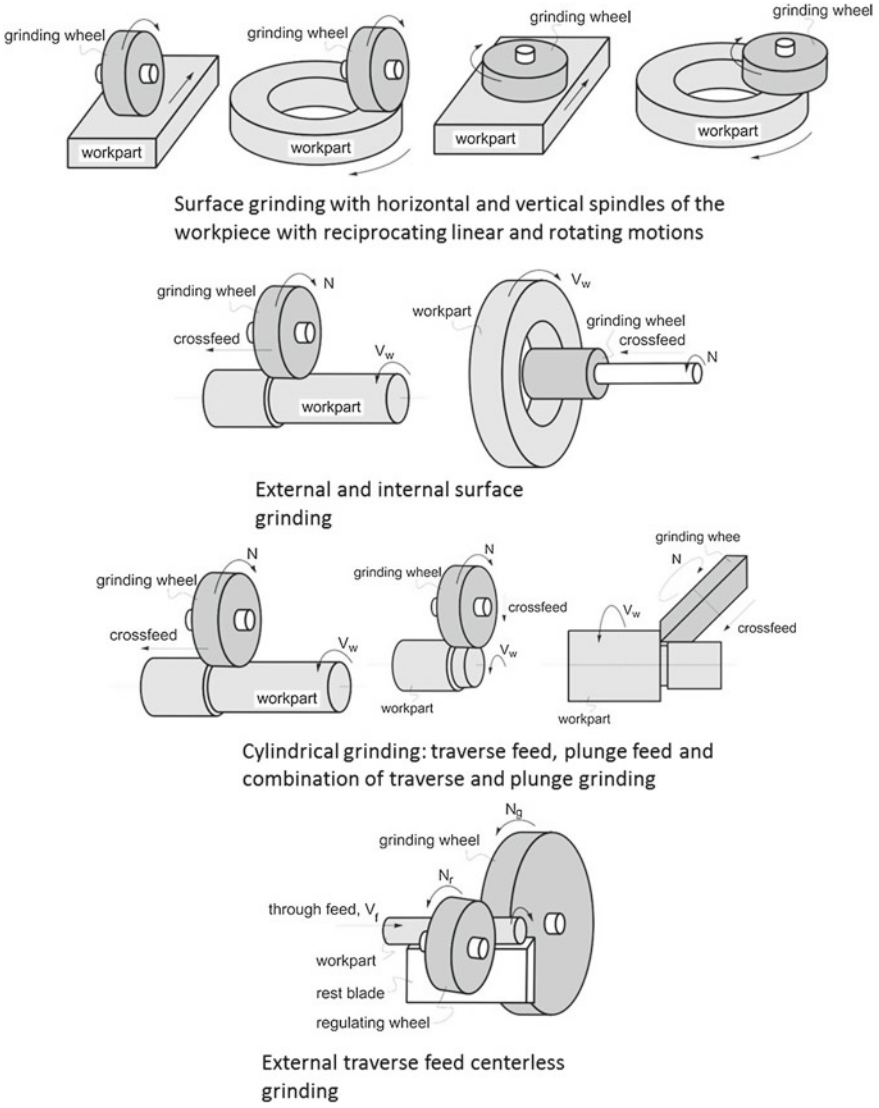

Fig. 2.6 Types of grinding

The attributes of grinding/abrasive machining are expressed in various manners. The grinding ratio, G correlates the amount of material removed (ground) with the grinding wheel/tool wear by the following formula.

$$G = \frac{Volume\ of\ material\ removed}{Volume\ of\ wheel\ material} \tag{2.7}$$

The grinding ratio depends upon type of wheel, workpiece material, grinding/cooling fluid, depth of cut, and speed of wheel and workpiece. In surface grinding operation (Fig. 2.7) [2] the length, l, of undeformed portion of the workpiece in contact of the grinding wheel is approximately represented by the following relationship.

$$l \approx (Dd)^{\frac{1}{2}} \tag{2.8}$$

where D is the diameter of the wheel and d is the wheel depth of cut. Assuming $v \ll V$ and width of the workpiece unity, the number of chips and the corresponding volume of the material removed per unit time are VC and vd respectively where V, v, and C are the tangential velocity of the grain on the periphery of the wheel, velocity of the workpiece, and the number of cutting points per unit area of wheel surface respectively. Furthermore, assuming the chip removed is of constant width, w, and rectangular in the cross section, the volume of the chip, V_{chip}, is represented by the following formula.

$$V_{chip} = \frac{wtl}{2} \tag{2.9}$$

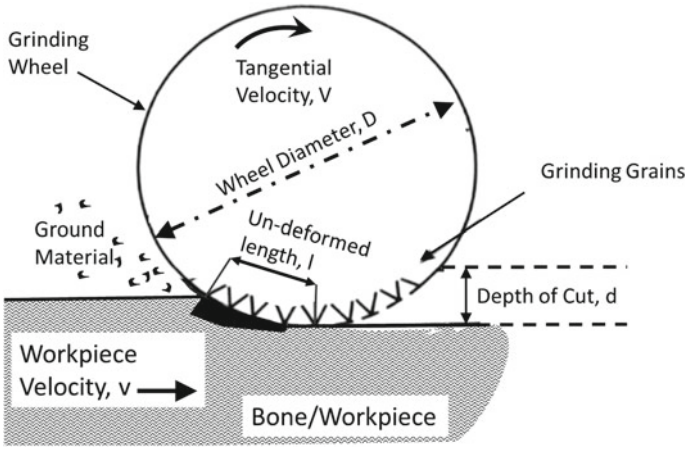

Fig. 2.7 Surface grinding operation

where t is the grain depth of cut (undeformed portion of the workpiece in contact with the wheel). Next, the volume of material removed per unit time is given by the following relationship.

$$Volume\ of\ workpiece\ material\ gound/time = \frac{Number\ of\ chips\ removed/time}{Volume\ of\ each\ chip} \tag{2.10}$$

that is

$$vd = VC.V_{chip} = \frac{VCwtl}{2} \tag{2.11}$$

Finally, t, the thickness of undeformed portion of the workpiece in contact with the wheel that is eventually removed as a chip of average thickness X, is given by

$$t = \frac{2v^{\frac{1}{2}}X^{\frac{1}{2}}d^{\frac{1}{4}}}{V^{\frac{1}{2}}C^{\frac{1}{2}}w^{\frac{1}{2}}D^{\frac{1}{4}}} \tag{2.12}$$

As the accuracy of dimensions of the surface precision grinding/abrasive machining is affected by the force on the grit, the force is proportional to the cross sectional area of the undeformed portion of the workpiece in contact with the wheel, the relative grit force is presented by

$$Relative\ grit\ force \propto \frac{vd^{\frac{1}{2}}}{VCD^{\frac{1}{2}}} \tag{2.13}$$

Finally, the temperature developed during grinding/abrasive machining can have adverse effects such as development of thermal and residual stresses in the surface and subsurface regions thereby introducing dimensional distortions in the workpiece. The temperature rise in surface and subsurface region, ΔT, is function of the total energy input to the surface area being ground and represented as

$$\Delta T \propto ud \tag{2.14}$$

where u is the specific energy consumed in producing a chip. If u is assumed to be varying inversely with the thickness of undeformed portion of the workpiece in contact with the wheel, t, then rise in temperature is given by

$$\Delta T \propto \frac{d}{t} \propto d^{\frac{3}{4}}V^{\frac{1}{2}}C^{\frac{1}{4}}D^{\frac{1}{4}}V^{\frac{1}{2}} \tag{2.15}$$

Although, localized temperatures at the wheel-workpiece contact region developed can be very high (>1000 °C) and time of contact being very short, depending upon the type of the workpiece material melting may or may not occur during grinding/abrasive machining.

2.4 Milling

Milling is a versatile machining (material removal) operation capable of producing a wide range of machined (cut) geometries including flat surfaces, pockets, angles, contours, steps, and slots [1, 2]. The tools or milling cutter employed for each of these operations are different and specialized. These tools/cutters have multiple teeth cutting edges configured around an axis that produce number of chips per revolution. The machining action is generated by rotation of the tool and the feed by motion of the workpiece. The combination of type of tool/cutter and feed mechanism together define types of milling operations and resulting milling geometries as schematically depicted in Fig. 2.8 [5].

The efficiency of the milling process can be realized through various critical machining parameters such as cutting/milling speed, V_m; feed per tooth, f_m; milling time, t_m; and material removal rate, MRR_{mill}. In milling, the cutting/milling speed, V_m is the peripheral speed of the tool/cutter and it is given by

$$V_m = \pi D_m N_m \tag{2.16}$$

where D_m is the cutter diameter and N_m is the rotational speed of the cutter as shown in Fig. 2.9. Feed per tooth, f_m and machine feed rate, V_m can be represented by the following equations.

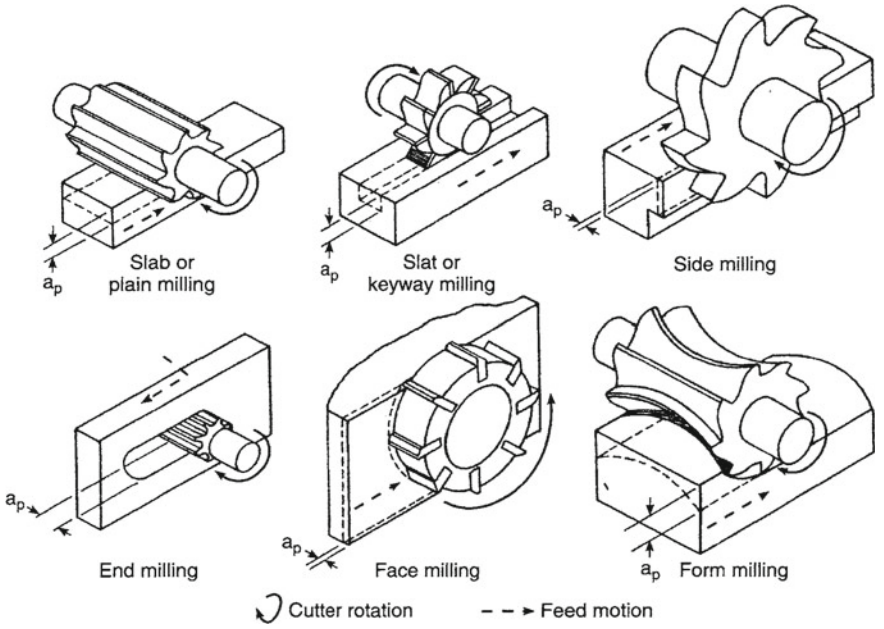

Fig. 2.8 Types of cutters and milling operations (reprinted from Grzesik [5] with permission. © Elsevier)

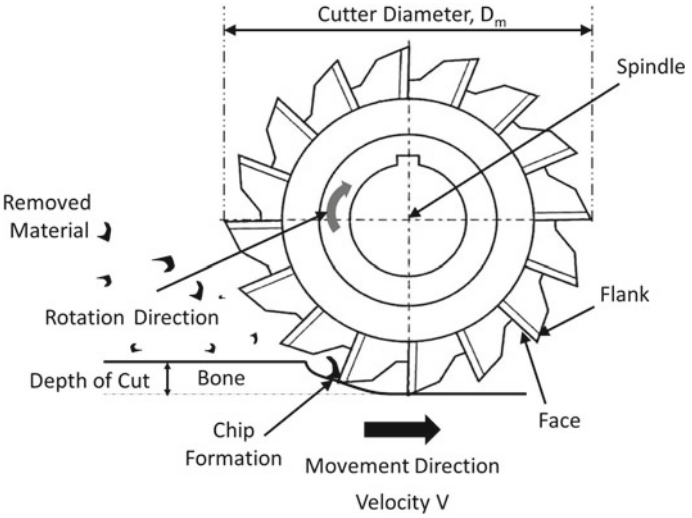

Fig. 2.9 Schematic of milling cutter with essential elements

$$f_m = \frac{v_m}{N_m.n} \tag{2.17}$$

where V_m is the machine feed rate (linear speed) of the workpiece and n is the number of teeth on the cutter periphery. Further, the milling time, t_m is expressed by the following equation.

$$t_m = \frac{l}{v_m} \tag{2.18}$$

where l is the length of the workpiece. Finally the material removal rate is given by

$$MRR_{mill} = \frac{lwd}{t_m} = wdv_m \tag{2.19}$$

where w is the width of the cut. Both power (Force × Velocity) and torque (power/milling speed) requirements in milling are dependent on the forces (tangential, radial, and axial) acting on the cutter of multiple teeth and complex geometry and hence they are very difficult to calculate. However, they can be measured experimentally for a variety of conditions. Furthermore, for rapid milling, feed per tooth (f_m) should be as high as possible. Such heavier feed, however is likely to exert greater load on the cutter teeth, workpiece, holding device, and milling machine. For a fragile material, a light feed is appropriate whereas a heavier feed is possible with soft materials. Irrespective of material type, a light feed leads to a good surface finish.

The various geometries such as flat surfaces, pockets, angles, contours, steps, and slots produced by milling are based on the following methods [1]. In slab milling or

peripheral milling, the axis of cutter rotation is parallel to the surface of the workpiece to be machined. Cutters used in slab milling possess straight or helical teeth and produce orthogonal or oblique sections. During this type of milling the operation can be conducted either as *up/conventional milling* or *climb/down milling* (Fig. 2.8). In up milling, the maximum chip thickness is at the end of the cut and hence tooth engagement is not a function of workpiece surface characteristics and the process is smooth. However, during the process the tool may chatter and the workpiece may need proper clamping to avoid its pulling upward. On the other hand, climb/down milling cutting starts with the thickest section of the chip and hence the downward component of cutting forces holds the workpiece in place. The surface characteristics influence the cutter teeth life during climb milling.

The milling process in which the cutter is mounted on a spindle with an axis of rotation perpendicular to the workpiece surface is called face milling (Fig. 2.8). During face milling, the cutter rotates at a rotational manner while the workpiece moves along a straight path in a linear manner. Like in slab milling, face milling operation can also be performed in up/conventional milling or climb/down milling mode. As the relative motion between the cutting teeth and the workpiece leaves feed marks on the machined surface during face milling, such surface roughness depends on insert corner geometry and feed per tooth. The method of *end milling* adopts the cutter with either sharp or tapered shank and rotates either on an axis perpendicular or tilted to the workpiece (Fig. 2.8). The end face of end mill with cutting teeth are used as a drill to start a cavity, whereas end mill with hemispherical ends produce curved surface and hollow end mill with internal cutting teeth machine the cylindrical surface of solid round workpiece. Other miscellaneous milling methods include straddle milling that is based on use of two or more cutters on an arbor to machine two parallel surfaces on the workpiece; and *form milling* to produce curved profiles using the cutters with specially shaped teeth.

2.5 Thermal Machining

A thermal machining using high energy density photon/electron heat sources such as laser, electron beam, and microwave is being extensively explored to machine various types of material systems [6, 7]. Although these techniques hold tremendous promise for machining various shapes, sizes, and materials they have not yet made inroads as routine commercial production techniques due to reasons such as but not limited to (1) lack of full understanding of interaction of these heat sources with material at atomic and molecular levels, (2) complexity and difficulty in maneuvering the heat source for delivery to workpiece during machining complex shapes, (3) lack of temperature dependent thermophysical properties of materials, and (4) safety issue with a reflected stray energy due to highly reflective nature of these intense heat sources with many types of materials. For all these prime and many other reasons, these thermal techniques are termed as non-traditional or un-conventional machining methods.

As these sources generate heat through interaction of the photons and electrons with the atoms and molecules in the surface and sub-surface regions of material. By controlling the intensity of incoming (input) high energy density photon/electron radiation, the temperature in heat source-material interaction region can be raised to the level to remove (machine) the material via melting or vaporization. The photonic/electronic radiation can be delivered in pulsed or continuous mode. The level (intensity or fluence) of energy delivered to the workpiece is function of power of the photon/electron source, traverse speed of photon/electron source or workpiece, photon/electron source coverage area on the workpiece surface, pulse frequency in case of pule mode delivery, and photon/electron energy absorption characteristics with the workpiece surface. Based on these process parameters and thermo-physical properties of the workpiece material such as thermal conductivity, density, and specific heat as function of temperature, one can develop a computational heat transfer, mass transfer, and fluid flow based model to predict photon/electron energy required for the purpose of raising the temperature of material to remove (machine) it via melting or vaporization for a desired removal (machining) rate [8, 9]. Several two and three dimensional computational models incorporating various details for intense heat based material machining have been proposed in the open literature [8–36]. Due to the complexity associated with the interaction of materials with high energy photon/electron radiation and associated multi-physics phenomena along with lack of data in the open literature on temperature based thermos-physical properties of various materials, these computational models exist with various limitations in accurately predicting the temperatures and material removal rates. Nonetheless, they continue to provide important guidelines for future developments.

Considering the dynamic nature of the high energy density photon/electron radiation based machining with very short interaction times ranging from mili-to picoseconds, it is extremely difficult to capture/realize various physical phenomena by in situ measurements of thermodynamic and kinetic parameters during machining process. In view of this, a multiphysics computational modeling approach incorporating physical phenomena such as heat transfer, fluid flow, convection mixing, surface tension, etc. remains the viable basis of computational efforts [8, 9]. Through understanding of correlations among these physical phenomena and in turn development of the correlation between these physical phenomena and processing parameters one can develop a better control on photon/electron energy based material removal (machining) rate and evolution of physical attributes (surface geometry and surface roughness) during machining operation. Furthermore, such methodology can be extended to optimization of the process to achieve higher machining efficiency.

During multidimensional high energy density photon/electron radiation based machining, material experiences various physical phenomena such as phase transition from solid-to-liquid-to-vaporization and material loss during evaporation. In addition, the material surrounding ablated region also experiences the transition dependent effects such as thermal expansion, melting, vaporization, along with generation of Marangoni convection in the melt and recoil pressure due to vaporization during heating as schematically presented in Fig. 2.10. These physical transitions are also associated with generation of various body and surface forces listed in Fig. 2.11

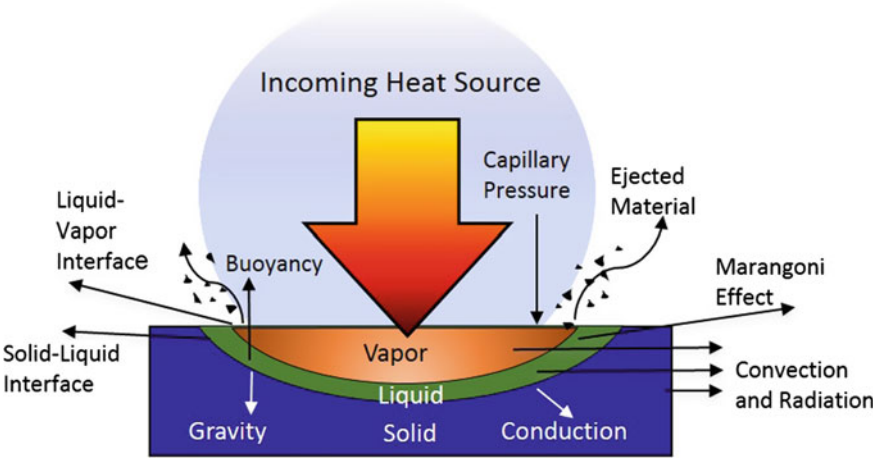

Fig. 2.10 Various physical phenomena within photon heat source-workpiece interaction region

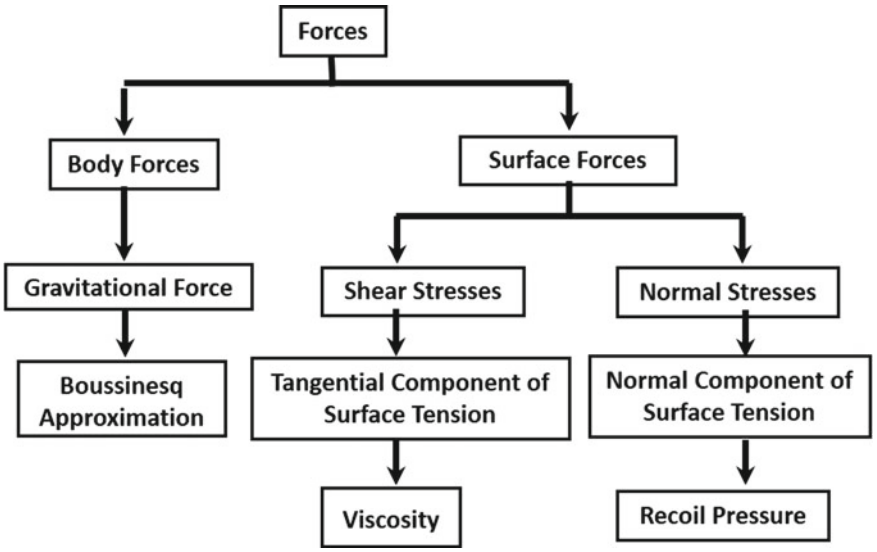

Fig. 2.11 Body and surface forces generated during thermal machining

[9] and depicted in Fig. 2.10. All these physical phenomena can be built into a complex computational model on the finite element platform. Such computational model based on the multiphysics approach can combine heat transfer, fluid flow, and structural mechanics for combinatorial effects of these physical phenomena. The model in turn can predict evolution of physical attributes/surface topography (depth, width, and geometry) of the machined region as schematically presented in Fig. 2.10 and corresponding machining rate.

The selective governing equations and boundary conditions for such multiphysics computational thermal models are presented below. As the material removal during such thermal machining is via controlled melting and vaporization, the prediction of temperature evolution is very important and can be determined by the solution of the equation governing the heat transfer given by

$$\rho C_P \left(\frac{\partial T}{\partial t}\right)_{(x,y,z)} = k\left[\left(\frac{\partial T}{\partial x}\right)_{(y,z,t)} + \left(\frac{\partial T}{\partial y}\right)_{(x,z,t)} + \left(\frac{\partial T}{\partial z}\right)_{(x,y,t)}\right] \tag{2.20}$$

Here, k is the thermal conductivity, C_p is the specific heat and ρ is the density of the material. Of course, temperature variation will be dependent on many complex physical phenomena occurring during various times of the heat source-material interaction period. Hence, the accuracy of temperature predicted by solution to this fundamental equation depends upon how diligently one can conceive and incorporate them into the computational model. Further, the photon/electron heat source-workpiece interaction region is assigned a heat flux boundary with a moving photon/electron heat source or workpiece defined by

$$-k\left[\frac{\partial T}{\partial x} + \frac{\partial T}{\partial y} + \frac{\partial T}{\partial z}\right] = PA + \epsilon\sigma[T^4 - T_0^4] + h[T - T_0] \tag{2.21}$$

Here, h is the heat transfer coefficient, ϵ is the emissivity, P is the photon heat source power, A is the absorptivity, σ is Stefan-Boltzman constant, and T_0 is the ambient temperature. All other surfaces are assigned convective cooling and surface to ambient radiation boundary conditions given by the following relationship

$$-k\left[\frac{\partial T}{\partial x} + \frac{\partial T}{\partial y} + \frac{\partial T}{\partial z}\right] = \epsilon\sigma[T^4 - T_0^4] + h[T - T_0] \tag{2.22}$$

The heat transfer model can be extended to (1) multi-pass photon/electron heat source processing to account for the reheating effects and (2) multiphase and multicomponent nature of the workpiece by adopting a rule of mixture approach for thermophysical properties. Furthermore, a level-set method can be adopted to predict the evolution of solid-liquid-vapor interface. Temporal tracking of such interface predicts the volume melted and/or vaporized from the photon/electron heat source-workpiece interaction region and in turn assists in estimation of the geometrical dimensions (depth and width) of machined region and machining rate during heat source based machining. As stated earlier, the nature of formulation of computational model depends upon consideration to details and complexity of the process and hence, accordingly it is likely to provide the accurate values of machining attributes such as surface roughness and machining rate. These details can be found in several references in the open literature on computational modeling of heat source based machining [8–36].

The basic description and key aspects of all above fundamental operations of machining are summarized in Table 2.1. The table reveals the primary characteristics

Table 2.1 Characteristics and key parameters of fundamental machining operations

Fundamental machining operation	Basic Description/characteristics	Key process aspects/parameters
Drilling	• A process used to produce a hole • A process also can be extended to enlarge a hole and then called core or counter drilling • Utilizes a drill to accomplish the material removal • A drill is a rotary end cutting tool having one or more cutting lips with single or multiple helical or straight flutes for passage of chips and injection of cutting fluid	• Drill type—a drill with helical grooves or flutes • Geometric parameters of drill—point angle, lip-relief angle, a chisel-edge angle, and a helix angle • Drilling peripheral speed—high and low • Depth of cut/ depth of the hole generated • Feed: The rate that the drill advances into the material • Thrust: The axial force required to drill • Torque: The twisting moment required to drill
Sawing	• A cutting process to remove material by moving a blade in linearly reciprocating or unidirectional linear or circular motion • Sawing blade is a tool with series of small teeth on its periphery • Due to a narrow width of kerf a saw removes small volume of material	• Saw material—low alloy steel, high-carbon steel, stainless steel, and high speed steel • Saw shape—liner and circular • Saw pitch—tooth spacing • Saw tooth size • Saw tooth form—straight, raker, and wave • Saw tooth tip type—welded/fused/inserted diamond and ferrous or non-ferrous carbides • Saw tooth flank • Saw tooth back clearance angle • Saw tooth rake angle • Gullet depth
Grinding/abrasive machining	• A process of material removal via accelerated wear/fracture of the surface • A grinding tool comprises of a multitude of hard and angular hard abrasive grits bonded or not bonded to a substrate	• Grit type—conventional (aluminum oxide and silicon carbide) and super (cubic boron nitride and diamond) abrasives • Physical nature of grit—hardness, toughness, resistance to attrition and fracture, friability

(continued)

Table 2.1 (continued)

Fundamental machining operation	Basic description/characteristics	Key process aspects/parameters
	• The material removal can be small fine or large scale • Typically abrasive/grinding machining is the last operation performed on the component to produce high quality surface finish tolerance	• Geometric nature of grit size and shape • Shape of grinding tool—disk, cylinder, cones and various geometric shapes • Grinding tool motion speed
Milling	• A machining operation to produce various surface geometries such a flat, pockets, angles, contours, steps, and slots • The machining action is generated by rotation of the tool and the feed by motion of the workpiece • The tools employed for milling have multiple teeth cutting edges configured around an axis that produce number of chips per revolution	• Type of milling tool—slab, face, end, straddle, slot/slit, angle, shell milling cutters • Milling tool rotary speed • Milling tool feed per tooth • Milling tool size • Maximum milling force, perpendicular and parallel to the milling direction • Axial Depth of cut • Number of end mill flutes
Thermal machining	• A machining operation involving removal of material by melting or vaporization • A machining tool can be an intense source of photonic beam of ultraviolet, infrared or microwave nature • The operation needs to be conducted in air or vacuum • Temperature required to remove material by melting or vaporization is generated through interaction of the photon source with the atoms or molecules of workpiece • Non-contact processes hence no mechanical stresses are involved	• Source of photon energy—laser, electron beam, microwave • Maneuverability of energy source—ability to focus/defocus, temporal and spatial distribution within and traverse speed of energy source • Power level of energy source • Operation mode of energy source—pulse and continuous

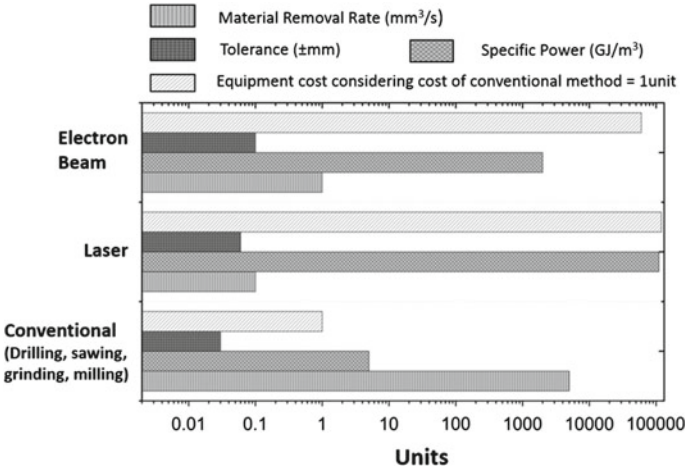

Fig. 2.12 Comparison of machining attributes of various machining operations

and/or parameters of these operations and important parameter that influence the machining performance under these operating modes. Of course, all these operations are complex and dependent on complex nature of interactions among of these primary parameters and additional secondary parameters that are not included in Table 2.1. Furthermore, comparison of attributes of these machining operations/methods are presented on Fig. 2.12. Due to several recent advancements in development of industrial high power lasers, the new lasers are highly efficient in terms of energy delivery through fiber optic as well as integration of them with the complex motion systems. The machining operations with such integrated laser systems are highly efficient and can provide much better characteristics than what is listed in Fig. 2.12. Also costs of these efficient lasers have dropped down substantially and can cost less than $100 K for 1 kW output power.

2.6 Machinability and Surface Quality

During all machining processes, the efficiency in terms of time and cost and desired outcome in terms of dimensions and surface finish of the process depend upon the machinability of a material that is being machined. In general, the machinability of a specific workpiece material can be expressed as the ease with which it can be machined which in turn can be rated in terms of surface finish of machined component, tool life, degree of dimensional control, machining force, and energy control which depends upon speed, depth, and feed [2, 37]. Although attempts have been made to rate machinability based on one or combinations of few above major factors,

due to the complex nature of any machining operation, establishing a quantitative relationship among these influencing factors to define a machinability for a specific material is difficult. This can further be complicated by the development and lack of control of temperature during machining. As a practical approach to this aspect, surface finish and tool life are considered prime factors in machinability.

In general, combination of good surface finish and integrity along with long tool life and requirement of low force and energy during machining are indication of good machinability. In metallic material systems, machinability ratings are based on comparing the machinability to AISI 1112 steel which is rated for its machinability at 100 or 1.0 [2, 37]. As there is no standard machinability rating for comparison available in non-metallic material systems, machinability rating of bones is difficult to find in the open literature. Furthermore, due to the multi-component nature in terms of chemical composition and physical architecture along with variation of these components as function of type (male and female) and age of the bone it is extremely difficult to quantify its machinability.

The surface quality produced during machining operation comprises of surface finish and surface integrity (physical and chemical properties). As stated above, resultant surface quality depends upon multiple factors such as machining force and energy control that in turn depend upon speed, depth, feed, and thermophysical and mechanical properties of the workpiece material [1]. Thus, controlling the machining process for desired surface quality is a complex and can be explored through experimental and computational efforts. The physical and chemical properties that affect the surface integrity are residual stresses, plastic deformation, fracture/cracking, and phase transformation. These physical and chemical properties affect mechanical (wear and fatigue) and corrosion/oxidation performances of machined workpiece. Apart from aesthetic appearance, surface finish directly and indirectly influences the physical and chemical performances of the machined workpiece.

The surface finish pertains to the geometric features of surface. According to the American National Standards Institute (ANSI), surface finish is defined with a set of standard terms such as profile, roughness, waviness, flaws, and lay. Profile is the contour of any section through a surface, roughness is relatively finely spaced surface irregularities, the spacing greater than roughness is waviness, and lay is the direction of the predominant surface pattern. The surface irregularities/imperfections occurring at infrequent interval and random locations are termed as flaws. These features are schematically illustrated in Fig. 2.13 [1]. According to ANSI/ASTM b46.1-1985 standard, surface roughness is quantitatively expressed as the arithmetic average, Ra, of deviation of the profile height (along the axis vertical to surface) increments from the centerline of the surface (Fig. 2.13b) and represented as follows.

$$R_a = \frac{1}{L}\int_{x=0}^{x=L} |y| dx \tag{2.23}$$

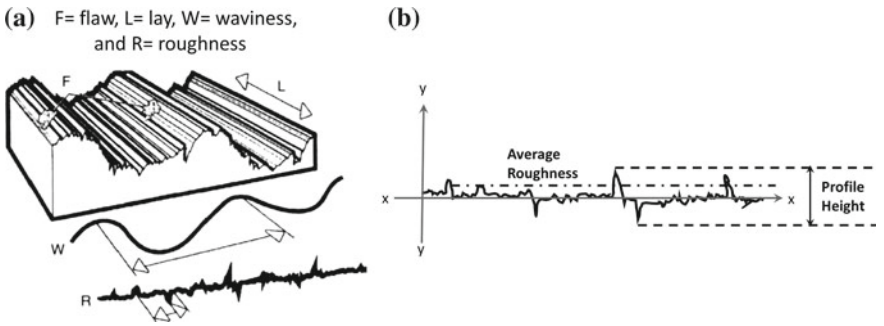

Fig. 2.13 Schematic of features of surface roughness showing, **a** 3D view and **b** 2D cross section (reprinted from Grzesik [5] with permission. © Elsevier)

where L is the sampling length along the surface. This also can be expressed as

$$R_a = \frac{y_a + y_b + y_c + \cdots + y_n}{n} \tag{2.24}$$

where surface profile heights at discrete locations a, b, c, …, n along the surface and number of locations (measurements) along the surface. Sometimes, roughness also can be expressed as the root mean square (rms), R_{rms}, the measurements from the centerline (Fig. 2.13b) given by the following equation.

$$R_{rms} = \left\{ \frac{\Sigma {y_i}^2}{n} \right\}^{\frac{1}{2}} \tag{2.25}$$

The range of surface roughness that can be achieved during these machining operations are presented in Fig. 2.14. Non-traditional applications are either the applications requiring very tight surface tolerances and high surface smoothness or the applications that can tolerate broad surface tolerances and rough surfaces. Also these conditions can be associated with machining of complex geometries and high volume and high production rate.

All above principles of machining of materials are recognized only for homogeneous material systems and do not take into account the material parameters such as multi-component (composite), multi-composition, and multi-phase nature along with the microstructural features such as grain size, grain shape, and grain distribution (uniform to multimodal). Even though these multiple features are likely to strongly influence the principles of machining and machining characteristics, they are often ignored due to the complex nature of the interactions between machine tool and multi-component/composition/phase material system. Hence, in spite of exploration or actual employment in real orthopaedic surgeries of these machining operations, their principles are not fully understood for machining of bones.

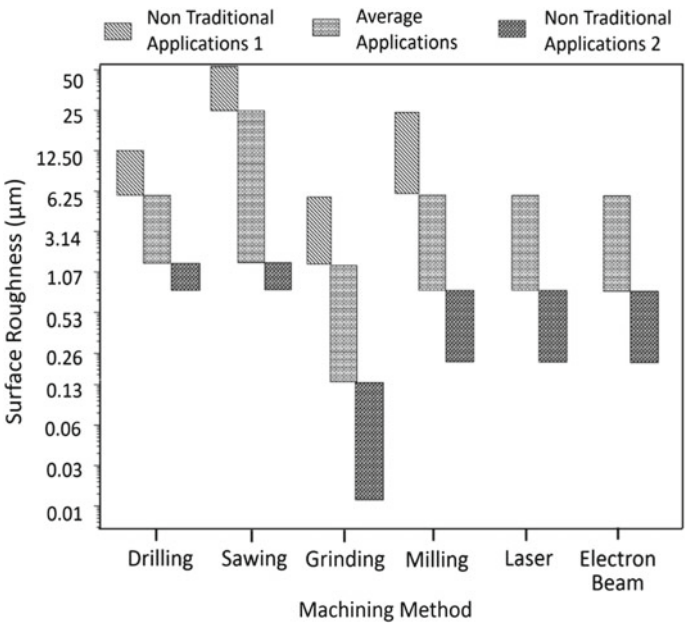

Fig. 2.14 Surface roughness generated during various machining processes

Especially, in case of bone, this is more so due to its multi-component (hydroxyapatite + cartilage + water), multi-composition (ceramic + organic + water), and multi-phase (solid + liquid) nature.

References

1. J.E. Lee, Y. Rabin, O.B. Ozdoganlar, A new thermal model for bone drilling with applications to orthopaedic surgery. Med. Eng. Phys. **33**(10), 1234–1244 (2011)
2. S. Kalpakjian, S.R. Schmid, C.W. Kok, *Manufacturing Processes for Engineering Materials* (Pearson-Prentice Hall, Upper Saddle River, 2008)
3. J. Schey, *Introduction to Manufacturing Processes* (McGraw-Hill Book Co, New York, 1987)
4. V. Marinov, in *Manufacturing Technology* (2006), p. 74
5. W. Grzesik, *Advanced Machining Processes of Metallic Materials: Theory, Modeling and Applications* (Elsevier, Amsterdam, 2008)
6. N.B. Dahotre, A. Samant, *Laser Machining of Advanced Materials* (CRC Press, Boca Raton, Louisiana, 2011)
7. A.N. Samant, N.B. Dahotre, J. Eur. Ceram. Soc. **29**(6), 969 (2009)
8. A. Samant, Laser machining of Structural Ceramics: Computational and Experimental Analysis, PhD Thesis, University of Tenesee, USA (2009)
9. H.H. Vora, Integrated Computational and Experimental Approach to Control physical Texture During Laser Machining of Structural Ceramics, PhD Thesis, University of North Texas, USA (2013)
10. I. Tuersley, A. Jawaid, I. Pashby, J. Mater. Process. Technol. **42**(4), 377 (1994)

11. N.B. Dahotre, S. Harimkar, *Laser Fabrication and Machining of Materials* (Springer Science and Business Media, Berlin, 2008)
12. A. Kuar, B. Doloi, B. Bhattacharyya, Int. J. Mach. Tools Manuf. **46**(12), 1301 (2006)
13. A. Stournaras, K. Salonitis, P. Stavropoulos, G. Chryssolouris, in *Proceedings of the 10th CIRP International Workshop on Modeling of Machining Operations* (2007), pp. 549–553
14. A.N. Samant, N.B. Dahotre, Ceram. Int. **35**(5), 2093 (2009)
15. A.N. Samant, N.B. Dahotre, Int. J. Mach. Tools Manuf. **48**(12), 1345 (2008)
16. S. Lei, Y.C. Shin, F.P. Incropera, J. Manuf. Sci. Eng. **123**(4), 639 (2001)
17. J.C. Rozzi, F.E. Pfefferkorn, F.P. Incropera, Y.C. Shin, Int. J. Heat Mass Transf. **43**(8), 1409 (2000)
18. M.A. Moncayo, S. Santhanakrishnan, H.D. Vora, N.B. Dahotre, Optics Laser Technol. **48**, 570 (2013)
19. J.C. Rozzi, F.P. Incropera, Y.C. Shin, Int. J. Heat Mass Transf. **43**(8), 1425 (2000)
20. H.D. Vora, N.B. Dahotre, Am. Ceram. Soc. Bull. **92**, 4 (2013)
21. J.C. Rozzi, F.E. Pfefferkorn, F.P. Incropera, Y.C. Shin, J. Heat Transfer **120**(4), 899 (1998)
22. J.C. Rozzi, F.E. Pfefferkorn, F.P. Incropera, Y.C. Shin, J. Heat Transfer **120**(4), 907 (1998)
23. H.D. Vora, S. Santhanakrishnan, S.P. Harimkar, S.K. Boetcher, N.B. Dahotre, J. Eur. Ceram. Soc. **32**(16), 4205 (2012)
24. S. Lei, Y.C. Shin, F.P. Incropera, Int. J. Mach. Tools Manuf. **40**(15), 2213 (2000)
25. F. Quintero, F. Varas, J. Pou, F. Lusquiños, M. Boutinguiza, R. Soto, M. Pérez-Amor, J. Phys. D: Appl. Phys. **38**(4), 655 (2005)
26. H. Vora, N. Dahotre, Int. J. Appl. Ceram. Technol. **12**(3), 665 (2015)
27. M. Sussman, P. Smereka, S. Osher, J. Comput. Phys. **114**(1), 146 (1994)
28. H.D. Vora, S. Santhanakrishnan, S.P. Harimkar, S.K. Boetcher, N.B. Dahotre, Int. J. Adv. Manuf. Technol. **68**(1–4), 69 (2013)
29. N. Pierron, P. Sallamand, S. Matteï, in *Proceedings of the Comsol Multiphysics Conference* (2005)
30. H.D. Vora, N.B. Dahotre, J. Manuf. Process. **19**, 49 (2015). http://dx.doi.org/10.1016/j.jmapro.2015.04.002. http://www.sciencedirect.com/science/article/pii/S1526612515000304
31. S. Sun, M. Brandt, M. Dargusch, Int. J. Mach. Tools Manuf. **50**(8), 663 (2010)
32. H.D. Vora, N.B. Dahotre, Lasers Manuf. Mater. Process. **2**(1), 1 (2015)
33. M. Van Elsen, M. Baelmans, P. Mercelis, J.P. Kruth, Int. J. Heat Mass Transf. **50**(23), 4872 (2007)
34. A.N. Samant, N.B. Dahotre, Int. J. Appl. Ceram. Technol. **8**(1), 127 (2011)
35. S. Harimkar, A. Samant, A. Khangar, N.B. Dahotre, J. Phys. D: Appl. Phys. **39**(8), 1642 (2006)
36. Y. Yan, L. Li, K. Sezer, D. Whitehead, L. Ji, Y. Bao, Y. Jiang, Int. J. Mach. Tools Manuf. **51**(12), 859 (2011)
37. J. Beddoes, M. Bibby, *Principles of Metal Manufacturing Processes* (Butterworth-Heinemann, Burlington, Massachusetts, 1999)

Chapter 3
Non-conventional and Hybrid Methods of Bone Machining

Having explored the basics of important fundamental contact (mechanical) and non-contact (thermal) operations involved in machining of the bones, the discussion will proceed towards some of the non-conventional techniques. These techniques have evolved as a result of research works on interaction of bones with various energy sources such as photon/electron beam and mechanical vibrations. Hybrids of fundamentals operations of machining have also been taken into account. Laser, microwave, and ion-beam based methods have been discussed under beam based techniques. Ultrasonic machining which has been extensively explored for bone application has been dealt in a separate section. Pneumatic and hydraulic machining have been taken into account under the section on hybrid machining. These non-conventional/hybrid techniques are not as popular as conventional ones but hold a huge potential for the future.

3.1 High Energy Beam Based Techniques

The high energy beam based methods employ some sort of radiation as the means of energy source for removal of the bone material. These techniques have mostly been employed previously in case of the structural materials. Unlike conventional mechanical contact methods employing physical tools which result in generation of heat as the secondary effect, beam based techniques employ heat as the primary means of tooling. The heat is generated by means of various electromagnetic waves within the electromagnetic spectrum such as ultraviolet, microwave, and infrared with various combinations for ranges of energy and wavelength (Fig. 3.1). As the combinations dictate the extent and mode of interaction of the energy source with the workpiece, any machining operation can be carried out with careful process control. Most common methods explored in this category include laser, ion-beam, and microwave machining which are discussed in detail in the following subsections.

N.B. Dahotre and S.S. Joshi, *Machining of Bone and Hard Tissues*,
DOI 10.1007/978-3-319-39158-8_3

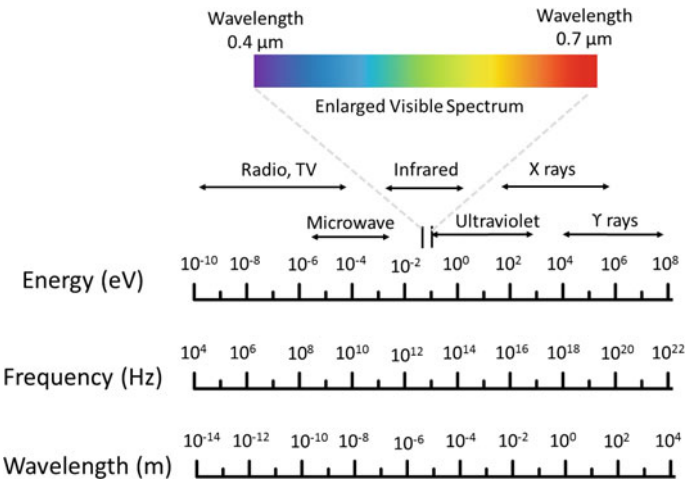

Fig. 3.1 Electromagnetic spectrum showing various regions with corresponding energy, wavelength, and frequency, and a magnified view of the visible spectrum

3.1.1 Laser Machining

Lasers (Light Amplification by Stimulated Emission of Radiation) have been used as a means of machining for quite some time now. Theoretically any wavelength within the electromagnetic spectrum can be made into a laser source. Principally, a lasing medium is excited using a energy source such as inert gas flash lamp. The input of energy (Fig. 3.2a) transfers the electrons within the atoms of the medium to higher energy state, technically termed as population inversion. On the other hand, the random absorption of energy gives rise to spontaneous emission (Fig. 3.2b). In case of population inversion, these electrons jump to lower energy state at the same time emitting photons of the same energy corresponding to difference between ground and excited state (Fig. 3.2c). A set of two mirrors, some times called resonators, one totally and the other partially reflecting, generates the chain reaction giving rise to highly concentrated beam coming out of the partially reflecting mirror (Fig. 3.3). This beam is monochromatic, coherent, and highly collimated in nature and can be employed for various applications depending on the wavelength. Operations of lasers have been described in great detail in the literature [1–3]. There are various types of lasers depending on the medium such as ytterbium aluminum garnet (YAG), inert gas, CO_2 gas. The most common types of lasers are pulsed and continuous. Important characteristics include input power, wavelength, beam diameter, scanning speed, and pulse duration. The interaction of matter with laser consists of absorption, reflection, and transmission as schematically shown in Fig. 3.4 [4] and dissipation of incoming energy, E, during the interaction is expressed mathematically in Eq. 3.1.

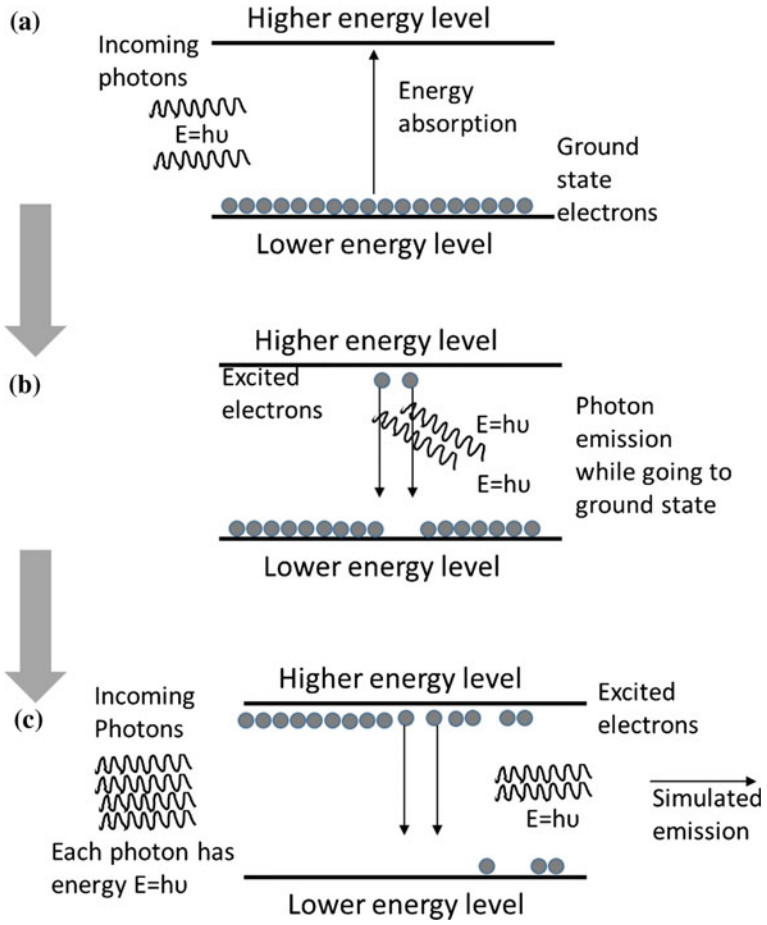

Fig. 3.2 Schematic energy diagram showing, **a** incoming photon of energy, and **b** spontaneous emission, and **c** simulated emission

$$E = rE + aE + tE \tag{3.1}$$

where r, a and t are coefficients of reflection, absorption, and transmission.

Laser are employed for variety of applications such as bar code scanners [5], sensing [6, 7], heat treatment [8–10], surface engineering [11, 12], and machining of various materials [2]. In the medical field, they have been used for various surgeries in the fields including dentistry, opthalmology, and orthopedics. However, only the lasers explored in case of bone machining will be discussed here. They include Ti-sapphire, CO_2, excimer, and YAG. In addition, it is worth mentioning here that, even though main focus of this book is hard tissues associated with the structural bones,

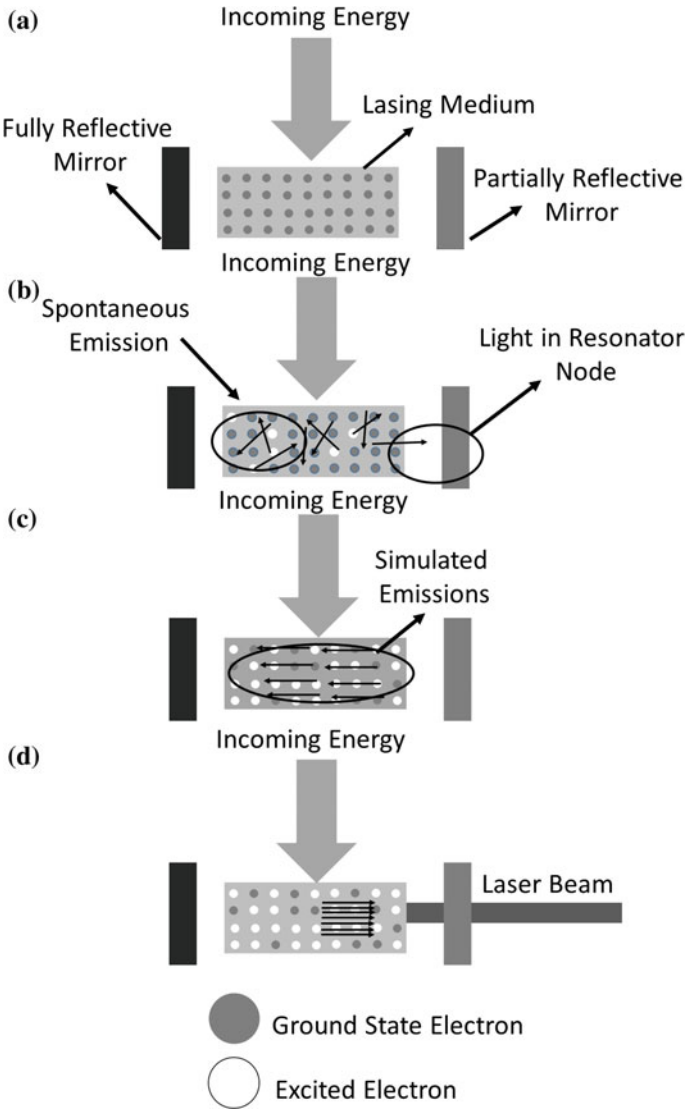

Fig. 3.3 Schematic of various steps in generation of laser beam

a majority of work conducted so far has been associated with machining of teeth. Hence a brief overview about laser machining of teeth will be presented prior to discussion about the main subject matter of machining of hard tissues of structural bones.

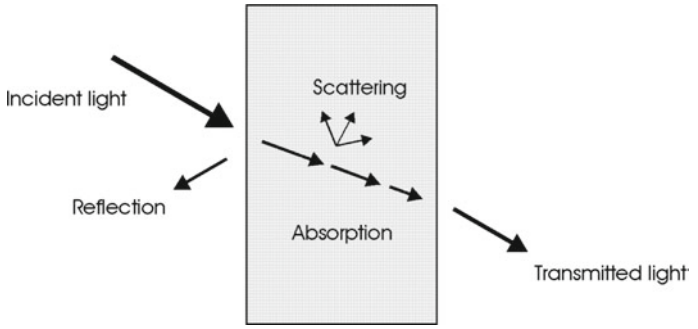

Fig. 3.4 Schematic of interaction of light with the matter showing the phenomena of absorption, reflection, and transmission (reprinted from Niemz [4] with permission. © Springer Science & Business Media)

3.1.1.1 Lasers in Dentistry

Lasers have been extensively researched for dental applications [13–19] with initial efforts dating back around 50 years [20]. The nature of interaction of tooth with various laser wavelengths is dictated by its overall structure (Fig. 3.5a [13]) and composition (Fig. 3.5b [13]). The arrangement starts with majority of hard mineral in the enamel. Within the sub surface layers, the percentage of hard mineral reduces, where as percentage of the water and the organic matter increases from dentin towards soft tissues. Such a complex assembly with continuous variation in the composition gives rise to different thermal absorbance and transfer characteristics within each layer and the behavior of laser interaction thus changes within each layer. This

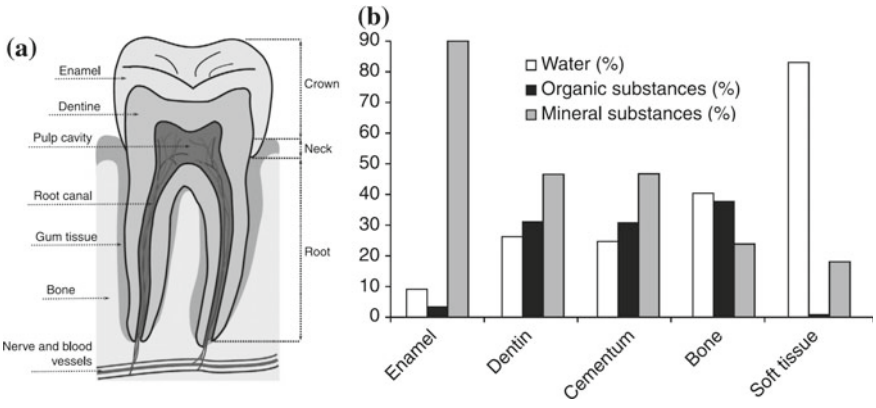

Fig. 3.5 Structure and composition of a tooth. **a** Schematic of structure of tooth and **b** compositional details of important constituents of the tooth (reprinted from Jelínková [13] with permission. © Elsevier)

leads to thermo-physical effects such as vapor build up and plasma formation. These phenomena in combination with instrumentation determine the ablation behavior of dental tissues.

The laser wavelengths considered for dental application range from ultraviolet to infrared. The interaction depends on three factors enlisted below.

- Absorbance of laser wavelength by bone constituents
- Time of radiance
- Direct chemical bond breaking

In the first case, the properties of bone material govern the ablation process. Infrared, Er:YAG, Nd:YAG, and CO_2 lasers are commonly tried for dental application. They thermally affect the enamel and dentin which have hydroxyapatite and water as the main constituents. CO_2 and Er:YAG lasers, on the account of high absorption in water and hydroxyapatite are absorbed near the tooth surface [13, 18]. This makes energy concentrated to smaller tissue volume making ablation possible. On the contrary, Nd:YAG laser due to its poor absorption in water and hydroxyapatite, penetrates deeply into the tissue thereby distributing a large quantity of energy.

In the second case, the control over instrumentation determines ablation process. Continuous wave CO_2 and Nd:YAG lasers when irradiate the tooth tissue for long time, evaporation and intense heating of the surrounding hard material occur. Reducing the exposure time by using a Q-switch Nd:YAG laser, thermal damage can be diminished but not prevented because of the poor tissue absorption [13]. On the contrary, short duration pulses of the order of 200 ps from Er:YAG laser along with it's better absorption coefficient with the tooth material results in thermo mechanical ablation. In case of a Guassian type of the beam, the central region of the beam cross section with highest energy gives rise to evaporation of the dental hard substances. On the other hand, the edge region of the beam does not provide heat enough for evaporation of hard tissues. But the energy is sufficient to abruptly heat up the water in dentin and enamel that eventually builds the pressure up driving the steam out resulting in thermo mechanical ablation. In addition, the lesser damage to adjoining region renders Er:YAG laser attractive for dental applications [13, 18].

The above described mechanisms are mainly driven by material absorbance and instrumentation. In case of excimer lasers however, laser pulses with high peak energy and extremely short duration of the order of few nano seconds are possible. The UV photons within these pulses are highly energetic to directly break the bond within organic material of the bone. A large number of photons are delivered very quickly in this process. This complex process is characterized by photo dissociation, plasma formation, and thermal effects. This combined effect causes ablation with minimal or no thermal damages.

All these mechanisms have been illustrated in Fig. 3.6 [18] which shows effects of various lasers on dentin. The best results were achieved by Er:YAG laser with 200 mJ input power with 10 pulses (Fig. 3.6a [18]). The surface was very smooth and uniform ablation occurred. On the other hand, ArF laser (an excimer laser) with input energy of 26 mJ required 300 pulses to achieve similar results (Fig. 3.6b [18]). A continuous wave CO_2 laser with 20 W power and residence time of 0.05 s, on

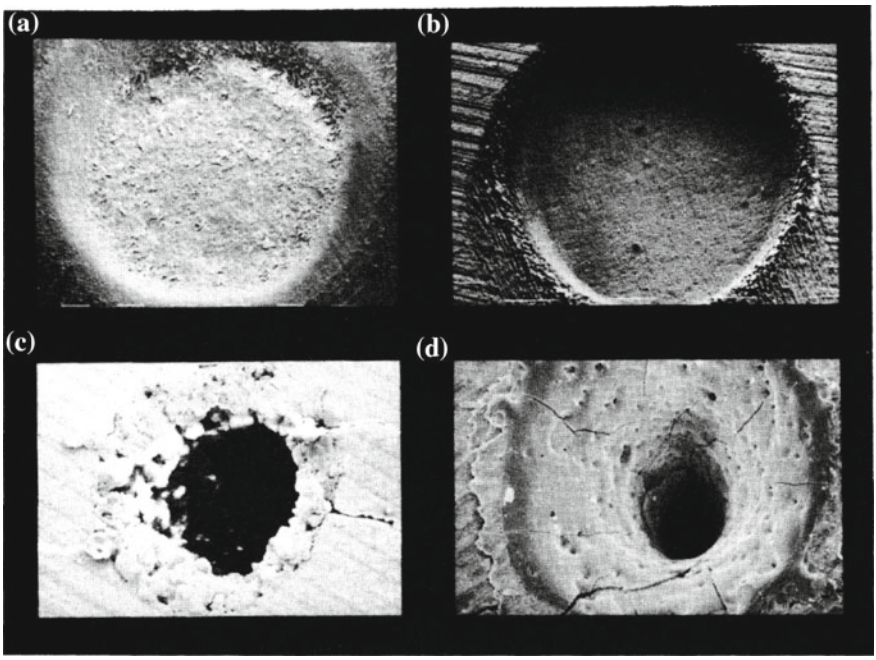

Fig. 3.6 Effects of various lasers on the dentin **a** Er:YAG laser, 200 mJ, 10 pulses (image at 80× magnification), **b** ArF laser, 26 mJ, 300 pulses, 3 Hz (image at 160× magnification), **c** continuous wave CO_2 laser, 20 W, 0.05 s (image at 160× magnification), and **d** Nd:YAG laser, 145 mJ, 100 pulses (image at 160× magnification) (reprinted from Keller [18] with permission. © SPIE)

the account of low absorbance resulted in deeper thermal damage (Fig. 3.6c [18]). Similar damage was observed in case of a pulsed Nd YAG laser (Fig. 3.6d [18]).

3.1.1.2 Lasers in Orthopedic Machining

Lasers have been considered for machining of structural bones. In contrast to conventional mechanical contact based methods, lasers use heat as the primary means of machining. The advantages associated with this technique are listed below [4, 21].

- No physical contact
- Shorter operation time
- Absence of traumatic vibration, bone dust or metal abrasion in incision
- Electronic control of the beam and amenability to automation leads to increased precision and easy operation.
- Stimulation of the granulation tissue initiating the healing process.
- Possibility of aseptic (free from contamination from bacteria, viruses and other microbes) and haemostatic (retarding bleeding) effects
- Cauterisation effect

Considering these advantages, lasers have been investigated/explored for machining of the structural bones. The bone material removal by laser is challenging due to diverse thermo physical properties of the bone constituents. The mineral (hydraxyapatite) has a high melting point (about 1000 °C) whereas organic matrix consisting of collagen starts to carbonize after evaporation of water (~100 °C). As a matter of fact, water plays a critical role in determining the ablation mechanism depending on the wavelength of the laser used (Fig. 3.7 [22, 23]). Some of the wavelengths are strongly absorbed by the water making it to quickly boil, while others are transmitted through it creating a possibility of damaging the tissues underneath. Copper vapor laser (wavelength = 511 nm) and Nd:YAG laser operating at 532 nm are easily transmitted through water. On the other hand, Er:YAG laser (wavelength = 2.940 μm) and Nd:YAG laser operated at 2900 nm wavelength are strongly absorbed by water. Other lasers absorbed by water are CO_2 lasers (wavelength = 10.6 μm), Yb-fiber laser (wavelength = 1.07 μm), and Nd:YAG laser operated at wavelength of 1.06 μm.

The interaction also depends on laser beam power density and its time of radiance. In addition, thermal transmittance plays a key role in determining how much depth the laser energy penetrates as illustrated in Fig. 3.8 [24] which also indicates more suitability of Er:YAG laser for the purpose of bone machining.

Ablation mechanism is critically influenced by the time of interaction and power density as schematically illustrated in Fig. 3.9 [13]. The dashed lines are constant laser fluence lines with lower line corresponds to 1 J/cm^2 whereas the upper line corresponds to 1000 J/cm^2. For exposures greater than 1 s, the laser is usually operated in a continuous wave mode giving rise to photochemical interactions. The time range of 1 min to 1 μs gives rise to thermal interactions. Often for the shorter interaction times, the laser operates in a pulse mode. The exposure time in the range of 1 μs to 1 ns results in photoablation. Extremely short exposure durations of the order <1 ns give rise to plasma-induced ablation and photodisruption. These mechanisms are briefly explained in the following discussion.

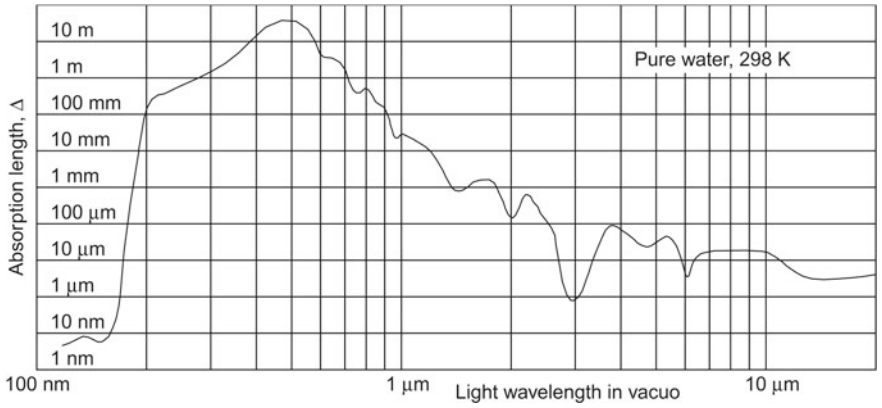

Fig. 3.7 Absorption characteristics of water at room temperature (reprinted from Kruusing [22] with permission. © Elsevier)

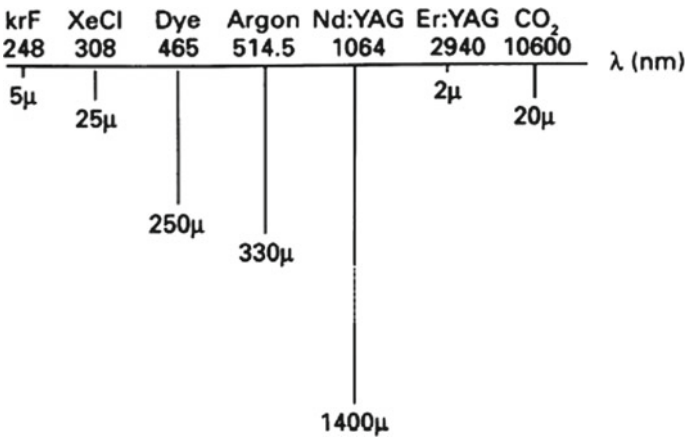

Fig. 3.8 Illustration showing penetration depth of various lasers into the bone (reprinted from Gudra and Muc [24] with permission. © Springer)

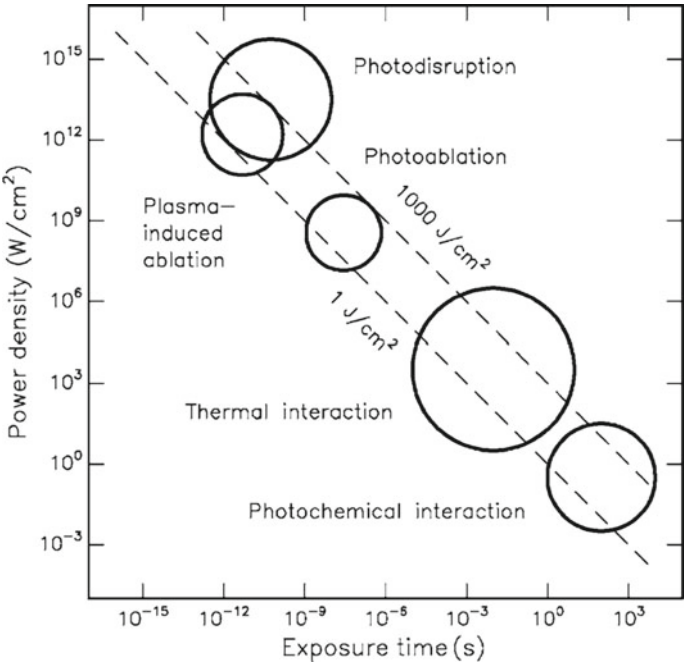

Fig. 3.9 Plot of laser-tissue interaction showing various mechanisms of interaction depending on power density and time of irradiance (reprinted from Jelínková [13] with permission. © Elsevier)

3.1.1.3 Photochemical Interaction:

The incoming light can induce chemical effects and reactions within macromolecules or tissues resulting in photochemical interactions. A very good example of such phenomenon is photosynthesis occurring in plants. Laser induced photochemical interactions occur at very low power densities (of the order of 1 W/cm^2) and long exposure times ranging exceeding seconds to continuous wave operation. These effects may not be very relevant from the machining point of view.

3.1.1.4 Thermal Interactions

During laser irradiation of bones and hard tissues, temperature rise as a result of heat input leads to occurrence of various thermal interactions. These interactions are very significant from the machining point of view and can take place in continuous as well as pulsed laser operation. Depending on the temperature and duration of exposure, the effects resulting of the thermal interactions include coagulation, carbonization, melting, and vaporization. As these thermal effects may lead to significant material damage, the processing in this regime requires a careful process control. Coagulation (clotting of the blood cells) occurs at temperatures of 60 °C where as carbonization commences at 100 °C. With further increase in temperature, occurrence of melting is followed by vaporization leading to thermo-mechanical ablation as discussed in the dentistry section. These thermal effects are tabulated in Table 3.1 [13] and the regions affected are schematically shown in Fig. 3.10 [13]. Thermal effects are usually observed in case of continuous and long duration pulsed type of CO_2, Nd:YAG, Er:YAG, Ho:YAG, argon ion, and diode lasers.

Thermal ablation effects have been heavily explored in laser machining of the bones. In one such study, comparison was done between the material removal characteristics of parietal bone of a rat during drilling operation with a burr and Er:YAG laser (wavelength of 2.94 mm, an output range of 30–350 mJ/pulse, a maximum pulse repetition rate of 10 Hz, and pulse duration of 200 μs), and a CO_2 laser (wavelength of 10.6 mm and output range of 0.5–5 W) [25, 26]. Energy output of 100 mJ/pulse was found to be clinically appropriate. Laser power employed was 1 W and bur drill was angled at 30°. Er:YAG laser resulted in grove formation, and two distinct

Table 3.1 Thermal effects of laser (reprinted from Jelínková [13] with permission. © Elsevier)

Temperature (°C)	Effect on tissue
37	No effect
45	Hyperthermia
50	Reduced enzyme activity
60	Denaturation of proteins and collagen, coagulation
80	Permeabilization of membranes
>100	Carbonization
>300	Melting

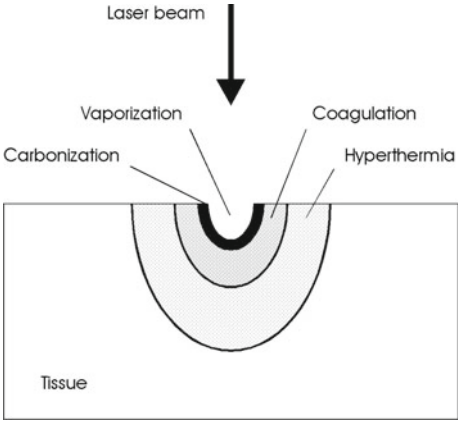

Fig. 3.10 Schematic of thermal effects of laser beam in the laser treated region and its vicinity (reprinted from Jelínková [13] with permission. © Elsevier)

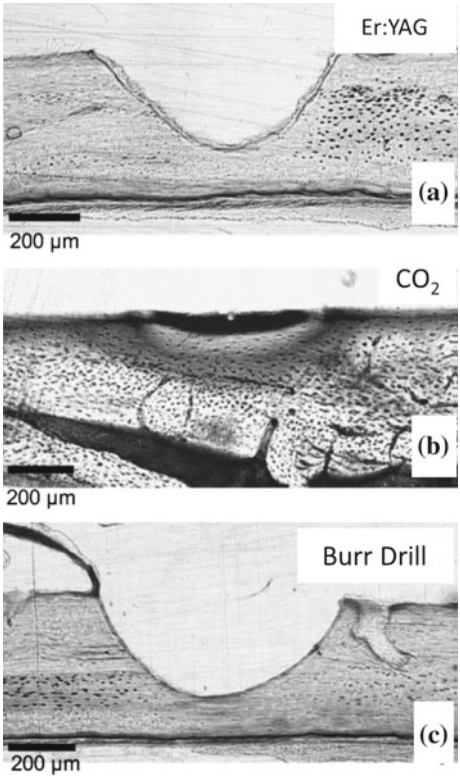

Fig. 3.11 Bone material removal from a rat parietal bone using, **a** Er:YAG, **b** CO_2 laser, and **c** burr drilling (reprinted from Sasaki et al. [25] with permission. © John Wiley and Sons)

layers were observed on the machined surface (Fig. 3.11a [25]). The drilled boundaries were precise and the average affected depth was 22 µm. CO_2 laser did not result in grove formation and damaged region was much larger (darker areas in Fig. 3.11b [25]). The laser affected region was divided in three zones: a completely carbonized

layer on the irradiated surface, a mildly carbonized intermediate layer, and a darkly stained layer at deeper sites of irradiation. Bur drill as expected, resulted in grove formation with presence of smear like region (Fig. 3.11c [25]).

TEM analyses indicated in case of Er:YAG laser irradiated bone that well oriented crystals were present in the unaffected region (Fig. 3.12a [25]) whereas less affected region revealed partly disorganized crystals (Fig. 3.12b [25]). Surface had totally random orientation (Fig. 3.12c [25]). All the regions had crystalline diffraction pattern. In case of CO_2 laser, partially carbonized region indicated round and large crystals (Fig. 3.13a [25]). Fully carbonized layer displayed complete fusion of the original apatites (Fig. 3.13b [25]). Bur drilling had an unaffected region similar to in case of Er:YAG laser, but smeared layer had a mixture of amorphous phase and needle like crystals (Fig. 3.14a, b [25]). This suggested that Er:YAG and bur drilling induced minimum damage in the regions underneath. EDS analysis suggested changes in Ca/P ratio in case of the Er:YAG laser and reason was thought to be formation of meta stable phases.

Even though bur and Er:YAG generated least damage in the bone, the post operation recovery was better in case of Er:YAG making it most beneficial method. The mechanism of ablation proposed took into account the composite nature of the bone.

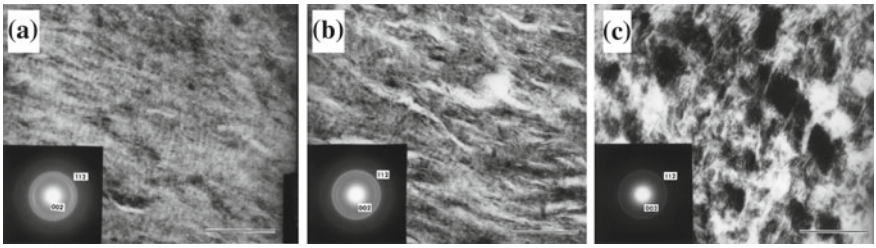

Fig. 3.12 Transmission electron micrographs and diffraction patterns (*inset*) of bone treated with Er:YAG laser showing, **a** base region, **b** laser affected sub surface region, and **c** surface region (reprinted from Sasaki et al. [25] with permission. © John Wiley and Sons)

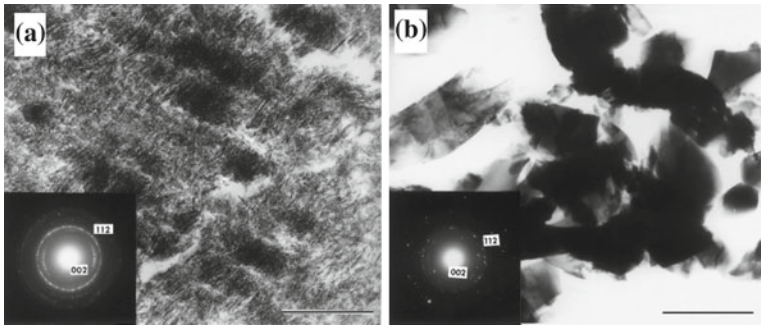

Fig. 3.13 Transmission electron micrographs and diffraction pattern (*inset*) of bone treated with CO_2 laser showing, **a** less affected region and **b** totally carbonized region (reprinted from Sasaki et al. [25] with permission. © John Wiley and Sons)

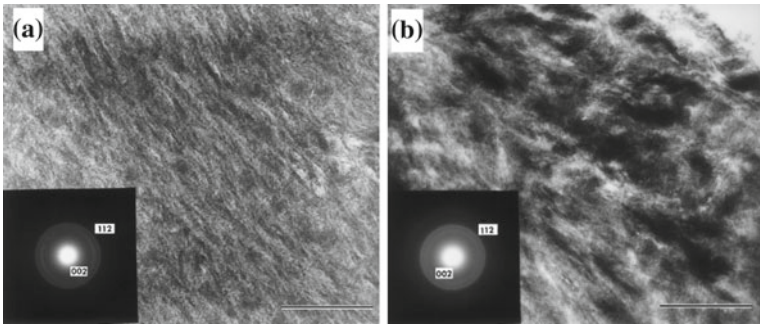

Fig. 3.14 Transmission electron micrographs and diffraction pattern (*inset*) of bone bur drilled showing, **a** base and **b** surface region (reprinted from Sasaki et al. [25] with permission. © John Wiley and Sons)

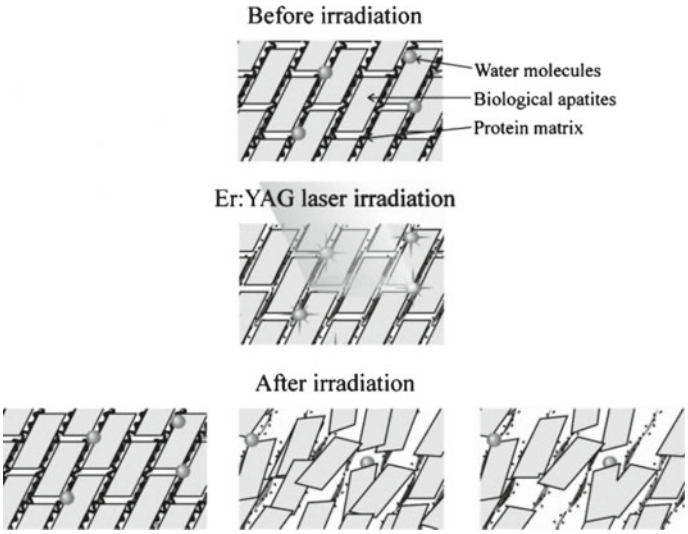

Fig. 3.15 Mechanism of ablation of bone by Er:YAG laser (reprinted from Sasaki et al. [25] with permission. © John Wiley and Sons)

The differential thermal properties of bone constituents lead to thermo-mechanical effects. The steps in ablation mechanism are schematically shown in Fig. 3.15 and enlisted below.

- The absorption of laser energy by the bone results in rise in temperature. Water content within the bone starts to boil building a vapor pressure.
- The built up pressure leads to a micro explosion. The micro-explosions eventually produce mechanical tissue ablation.
- A two layered structural zones are generated where in subsurface layer which accumulated energy undergoes micro explosions whereas surface with direct exposure to the intense laser energy instantly undergoes micro cracking.

Surface profile generated by Er:YAG laser was investigated by scanning white-light interferometry to capture a detailed three-dimensional image (Fig. 3.16 [27]). Laser cutting was carried out by hand held laser head and a fixed cutting rig. The surface profile data indicated that the lased surface was rougher than that of the original bone. Although many researchers explored beneficial nature of the rough surface [12, 28], this group of researchers pointed towards careful choice of processing parameters.

Another study compared ablation characteristics of Er:YAG, continuous wave CO_2, and a pulsed CO_2 laser (Fig. 3.17 [29]). Er:YAG again was proved to be the best laser by providing least damage to the exterior of the bone as well as the cartilage and machining was achieved at much faster rates at lower energy densities (Fig. 3.17 [29]). This was attributed to 10 times higher absorption coefficient of bone at 2.94 μm wavelength of Er:YAG laser than that of CO_2 laser of 10.6 μm. In addition, pulsed lasers were found to be helpful because they allowed a cool down time.

Considering superior capability of Er:YAG laser, the technique was compared with various other hybrid as well as conventional techniques [30, 31]. Comparing

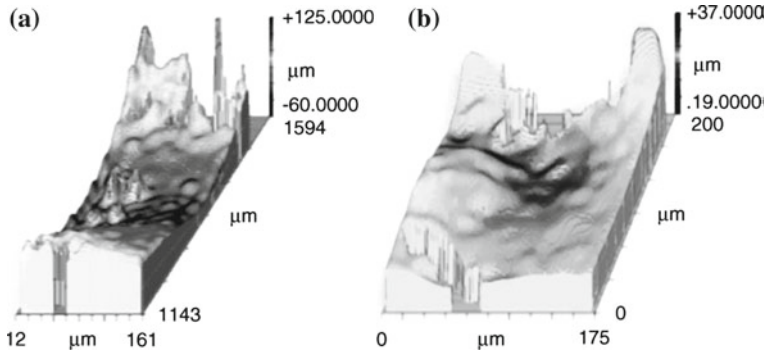

Fig. 3.16 Surface profiles on bone generated using Er:YAG laser. **a** Hand held head and **b** Fixed (reprinted from Wallace et al. [27] with permission. © Elsevier)

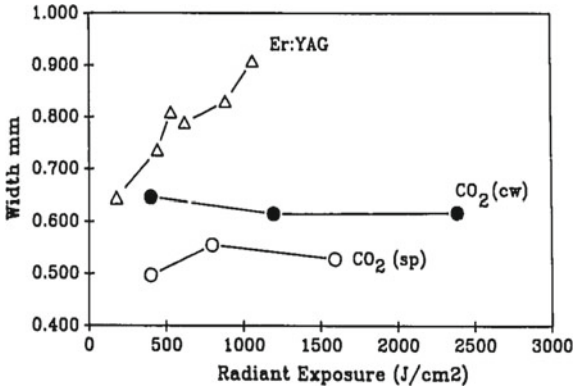

Fig. 3.17 Comparison between widths of machined holes in a bone by Er:YAG and CO_2 (pulsed and continuous) laser (reprinted from Gonzalez [29] with permission. © John Wiley and Sons)

with pizoelectric cutter, more bleeding was observed in case of Er:YAG laser cut in a minipig bone (Fig. 3.18 [31]). The bleeding in fact was a sign of anatomically open and biologically active surface, which was thought to promote the healing process. Such a biological response was a result of formation of smear layer in case of pizoelectric cutter which did not form during Er:YAG laser cutting and hence did not block the blood flow. The smear layer was very similar to the one observed in dental tissues that underwent mechanical cutting, however, the exact mechanism of the layer formation was not clear (Fig. 3.19 [31]). The Er:YAG technique was also compared with high and low speed diamond coated tools as well as pizo tools in a cutting operation of pig cadaver bone [30]. Sharpness and depth of the cuts achieved by Er:YAG laser were much higher than the other techniques. Carbonization was completely absent and minimum bone fragments formed during Er:YAG laser cutting. At the same time the importance of careful choice of parameters based on the laser system and laser-tissue interaction was emphasized.

To overcome the adverse effects of CO_2 laser, an effort was made to design a suitable processing setup [32]. A computer control was introduced and pilot laser beams were utilized for careful positioning of the bone. Pressurized airflow protected the laser beam head by driving away the ablation products. The incision area was cooled down by two fine spray nozzles spraying isotonic NaCl solution. The laser pulse duration was reduced to less than 80 μs and multi pass machining was performed

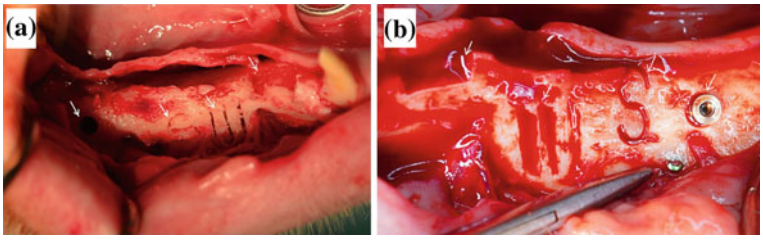

Fig. 3.18 Cut surface of mandibular ridge of Gottingen minipigs done by **a** piezoelectric tool and **b** Er:YAG laser (reprinted from Baek et al. [31] with permission. © John Wiley and Sons)

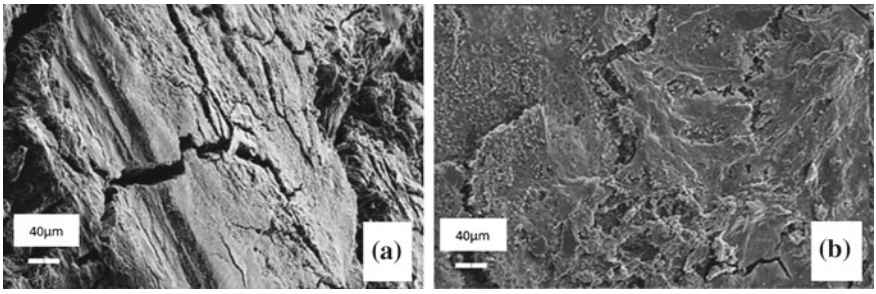

Fig. 3.19 SEM micrographs showing, **a** smear layer on bone surface cut by pizoelectric cutter and **b** Er:YAG laser cut surface without a smear layer (reprinted from Baek et al. [31] with permission. © John Wiley and Sons)

with high beam velocity of 480 mm/s. This shifted the laser effect to half of the diameter of bone tissue protecting it from thermal damage and carbonization. This effort established a possibility of bone machining by CO_2 laser while the same time emphasizing the need for automated control. Another study explored the possibility of usage of various liquids instead of water or saline [32]. The method consisted of soaking bones in the liquid prior to ablation. It was concluded that longer times of soakings were required to double the ablation rate. The novelty of this study was the application of confocal microscopy for 3D reconstruction of the ablated craters for geometry analysis (Fig. 3.20 [32]).

Taking this idea forward, quantification of ablation by CO_2 laser by water-air spray method was carried out [33, 34]. The idea was based on the time required to input the laser energy, that is the pulse duration (τ_L) and time required for dissipation of this heat, termed as thermal relaxation time (τ_T). τ_T was a function of thermal conductivity, κ, and absorbance μ_a expressed in Eq. 3.2 [35]. The equation indicates an inverse relationship between τ_T and μ_a. The value of τ_T was reported as 20–30 μs in the case of cortical tissue irradiation at 9.6 μm wavelength of the CO_2 laser. On the contrary, it was suggested that relaxation times were expected to be much smaller for Er:YAG laser compared to CO_2 laser [36]. A quantity termed as effective number of pulses, N_{eq}, was defined according to Eq. 3.3.

$$\tau_T = (4\kappa\mu_a^2)^{-1} \tag{3.2}$$

$$N_{eq} = total\ pulse\ number * \frac{spot\ radius}{cut\ length} \tag{3.3}$$

The cut profiles indicated narrowing of the cuts with increased value of N_{eq} and depth, D, naturally increased (Fig. 3.21 [33]). It was concluded that, in initial stages the ablation was uniform regardless of number of pulses. There was a reduction in ablation rate as cut depth increased. Ratio of diameter (d) to effective width

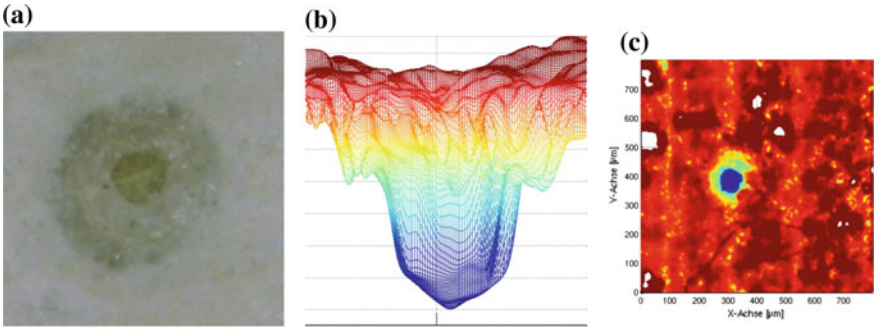

Fig. 3.20 Confocal microscopy views of laser ablated crater showing, **a** top view, **b** 3D confocal reconstruction in cross section, and **c** top view of the reconstruction (reprinted from Mehrwald et al. [32] with permission. © SPIE)

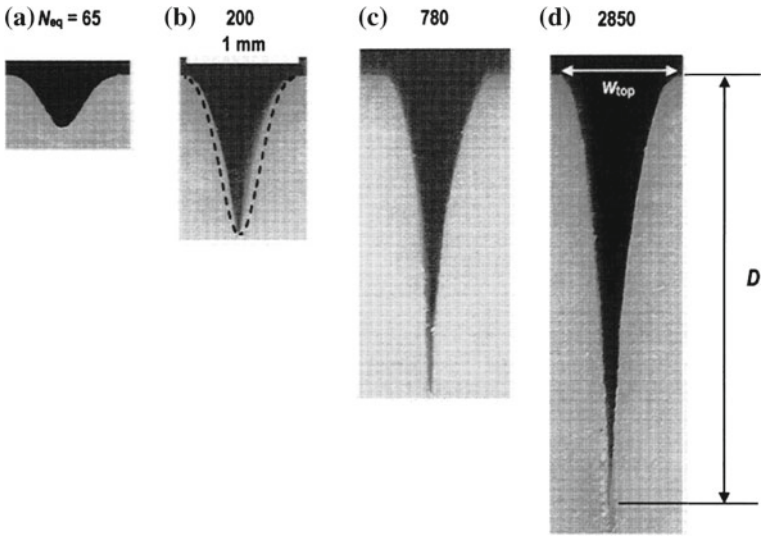

Fig. 3.21 Depth profiles of machined cortical bone tissue of young bull as a function of effective number of pulses (reprinted from Ivanenko et al. [33] with permission. © SPIE)

(W_{eff}) was used as a geometric parameter to define a modified relaxation time, τ_T', expressed according to Eq. 3.4. It was clear that as depth increased the heat dissipation time reduced (75 ns for the depth of 4.5 mm). The threshold value for fluence to begin ablation (Φ_{th}) along with the fluence used for the experiment (Φ) to predict the maximum possible depth D_{max} at that processing condition are expressed in Eqs. 3.5 and 3.6 respectively. Φ_{th} was found to be directly related to E_{abl} (J/mm^3). The minimal specific necessary to start the ablation process. The value of E_{abl} was calculated as 1.2 J/mm^3 based on thermo-physical properties of the bone. It was suggested that with increase in cut depth the products are concentrated in a narrower space without the possibility of escaping to the sides unlike in a shallow cut. Thus it was also observed that with increase in the effective width of the cut, the ablation energy reduced and cutting depth increased. In another study based on a similar quantification approach by the same group, the W_{eff} was predicted based on beam radius, r, as per the Eq. 3.7 and plotted in Fig. 3.22 [36].

$$\tau_T{}' = \frac{\tau_T}{1 + \left(\frac{D}{w_{eff}}\right)^2} \tag{3.4}$$

where

$$\Phi_{th} = E_{abl} d_a = \frac{E_{abl}}{\mu_a} \tag{3.5}$$

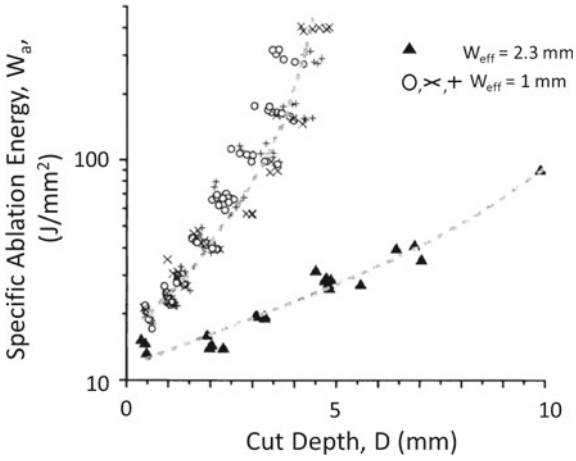

Fig. 3.22 Effect of width of cut on ablation energy and depth of cut achieved (reprinted from Ivanenko et al. [33] with permission. © SPIE)

$$D_{max} = w_{eff}\sqrt{\frac{\Phi\ \tau_T}{\Phi_{th}\ \tau_L}} \tag{3.6}$$

$$W_{eff} = r\sqrt{ln\left(\frac{\frac{\Phi}{\Phi_{th}}}{2}\right)} \tag{3.7}$$

In addition, the effect of water and air spray with optimized laser processing conditions revealed no thermal damage and cut surface was very uniform (Fig. 3.23a [34]). On the contrary, cutting with conventional diamond saw had significant damage with non uniform cut surface (Fig. 3.23b [34]). Important facts derived from these studies are listed below. They are based on quantification, experimental observations, and previously published literature. In general, these facts are applicable to laser ablation irrespective of the type of laser used.

1. The higher the ablation efficiency, the smaller thermal side-effects will be induced in the tissue.
2. The thermomechanical tissue ablation is a threshold process. It starts, if the accumulated energy is large enough to evaporate the tissue liquid and to build high internal pressure.
3. A reasonably strong tissue absorption at the laser wavelength, high radiant exposure, and high peak irradiance in the focus are essential preconditions of an effective ablation.

Instrumentation modification in case of Er:YAG laser was also explored [37]. Optical simulations were performed in order to determine the best focusing conditions. Thus the improved Er:YAG laser was able to fine tune for optimum ablation rate and surface quality. The test setup used was very similar to the study discussed in [29] (Fig. 3.24). The effect of water content on ablation performance of Er:YAG

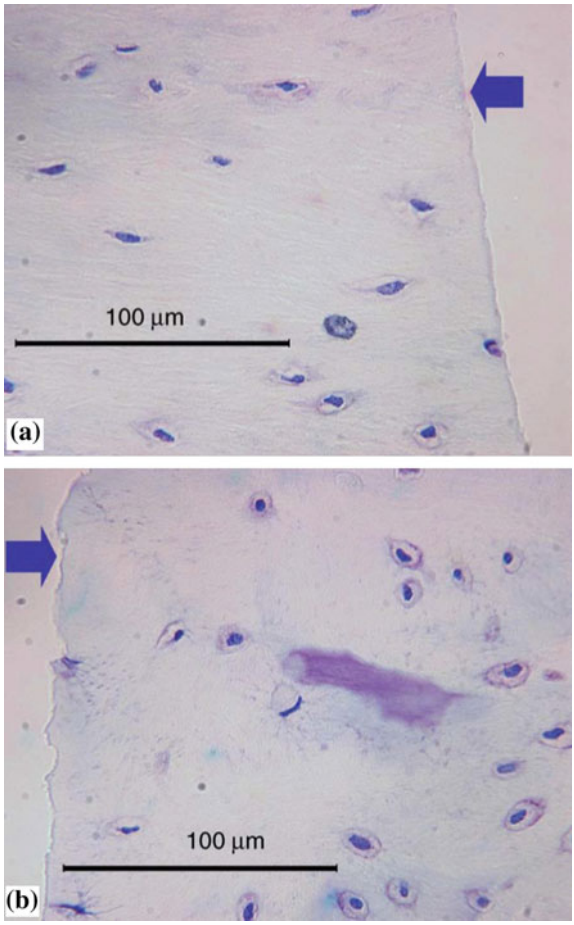

Fig. 3.23 Comparison between a pig rib bone cut by **a** CO_2 laser and **b** diamond saw. The cut surface indicated by an *arrow* (reprinted from Ivanenko et al. [34] with permission. © Elsevier)

laser was investigated [38]. Relative transmittance was measured in the fresh bone and also in completely air dried and oven dried bones. A real time mass loss was monitored during laser ablation using computer assisted balance. Even though there was a huge difference between relative transmittance, being higher for oven dried bone, the ablation rates were only slightly lower (Fig. 3.25). This was attributed to poor contact between dried bone and test crystal highlighting difficulties in measurement and need for careful instrumentation in case of bone property measurement. Similar observations have been made in case of a CO_2 laser wherein more ablation energy was necessary for a dry bone [36].

Apart from Er:YAG and CO_2 lasers, other types of lasers causing thermal effects also have been tried for the bone ablation process. Nd:YAG (λ = 1:06 mm, τ_L = 100 μs-cw) and Ho:YAG (λ = 2.12 nm, τ_L = 150–800 µs) have been used in majority during these studies [39–43] because of the main advantage that these lasers can be conveniently transmitted via a glass fiber. From practical point of view, this

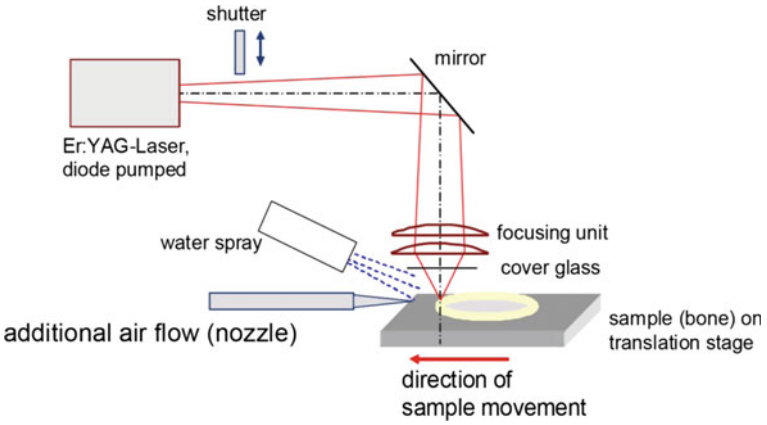

Fig. 3.24 Modified laser setup with water and air spray for better ablation characteristics (reprinted from Stock et al. [37] with permission. © SPIE)

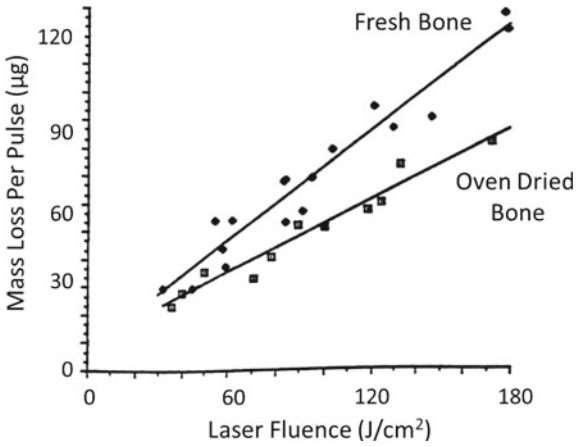

Fig. 3.25 Difference between ablation rates of fresh and dry bones by Er:YAG laser (reprinted from Walsh Jr and Hil [38] with permission. © SPIE)

characteristic becomes very important because in a actual surgery setup, maneuverability of the surgical tools plays a key role in order to carry out the operations optimally. Thus, with the usage of transmittable lasers, it is possible to keep the laser system away from the patient and surgeons and transmit the beam via fiber to a hand held laser head thereby providing a lot of convenience. Nonetheless, these lasers induce undesired damage within the bones. The wavelengths of these lasers are strongly scattered by the water as well as the mineral with scattering of the order of 350–400 cm^{-1} [34]. Uneven distribution of energy leads to heavy damage to the bone tissues. Apart from these commercially available medical lasers, other types of lasers such as Nd:YVO_4 and free electron laser (FEL) have been tried successfully for bone material removal. Nd:YVO_4 laser resulted in heavy carbonization (charring) during ablation [44]. A tunable FEL was used for investigating effect of various wavelengths (2.79, 2.9, 6.1, and 6.45 µm) on the bone ablation (Fig. 3.26)

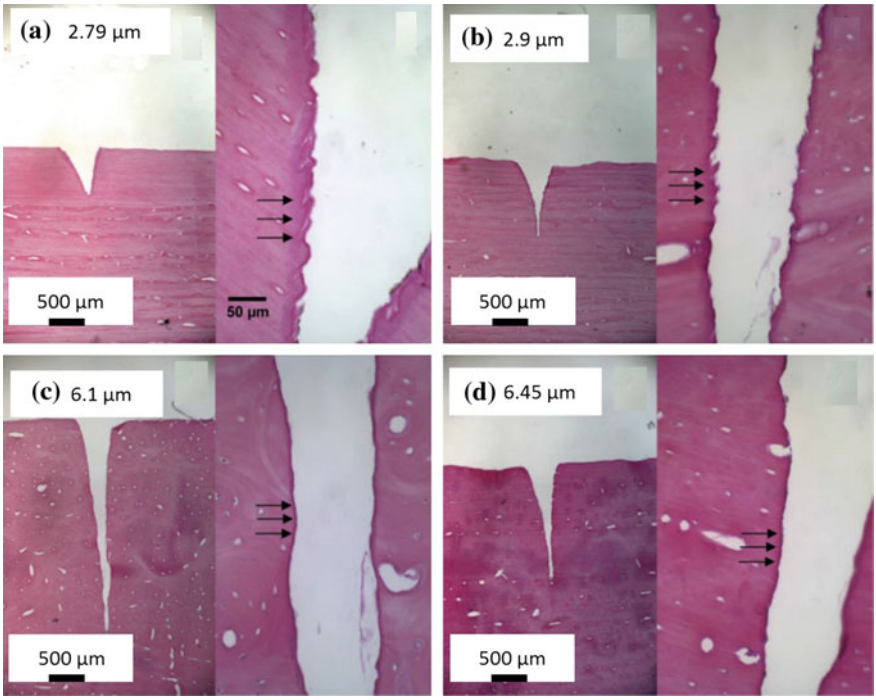

Fig. 3.26 Set of hematoxylin and eosin stained histologic sections of cortical bone showing carters produced using lasers of various wavelengths. The *arrows* indicate damaged regions (reprinted from Youn et al. [45] with permission. © John Wiley and Sons)

[45]. The wavelength of 6.1 μ was the most efficient in terms of ablation and had least thermal damage on the bone tissues (Fig. 3.27 [45]). The reason was again related to optimum absorption of this wavelength by water as well as bone mineral. These set of studies pointed towards need for continuing research so as to develop instrumentation that would overcome the adverse effect of currently available lasers such as Nd:YAG and coming up with new laser types feasible for bone ablation.

So far discussion has been focused on ablation behavior of various lasers based on thermal effects. Another important aspect of this field is post operation healing process. In this case as well, Er:YAG laser seems to outperform other lasers with rapid healing of cut bone regions [25, 29, 46–50]. After Er:YAG laser ablation, pronounced revascularization, faster bone healing, and more favorable surface for cell attachment in calvary bones were observed as compared to CO_2 laser and mechanical techniques [48]. In another investigation, bone healing after Er:YAG treatment showed presence of new immature trabecular bone on 14th day after treatment which was not observed in bur drilling. But after 21 days there was no significant difference between both the histologies [49]. Another study again pointed out the precise nature of Er:YAG but the healing times were similar compared to tool based material removal [50]. The diode laser treatment yielded the results on the same line

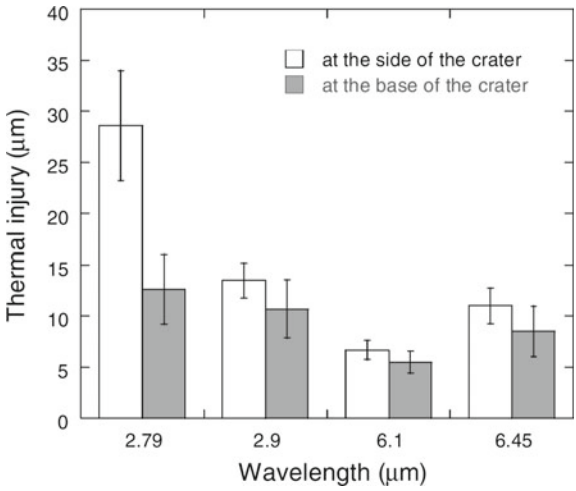

Fig. 3.27 Effect of wavelength on thermal damage during FEL ablation of bovine cadaver knee bone (reprinted from Youn et al. [45] with permission. © John Wiley and Sons)

although a potential of better healing by careful process control in case of lasers was also pointed out [51]. For FEL, the initial healing was faster (Fig. 3.28) but after 10 weeks the samples machined with conventional techniques showed equivalent recovery (Fig. 3.29) [52].

Although it is beyond the scope of this book to explore the exact healing mechanism and role of surface texture on machined bone in this process, it can be deduced that selection of laser processing parameters again becomes important in case of healing response. In addition, there is a need for complete experimentation approach which includes ablation process itself, analysis from the machining point of view, biological and cellular damage evaluation, geometrical reconstruction of ablated area with available and novel techniques, and finally the healing response. At this stage of research, Er:YAG performs the best but the new studies can be directed towards

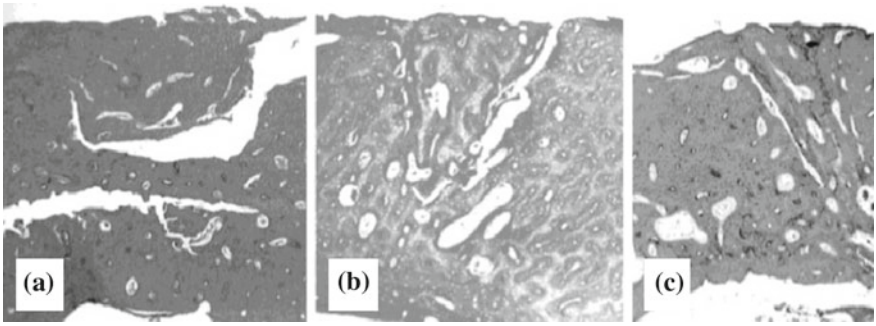

Fig. 3.28 Healing response of cortical bone of a rabbit: **a** saw cut showing no evidence of a healing response, **b** partial FEL cut and **c** completely FEL cut samples and completely filled with trabecular bone and loose connective tissue (reprinted from Payne et al. [52] with permission. © John Wiley and Sons)

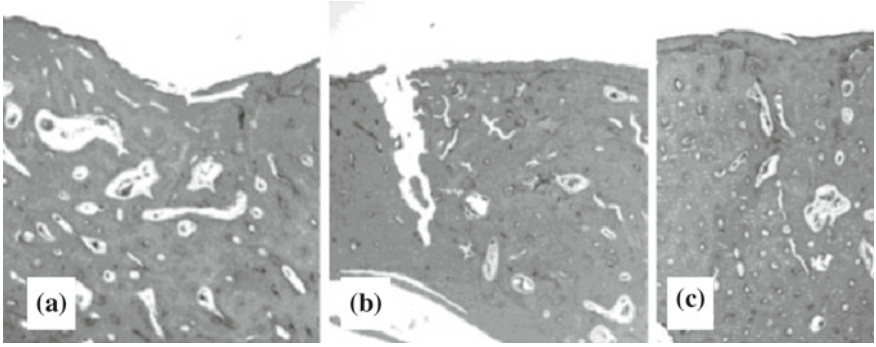

Fig. 3.29 Similar healing responce of cortical bone of a rat in 6 weeks following osteotomy for **a** saw cut, **b** partially FEL cut and **c** completely FEL cut surfaces (reprinted from Payne et al. [52] with permission. © John Wiley and Sons)

lasers such as FEL. Additionally, CO_2 laser with air-water spray which has shown promising results can be evaluated comprehensively with the suggested approach. These efforts are likely to lead the prevalent implementation of lasers as orthopedic surgical tool.

So far, extensive coverage was given to thermal effects on bone and lasers causing them. The state of the art of the research in this area was presented in a comprehensive manner. Hereafter, the focus will be directed towards modern lasers operating in the regime of fempto to picoseconds. In these time frames, mechanisms such as photo ablation and plasma induced ablation become active. Firstly these mechanisms will be described followed by a review of the latest research in this field.

3.1.1.5 Photoablation

With reduction in the laser pulse duration coupled with very high power density of the order of 10^7–10^8 W/cm^2, the tissues undergo decomposition and are etched out of the surface. This phenomenon is technically termed as photo ablation. The dimensions of ablated region depend on beam characteristics. The material removal is very precise in nature and thermal damages in the surrounding region are minimal. This phenomenon was first discovered in case of polymers and the theory of material removal is applicable in case of tissues as well [13, 53]. As soon as the laser hits polymeric material, each monomer unit (building blocks of polymer) undergo excitation. As a result, they are transfered to repulsive state from the excited one. This causes change in volume occupied by monomer units giving rise to transfer of momentum, causing the process of ablation to happen. These time frames from a computer simulation of photo-ablation of poly methyl methaacrylate (PMMA) are shown in Fig. 3.30 [13, 53]. Even though this technique is not heavy on bone material removal, it is used for the treatment of removing cancerous growth in bones. The process is typical for but not limited to excimer lasers.

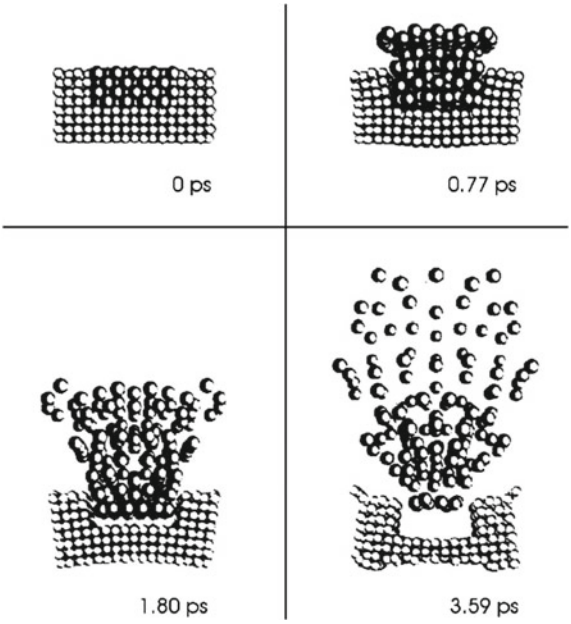

Fig. 3.30 The process of photo-ablation predicted by computer simulations (reprinted from Garrison and Srinivasan [13, 53] with permission. © AIP Publishing LLC)

3.1.1.6 Plasma-Induced Ablation

In the exposure duration time range applicable to photo-ablation, if the input power density is further higher of the order of 10^{11} W/cm^2, the material enters the regime of plasma-induced ablation. This is driven by a phenomenon termed as optical breakdown which happens in the material being irradiated resulting in plasma formation. First investigations in this area date back to late 1980s [54, 55]. The electric field strength associated with the material and the local power density (P_{ef}) determines the point of optical breakdown as expressed by Eq. 3.8 [13].

$$P_{ef} = \frac{1}{2}\epsilon_0 c E^2 \tag{3.8}$$

where ϵ_0 is the dielectric constant, and c is the speed of light, and E is the electric field strength. The field strength of 10^7 V/cm corresponding to power density of 10^{11} W/cm^2 is able to cause plasma ionization. This happens because the electric filed becomes comparable to Coulombic field within the atoms/molecules of the material. In case of Q-switched mode, the thermionic emission effect acts as the main driver behind plasma formation resulting in localized microplasma. At the same time, the plasma temperatures achieved are unusually high. On the other hand, in a mode locked laser, the multi-photon ionization takes place. Many photons are absorbed providing energy leading to ionization. In both the cases, electrons are knocked out of the atom, some of which coherently (without loss of energy) collide with other atoms releasing more electrons further driving the process of ionization in a sort of chain reaction [13]. The action of Q-switched and mode locked lasers in

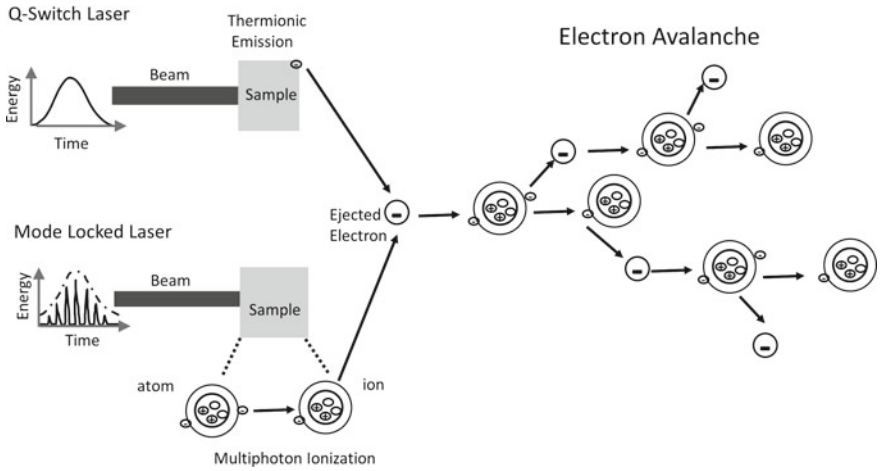

Fig. 3.31 Schematic illustration of plasma ionization in Q-switched and a mode locked lasers

plasma formation is illustrated in Fig. 3.31. The resulting ablation action gives a very clean and well-defined removal of tissue without any thermal or mechanical damage. The plasma induced ablation commonly occurs in case of the exposure times of the range of few hundreds of fempto seconds to pico seconds. Common lasing materials working in this regime are Nd:YAG, Nd:YLF, and Ti:Sapphire and plasma ablation is considered as the ideal micro machining mechanism for the bones.

3.1.1.7 Photodisruption

When the energy density is higher than that required for the process of plasma induced ablation, the side effects of plasma formation become profound. These effects are mechanical in nature and are directly proportional to the input laser energy. The optical breakdown leads plasma formation followed by shock wave generation, cavitation, and jet formation. Shock waves become predominant at high energy input for extremely short interaction time. These mechanical effects disrupt the tissues and also has an effect on surrounding tissues. Cavitation occurs when the regions inside a tissue undergo vaporization causing bubble to form and finally disrupt the tissues. If the biological fluids are in the vicinity of caviation, the collapse of a bubble results in jet formation. This phenomenon results in fragmentation and cutting of tissue by mechanical forces. Time of exposure ranges within fempto to nano seconds and lasing systems are similar to that produce plasma induced ablation. Major applications include eye lens fragmentation or surgery involving breaking of unwanted entities such as kidney stone within the body via shock wave [4].

Having covered the important mechanism operative in femto-nano second regime, the literature review about ablation of hard tissues with these type of lasers will be presented. Firstly, there are many advantages of the ultra short laser pulses as

discussed by Neev et al. in one of the popular invited papers [56] which are enlisted below. These advantages are exclusive to the ultrashort regime and apart from these, ultrashort pulsed lasers also posses all the advantages of laser machining in general.

1. Requirement of small input of laser energy per ablated volume of tissue and the resulting decrease of energy density needed to ablate material. As a result ablation happens in very efficient manner
2. Minimum mechanical damage to tissues on the account of efficient ablation and short duration of stress impulse.
3. Minimum thermal damage because of small interaction time and heat transportation away from the bones with the ablated tissues.
4. Minor influence of tissue properties on ablation process, threshold, and rate in particular.
5. High degree of machining precision with smaller material removal in each pulse. Number of pulses are easily controllable by a feedback mechanism based on the progress of ablation.
6. Silent operation due to lower acoustical noise (as compared to the high-speed drilling or use of other laser systems).
7. Minimum pain due to localized nature of the process.
8. Ability to control the surface texture on the ablated bone.
9. Precise spatial control due to the intensity dependent and multiphoton process that self-ensures that the tissue below or laterally removed from the beam focus will not experience ablative interaction.
10. Since ultrashort pulses interact strongly with all matter regardless of specific linear absorption characteristics, efficient processing of almost all tissue types is possible.

Ti-sapphire laser ($\lambda = 1.06\ \mu m$, 100 fs pulse duration, frequency 83.6 MHz, input power 400 mW) was employed to study ablation of hard teeth tissue, human nail, and incus midear bone [56]. Seed pulses of 100 fs from a mode-locked Ti:Sapphire oscillator were stretched to 1 ns in a four-pass, single-grating pulse stretcher. TEM_{∞} mode was operated at 10^6 mJ and further amplification to the 60-mJ level was achieved in a Ti:Sapphire ring regenerative amplifier, which supported a larger (2.3 mm) beam diameter and reduced nonlinear effects. The ablation was damage free. Similar study compared response of bone to conventional drilling and Ti:Saphhire laser drilling [57]. The laser drilling resulted in cleaner drilled surfaces. Extent of necrosis was minimal in case of laser drilling (Fig. 3.32a, b [57]). The healing recovery was much better in case of laser osteotomy compared to mechanical (drill) osteotomy as illustrated in photos as well as bar charts (Fig. 3.33a, b [57]). However, even though the clean nature of femto second lasers is attractive and post osteotomy healing is also better, some problems associated with fs lasers pointed in the literature are listed below [56].

- The amount of ablated tissue per pulse is relatively small, of the order of a single micron of tissue thickness per pulse.

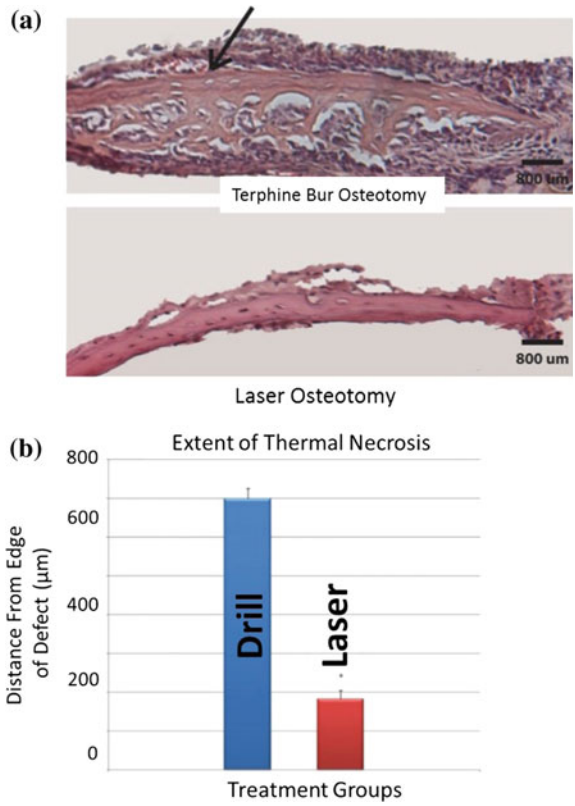

Fig. 3.32 Observation of osteotomy defects in post surgery h and E stained bone samples **a** trephine bur osteotomy (*top*) and Ti:Sapphire laser (*bottom*) and **b** the extent of osteonecrosis delineated by measuring the distance the empty osteocyte lacunae extended from the edge of the calvarial defect (reprinted from Lo et al. [57] with permission. © John Wiley and Sons)

- Ablation efficiency rapidly reduced with increase in laser fluence made in an attempt to increase ablation rate.

The reduction in ablation with increase in fluence was explained on the basis of the physics behind the process [56, 58]. Considering the biological tissues as wide band gap materials, input energy causes phonon scattering (Joule heating), and once the electrons have high enough energy to get knocked out, ionization occurs. This leads to multi photon absorption in case of ultrashort pulsed lasers and the avalanche process induced by the electromagnetic field that follows, generates free electron in an exponential function. Laser power also increases exponentially. These electrons in the plasma absorb the incoming laser energy thus making process independent of the physical properties of the bone. However, when the electron density reaches critical value, n_c, ($10^{21}/cm^3$ for Ti-Saphire laser wavelength [58]), the plasma becomes highly reflective. This causes absorption to be confined to a very thin layer. The penetration depth, δ, is expressed as a function of laser wavelength, λ, as per Eq. 3.9.

$$\delta = \frac{\lambda}{2\pi\sqrt{|\epsilon|}} = \frac{\lambda}{\pi\sqrt{1-\frac{n}{n_c}}} \tag{3.9}$$

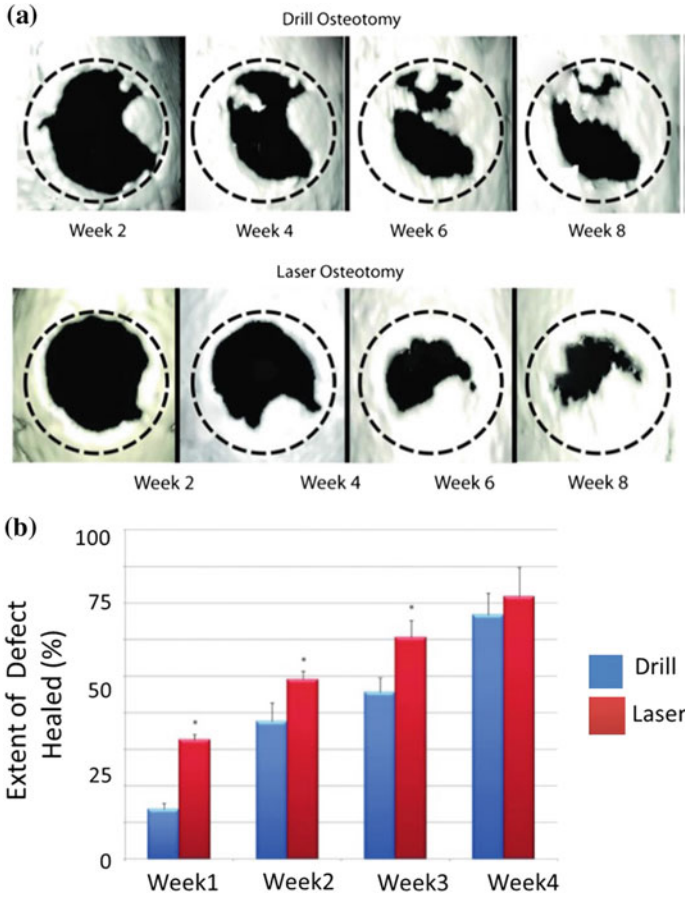

Fig. 3.33 Healing response of bone to Ti:Saphire femtosecond laser and conventional drilling. **a** photographs of bone recovery and **b** bar charts giving percent recovery (reprinted from Lo et al. [57] with permission. © John Wiley and Sons)

where ϵ is the electrical permitivity of the plasma, and n is the number of electrons. Thus after a certain energy input, ablation rate does not improve and a choice needs to be made for the requirement between ultrashort pulsed laser or conventional thermal effect laser. A clean, negligible-damage ablation of the short pulses remove only a minute amount of material with each pulse, whereas conventional lasers lead to thermal and mechanical collateral damage.

Another effort explored ablation of rat skull bones by excimer laser [59]. Two types of lasers were employed, one with wavelength of 248 nm and a maximum output of 500 mJ/cm^2 while the other with wavelength of 193 nm and a maximum output of 250 mJ/cm^2. These investigations also observed saturation in the ablation rate with increase in laser fluence indicating effect of critical electron density (Fig. 3.34 [59]). They also compared this process to infrared lasers, Nd:YAG and CO_2 and

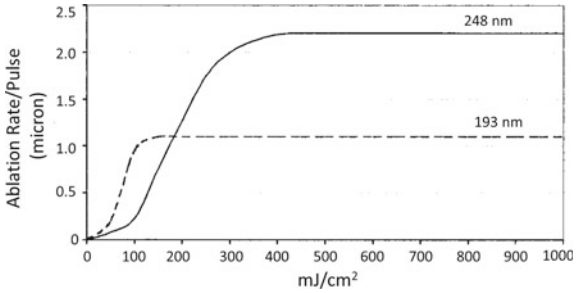

Fig. 3.34 Plots indicating saturation of ablation rates for two laser wavelengths with an increase in laser fluence (reprinted from Walter et al. [59] with permission. © John Wiley and Sons)

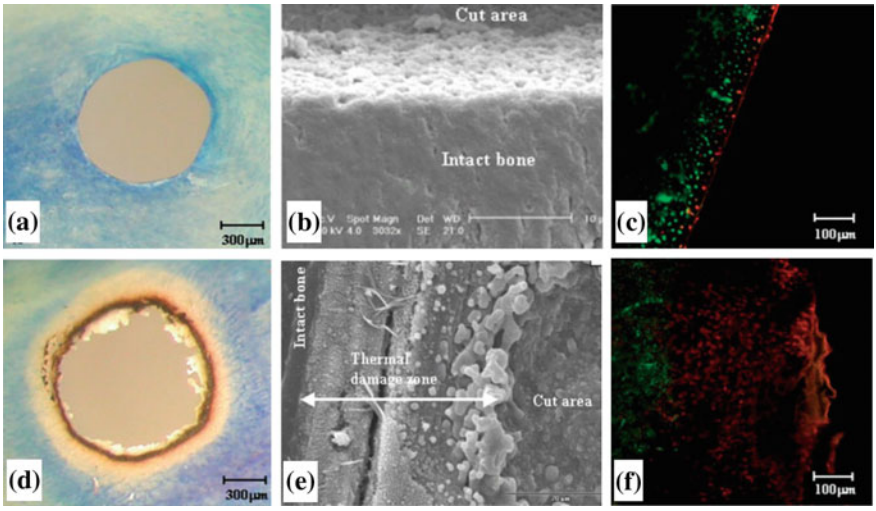

Fig. 3.35 Set of micrographs showing ablated surface of by fs laser and nano second laser. The sub figures **a**–**c** correspond to fs laser whereas **d**–**f** to nano second laser. **a** and **d** optical images, **b** and **e** SEM micrographs, **c** and **f** confocal images (reprinted from Girard et al. [62] with permission. © John Wiley and Sons)

indicated that excimer lasers produced much uniform cuts and minimum zone of thermal damage. Although it has to be noted here that the most attractive infrared laser, Er:YAG was not compared. Similar observations about ablation characteristics were made by other researchers in case of excimer [60] and Yb:KYW lasers [61].

Thermal effects were quantified during Ti-Saphire fs ablation of the bones and compared with nano second laser using confocal and SEM/EDS analyses in a study by Girrad et al. [62]. Confocal microscopy and SEM imaging revealed damaged zone of only 14 µm for fs laser which extended to 435 µm for a nano second laser (Fig. 3.35 [62]). Carbon was depleted in the recoiled material as indicated by EDS analysis thus indicating degradation of organic matter in the ablated recoiled bits of bone suggesting the occurrence carbonization.

One of the latest significant works has compared Er:YAG and femtosecond lasers from various aspects (Table 3.2) [61]. This study clearly pointed out that although Er:YAG was much faster, it was less precise and produced rougher surfaces than fs lasers. It also had higher degree of damage than fs lasers. Apart from these positive points, the fs lasers were much slower in terms of ablation rate and expensive from economics point of view. This study pointed towards further research on ultrashort pulsed lasers to make them surgically feasible in terms of time and cost. It is intuitively thought that these lasers will be of great significance become of a great significance where precision becomes a priority over other factors.

Having covered all types of lasers used for machining of the bone tissues and summarizing their characteristics in Table 3.3, the discussion will be advanced towards other beam based techniques namely microwave and ion beam. These are still in the experimental phase and will need significant amount of work to make them as established as lasers are today. Nonetheless, important operation and ablation mechanisms have been discussed and preliminary efforts in this field have been explored.

3.1.2 Microwave Machining

Microwaves form the part of electromagnetic spectrum belonging to the frequency range of 300 MHz–300 GHz (Fig. 3.1). For heating purposes, the frequencies used are 0.915 and 2.45 GHz (Fig. 3.1) as reserved by Federal Communications Commission (FCC) [63, 64]. The microwave interacts in three ways depending upon the type of material [65] as illustrated in Fig. 3.36. Metallic materials reflect microwaves. High dielectric loss materials absorb the microwaves. Low dielectric loss materials or insulating materials permit microwaves to pass through. Bones having calcium phosphate as the major component fall under the last category. Microwaves react with the hard tissues causing heat generation by resistive losses of moving charged-ions and oscillations of charged molecules [66, 67]. This heat is then transfered by the induced movements of charged ions. At temperatures over 50 °C, tissues may undergo vaporization and carbonization. Higher temperatures may cause desiccation, protein denaturation, coagulation, and finally welding and cavitation [66, 67].

In order to carry out machining operations of bone, an external tool which would absorb the microwave energy and serve as a heat source is required (Fig. 3.37 [68]). This tool, technically termed as the near field concentrator acts as both receiver and transmitter of the microwaves. Heating takes place on the localized region at the tip of the tool resulting in creation of a hot spot on the bone surface. George et al. demonstrated drilling of a cow rib bone in dry and wet conditions using a microwave oven [69]. The drilling setup shown in Fig. 3.37 was kept inside the oven [68, 70]. A frequency of 2.45 GHz and power of 600 W was employed for this purpose. The total time required for drilling through the 6 mm thick bone was 15 s in both the cases. However, thermal damage was much less in case of the wet bone [69]. Although this study established possibility of drilling of bones using microwaves, it did not investigate into machining parameters like drilling force.

Table 3.2 Comparison of parameters and process characteristics of Er:YAG and fs lasers

Type of laser	Characteristics										
	Wavelength (mm)	Energy per pulse (J)	Frequency (Hz)	Laser fluence (J/cm^2)	Ablation rate (mm^3/min)	Depth of ablation (mm)	Surface	Damage	Time required	Cost	Precision
Er:YAG Laser	2.94	0.57	1	18	4.4	1.3	Rough	Little	Quick	Less	Reasonable
Fempto second laser type 1	1.70	60	5000	N/A	0.0048	0.86	Smooth	Little	Long time	More	Very precise
Fempto second laser type 2	1.05	3	30,000	N/A	0.0018	0.16	Smooth	Not visible	Long time	More	Very precise

Table 3.3 Lasers for orthopedic application

Laser type	Wavelength	Time	Mechanism	Key points
Er:YAG	2.9 μm	μs	Thermal	•Good absorption by water •Most attractive laser from surgery point of view •Excellent bone healing after the ablation
CO_2	9.6–10.6 μm	μs cont.	Thermal	•Good absorption by mineral •Significant thermal damage •Improved instrumentation with air-water spray
Nd:YAG	1.064 μm	μs cont.	Thermal	•Bad absorption characteristics •Heavy thermal damage to bones •Easily transmitted by fibers
Ho:YAG	2.61 μm	μs	Thermal	•Bad absorption characteristics •Heavy thermal damage to bones •Easily transmitted by fibers
FEL	Tunable	μs	Thermal	•Wavelength of 6.1 μm most effective •Controlled thermal damage •Decent healing characteristics
Ti- Sapphire	0.60–1.053 μm	fs	Plasma	•Very precise ablation •Minimum thermal damage •Relatively slow ablation •High cost
Excimer	Depends on lasing media	fs-ns	Plasma	•In fs regime the characteristics similar to Ti-Saphire •In ns regime thermal damage is relatively high

μs—microsecond; cont.—continuous wave; fs—fempto second; ns—nano second

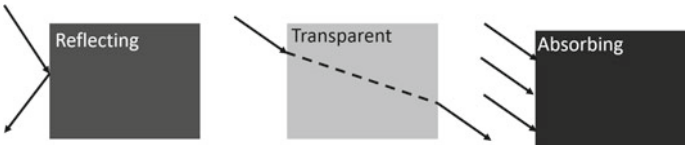

Fig. 3.36 Interaction of microwaves with the condensed material

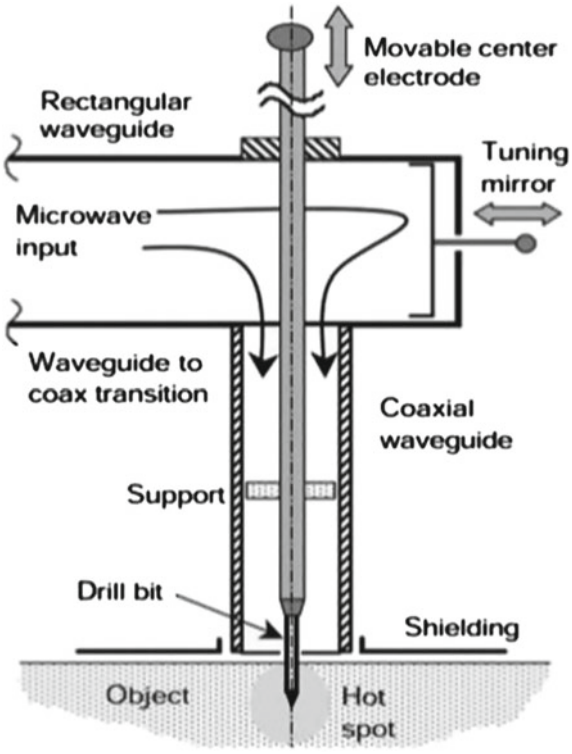

Fig. 3.37 Schematic of microwave drilling of a material [68] (reprinted from Jerby and Dikhtyar [70] with permission. © Springer)

Eshet et al. carried out detailed investigation of the mechanical properties of microwave drilled bones [71]. Frequency of 2.45 GHz and power of 150–200 W was used. The drilled holes were smooth and uniform in case of microwave drilling compared to conventional mechanical drilling process. The variation of power and drill depth as a function of time in case of mid-shaft of bovine tibial bone (cortical bone) and bovine trabecular bone is presented in Table 3.4. Mechanical properties such as strength and fatigue life of microwave drilled, conventionally drilled, and raw bones were very similar. This study also pointed out that microwave drilling of bones was possible and it was safer than radio frequency technology but at the same time constraints in implementation of this technology were pointed out. These constraints included in vivo set up design, safety concerns for personnel operating the microwave equipment, and patient undergoing surgery. In addition, the studies explored here did not investigate important machining parameters such as force and temperature rise.

Table 3.4 Effective power and drilling depth expressed as function of time for two types of bones

Time (s)	Effective power (W)		Drilling depth (mm)	
	Midshaft	Bovine tracebular	Midshaft	Bovine tracebular
0	200	200	0	0
0.5	225	175	0.5	1.1
1.0	170	130	1.0	1.8
1.5	160	100	2.0	2.0
2.0	150	130	2.2	2.5
2.5	140	120	2.7	2.8
3.0	130	100	3	3.8

Thus a further detailed investigative efforts are needed before microwave technology becomes implementable in actual practice.

3.1.3 Ion-Beam Machining

Focused ion beam has come up as a novel micro machining technique. It primarily utilizes an gallium ion source. These ions are accelerated towards the sample surface by application of voltage. Impingement of high velocity ions results in energy exchange with the sample atoms setting them into motion. If the energy is high enough, the atoms get knocked out causing the machining action. In addition, it is possible to carry out beam assisted deposition. Further, the ions reflected back can be used for imaging purposes. These three modes have been schematically shown in Fig. 3.38.

As far as bio application is concerned, ion beam assisted deposition has been tried in case of bone-implants where in hydroxyapatite coatings were produced on implant materials [72–74]. In case of machining operations however, the ion beam has been employed only for the purpose of machining out the samples for micro

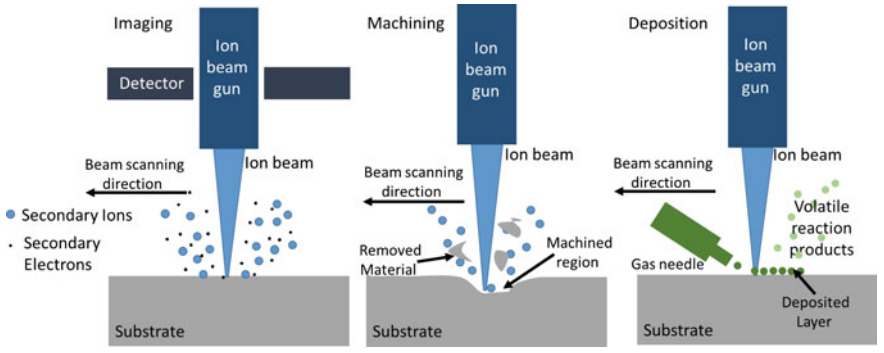

Fig. 3.38 Schematic of three operations of ion beam based processing

scale testing [75, 76]. The main difficulty is the need for vacuum which requires extensive dehydration of bones before the machining and making the bone samples electronically conductive by gold coating prior to machining. Nonetheless, it is very helpful technique in lifting out site specific bone constituent samples. The length scales as low as 5 μm can be prepared and tested. These abilities make ion beam an unique tool for research purpose. Even though, currently, this technique is not feasible for bone machining operations, it holds a great potential in the situation where micro machining of bones may become critical.

3.2 Ultrasonic Machining

Ultrasonic machining as the name suggests employs conversion of high frequency electrical energy into mechanical vibrations through a transducer/booster combination [77–79]. These vibrations are then transfered to a mechanical tool and abrasive particles present in the slurry that is passed between the workpiece and tool. The vibrations of the tool with the applied feed force make the abrasive particles perform material removal by the mechanism of microchipping. The general features of the equipment along with the enlarged views of the tool-abrasive slurry arrangement employed during ultrasonic machining has been schematically depicted in Fig. 3.39 [77]. The further essentials of ultrasonic machining are described below.

3.2.1 Setup Components

The ultrasonic machining setup comprises of combination of various types instrumentation. These consist of mechanical tools, electric generators, and converters.

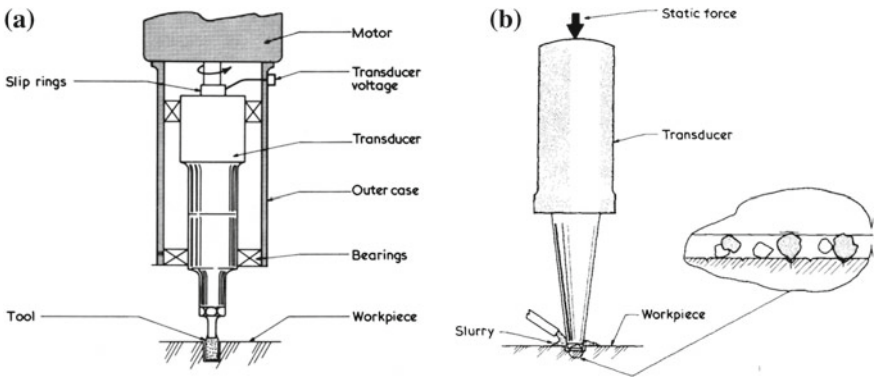

Fig. 3.39 Schematic of ultrasonic machining set-up. **a** full assembly and **b** abrasive slurry tool (reprinted from Graff [77] with permission. © Elsevier)

The current subsection provides a brief description about the general instrumentation required for ultrasonic machining.

3.2.1.1 The Ultrasonic Generator and Ultrasonic Transducer

The generator operates on high frequency which matches with natural frequency of the tool-horn assembly. The generator is designed to accommodate minor tool wear and tear resulting in minimum heat generation and minimum loss of acoustic energy. The high frequency generated is then transferred to the transducer. The conversion of electrical energy is then made into the mechanical vibrations. The transducer is usually magnetostrictive or piezoelectric. Magnestostrictive transducer provides better flexibility with frequencies felicitating tool design. On the other hand, it has high electrical losses thus resulting in low efficiencies of the order of 55 % and require cooling arrangements to take care of heat generated due to these losses. Piezoelectric transducer on the other hand has high energy efficiencies (90–95%) and hence does not require cooling.

3.2.1.2 Horn and Tool

Horn is also refereed to as acoustic coupler, velocity/mechanical transformer, and concentrator or stub. Usually, the vibrational amplitude at the traducer is of the order of few microns and horn amplifies these vibrations to achieve reasonable machining rates. Tool is attached to the horn and needs to vibrate with maximum amplitude. The tool can be joined with horn by brazing or mechanical fixing. Another important requirement for the tool is high hardness, wear resistance, and good fatigue life. A photograph of set of horns and tools have been shown in Fig. 3.40 [79].

3.2.1.3 Tool Feed and Abrasive Feed Mechanisms

The tool acts under a static load holding itself against the workpiece. The tool feed mechanism helps in application of the uniform load on the workpiece. The slurry is pumped using jet flow or suction between the workpiece and the tool. Some systems employ combination of both the mechanisms. In some cases such as drilling with relatively deeper holes, the slurry can be fed through the horn and tool assembly itself. The slurry not only serves to supply the abrasive particles but also acts as the coolant for the tool. Important delivery mechanisms are schematically shown in Fig. 3.41 [79].

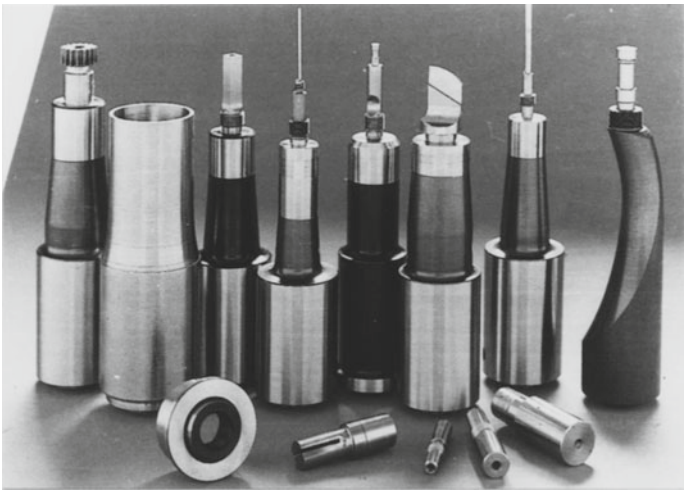

Fig. 3.40 Photo of horn with or without tool heads (reprinted from Thoe et al. [79] with permission. © Elsevier)

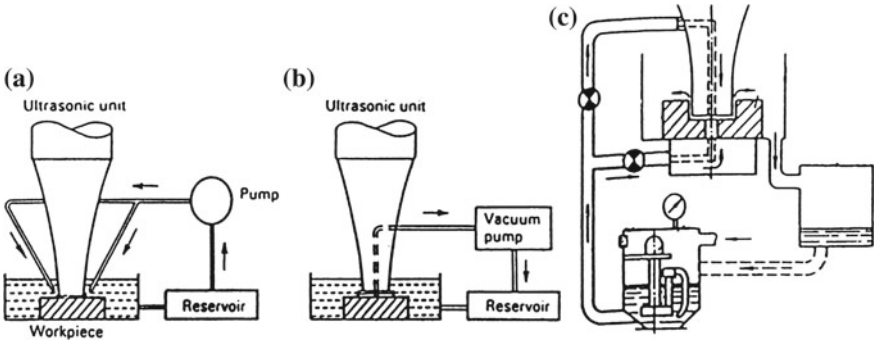

Fig. 3.41 Abrasive slurry delivery mechanisms, **a** jet flow, **b** suction, and **c** combination of both (reprinted from Thoe et al. [79] with permission. © Elsevier)

3.2.2 Machining Mechanisms

As a result of combined action of abrasive particles and horn-tool setup the material removal takes place. Ultrasonic technique can be employed for various modes of machining such as cutting, drilling, and grinding. These mechanisms can act in individual or combined fashion depending on the material, applied load and frequency. The mechanisms are listed below.

- Mechanical abrasion by direct hammering of the abrasive particles against the workpiece surface
- Micro chipping by impact of the free moving abrasive particles
- Cavitation effects from the abrasive slurry
- Chemical action associated with the fluid employed

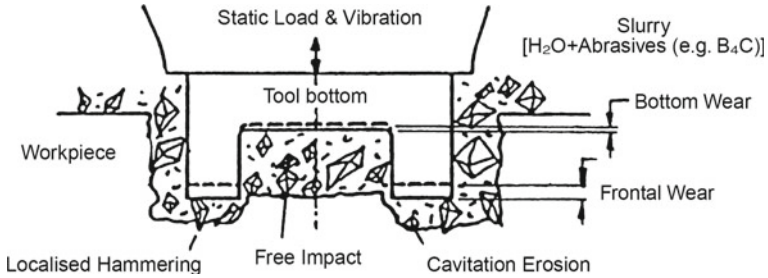

Fig. 3.42 Mechanisms of material removal during ultrasonic machining (reprinted from Thoe et al. [79] with permission. © Elsevier)

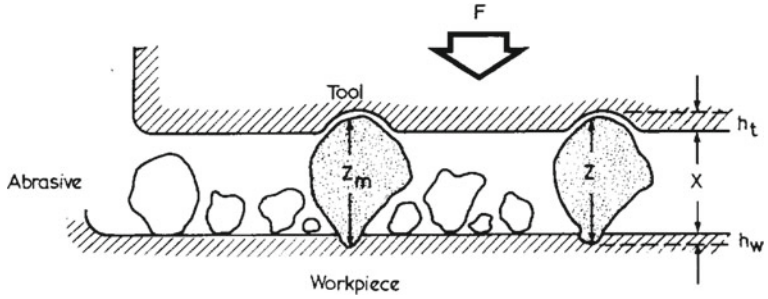

Fig. 3.43 Abrasive particles in the space between tool and workpiece (reprinted from Kazantsev and Rosenberg [80] with permission. © Elsevier)

Figure 3.42 summarizes these mechanisms in a schematic fashion. For mathematical expression of the ultrasonic machining, the various aspects/components are schematically depicted in Fig. 3.43

The force acting on each particle is expressed as

$$F = N \int_{x}^{Z_m} \Phi_z(z-x)\Psi_z dz \tag{3.10}$$

The volume machined in one cycle is expressed as

$$V = N \int_{x}^{z_m} V_z(z-x)\Psi_z dz \tag{3.11}$$

where N is the number of particles, z is the height of the particle, z_m is the maximum height, Ψ_z is the size distribution function, V_z is volume of material machined out by an abrasive particle. The effect of particle size is expressed as

$$\Psi_z = \frac{1.0095}{z}\left[1 - \left(\frac{z-\bar{z}}{\bar{z}}\right)^2\right]^3 \tag{3.12}$$

where $\bar{z}$ is the average diameter of particles. Depth of the material removal from the workpiece is inversely proportional to the hardness as expressed by the following equation.

$$h_t = \frac{1}{4H_t\bar{z}}\Phi_z \tag{3.13}$$

where h_t is the depth to which the depth of material removed and H_t is the hardness of the material. The relationship between volume removed and force is expressed as

$$\frac{V}{N} = C_{(\bar{z})}\left(\frac{F}{N}\right)^{q_{(\bar{z})}} \tag{3.14}$$

where $C_{(\bar{z})}$ and $q_{(\bar{z})}$ are factors which depend on average grain size of the abrasive. Finally the machining rate during ultrasonic machining is expressed in terms of pressure (σ_m = force/machined area) and concentration of abrasive particles (N_s= number of particles/machined area) as

$$v = C_{(z)}\frac{\sigma_m}{N_0}^{q_{(\bar{z})}} N_0 f \tag{3.15}$$

where N_0 is the ratio N/s and f is the frequency of vibration.

Finally, to consider the effect of ultrasonic vibrations the pressure acting on the particles is related to vibrational amplitude and applied static load as

$$\sigma_m = Q(\xi_m^2 P_l)^{\frac{1}{3}} \tag{3.16}$$

where Q is the constant, ξ is the amplitude of vibration, P_l is static load applied.

Having discussed the mechanisms of material removal, there are various modes of operation in which the equipment can be operated. These modes are basically based on the direction of vibration of the tool and listed below

- Longitudinal
- Torsional
- Compound motion
- Wire transverse

The first three modes can be put to work with any tool whereas the last one needs a thin wire attached to the equipment. Based on the required machining action, the proper mode of action of the equipment can be chosen. Apart from these modes, there are some unwanted actions which are termed as unwanted modes. These modes can cause damages to the tissues by having undesirable effects such as stress concentration and non longitudinal vibrations. Detailed description of these modes have been given in the publication referenced here [81].

3.2.3 *Ultrasonic Machining of Bone and Hard Tissues*

Having discussed the basics of the setup and the mechanisms of material removal during ultrasonic machining, hereafter the focus will be towards ultrasonic machining of bones. Ultrasonic technique has been applied in case of machining of hard tissues as early as 1950s [82–84]. Many efforts have been in the field of dentistry and many relevant publications are patents [82, 85–90]. An example of alveolar bone cut using ultrasonic chisel during a extraction procedure has been shown in Fig. 3.44 [90].

This technique has also been explored for structural bones. Khambay and Walmsley explored the cutting abilities of ultrasonic technique in case of freshly procured bovine bone [91, 91]. The initial study concluded that ultrasonic cutting when compared to traditional burr produces superficial cuts which can be advantageous in controlling tissue damage. In another study the clinicians needed to be trained in order to handle ultrasonic equipment in a standardized manner [91]. In a subsequent study, effect of various process parameters was investigated. The variation in longitudinal downward force during ultrasonic chisel cutting of bovine bone with rake angle of 0° is shown in Fig. 3.45 [91]. The effect of vibrations induced by transducer horn assembly can be clearly seen. Furthermore, the effect of rake angle was investigated (Fig. 3.46) on the downward and longitudinal forces (Fig. 3.47 [91]). It is clear that even though there is not significant change in longitudinal force, the downward force slightly increases up to rake angle of 10° and then reduces rapidly for higher rake angle. This has a significant effect on depth of cut which reduces as the downward force does. This is clearly reflected in variation in cutting force as a function of rate of cut (Fig. 3.48 [91]).

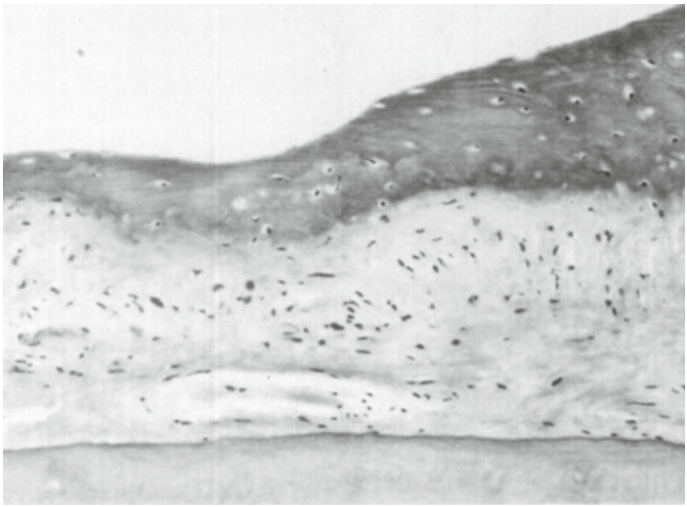

Fig. 3.44 Ultrasonically cut alveolar bone during tooth extraction (reprinted from Horton et al. [90] with permission. © Elsevier)

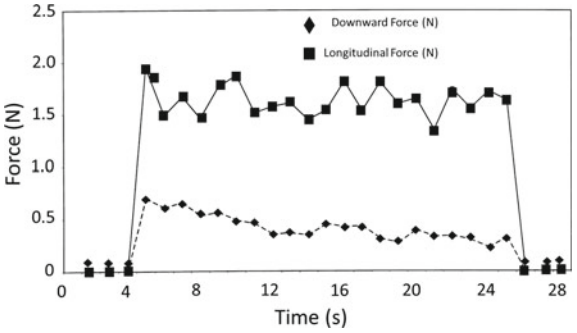

Fig. 3.45 Variation in longitudnal force and downward force during ultrasonic chisel cutting of bovine bone (reprinted from Khambay and Walmsley [91] with permission. © Elsevier)

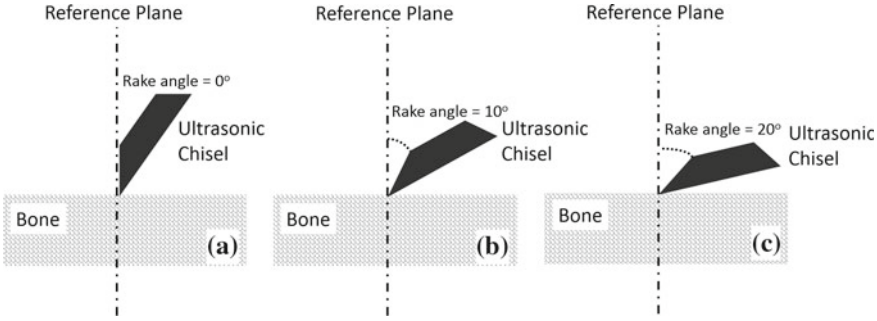

Fig. 3.46 Various rake angles investigated by Khambay et al. [91]

Fig. 3.47 Effect of rake angle on downward and longitudinal forces (reprinted from Khambay and Walmsley [91] with permission. © Elsevier)

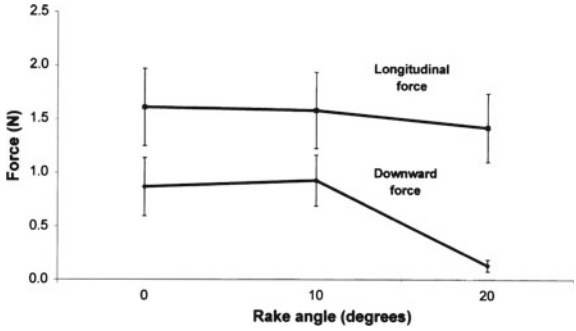

One of the primary characteristics which brings ultrasonic machining more superior to conventional machining is that it essentially brings down the cutting temperature while operating upon the bone and thus helps the long-term goal of avoiding any detrimental after-effects to the bone. In this field, Cardoni et al. [92] directed study gathered that when ultrasonic energy is absorbed by natural materials, their thermal responses are altered dramatically for a favorable outcome. The post ultrasonic cutting observations by Lucas et al. [93] also supported that by controlling cutting parameters such as load, tuning frequency, and vibration velocity of the blade tip,

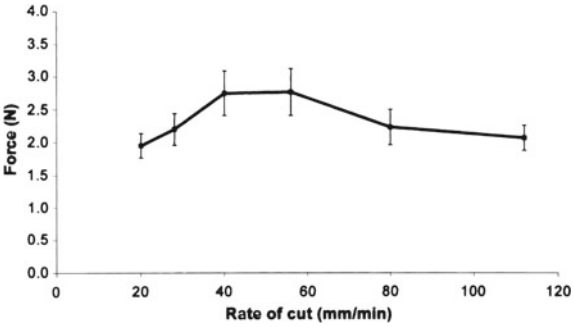

Fig. 3.48 Variation in cutting force as a function of rate of cut (reprinted from Khambay and Walmsley [91] with permission. © Elsevier)

Fig. 3.49 20 kHz (*long*) and 35 kHz (*short*) ultrasonic cutting blades (reprinted from Cardoni et al. [92] with permission. © Elsevier)

the thermal response of material can be altered for elimination of additional cooling system. Two different types of blades used in this study are shown in Fig. 3.49 [93]. Besides the above-mentioned research works related to the influence of process parameters on temperature, a number of attempts were also made to come up with innovative designs [94, 95] for the cutting blades to distinctively decrease the frictional heat during site specific cutting.

Another dimension to the domain of ultrasonic machining is the introduction of piezosurgery based on piezoelectric ultrasonic vibrations. Robiony et al. [96] have reported extensive use of piezosurgery in maxillary osteotomies. The piezoelectric device shown in Fig. 3.50 [96] observed to produce relatively safer cuts, without any trace of damage from osteonecrosis. In addition, the technique is also suitable for cutting delicate structures without encountering any difficulties associated with intra operative visibility. Other studies too [97, 98] have contributed significantly to this promising field of piezosurgery and many suggestions centering around new bone cutting methodologies [99] were proposed.

Alongside the studies pertaining to cutting blade design, and parametric studies on temperature effects, several other research works also mention regarding the fracture occurring in bones and its probable causes. As Aro et al. [100] did not observe any micro-fractures during ultrasound sawing it was not considered as one of the major

Fig. 3.50 The piezosurgery device with a piezoelectric hand piece (reprinted from Robiony et al. [96] with permission. © Elsevier)

mechanisms for bone destruction. Furthermore, differentiations were made between the short-term and long-term consequences of using an oscillating saw as against an ultrasonic one on scapula of a rabbit by carrying out histological and scanning electron microscopic investigations. Their conclusions were that application of ultrasonic technology did not induce any micro-fractures whatsoever. It is known that eminent researchers have also resorted to finite-element modeling [101] to better explore the fracture phenomenon while cutting brittle materials ultrasonically. Thus, they provided valuable insights into the fracture mechanism based on crack-propagation for successful cutting of friable materials. These efforts related to modeling have been discussed in detail separately in Chap. 6.

3.3 Pneumatic and Hydraulic Machining

Pneumatic machining basically involves tools driven by pneumatic technology rather than electric or hydraulic. Compressed gas/air is used to drive tools such as drills. Pneumatic techniques offer major advantage from biological point of view that it is a cleaner way of operating the tools. Several innovative and modernistic designs have been developed over the years and constant advancements are being witnessed. Though generally the pneumatic technology is primarily used in the motors that drive the cutting tools for machining of bones, Forest Barber and Tidwell [102] invented a replicator for resecting bone in which they have incorporated a high speed cutting tool that utilizes the pneumatic technology. Ham et al. [103] interestingly experienced far

generation of superior surface flatness during robot-assisted surgery wherein one of the motors was pneumatic based. Furthermore, Jakopec et al. [104] brought in the pneumatic tourniquet in their study on a hands-on robotic framework based total knee replacement involving of several individual robots. Another different, attempt by Zegunis et al. [105] compared the thermal effects in a pneumatic hammer drilling and conventional drill-bit based drilling by embedding k-type thermocouples in the bone. The observations revealed that under similar conditions, the hammering generated an average maximum temperature of 31 °C while that recorded for conventional drilling generated was 47 °C.

In their study, Mimnaugh et al. [106] used a pneumatic hand grinder in quest of obtaining small bone particles for further study on the influence of entrapment of these particles on the surface morphology and wear characteristics. In another invention, Meredith [107] specifically used the pneumatically operated cylinders with a vacuum of 28″ of mercury in their advanced design concerning with an intention to blend the constituents and form composites similar to natural bone. The patent by Tarasius and Spiering [108] includes the use of electrically or pneumatically operated motors as a design modification in place of a hand driven handle for the purpose of exclusively milling bones and hard tissues. Despite its varied advantages and enhanced capabilities, pneumatic designs are continually being modified and battery-operated saws are becoming more popular. Notable proposition in this line of machining has been given by Troccaz et al. [109] whose research probed the dependability of surgical robots, for automation and accuracy during machining of bones. This design incorporated a pneumatic artificial muscle actuators emphasizing the nedd for robotic intervention in operations such as precise milling of femur and the inserted stem's alignment.

Another development in this field was undertaken by Park et al. [110], where they attached a pneumatic milling tool to the femur and subsequent tasks were performed sequentially as required for total hip arthroplasty. The efforts are also being conducted to reduce the error generated due to human interaction. In general, pneumatically-operated milling tools lead to reduction in machining time with machining errors within acceptable range. Malvisi et al. [111] compared three different types of pneumatic milling cutters and established that milling can totally replace sawing, especially in cases of major re-sectioning of bones. Their work further indicated that pneumatic milling operation can be carried out in the absence of irrigation and within the stipulated time frame for allowable range of accuracy and temperature elevations. Since the use of pneumatic tools such as drills, mills, hammers, cutters, shapers, and grinders is well established machining of conventional metallic and non-metallic materials, with several modifications in designs mentioned above, they are being considered also for bone machining. For instance, Chung et al. [112] incorporated a pneumatic drill and slider for driving the tool in their construction of a compact, robust, complex and miniature intramedulla gage for stem implantation in femurs.

As described above, several bone machining techniques are supplemented with haydraulic jets to assist in cooling and/or enhance the cutting action. However, another technique based on hydraulics, waterjet machining utilizes water (fluid), primarily for the purpose of machining. Promising works have been done in the field of waterjet machining of the bones and they are discussed in the following section.

3.4 Waterjet Machining

Waterjet machining as the name suggests employs high pressure jet of water in order to perform material removal. On the account of its precision, waterjet machining has been employed in variety of industries related to metal cutting, paper and cardboard cutting, and frozen food cutting reflecting the versatile nature of the process [113–115]. In case of bone and hard tissue cutting, this process offers some specific advantages listed below [116–119].

- No heating of the tissues
- Precise and clean cuts
- Better accessibility for deployment in operation theater via flexible waterjet tubing
- Water is not biologically harmful

The basic principle behind waterjet machining is expressed by the following Bernuli's equation [117].

$$V_{liquid} = \mu_v \sqrt{\frac{2P}{\rho}} \tag{3.17}$$

where V_{liquid} is the waterjet velocity (m/s), μ_v is the constant with value between 0.86 and 0.92 depending on the waterjet setup, ρ is the density of water (kg/m^3), P is the pressure (Pa). Considering that μ_v and ρ remain constant, any increase in the pressure would also increase the water jet velocity. Depending on movement of the water jet stream, the various machining actions can be performed. For example, during cutting, the waterjet is moved over the material and during drilling, waterjet does not continue path through the material but changes its trajectory by 180° after reaching the desired depth (Fig. 3.51). The control of pressure plays a key role and should be exercised carefully. The general setup for waterjet machining consists of a high pressure water pump, a transducer for monitoring real time pressure, a jet nozzle with adjustable diameter, and specimen holding arrangements [119].

The diameter of the waterjet also plays a critical role especially in case of bones which have a porous composite structure [117]. The diameter is related to the volume of water in contact with the material expressed in the following Eq. 3.18. While, water jet with a smaller diameter than the trabucular spacing (Tb.Sp.) can pass through the cavities of the bone without removing the bone itself and tubercular struts (Fig. 3.52a [117]), water jet with a larger diameter can cut through the bone (Fig. 3.52b [117]).

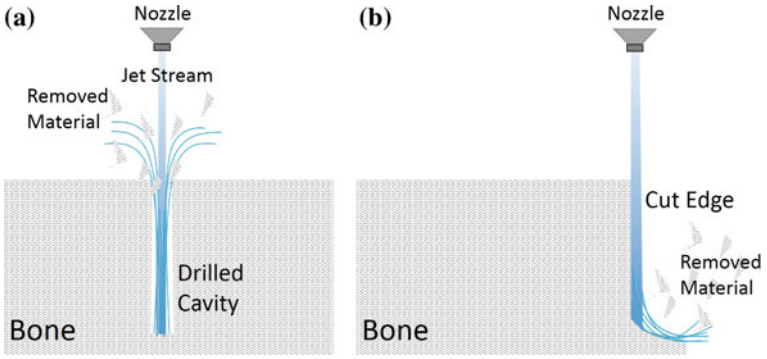

Fig. 3.51 Schematic of waterjet machining. **a** drilling and **b** cutting

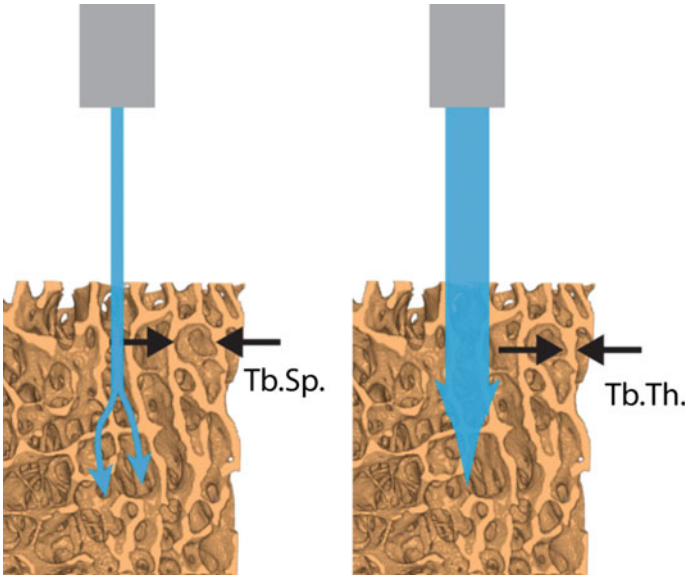

Fig. 3.52 Effect of jet diameter on its transmission during waterjet drilling of bone (Tb.Sb: trabecular spacing and Tb.Th: trabecualar thickness) (reprinted from Den Dunnen and Tuijthof [117] with permission. © Steven den Dunnen and Gabrielle Tuijthof)

$$Vol_{water} = \frac{1}{4}\pi D^2 V_{liquid}.t \tag{3.18}$$

where Vol_{water} is the volume of water (m^3), D (m) is the water jet diameter and t (s) is the time of interaction between the waterjet and material being cut and t is given by $D/V_{scanning}$, $V_{scanning}$ being the jet scanning/rastering velocity.

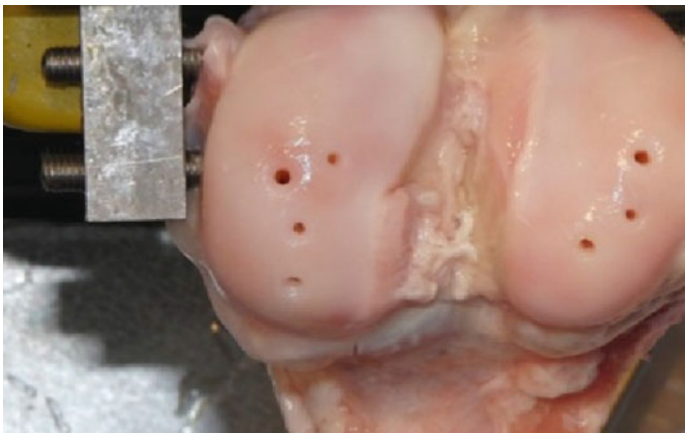

Fig. 3.53 Waterjet drilled holes in the famour bone (reprinted from Den Dunnen and Tuijthof [117] with permission. © Steven den Dunnen and Gabrielle Tuijthof)

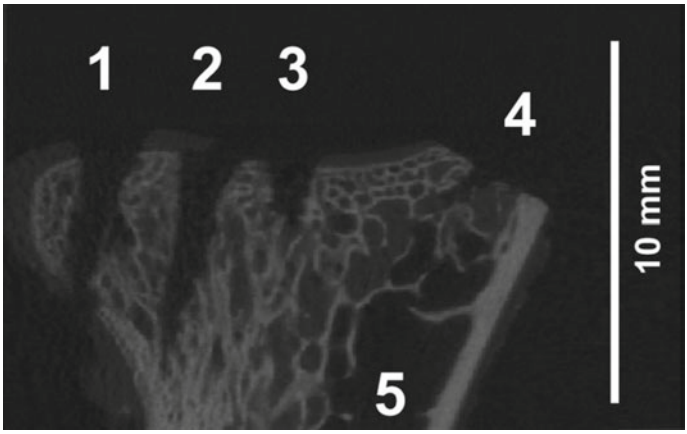

Fig. 3.54 A micro CT scan image of watetjet drilled holes in the goat bone. (*1*) full penetration of the bone, (*2*) and (*3*) cone shaped holes, (*4*) the sawed-off protrusion, and (*5*) natural cavity in the bone (reprinted from Dunnen et al [119] with permission. © Strojniški vestnik—Journal of Mechanical Engineering)

With this basis, actual trials of bone machining have been carried out. An example of drilling has been shown in Fig. 3.53 [117]. The precisely drilled holes are clearly seen. The similar technique was also used for making cuts and drill various shaped holes (Fig. 3.54 [119]). In the same publication, the mechanism of drilling of bones by waterjet was also suggested. Depending on the input waterjet pressure, various

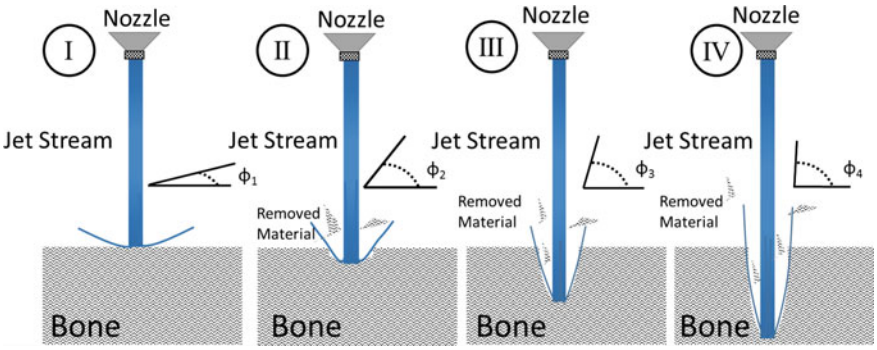

Fig. 3.55 Schematic of the stages in waterjet drilling as suggested in [119]: **I** reflection tangential to the surface, **II** small cavity changes reflection angle, **III** incoming and outgoing waterjets start to interfere, widening the hole beyond the waterjet diameter, and **IV** hole depth and diameter are further increased

responses from the bone are generated. If the pressure threshold is not met, the water jet gets reflected from the bone material and may damage surrounding organs or cartilage (Fig. 3.55a). As soon as the waterjet pressure threshold is reached, corresponding cuts are achieved with a small dent in the water jet and with increase in depth of cut the angle of reflection continues to increase (Fig. 3.55b). With further time, the hole widens greater than the jet diameter and hole depth becomes deeper with root diameter smaller than opening diameter giving the characteristic conical shape (Fig. 3.55c, d). In the same study, effect of pressure was investigated on human, sheep, goat, and pig bones and it was concluded that the pressure of 30 MPa was good enough for successful drilling in each case [117].

It is clear that, waterjet is suitable for machining of the bones, however, traditionally waterjet technology employs suspended abrasive particles [113]. Although this leads to faster machining, but in case of bones abrasive might pose some adverse issues. These include biocompatibility, excessive mechanical damage, and danger of residual particles. In order to deal with such issues, some of the biofriendly and soluble abrasives have been tried [118, 120]. Sugar and sorbitol were found comparatively effective. However, the bio friendly abrasives need further research in order to reach implementation stage. Another issue with waterjet technology is real time surgical application, where clamps used for research purposes are not feasible. A possible operation theater setup has been proposed. Similar to many non conventional techniques like laser, in case of waterjet machining the surgeons would need to undergo intense operational and safety training before it is implemented in clinical environments.

So far, the conventional and non-conventional techniques of bone machining have been discussed. Figure 3.56 summarizes these all techniques in the form of a flow diagram and summary of the key variables and process parameters along with important features of these machining techniques are presented in Table 3.5. While this chapter

Table 3.5 Parameters and key characteristics of non-conventional machining operations

Non-conventional method	Process parameters	Features
Laser	• Wavelength • Time of interaction • Input power • Beam diameter • Beam shape and pulse width	• A concentrated source of energy • Induces phase transformation from solid to liquid to vapor in short time frames • Optical properties of bone determine the laser wavelength absorbed • Available in variety of types, only some of those suitable for bone • Mechanism of ablation include thermal, photodisruption, photoablation, plasma ablation depending upon laser power and interactio time • Minimally invasive with superior healing • Performs various operations like cutting, drilling, grinding in a versatile manner
Microwave	• Input power • Generation frequency • Type of tool attached	• Microwave energy absorbed by the bone • Heats the bone via induction of atomic vibrations • Heat generated evaporates the fluids within the bone leading to ablation • Adaption of the technique is in developmental stage • Causes undesired damage and necrosis of the surrounding region
Ion Beam	• Accelerating voltage • Ion current • Type of ion source • Microwave energy absorbed by the bone	• Ions accelerated knock off the atoms within the bone • Very suitable for micro/sub micro level machining • Interaction region is very small resulting less damage

(continued)

Table 3.5 (continued)

Non-conventional method	Process parameters	Features
Ultrasonic	• Ultrasonic frequency • Rake angle • Longitudinal and transverse force • Applied static load • Types of abrasive	• Ultrasonic vibrations are transfered to a tool head under a static load • Employs abrasive particles along with the vibrating tool for material removal • Various types of tool head determine the machining action/operation • Abrasive slurry also acts a coolant • Material removal by micro chipping, abrasion, cavitation
Waterjet	• Waterjet diameter • Velocity of water • Head pressure	• Waterjet is a cutting tool • Waterjest also acts like a coolant • Precise machining in various operations such as cutting and drilling possible • Use of biofriendly abrasives can lead to increased machining rates without adverse effects

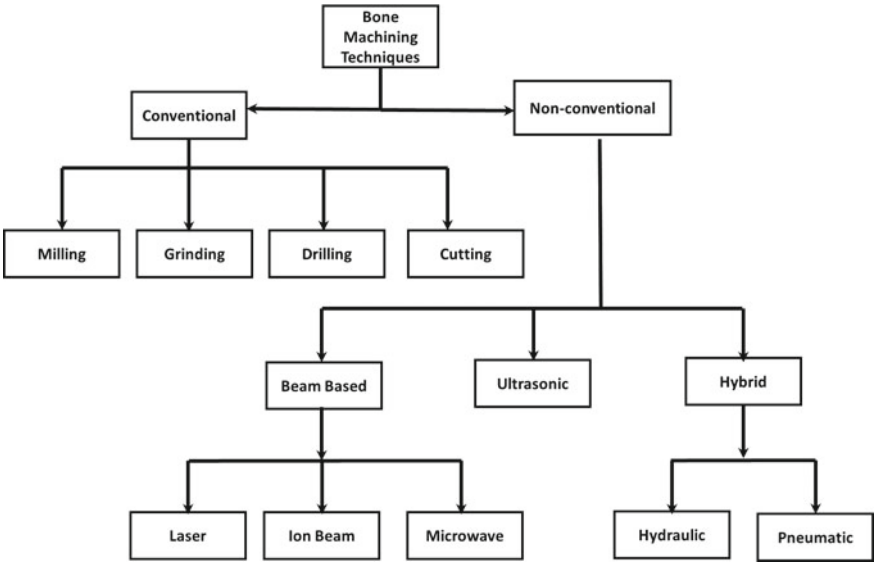

Fig. 3.56 Flow diagram summarizing all the conventional and non-conventional machining processes

has given basic description of these processes the following chapter carries forward the detailed discussion on physical attributes of bone machining such as machining forces and crack propagation.

References

1. H.J. Foth, *Principles of Lasers* (Wiley, New York, 2008)
2. N.B. Dahotre, S. Harimkar, *Laser Fabrication and Machining of Materials* (Springer Science & Business Media, Berlin, 2008)
3. R.E. Hummel, *Electronic Properties of Materials* (Springer Science & Business Media, Berlin, 2011)
4. M.H. Niemz, *Laser-Tissue Interactions: Fundamentals and Applications* (Springer Science & Business Media, Berlin, 2013)
5. E.P. Batterman, D.G. Chandler, Hand-held Bar Code Reader with Laser Scanning and 2D Image Capture (2001). US Patent 6,223,988
6. J. Mandal, S. Pal, T. Sun, K.T. Grattan, A.T. Augousti, S.A. Wade, Photonics Technology Letters. IEEE **16**(1), 218 (2004)
7. P. Urayama, W. Zhong, J. Beamish, F. Minn, R. Sloboda, K. Dragnev, E. Dmitrovsky, M.A. Mycek, Appl. Phys. B **76**(5), 483 (2003)
8. V.G. Gregson, *Laser Materials Processing*, pp. 201–233 (1983)
9. S.S. Joshi, A.V. Gkriniari, S. Katakam, N.B. Dahotre, J. Phys. D: Appl. Phys. **48**(49), 495501 (2015)
10. S.S. Joshi, P. Samimi, I. Ghamarian, S. Katakam, P.C. Collins, N.B. Dahotre, J. Appl. Phys. **118**(16), 164904 (2015)
11. S.S. Joshi, S. Katakam, H. Singh Arora, S. Mukherjee, N.B. Dahotre, *Critical Reviews in Solid State and Materials Sciences*, pp. 1–46 (2015)
12. A. Kurella, N.B. Dahotre, J. Biomater. Appl. **20**(1), 5 (2005)

13. H. Jelínková, *Lasers for Medical Applications: Diagnostics, Therapy and Surgery* (Elsevier, Amsterdam, 2013)
14. J. Moss, B. Patel, G. Pearson, G. Arthur, R. Lawes, Biomaterials **15**(12), 1013 (1994)
15. S. Chaiyavej, H. Yamamoto, A. Takeda, H. Suda, Lasers Surg. Med. **27**(4), 341 (2000)
16. S. Stübinger, K. Biermeier, B. Bächi, S.J. Ferguson, R. Sader, B. von Rechenberg, Lasers Surg. Med. **42**(7), 652 (2010)
17. M. Frentzen, H. Koort, Int. Dental J. **40**(6), 323 (1990)
18. U. Keller, in *Berlin-DL Tentative* (International Society for Optics and Photonics, 1991), pp. 282–288
19. D. Clarkson, Dental Update **19**(3), 115 (1992)
20. T.H. Maiman, *in Esentials of Lasers: The Commonwealth and International Library: Selected Readings in Physics* (Elsevier, Amsterdam, 1960), pp. 136–143
21. J.Y. Giraud, S. Villemin, R. Darmana, J.P. Cahuzac, A. Autefage, J.P. Morucci, Clin. Phys. Physiol. Meas. **12**(1), 1 (1991)
22. A. Kruusing, Opt. Lasers Eng. **41**(2), 307 (2004)
23. S. Rupprecht, K. Tangermann-Gerk, J. Wiltfang, F.W. Neukam, A. Schlegel, Lasers Med. Sci. **19**(2), 81 (2004)
24. T. Gudra, S. Muc, Eur. Phys. J. Spec. Topics **154**(1), 85 (2008)
25. K.M. Sasaki, A. Aoki, S. Ichinose, I. Ishikawa, Lasers Surg. Med. **31**(5), 322 (2002)
26. J.T. Walsh, T.F. Deutsch, Lasers Surg. Med. **9**(4), 327 (1989)
27. R. Wallace, C. Whitters, J. McGeough, A. Muir, J. Mater. Process. Technol. **149**(1), 557 (2004)
28. S.R. Paital, N.B. Dahotre, Mater. Sci. Technol. **24**(9), 1144 (2008)
29. C. Gonzalez, W.P. Van De Merwe, M. Smith, L. Reinisch, The Laryngoscope **100**(1), 14 (1990)
30. U. Romeo, A. Del Vecchio, G. Palata, G. Tenore, P. Visca, C. Maggiore, Braz. Dental J. **20**(2), 162 (2009)
31. K.W. Baek, W. Deibel, D. Marinov, M. Griessen, M. Dard, A. Bruno, H.F. Zeilhofer, P. Cattin, P. Juergens, Lasers Surg. Med. (2015)
32. M. Mehrwald, J. Burgner, C. Platzek, C. Feldmann, J. Raczkowsky, H. Wörn, in *BiOS* (International Society for Optics and Photonics, 2010), pp. 75,620P–75,620P
33. M.M. Ivanenko, T. Mitra, P. Hering, in *EOS/SPIE European Biomedical Optics Week* (International Society for Optics and Photonics, 2000), pp. 46–51
34. M. Ivanenko, M. Werner, S. Afilal, M. Klasing, P. Hering, Med. Laser Appl. **20**(1), 13 (2005)
35. A. McKenzie, Phys. Med. Biol. **35**(9), 1175 (1990)
36. M. Ivanenko, P. Hering, Appl. Phys. B **67**(3), 395 (1998)
37. K. Stock, R. Diebolder, F. Hausladen, R. Hibst, in *SPIE BiOS* (International Society for Optics and Photonics, 2014), pp. 89,263P–89,263P
38. J.T. Walsh Jr, D.A. Hill, in *Optics, Electro-Optics, and Laser Applications in Science and Engineering* (International Society for Optics and Photonics, 1991), pp. 27–33
39. K. Trauner, N. Nishioka, D. Patel, Am. J. Sports Med. **18**(3), 316 (1990)
40. J.P. Winkler, A temperature study of laser-irradiated bone. PhD Thesis, University of Tennessee, USA (1997)
41. B. Fink, T. Schneider, S. Braunstein, G. Schmielau, W. Rüther, Arthroscopy: J. Arthrosc. Relat. Surg. **12**(2), 217 (1996)
42. I.M. Stubig, P.A. Reder, G. Facer, H.G. Rylander, A.J. Welch, in *OE/LASE'93: Optics, Electro-Optics, & Laser Applications in Science& Engineering* (International Society for Optics and Photonics, 1993), pp. 10–16
43. L.R. Friesen, C.M. Cobb, J.W. Rapley, L. Forgas-Brockman, P. Spencer, J. Periodontol. **70**(1), 75 (1999)
44. Y.M. Lee, R. Tu, A. Chiang, Y.C. Huang, J. Biomed. Opt. **12**(6), 060505 (2007)
45. J.I. Youn, P. Sweet, G.M. Peavy, Lasers Surg. Med. **39**(4), 332 (2007)
46. J.S. Nelson, A. Orenstein, L.H.L. Liaw, M.W. Berns, Lasers Surg. Med. **9**(4), 362 (1989)
47. R.J. O'Donnell, T.F. Deutsch, T.J. Flotte, C.A. Lorente, W.W. Tomford, H.J. Mankin, K.T. Schomacker, J. Orthopaedic Res. **14**(1), 108 (1996)

48. A. Pourzarandian, H. Watanabe, A. Aoki, S. Ichinose, K.M. Sasaki, H. Nitta, I. Ishikawa, Photomed. Laser Therapy **22**(4), 342 (2004)
49. E.D.A. de Mello, R.M. Pagnoncelli, E. Munin, M. Sant, Ana Filho, G.P.S. de Mello, E.A.L. Arisawa, M.G. de Oliveira, Lasers Surg. Med. **23**(3), 253 (2008)
50. U.K. Akyol, M. Güngörmüs, C. Gündogdu, H. Erdem, J Contemp. Dent p. 2 (2009)
51. H. Pretel, R. Lizarelli, L. Ramalho et al., Lasers Surg. Med. **39**(10), 788 (2007)
52. J.T. Payne, G.M. Peavy, L. Reinisch, D.C. Van Sickle, Lasers Surg. Med. **29**(1), 38 (2001)
53. B.J. Garrison, R. Srinivasan, J. Appl. Phys. **57**(8), 2909 (1985)
54. D. Stern, R.W. Schoenlein, C.A. Puliafito, E.T. Dobi, R. Birngruber, J.G. Fujimoto, Arch. Ophthalmol. **107**(4), 587 (1989)
55. P. Teng, N.S. Nishioka, R. Anderson, T.F. Deutsch, IEEE J. Quant. Electron. **23**(10), 1845 (1987)
56. J. Neev, L.B. Da Silva, M.D. Feit, M.D. Perry, A.M. Rubenchik, B.C. Stuart, IEEE J. Sel. Topics Quant. Electron. **2**(4), 790 (1996)
57. D.D. Lo, M.A. Mackanos, M.T. Chung, J.S. Hyun, D.T. Montoro, M. Grova, C. Liu, J. Wang, D. Palanker, A.J. Connolly et al., Lasers Surg. Med. **44**(10), 805 (2012)
58. J. Ihlemann, B. Wolff, P. Simon, Appl. Phys. A **54**(4), 363 (1992)
59. M.L. Walter, M.E. Domes, R.A. Diller, J. Sproedt, U.H. Joosten, Lasers Surg. Med. **25**(2), 153 (1999)
60. R. Sarkar, R.L. Fabian, R.C. Nuss, C.A. Puliafito, Am. J. Otolaryngol. **10**(2), 76 (1989)
61. Y. Liu, M. Niemz, Lasers Med. Sci. **22**(3), 171 (2007)
62. B. Girard, D. Yu, M. Armstrong, B. Wilson, C. Clokie, R. Miller, Lasers Surg. Med. **39**(3), 273 (2007)
63. D.E. Clark, D.C. Folz, J.K. West, Mater. Sci. Eng.: A **287**(2), 153 (2000)
64. E. Thostenson, T.W. Chou, Compos. Part A: Appl. Sci. Manuf. **30**(9), 1055 (1999)
65. H.S. Ku, E. Siores, A. Taube, J.A. Ball, Comput. Ind. Eng. **42**(2), 281 (2002)
66. G.S. Gazelle, S.N. Goldberg, L. Solbiati, T. Livraghi, Radiology **217**(3), 633 (2000)
67. A. Copty, F. Sakran, M. Golosovsky, D. Davidov, A. Frenkel, Appl. Phys. Lett. **84**(25), 5109 (2004)
68. E. Jerby, V. Dikhtyar, Bayreuth (2001)
69. T.J. George, A.K. Sharma, P. Kumar, R. Kumar, S. Das, in *International Conference on Emerging Trends in Manufacturing Technology Toc H Institute of Science & Technology Kerela* (2012)
70. E. Jerby, V. Dikhtyar, *Advances in Microwave and Radio Frequency Processing* (Springer, Berlin, 2006)
71. Y. Eshet, R.R. Mann, A. Anaton, T. Yacoby, A. Gefen, E. Jerby, IEEE Trans. Biomed. Eng. **53**(6), 1174 (2006)
72. J.M. Choi, H.E. Kim, I.S. Lee, Biomaterials **21**(5), 469 (2000)
73. I.S. Lee, B. Zhao, G.H. Lee, S.H. Choi, S.M. Chung, Surface Coatings Technol. **201**(9), 5132 (2007)
74. T. Hayakawa, M. Yoshinari, H. Kiba, H. Yamamoto, K. Nemoto, J.A. Jansen, Biomaterials **23**(4), 1025 (2002)
75. Y. Chan, A. Ngan, N. King, J. Mech. Behav. Biomed. Mater. **2**(4), 375 (2009)
76. K.J. Altman, Microscale Machining and mechanical characterization of bone tissue. PhD Thesis, The Ohio State University, USA (2009)
77. K. Graff, Ultrasonics **13**(3), 103 (1975)
78. D. Kremer, S. Saleh, S. Ghabrial, A. Moisan, CIRP Ann. Manuf. Technol. **30**(1), 107 (1981)
79. T. Thoe, D. Aspinwall, M. Wise, Int. J. Mach. Tools Manuf. **38**(4), 239 (1998)
80. V. Kazantsev, L. Rosenberg, Ultrasonics **3**(4), 166 (1965)
81. B. Estabrook, S. DiMatteo, P. Smith, Damping ultrasonic transmission components (1999). US Patent 5,989,275
82. A.G. Nielsen, J.R. Richards, R.B. Wolcott, J. Am. Dental Assoc. **50**(4), 392 (1955)
83. L. Balamuth, Sound: Its Uses Control **2**(2), 15 (1963)
84. M.C. Catuna, Ann. Dent. **12**(3), 100 (1953)

85. W. Lefkowitz, J. Am. Dental Assoc. **52**(4), 406 (1956)
86. E.V. Street, J. Prosthet. Dentist. **9**(1), 132 (1959)
87. J.R. Richards, High frequency dental tool (1959). US Patent 2,874,470
88. B. Lewis, K. Manuel, K. Arthur, Ultrasonic dental and other instrument means and methods (1975). US Patent 3,924,335
89. A. John E. Brantly, M.B. Bowers, Fluid circulating dental drill and bit (1948). US Patent 2,442,033
90. J.E. Horton, T.M. Tarpley, J.R. Jacoway, Oral Surgery. Oral Med. Oral Pathol. **51**(3), 236 (1981)
91. B. Khambay, A. Walmsley, J. Dentist. **28**(1), 31 (2000)
92. A. Cardoni, A. MacBeath, M. Lucas, Ultrasonics **44**, e37 (2006)
93. M. Lucas, A. Cardoni, A. MacBeath, CIRP Ann. Manuf. Technol. **54**(1), 195 (2005)
94. A. Cardoni, M. Lucas, M. Cartmell, F. Lim, Ultrasonics **42**(1), 69 (2004)
95. M. Lucas, J. Petzing, A. Cardoni, L. Smith, J. McGeough, CIRP Ann. Manuf. Technol. **50**(1), 149 (2001)
96. M. Robiony, F. Polini, F. Costa, T. Vercellotti, M. Politi, J. Oral Maxillofacial Surg. **62**(6), 759 (2004)
97. T. Vercellotti, A. Crovace, A. Palermo, A. Molfetta, Medit. J. Surg. Med. **9**(4), 89 (2001)
98. D.J. Hoigne, S. Stübinger, O. Von Kaenel, S. Shamdasani, P. Hasenboehler, BMC Musculoskeletal Disorders **7**(1), 36 (2006)
99. M. Politi, T. Vercellotti, F. Polini, et al., in *Proceedings of the 2nd International Meeting on Distraction Osteogenesis of the Facial Skeleton, Bologna, Italy, September* (2002)
100. H. Aro, H. Kallioniemi, A. Aho, P. Kellokumpu-Lehtinen, Acta Orthopaedica **52**(1), 5 (1981)
101. A. Smith, A. Nurse, G. Graham, M. Lucas, Ultrasonics **34**(2), 197 (1996)
102. F.C. Barber, D.G. Tidwell, Replicator for resecting bone to match a pattern (1993). US Patent 5,190,547
103. G. Van Ham, K. Denis, J. Vander Sloten, R. Van Audekercke, G. Van der Perre, J. De Schutter, E. Aertbeliën, S. Demey, J. Bellemans, Comput. Aided Surg. **3**(3), 123 (1998)
104. M. Jakopec, S. Harris, F. Rodriguez y Baena, P. Gomes, J. Cobb, B. Davies, Comput. Aided Surg. **6**(6), 329 (2001)
105. V. Zegunis, S. Toksvig-Larsen, R. Tikuisis, Acta Orthopaedica **64**(5), 592 (1993)
106. K.D. Mimnaugh, J.Q. Yao, M.P. Laurent, R. Crowninshield, J.J. Mason, C. Blanchard, J. Arthroplasty **24**(2), 303 (2009)
107. T. Meredith, Composite bone material implant and method (2002). US Patent App. 10/128,219
108. P.T.J. Spiering. Mill, In particular for milling of bone, as well as a drum, provided with cutting members, applicable in the mill (2001). US Patent 6,318,651
109. J. Troccaz, P. Berkelman, P. Cinquin, A. Vilchis, in *Proceedings of the IARP Workshop on Robot Dependability, France* (2002)
110. S. Park, N. Kim, H. Shin, K. Lim, Y.S. Yoon, Int. J. Arm **8** (2007)
111. A. Malvisi, P. Vendruscolo, F. Morici, S. Martelli, M. Marcacci, in *Medical Image Computing and Computer-Assisted Intervention–MICCAI 2000* (Springer, 2000), pp. 1238–1244
112. J.H. Chung, S.Y. Ko, D.S. Kwon, J.J. Lee, Y.S. Yoon, C.H. Won, IEEE Trans. Robot. Autom. **19**(5), 885 (2003)
113. J. Folkes, J. Mater. Process. Technol. **209**(20), 6181 (2009)
114. D.A. Summers, *Waterjetting Technology* (CRC Press, London, 2003)
115. R. Kovacevic, M. Hashish, R. Mohan, M. Ramulu, T. Kim, E. Geskin, J. Manuf. Sci. Eng. **119**(4B), 776 (1997)
116. S. Hloch, J. Kl'oc, P. Hreha, D. Magurová, D. Kozak, L. Knapčíková, Hip **3500**(4000), 4500 (2013)
117. S. Den Dunnen, G. Tuijthof, Mech. Sci. **5**(2), 53 (2014)
118. P. Hreha, S. Hloch, D. Magurovd, J. Valicek, D. Kozak, M. Harnicdrovd, M. Rakin, Tehnicki Vjesnik **17**(2), 237 (2010)
119. S. den Dunnen, G. Kraaij, C. Biskup, G.M. Kerkhoffs, G.J. Tuijthof, Strojniški Vestnik-J. Mech. Eng. **59**(7–8), 425 (2013)
120. F. Pude, S. Schmolke, K. Schwieger, M. Honl, H. Louis, in *Proceedings of the 6th International Conference on Management of Innovative Technologies MIT2003, Ljubljana* (2003)

Chapter 4
Attributes of Bone Machining

Any machining operation has certain key attributes depending upon the material undergoing the process, the type of process, and choice of process parameters. In case of bones and hard tissues, which are composite materials, these attributes very much characterize the uniqueness of their machining operations. Having discussed the basics about state of the art of orthopedic surgery, nature of bones, and fundamentals of various machining processes (conventional and non conventional), the current chapter takes the discussion ahead with attributes of machining process. The key attributes considered here are

- Effect of microstructure
- Effect of aging
- Effect of machining parameters
- Crack propagation
- Chip formation
- Temperature rise

It is worth noting here that above mentioned attributes are equally important in case of all the materials. However, temperature rise becomes critically important due to thermally induced necrosis and hence, a need for careful control of temperature. In light of this, a separate chapter has been dedicated to temperature rise during machining of bones whereas other attributes have been discussed in the following sections.

4.1 Microstructure and Materials Aspects

As a result of composite nature of the bone, the mechanical and thermal loading direction critically determines the response of bone to the mechanical machining. However, Factors such as porosity, mineralization, orientation, diameters and spacing of collagen fibers, and other aspects of histological structure play a deterministic role in case of mechanical response and thus the machining process as well [1, 2]. This makes a distinct impact in differentiating the material response in case of a

N.B. Dahotre and S.S. Joshi, *Machining of Bone and Hard Tissues*,
DOI 10.1007/978-3-319-39158-8_4

homogeneous and a complex material such as bone. This situation is illustrated in Fig. 4.1 [1], which shows (a) various loading directions in a bone, formation of microcracks in (b) homogeneous material and (c) bone. In a transverse direction, the important responses of bone constituents to mechanical loading have been tabulated in Table 4.1. In addition, it has also been reported that, bones are much stronger when loaded in either compression or tension in longitudinal direction. On the other hand, even though the overall strength of bone drops down in transverse loading, it reflects higher strength in compression than tension. It has been well documented in the literature that the mechanical response changes drastically depending upon loading

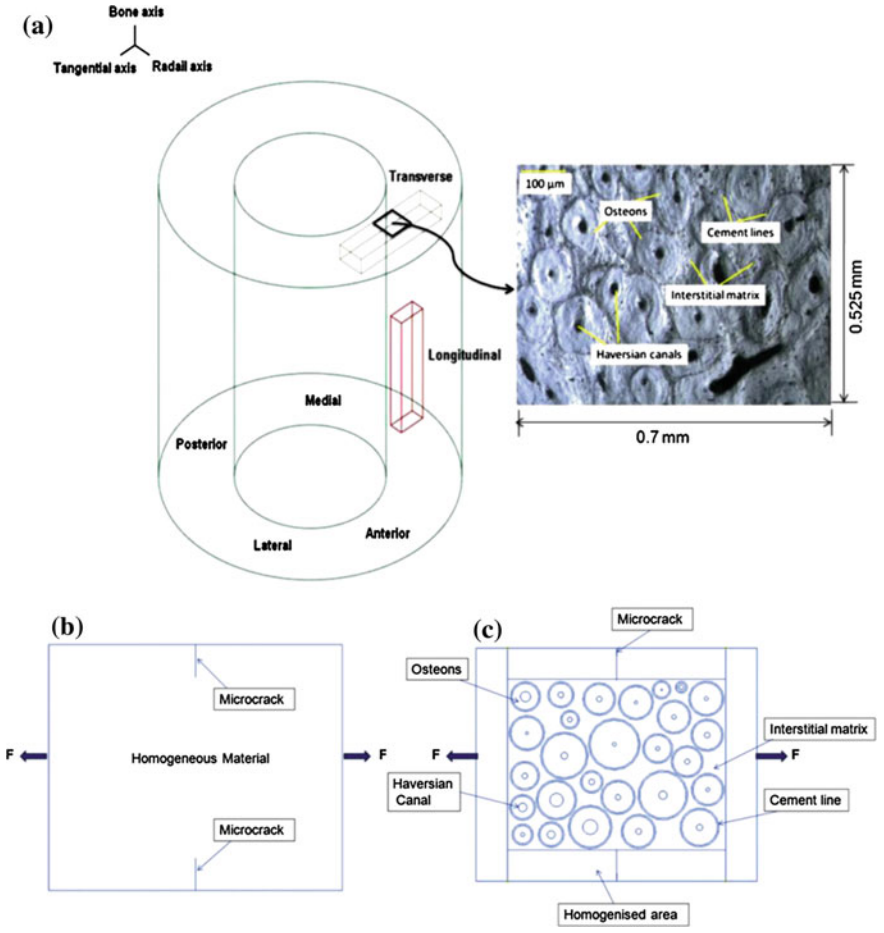

Fig. 4.1 An osteonal bovine cortical bone tissue. **a** Optical micrograph of cross sectional view and its position in transverse-radial cross-section and schematic illustration of mechanical response of **b** homogeneous material, and **c** bone (reprinted from Abdel-Wahab et al. [1] with permission. © Elsevier)

Table 4.1 Mechanical properties of various microstructural components of bone

Component	Elastic modulus (GPa)	Poisson's ratio	Strain energy release rate (N/mm)
Osteons	9.13	0.17	0.86
Interstitial matrix	14.1	0.15	0.23
Cement lines	6.85	0.49	0.14

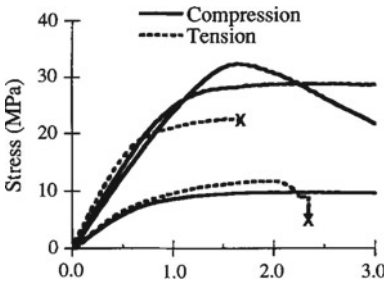

Fig. 4.2 Typical stress-strain curves for compressive (*solid lines*) and tensile (*dashed lines*) loading of bone specimens with different moduli. The tensile specimens fractured as shown (X). These curves illustrate how the difference between the tensile and compressive strengths is large for high modulus specimens, but small for low modulus specimens (reprinted from Keaveny et al. [3] with permission. © Elsevier)

direction (Fig. 4.2 [3]) and orientation of microstructural features with respect to it [4]. Furthermore, studies into the internal structure of the bone reveal prevalence of anisotropy and heterogeneity. This makes it more difficult to predict the exact response of bone to machining operation. In another of such studies [5], it was concluded that heterogeneity and anisotropic nature of the bone have a direct effect on the properties at continuum level. As a result of anisotropy, the elastic modulus was observed to vary 50–100 folds in the region of similar metaphysis. Another good example depicted in Fig. 4.3 [6], which clearly shows that elastic modulus in various loading modes is heavily influenced by apparent bone density. Therefore, it was recommended that properties of bone be reported along with its type, loading direction, anatomic site, and age.

This brings the discussion to another variable, that is the age which critically influences the bone regeneration based on diet habits, geographic location, and gender. Giving attention towards the fact that bone is a living organ, it undergoes continuous changes with respect to its structure. Inherent ability of repair results in regeneration of the damaged bone. However, as the bones age, this ability continuously reduces which is a clear indication of reduction in ultimate tensile strength (UTS) with increase in age shown in Fig. 4.4.

It has been reported that, even exercise does not improve the response of aged bones to loading [8]. In fact, the porosity of bony structure has been reported to increase with age as indicated in the results predicted by aging model (Fig. 4.5)

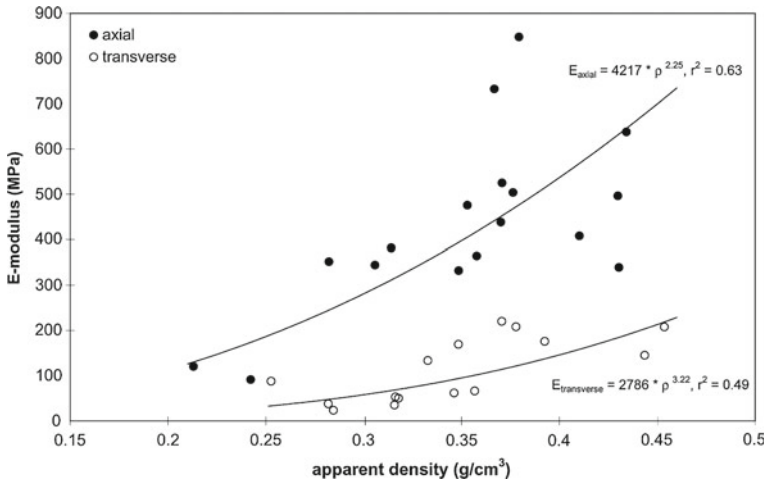

Fig. 4.3 Scatter plot of E-modulus versus apparent density, *filled circles* axial-group, *open circles* transverse-group. The fitted line through each group is the power relationship shown in the figure (reprinted from Giesen et al. [6] with permission. © Elsevier)

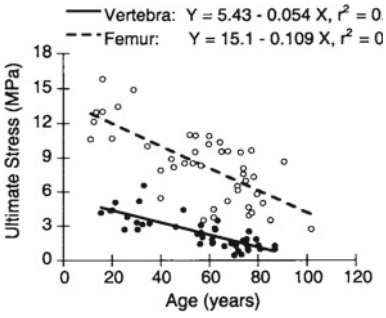

Fig. 4.4 Dependence of ultimate stress on age for trabecular bone from the human vertebra and femur. For both anatomic sites, strength decreases approximately 10 %/decade (reprinted from Kutz [7] with permission. © McGraw Hill)

[9]. It has also been reported that, even though the porosity increases with age, the mineral content is not greatly affected by age [10]. At the same time, linear regression analysis has indicated that ultimate tensile strength, ultimate strain, and energy absorption decrease by 5, 9, and 12 % respectively per decade as the bone ages. Furthermore, the same study also indicated that increase in porosity predominantly contributed to reduction in strength. In addition to age, the gender is also considered as a determining factor. It was reported that female bones underwent compensatory hypertrophy (increase in size to perform work of dead tissues) which did not happen in case of male bones.

Thus it is very much clear that as a result of highly heterogeneous and continuously changing nature of bones, it is highly difficult to exactly predict the bone response to

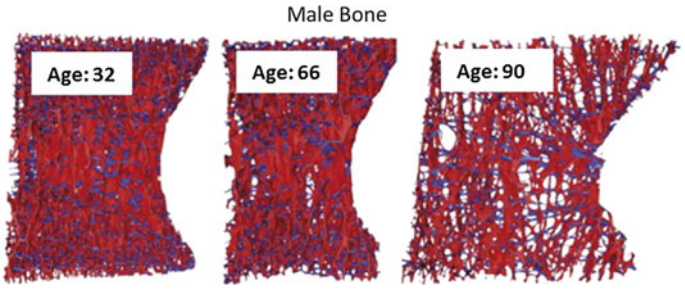

Fig. 4.5 Effect of aging on male trabecular bone (reprinted from Thomsen et al. [9] with permission. © Elsevier)

machining. The macro-level mechanical response of bones is heavily dependent on loading direction with respect to various micro level constituents. In addition, factors such as age and gender also play a very critical role. This discussion overall points towards designing a patient specific treatment in order to achieve higher success rates in case of orthopedic treatments.

4.2 Effect of Machining Parameters

Apart from material undergoing the machining, the choice of parameters also plays a key role in determining the overall outcome of the machining. In the current section, important parameters with respect to general mechanical machining processes have been discussed. These parameters include

- Applied force/load
- Cutting speed
- Feed rate
- Depth of machining
- Rake angle
- Tool dimensions
- Generated torque

In general, it is accepted that the applied force, whether it is a conventional tool or ultrasonically assisted tool, should not exceed the safe limit of material (fracture strength, thermal strength, and carbonization or necrosis temperature). The excessive force as discussed in previous chapters may lead to undesirable mechanical damage as well as thermally driven necrosis in the bone and hard tissues. In addition, there is a large variation in force as a result of heterogeneous structure of bone as discussed previously. Another important aspect produced by the force is torque. So, the average forces timed over the whole machining process gives a better insight and can be henceforth be compared to the forces predicted by the modeling exercises. As feed rates and speeds increase, torque values witness a surge along with a slight increase on the thrust values.

Torsional yielding in a human cortical bone was investigated for the effect of torque [11]. A correlation was drawn with the damage density and stiffness degradation was evaluated. Since the bone is exposed to severe thrust forces and torques for the purpose of cutting through it, it is important to ensure that the torque experienced by the bone during the cutting operation does not exceed the torsional yield point of human bone. In the latter case, the properties of the human bone will undergo undesirable changes and issues concerning bio-compatibility would arise. Finite element analysis has been time and again used to calculate the force and torque parameters during the cutting process. Real-life bone cutting conditions were simulated and the bone-tool interaction predicted based on various parameters. Cutting force as function of depth of cut, tool velocity, lubrication, coolant, and tool nose radius have been established. The final conclusion was that the material removal rate (MRR) and lubricating conditions (oil, coolant, fluids, the flow rate, additives) have the most profound impact on the cutting force. Utilizing the crucial information reported in works of Alam et al. [12], bone machining procedures can be optimized and can be done using minimum invasion. The force analysis has been primarily focused upon. Additionally, estimation of torque was carried out simultaneously by Jacob et al. [13] and the findings were reported in their research paper on bone drilling and graphically presented in Fig. 4.6 as comparison between computationally and experimentally derived torque as function of rotational speed during bone drilling operation. The summary of observations is presented below.

1. As the depth of cut decreases, the specific cutting force experiences an increment which can be justified by the theory on size effect. These observations comply with the expected results as per the Modified Merchant Analysis.
2. The specific cutting force is a function of depth of cut only (Fig. 4.7 [14]).
3. The shear strength measured in a direction perpendicular to the bone axis is double that in the other two directions due to the presence of the osteon that has spiral collagen fibers.

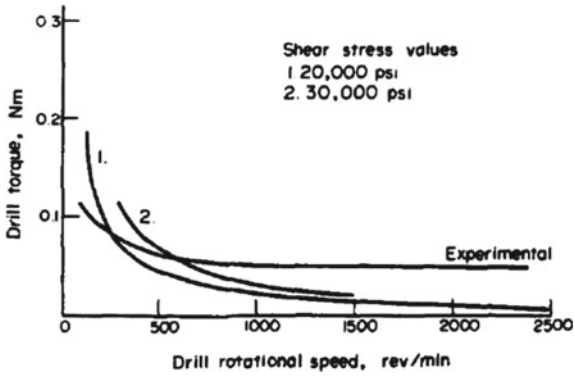

Fig. 4.6 Comparison of torque estimated by Cook model with experimental data as a function of rotational speed in drilling of bone (reprinted from Jacob et al. [13] with permission. © Elsevier)

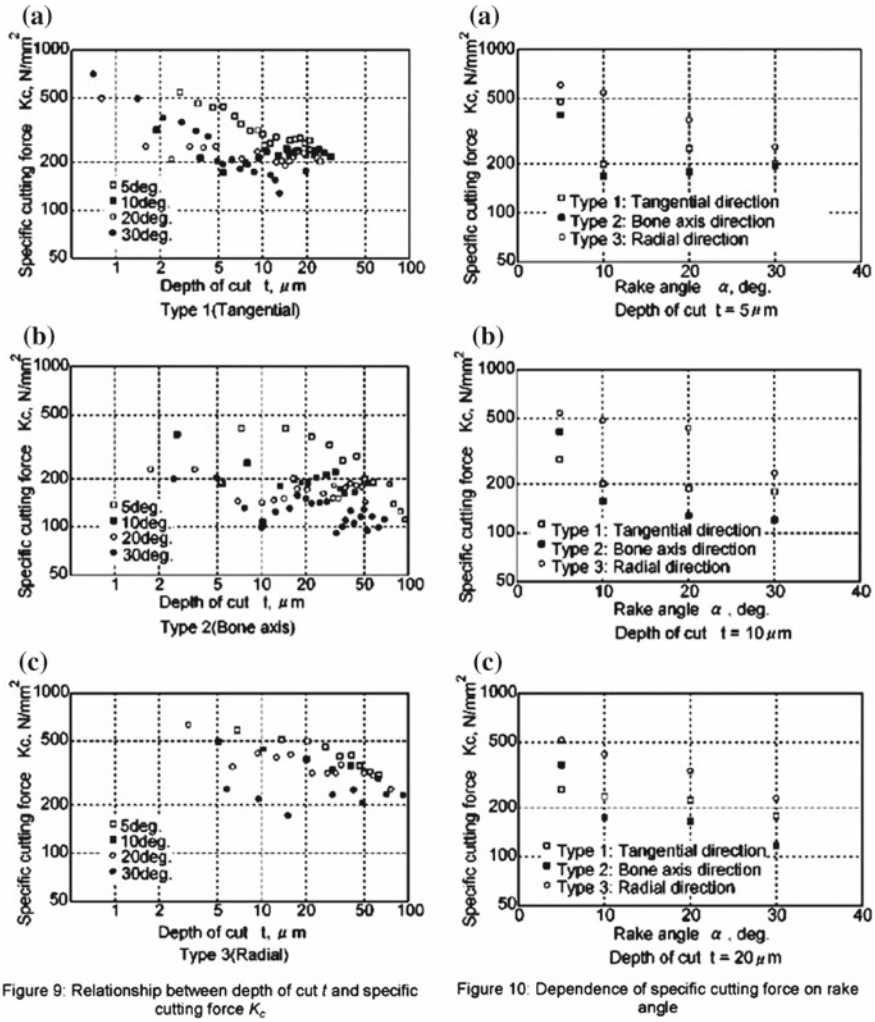

Fig. 4.7 Dependence of specific cutting force on depth of cut, rake angle, and specific cut angle (reprinted from Mitsuishi et al. [14] with permission. © Elsevier)

Another study conducted orthogonal cutting experimentation on bovine cancellous bone specimens [15]. Variations were made in cutting speed, rake angle, and depth of cuts. The final objective was to attain a particular set of these variables which would ultimately contribute to reducing the specific cutting energy, avoid unnecessary and undesirable fragmentation, and also assist in extrusion of the bone marrow. It was observed that specific cutting energy reduced as both the cutting speed (Fig. 4.8 [15]) and the depth of cut increased (Fig. 4.9a [15]). The optimum results corresponded to a 60° tool rake angle (Fig. 4.9b [15]).

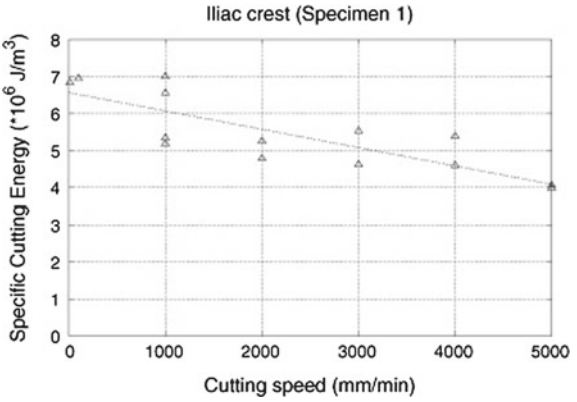

Fig. 4.8 Specific cutting energy as a function of cutting speed (reprinted from Malak and Anderson [15] with permission. © Elsevier)

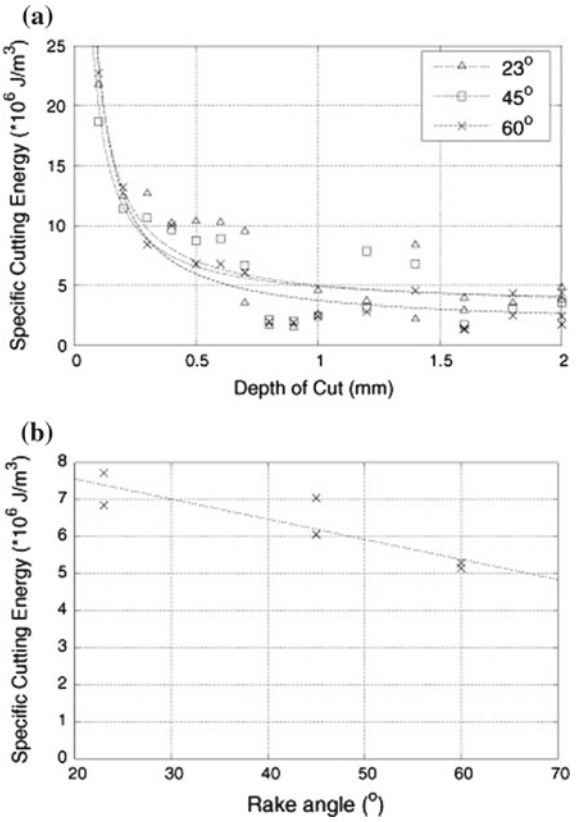

Fig. 4.9 Specific cutting energy as a function of depth of cut for various rake angles in case of **a** femur and **b** iliac crest bone (reprinted from Malak and Anderson [15] with permission. © Elsevier)

4.3 Crack Formation and Propagation

Crack formation and propagation is an important attribute of machining process as it governs the way bone fails during machining and finally resulting in material removal. It also reflects the toughness of the bones. The toughness depends on type of loading and direction of crack propagation. Basic mechanisms of crack generation and propagation are classified in three modes as Mode I: crack opening where loading direction is perpendicular to prorogation; Mode II: in plane shearing where loading direction is in plane and parallel to propagation; Mode III: tearing where loading direction is in shear to the propagation (Fig. 4.10 [16]).

Toughness is mainly governed by not the composition but the way constituents are arranged within the bone which dissipate the energy effectively [17]. For example, Table 4.2 quotes fracture toughness of various anatomic sites in terms of fracture energy release rate G_{Ic} in Mode I loading and G_{IIc} in Mode II loading respectively [18]. The general mechanisms of toughening are viscoplastic flow in case of gel like substances or polymers which toughen by formation of non connected microcracks. In case of ceramics however, the toughening takes place by crack bridging and deflection. Interestingly, owing to the composite nature of of the bone, all of these modes have been found to be operative in bones [19–27]. Interesting observation about crack path angle relative to collagen fibrils was made by Peterlik et al. [17]. Their observations indicated that depending upon these values, the bone transitions from totally brittle to ductile fracture. Such a behavior is indicated in Fig. 4.11a [17] where in variation of crack extension energy is shown as a function of collagen

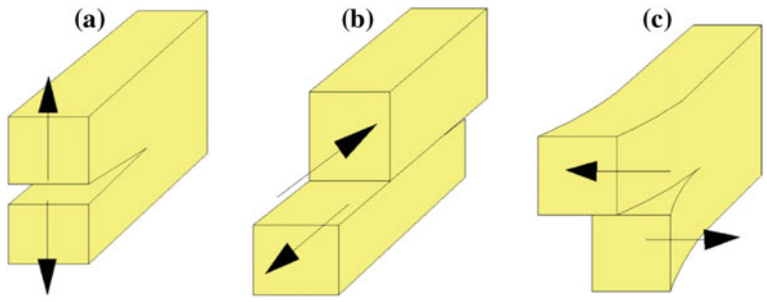

Fig. 4.10 Main modes of fracture displacements in reference to loading conditions in an isotropic material **a** Model I (Opening). **b** Model II (In-Plane Shearing). **c** Model III (Tearing) (reprinted from Liao and Axinte [16] with permission. © Elsevier)

Table 4.2 Site specific fracture toughness values of bone anatomies

Anatomic site	Femoral neck	Femoral shaft	Tibial shaft
$\mathbf{G}_{Ic}$	1128 ± 344	706 ± 288	816 ± 327
$\mathbf{G}_{IIc}$	5642 ± 1272	1817 ± 1090	5570 ± 1749

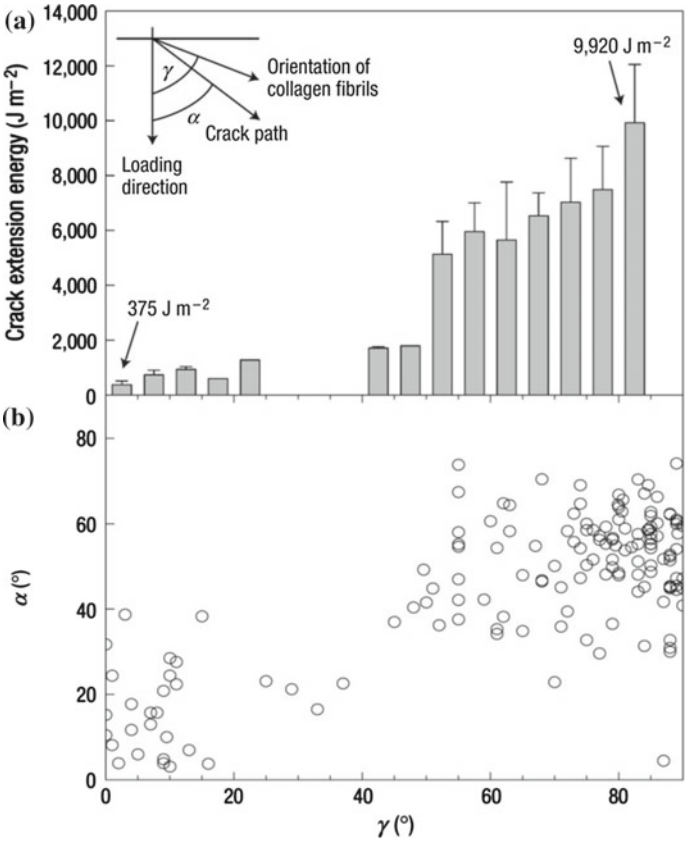

Fig. 4.11 Crack extension as a function of the collagen angle γ. **a** The energy required for crack extension and **b** the standard deviation of the crack path angle α (reprinted from Peterlik et al. [17] with permission. © Nature Publishing Group)

orientation. As the angle gets larger, the energy required is more indicating transition from ductile to brittle type of behavior. In addition, variation in crack path orientation with respect to loading direction was monitored as a function of collagen orientation (Fig. 4.11b). This plot also indicated a similar trend with an increase in value for large angle of collagen fibril orientation.

To further investigate such a behavior, the cracks in different modes were carefully observed in micrographs (Fig. 4.12) [17]. When the orientation of the cracks was aligned perfectly with the fibrils, the crack surface appeared smooth indicating predominantly brittle mode of fracture (Fig. 4.12a). Furthermore, when the crack became perpendicular, the crack surface became zig zag in nature with heavy distortion and torn areas (Fig. 4.12b). This confirmed the transition from brittle to ductile mode. Another study trying to probe the ductile to brittle transition pointed out the importance of water content in fracture toughness evaluation [4]. It was reported that water content greatly helped in increasing the fracture toughness. Furthermore,

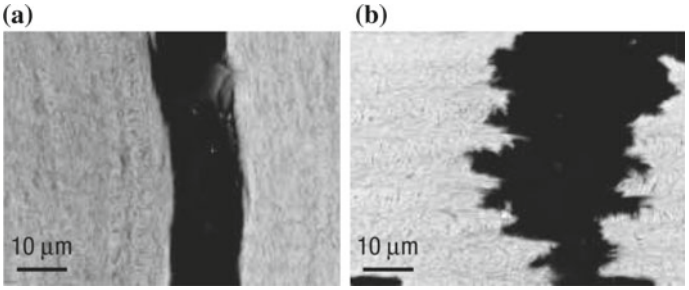

Fig. 4.12 Scanning electron micrographs of the crack path. **a** Longitudinal crack extension, where the crack flanks appear straight and smooth, and **b** circumferential crack extension, where the crack flanks appear deflected and heavily distorted (reprinted from Peterlik et al. [17] with permission. © Nature Publishing Group)

the plastic component of the fracture toughness was found to be higher by 80 % in wet specimen. In the same study, it was also reported that with an increase in crack length, the value of apparent fracture toughness also increased.

Another study noted that irrespective of age and gender, the human bones possessed greater resistance to crack growth under shear than the tension [28]. The tensile fracture toughness had a value of 339 N/m compared to 4200 N/m of shear toughness. It was concluded that bone has inherent crack growth prevention mechanism because of its microstructural features in shear which also is concurrent with natural design where majority of the loading on bone and joints is compressive or shear. In addition, another important observation made was that the bone toughness is equivalent in men and women and bone toughness gradually decreases with age 55 and beyond. Furthermore, the mechanism of decrease in fracture toughness was investigated in a separate study [29]. Age-related embrittlement of bone fracture was linked to the higher near-tip strains by lamellar shear and crack deflection at lamellar interfaces in the young bone and their absence in the old bone [29]. The chemical changes in the bone also play a role. The different near-tip deformation behaviors were considered to be driven by presence of Si and Zn in the young bone but more Ca and P along with the lack of Si and Zn in the old bone.

In order to achieve further understanding about microcrack mechanism which is generally how the toughening in bones takes place, fracture toughness tests were conducted [30]. When the samples were put in the scanning electron microscope for further evolution, the researchers observed a frontal process zone and a notable process zone similar to those in quasi-brittle solids. It was also reported that the crack propagation velocity and crack extension obey an inverse relationship with each other [30]. The schematic of crack propagation model characteristics are presented in Fig. 4.13 [30].

Furthermore, the crack propagation model was compared to crack initiation model by the same investigators [31]. It was found that the slope of crack-growth using the crack-propagation mode presents a more realistic framework to evaluate fracture toughness instead of parameters derived from the crack-initiation model. The crack growth resistance increased as a function of square root of crack extension (Fig. 4.14).

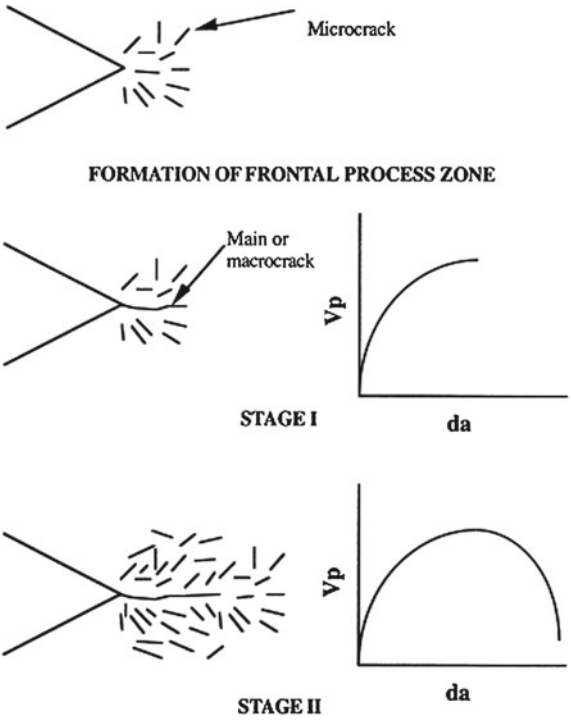

Fig. 4.13 Schematic of crack propagation model showing the development of microcracking in cortical bone. The application of loading initially results in the formation of microcracks around the notch. With continued loading a main crack originates from the notch and accelerates through this zone (Stage I). Acceleration of the main crack brings it into uncracked material decelerating the crack. Microcrack formation occurs ahead and behind the tip of the main crack as it moves slowly under continued loading (Stage II) (reprinted from Vashishth et al. [30] with permission. © Elsevier)

Formation of microcarks during the propagation of the main crack actually mitigated further growth of the main crack. It was also emphasized that initiation of a crack is not a crucial step for fracture; rather it is the ease of growth or penetration through the bone is the key step in the whole process.

In actual day to day life, the bone experiences variation in loading cycle and hence undergoes fatigue loading. One of the initial studies on fatigue loading of bones investigated the effect of nature of strains [32]. The bone specimens subjected to tensile strains generated an extensive network of fine cracks at ultrastructural level. On the other hand, those subjected to compressive strains generated linear cracks at the interstitial sites. It has also been reported that, if the bone is loaded beyond its yield strength followed by unloading and reloading, there is a significant reduction in elastic modulus [7, 33–36]. This behavior is schematically illustrated in Fig. 4.15. Another important parameter that characterizes the fatigue behavior is the secant modulus defined by secant drawn from the loading point to the first unloading point [7, 36, 37]. It is usually accepted that 5 % reduction in secant modulus results in fatigue failure leading to rapid decrease in stiffness and a failure [37, 38]. Such reduction in modulus is accompanied by increased dissipation of mechanical energy per loading cycle [7, 39]. A general empirical law was derived from strain amplitude controlled tests for expressing fatigue behavior of human femoral cortical bone according to Eq. 4.1 [39].

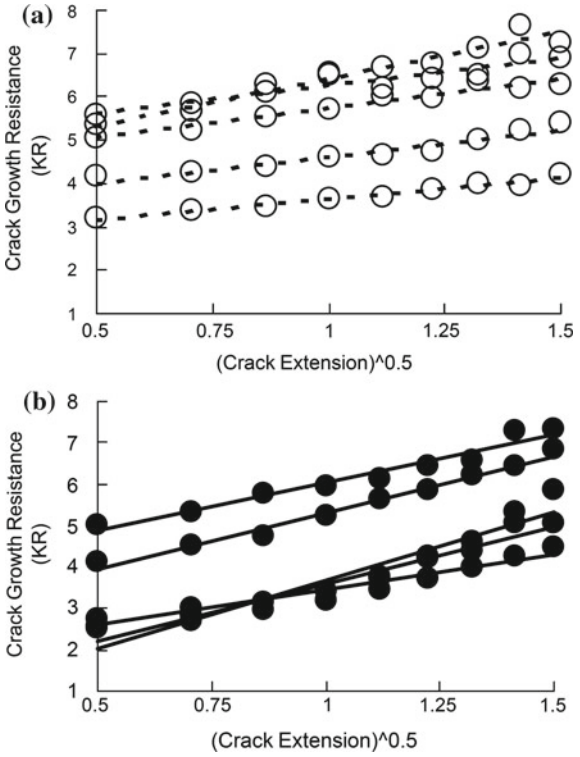

Fig. 4.14 Crack growth resistance (KR) versus crack extension of cortical bone of **a** bovine and **b** antler. Each line represents one specimen. The coefficients of linear regression (r^2) for bovine bone specimens were 0.86, 0.93, 0.94, 0.95 and 0.96. The coefficients of linear regression (r^2) for antler bone specimens were 0.90, 0.95, 0.95, 0.96 and 0.98 (reprinted from Vashishth [31] with permission. © Elsevier)

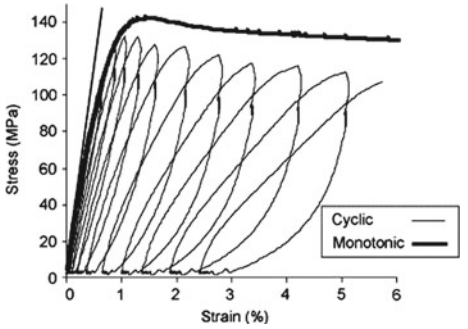

Fig. 4.15 Comparison between the stress-strain curve of monotonic loading test and the envelop of the stress-strain curve of the progressive cyclic loading test on bone specimens from the same donor (reprinted from Leng et al. [36] with permission. © Elsevier)

$$N_f = (2.94 \times 10^{-9})\Delta\epsilon^{-5.342} \tag{4.1}$$

where N_f is the number of cycles to failure, and $\Delta\epsilon$ is the applied strain amplitude. In addition, creep strains were found to be associated with the fatigue loading. When fatigue and creep behaviors are expressed as functions of stress to modulus versus

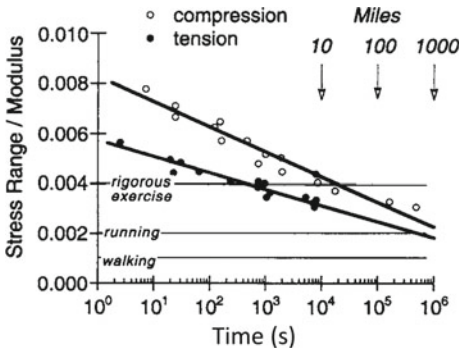

Fig. 4.16 Fatigue and creep behaviors of human cortical bone versus time to failure. For fatigue loading, the ordinate on this graph can be converted to number of cycles by multiplying the time to failure by the frequency, which is typically one cycle per second for normal walking. Note that both creep and fatigue resistance are lower in tension, consistent with monotonic behavior (reprinted from Carter et al. [39] with permission. © Taylor & Francis Ltd (www.tandfonline.com))

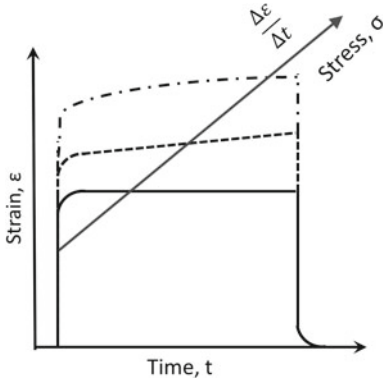

Fig. 4.17 Schematic of creep response of cortical bone for three different stress levels. When a low stress is applied to the bone, the strain remains constant over time, and there is no permanent deformation after unloading. For stresses just below yield, strains increase with time at a constant rate, and a small permanent deformation exists after unloading. As the magnitude of the stress is increased, the rate of creep increases, and a larger permanent deformation exists after unloading

time to failure, fatigue life is independent of frequency (0.2- to 2.0-Hz range), and substantial similarities appear between the fatigue and creep behaviors (Fig. 4.16). It further confirms that in general, bones act stronger in compression than tension. It also points out that the exercise schedule should be carefully controlled. From machining point of view, the bone under machining should not be subjected to higher stress in any case and stress duration has to be cautiously controlled depending upon patient specific nature of bone. Furthermore, as expected, the stress level plays a critical role in determining level of generation of creep strains (Fig. 4.17 [40]). At low stress levels, the creep stress generation rate is zero whereas it gradually increases for intermediate stresses and rapidly for higher stresses.

Effect of temperature was investigated on bone fatigue behavior [41]. It was concluded that, with reduction in temperature from 45 to 21 °C, the fatigue life of bone improved thrice (Fig. 4.18 [41]). Even-though, these observations clearly indicates that people living in moderate temperatures would have better bone fatigue performance, the results in sub-zero temperature conditions were not reported and further research is needed to get complete picture. In the same study, it was also shown that an increase in mineral density by 6 % enhanced the fatigue life by threefold. The same group further investigated the effect of bone type on fatigue behavior [41]. It was reported that the secondary bones were much weaker in fatigue as a result of lower density and inherently weak structure (Fig. 4.19 [42]).

Another study reported that during a mix fatigue loading of the bone, the compressive strains are predominant [43]. A number of fluorescent chelating agents were applied to intricately monitor the changes accompanying the straining procedure. It was also observed that the crack growth was large. The barrier effects were offered by the cement lines (boundaries between osteons). In addition, the longitudinal cracks were lengthier than the transverse cracks. On microstructural level, an investigation related to fatigue cracks indicated that micro cracks of short length (lesser than 100 μm) were completely inhibited by cement lines encompassing osteons [44]. However, with an increase in the crack length to those of intermediate range (100–300 μm) the cracks had their path deviated from the main course. Cracks longer than 400 μm failed to inhibit the growth. It was concluded that under certain cyclic

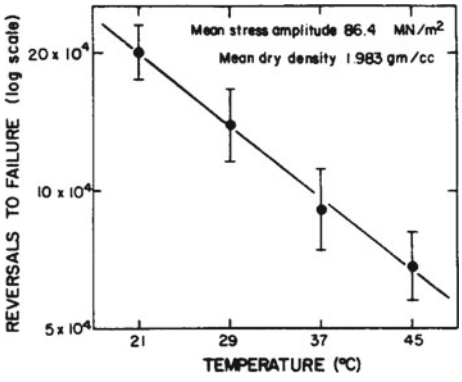

Fig. 4.18 Reversals to failure against bone temperature (reprinted from Carter and Hayes [41] with permission. © Elsevier)

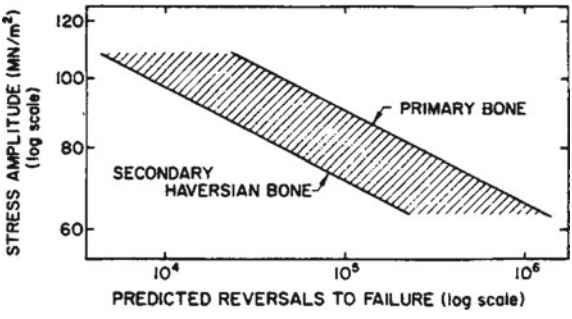

Fig. 4.19 Fatigue behavior of primary and secondary bones (reprinted from Carter et al. [42] with permission. © Elsevier)

loading, it becomes more essential to prevent propagation than initiation of cracks in bones because micro-cracks keep originating on the surface due to the cyclic stress sustained by the bone.

Important attribute that follows after crack formation and propagation is the chip formation. The chips are the footprints of the material undergoing machining as well as the machining parameters employed. Following section elucidates the importance of chip formation, key mechanisms, and how the process parameters should be controlled to obtain the desired quality chips with appropriate length and continuous in nature.

4.4 Chip Formation

During any machining process, independent of type of material, the process of material removal takes place in the form of chip formation. Investigating such a removed of material can provide important information regarding overall process of machining as well as the microstructural changes during that process. Also, key information can be extracted with regards to the improvement in the choice of machining parameters, improvements in tool/tool tip design or additional changes such as cooling systems. Another important aspect of chips is that they are also chunk of heat carrier. Main reason behind this is very high surface to volume ratio associated with them. Chips can form in various forms such as continuous, discontinuous, and intermittent fragments. They not only provide evidence of the type of machining but also nature of material (brittle or ductile.)

The process attributes which drastically influence the process of chip formation are depth of cut, tool velocity, and rake angle. In case of rake angle, the higher values are preferred for continuous chip formation [15]. This is illustrated by a photograph of chips forming in real time at a tool rake angle of 23° compared to 45° (Fig. 4.20 [15]). In first case, just by visual observation, one can easily make out the brittle nature of the bone being cut. On the other hand, an increase in rake angle transforms the chip to a continuous one very similar to the one observed in case of ductile metals. The physical reason considered behind such a change in behavior is, with an increase in cutting rake angle, the force eases out. Another important observation made about processing parameters is that the depth of cut has equal importance as that of rake angle concerning chip formation. It was observed that as the depth of cut increased the mechanism of chip formation changed from shear plane driven to discrete fracture.

Another investigation reported about the chip formation behavior as a function of uncut chip thickness (UCT) and relative orientation of osteons with respect to the tool (Fig. 4.21 [16]). It was observed that chip formation for minimum UCT in the parallel direction was easiest. Even though, the chip formation looked similar in all directions and uncut chip thicknesses, the closer observation clearly indicated the difference in fracture direction. In addition, as the UCT increased the fractured length also increased. Similar observation has also been reported by other investigators as

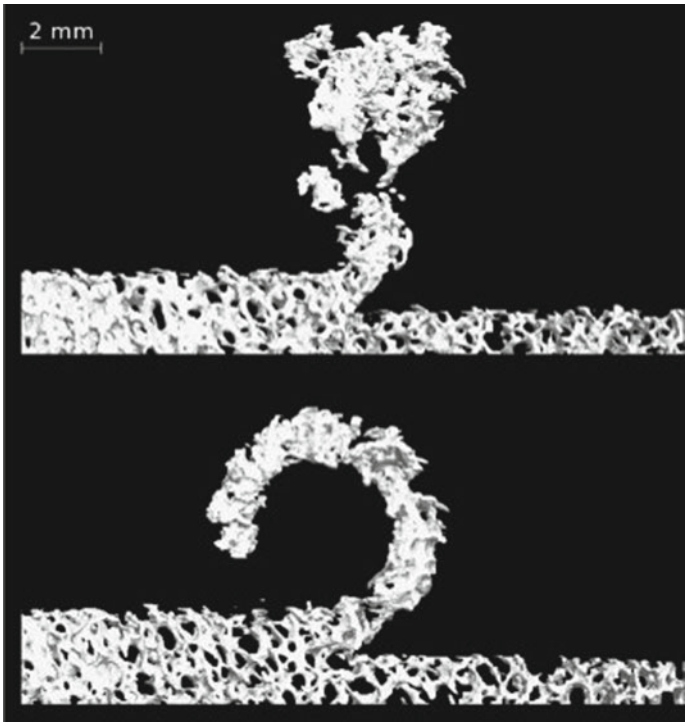

Fig. 4.20 CT scans showing discontinuous chip at rake angle of 23° (*top* photograph) and continuous chip for rake angle of 45° at 1.2 mm depth of cut (*bottom* photograph) (reprinted from Malak and Anderson [15] with permission. © Elsevier)

well (Fig. 4.22 [45]). Furthermore, irrespective of the cutting direction, as UCT increased, the mode of chip formation changed. These mechanisms are described below.

- **Shear Cutting (SC) Mode**: This model is valid for smaller depth of cut. The bone behaves like a ductile material in this regime. The energy released is smaller than fracture toughness and thus fracture does not take place, forming the chips in continuous manner instead. The heat is concentrated in narrow band of deformation zone and plastic deformation is predominant.
- **Shear Crack Cutting (SCC) Mode**: As the UCT increases, the chip morphology becomes zig-zag in nature. The chip formation starts by accumulation of the plastic deformation. The energy released soon exceeds the energy released during mode II fracture of the bone. As a result, the visible crack forms, thus the name shear crack cutting.
- **Fracture Cutting (FC) Mode**: With further increase in UCT, the fracture energy exceeds in all the directions. Cracks formed have mixed mode I and mode II nature. The propagation takes place in the direction of cutting.

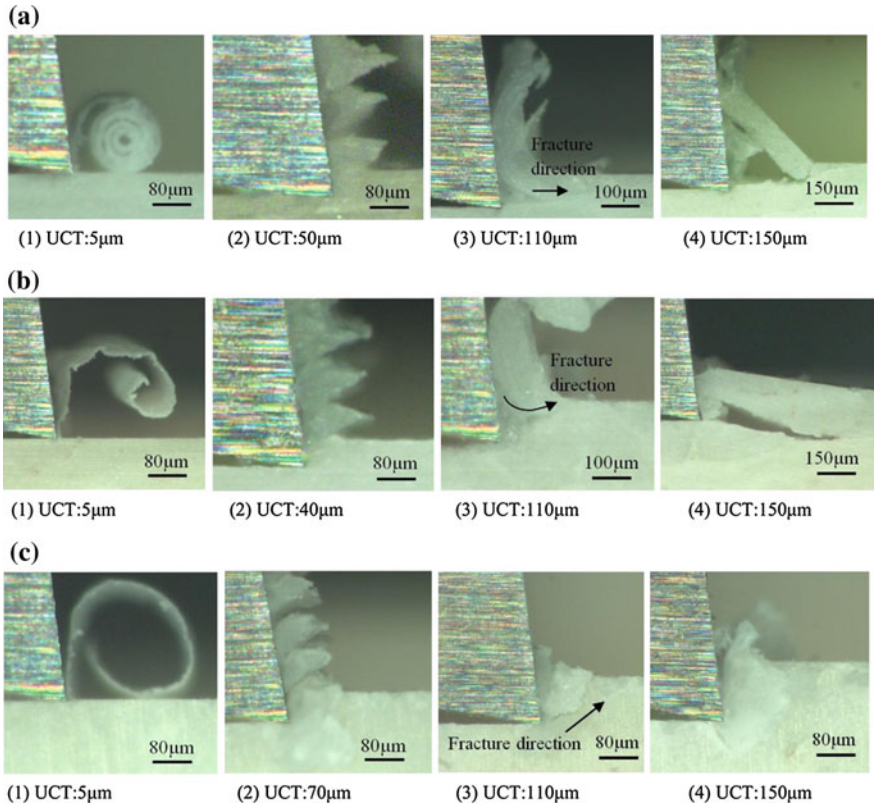

Fig. 4.21 Chip morphologies when various UCT and cutting direction relative to osteon orientation **a** Parallel cutting direction. **b** Across cutting direction. **c** Transverse cutting direction (reprinted from Liao and Axinte [16] with permission © Elsevier)

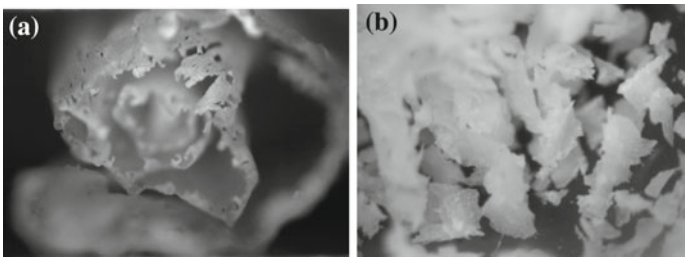

Fig. 4.22 Macroscopic images illustrating different chip formation mechanisms for various depths of cut. **a** 2 μm (*left*) and **b** 200 μm (*right*) (reprinted from Plaskos et al. [45] with permission. © Springer)

To understand chip formation during drilling, the chip morphology was monitored as a function of drilling speed (Fig. 4.23 [46]). While, at lower speeds the chips formed continuously (Fig. 4.23a [46]), with an increase in speed the chips formed in a fragmented manner (Fig. 4.23b [46]) and for the highest speeds, they formed in a powdery fashion (Fig. 4.23c [46]). In case of continuously formed chips were termed

Fig. 4.23 Variation of chip morphology in bone drilling at various rotational speeds: **a** continuous-12 m/min; **b** fragmented-30 m/min; **c** powdery-48 m/min (reprinted from Liao and Axinte [46] with permission. © Elsevier)

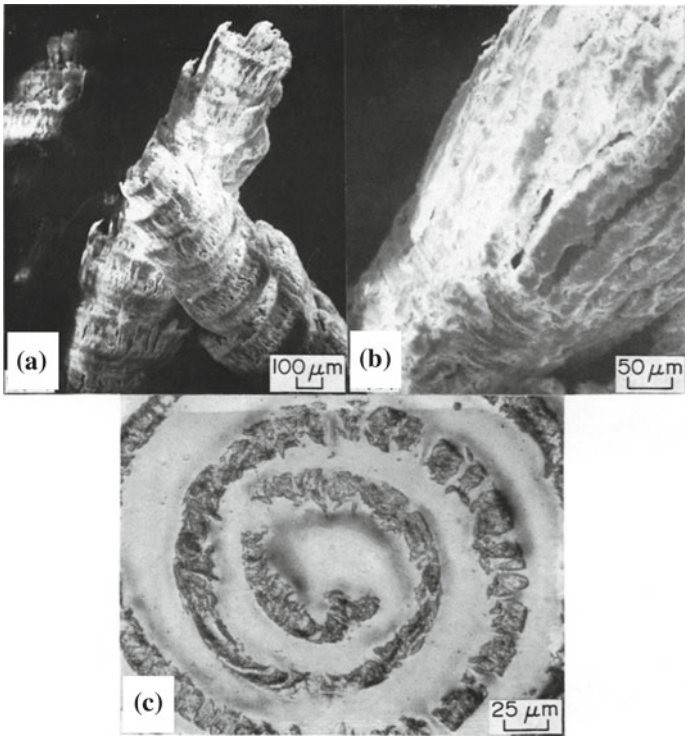

Fig. 4.24 Scanning electron micrographs of drilling chips: general purpose twist bit, 40 rpm, d = 1.98 mm, p = 14.4 N/mm^2. **a** spiral shape of chip and **b** higher magnification, note back side of chip towards center of drill bit near lower *left corner*. **c** Optical micrograph showing cross-section through spiral chip: general purpose twist bit, 40 rpm, d = 1.98 mm, p = 7.2 N/mm^2 (reprinted from Wiggins and Malkin [47] with permission. © Elsevier)

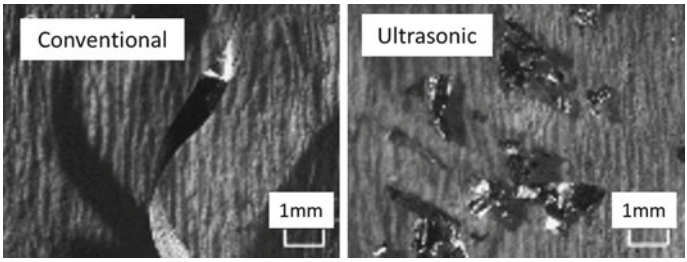

Fig. 4.25 Comparison between chips generated in conventional and ultrasonic drilling (reprinted from Chang and Bone [48] with permission. © Elsevier)

under-broken chips. Although, these type of chips can be removed easily, there is always a danger of damaging the drill surface by the process of clogging. This also poses a risk of force/torque built up and breaking of the drill inside the drilled hole. The powdery chips formed for highest drill speeds are also termed as over broken chips. They pose danger of undesirable scattering and vibration. Therefore, the drill speed needs to be optimum to form fragmented/adequately broken chips.

Furthermore, to get deeper understanding about the process of chip formation, SEM analysis was employed (Fig. 4.24 [47]). The chips from drilling process were analyzed. The chip formation took place via continuous fracture as a result of localized deformation. The process took place during the interaction of chiseled portion at the tip of drill bit with the bone. The segmental behavior of material removal was clear as evident in Fig. 4.24a, b [47]. In addition, Fig. 4.24c [47] clearly demonstrates that the process in drilling is different than orthogonal cutting. The circumferential striations and smearing present these differences.

Another aspect about the chip formation is that even though the continuous chip formation indicates better machining process, the continuously formed chips can pose inconvenience to the surgeon or the operator. In order to address this issue, some of the special tools have been opted for chip breaking [48]. These attachments help in cutting the chips at periodic intervals for maintaining the chip length at optimum level for desired chip morphology. Furthermore, it has been reported that carefully optimized ultrasonic machining results in desired length of chips compared to conventional machining (Fig. 4.25 [48]). Such optimally formed chips not only increase the convenience of surgeon/operator but also help in restricting the surface damage caused by the chips. Continuing the discussion on these lines brings the it to the final attribute, that is surface finish after bone machining and is discussed in the following section.

4.5 Machined Surface

Even though this topic in general in terms of surface quality has been already discussed separately in Chap. 2 already, a brief description has been provided in the current section in specific connection with bone. Final attribute of the machining

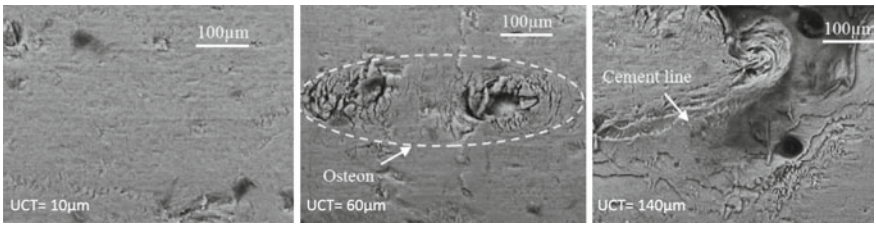

Fig. 4.26 Effect of uncut chip thickness (UCT) on surface quality (reprinted from Plaskos et al. [45] with permission. © Springer)

is the nature of the machined surface. It is usually judged by certain quality parameters. The surface quality indicates the amount of damage induced in the bone as a result of machining process. Furthermore, it also determines the process of post machining oseointigration during the healing process. Surface accuracy and fine finish play a major role in all applications since time immemorial. In case of bone milling operations, the surface quality observations have been notably made. A lot of milling parameters influence the resultant surface quality/flatness and post-operation osseointegration. It holds tremendous importance especially in total knee arthroplasty (TKA) [49]. Surface flatness obtained as a result of optimized milling operation resulted in maximized bone ingrowth. This gave better healing characteristics. It was also concluded that to ensure a good surface finish, temperature rise needed to be critically controlled. Moreover, there was not much variation in surface quality on changing the feed rate or the milling speed.

In another study related to cutting oration, it was observed that when the cutting direction was exactly perpendicular to the osteons, the surface roughness was the highest a large volume of sub-surface damage [50]. Experiments also showed that positive rake angles fared poorly as against negative rake angles from the surface roughness perspective. Increase in depth of cut increased surface roughness. Similar observations were made related to depth of cut by different researchers who quantified it in terms of UCT discussed before [45]. The smooth surface is evident for minimum UCT where as various bone elements disintegrated as with increase in UCT (Fig. 4.26).

References

1. A.A. Abdel-Wahab, A.R. Maligno, V.V. Silberschmidt, Comput. Mater. Sci. **52**(1), 128 (2012)
2. R.B. Martin, D.B. Burr, *Structure, Function, and Adaptation of Compact Bone* (Raven Pr, New York, 1989)
3. T.M. Keaveny, E.F. Wachtel, C.M. Ford, W.C. Hayes, J. Biomech. **27**(9), 1137 (1994)
4. F. Libonati, L. Vergani, Procedia Eng. **74**, 464 (2014)
5. T.M. Keaveny, W.C. Hayes, J. Biomech. Eng. **115**(4B), 534 (1993)
6. E. Giesen, M. Ding, M. Dalstra, T. Van Eijden, J. Biomech. **34**(6), 799 (2001)

7. M. Kutz, *Standard Handbook of Biomedical Engineering and Design* (McGraw-Hill, New York, 2003)
8. L.B. Meakin, C. Udeh, G.L. Galea, L.E. Lanyon, J.S. Price, Bone **81**, 47 (2015)
9. J.S. Thomsen, A.S. Niklassen, E.N. Ebbesen, A. Brüel, Bone **57**(1), 47 (2013)
10. R. McCalden, J. McGeough, M. Barker et al., J. Bone Joint Surg. **75**(8), 1193 (1993)
11. K.J. Jepsen, D.T. Davy, D.J. Krzypow, J. Biomech. **32**(3), 303 (1999)
12. K. Alam, A. Mitrofanov, V.V. Silberschmidt, Comput. Mater. Sci. **46**(3), 738 (2009)
13. C. Jacob, J. Berry, M. Pope, F. Hoaglund, J. Biomech. **9**(5), 343IN3345 (1976)
14. M. Mitsuishi, S. Warisawa, N. Sugita, M. Suzuki, H. Moriya, H. Hashizume, K. Fujiwara, N. Abe, H. Inoue, K. Kuramoto et al., CIRP Ann.-Manuf. Technol. **54**(1), 41 (2005)
15. S.F. Malak, I.A. Anderson, Med. Eng. Phys. **30**(6), 717 (2008)
16. Z. Liao, D.A. Axinte, Int. J. Mach. Tools Manuf. **102**, 41 (2016)
17. H. Peterlik, P. Roschger, K. Klaushofer, P. Fratzl, Nat. Mater. **5**(1), 52 (2006)
18. C.U. Brown, Y.N. Yeni, T.L. Norman, J. Biomed. Mater. Res. **49**(3), 380 (2000)
19. J.B. Thompson, J.H. Kindt, B. Drake, H.G. Hansma, D.E. Morse, P.K. Hansma, Nature **414**(6865), 773 (2001)
20. G.E. Fantner, T. Hassenkam, J.H. Kindt, J.C. Weaver, H. Birkedal, L. Pechenik, J.A. Cutroni, G.A. Cidade, G.D. Stucky, D.E. Morse et al., Nat. Mater. **4**(8), 612 (2005)
21. P. Zioupos, J. Currey, J. Mater. Sci. **29**(4), 978 (1994)
22. P. Zioupos, X. Wang, J. Currey, Clin. Biomech. **11**(7), 365 (1996)
23. D. Vashishth, K. Tanner, W. Bonfield, J. Biomech. **36**(1), 121 (2003)
24. D. Liu, S. Weiner, H.D. Wagner, J. Biomech. **32**(7), 647 (1999)
25. R.K. Nalla, J.H. Kinney, R.O. Ritchie, Nat. Mater. **2**(3), 164 (2003)
26. R.K. Nalla, J.J. Kruzic, R.O. Ritchie, Bone **34**(5), 790 (2004)
27. R.K. Nalla, J.J. Kruzic, J.H. Kinney, R.O. Ritchie, Biomaterials **26**(2), 217 (2005)
28. T.L. Norman, S.V. Nivargikar, D.B. Burr, J. Biomech. **29**(8), 1023 (1996)
29. K.S. Chan, C.K. Chan, D.P. Nicolella, Bone **45**(3), 427 (2009)
30. D. Vashishth, K. Tanner, W. Bonfield, J. Biomech. **33**(9), 1169 (2000)
31. D. Vashishth, J. Biomech. **37**(6), 943 (2004)
32. T.M. Boyce, D.P. Fyhrie, M.C. Glotkowski, E.L. Radin, M.B. Schaffler, J. Orthop. Res. **16**(3), 322 (1998)
33. A.C. Courtney, W.C. Hayes, L.J. Gibson, J. Biomech. **29**(11), 1463 (1996)
34. M. Fondrk, E. Bahniuk, D. Davy, J. Biomech. Eng. **121**(5), 533 (1999)
35. M.T. Fondrk, An Experimental and Analytical Investigation Into the Nonlinear Constitutive Equations of Cortical Bone, PhD Thesis, Cleavland State University, USA (1989)
36. H. Leng, X.N. Dong, X. Wang, J. Biomech. **42**(4), 491 (2009)
37. M.C. Michel, X.D.E. Guo, L.J. Gibson, T.A. McMahon, W.C. Hayes, J. Biomech. **26**(4–5), 453 (1993)
38. M. Schaffler, E. Radin, D. Burr, Bone **11**(5), 321 (1990)
39. D.R. Carter, W.E. Caler, D.M. Spengler, V.H. Frankel, Fatigue behavior of adult cortical bone:the influence of mean strain and strain range. Acta Orthop. Scand. **52**(5), 481 (1981)
40. M. Fondrk, E. Bahniuk, D. Davy, C. Michaels, J. Biomech. **21**(8), 623 (1988)
41. D. Carter, W.C. Hayes, J. Biomech. **9**(1), 27 (1976)
42. D. Carter, W.C. Hayes, D.J. Schurman, J. Biomech. **9**(4), 211 (1976)
43. F.J. O'Brien, D. Taylor, T.C. Lee, J. Biomech. **36**(7), 973 (2003)
44. S. Mohsin, F. O'Brien, T. Lee, J. Anat. **208**(1), 81 (2006)
45. C. Plaskos, A.J. Hodgson, P. Cinquin, in *Medical Image Computing and Computer-Assisted Intervention-MICCAI 2003* (Springer, Berlin, 2003), pp. 254–261
46. Z. Liao, D.A. Axinte, J. Mater. Process. Technol. **229**, 82 (2016)
47. K. Wiggins, S. Malkin, J. Biomech. **9**(9), 553 (1976)
48. S.S. Chang, G.M. Bone, Robot. Comput.-Integr. Manuf. **21**(4), 442 (2005)
49. K. Denis, G. Van Ham, J. Vander Sloten, R. Van Audekercke, G. Van der Perre, J. De Schutter, J.P. Kruth, J. Bellemans, G. Fabry, in *International Congress Series*, vol. 1230 (Elsevier, Amsterdam, 2001), pp. 300–306
50. C. Yeager, A. Nazari, D. Arola, Mach. Sci. Technol. **12**(1), 100 (2008)

Chapter 5
Temperature Evolution During Bone Machining

The heat evolved during any machining operation as a secondary effect (in mechanical machining) and/or primary or inherent effect/source (in beam based machining) results in temperature increase of the bone. As discussed in Chap. 2, rise in temperature leads to thermal necrosis of the bones and as a result becomes very critical aspect. A lot of studies have investigated temperature rise during various conventional and non-conventional bone machining processes [1–5]. The current chapter is exclusively dedicated to temperature evolution. Various efforts exploring role of machining parameters on temperature evolution are discussed. Firstly, some general considerations are given to the topic. Then, the chapter moves to the discussion about temperature measurement techniques. With this background, various conventional and non-conventional processes are discussed. Finally, the efforts regarding reducing the temperature are taken into account.

5.1 General Considerations

In any machining process in general, the temperature evolution depends on thermophysical properties of the material undergoing the process and can be numerically expressed in Eq. 5.1 [6, 7].

$$T = C_0 K_s V^{2n} A^n \; or \; W^{2n} h^{1.2n} \tag{5.1}$$

where K_s is the specific cutting energy, V the cutting velocity, A the chip cross-sectional area, W the thermal conductivity of work material, and h the thermal capacity (density specific heat) of work material. C_0 and n are constants and can be obtained experimentally. Thus the temperature rise depends on input machining energy and thermal properties of the bone. Especially, the input energy in conventional mechanical machining is dependent on shear strength of the bone as machining is a shear failure process. The heat generated is partly dissipated with the chips and rest contributes towards temperature rise. The heat capacity of the bones being much

N.B. Dahotre and S.S. Joshi, *Machining of Bone and Hard Tissues*,
DOI 10.1007/978-3-319-39158-8_5

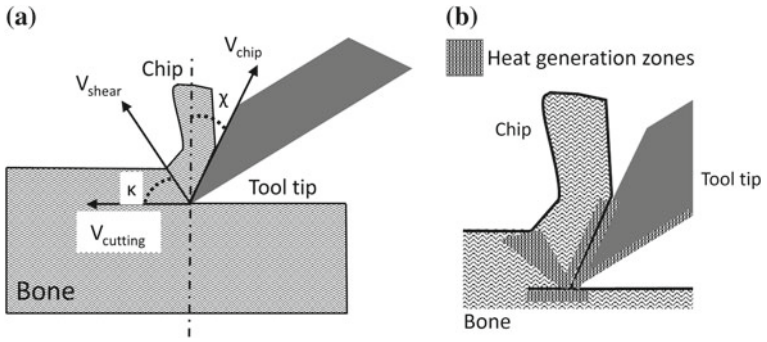

Fig. 5.1 Tool-bone interaction showing **a** process of chip formation by shear force and **b** zones of heat generation in the interaction region

lower, and hence comparatively temperature rise is low chips carry less amount of heat when compared to the metals. The process of chip formation along with the zones of heat generation is schematically illustrated in Fig. 5.1.

Research related to the temperature effects and necrosis in bones dates back to 1941 [8]. Since then, efforts are being made to understand the temperature development and its effect on bone tissues as well as in developing bone machining techniques operating at safe temperature levels. Hence, the discussion will move forward to various machining processes with specific emphasis on temperature related aspects.

5.2 Temperature Measurement

Monitoring temperature accurately is the necessary requirement to determine the exact effect of machining parameters. The most common ways of temperature measurement are enlisted below [9].

- Thermocouples/thermoresistors
- Infrared thermographic camera

Thermocouples are the sensors based on a pair of different conductors. As the temperature changes between ends of both the conductors, there is a proportional change in the voltage between the two. It is worth mentioning here that, other sensors such as thermistors are used where resistance is monitored as a function of temperature [10]. These sensors can be placed in a pre-drilled holes in the vicinity of volume of bone material being removed prior to the machining experiments. At the same time, it is difficult to measure the exact temperature at the point of tool contact. In some efforts, the thermocouple was placed right above (Fig. 5.2a) [11] or very nearby (Fig. 5.2b) [12] the tool so that temperature could be monitored with the movement of the tool. Other means are putting number of thermocouples at various locations on the surface (Fig. 5.2c) or at the depth (Fig. 5.2d). This allows to capture extent of effect of temperature rise based on anisotropic nature of the bone.

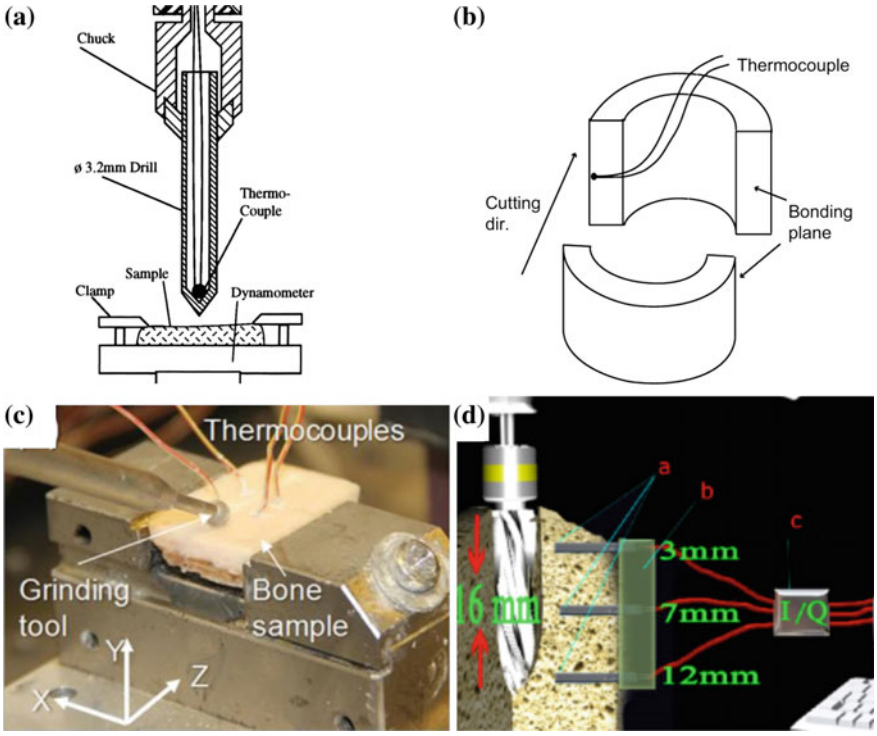

Fig. 5.2 Various arrangements of temperature sensors: **a** (reprinted from Hillery and Shuaib [11]. © Elsevier), **b** (reprinted from Sugita et al. [13] with permission. © Elsevier), **c** (reprinted from Tai et al. [14] with permission. © Elsevier) themocouples and **d** thermistors (reprinted from Sener et al. [10] with permission. © John Wiley and Sons)

Although thermocouples have been popular in research studies, they have inherent limitations that they can not measure the surface temperature directly. To overcome this difficulty, infrared thermography technique was employed [15–17] (Fig. 5.3). It is based on infrared radiation emitted by the material which is sensed using an infrared sensor. The signals acquired are used for constructing the 2D thermal image. Combining 2 or more cameras, a 3D surface can be reconstructed [9]. Another major advantage of this technique is that, this method is non-contact type and thus is more feasible during in vivo studies or actual surgeries. In addition, the temporal resolution is reported to be high for this technique when using high speed infrared camera [18, 19] making it potentially suitable for non-conventional machining techniques such as lasers based machining. A complete heat map generated gives the spatial distribution of the heat and spread of the affected areas.

Having considered the advantages of infrared thermography, there are some limitations imposed either by lack of availability of exact thermal properties of the bone or by the technique itself. For example, knowledge about emissivity of bone is critical [15] and in case of instrument a thorough calibration using thermocouple is required

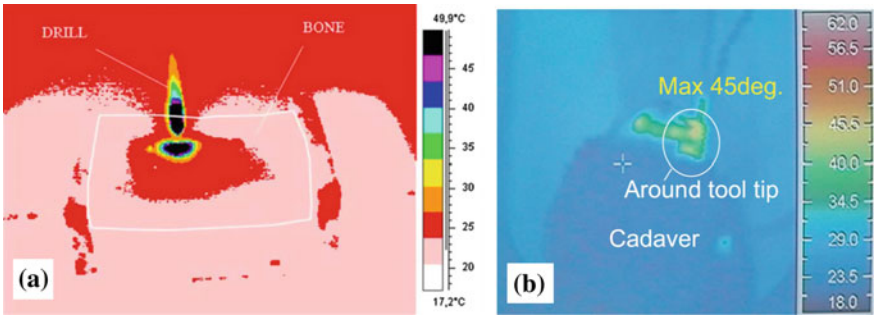

Fig. 5.3 Infrared thermography during, **a** drilling (reprinted from Augustin et al. [15] with permission. © Springer) and **b** cutting (reprinted from Sugita et al. [13] with permission. © Elsevier)

before temperatures can be accurately predicted [9]. In addition, measurement of the temperature beneath the surface being difficult if not impossible, the extent of depth of necrotic regions can not be realized. To get an overall idea of temperature profile, infrared thermography needs to be used along with thermocouples [20]. In spite of these efforts, the technology needs advancement towards real time temperature monitoring during an actual surgical operation. On a different note, computational models can also help in predicting temperatures during machining and help choose right parameters for the machining operation. The field of modeling related to bone machining has been explored in a separate chapter. Nonetheless it is clear that work needs to be done related to temperature measurement to implement it in the operation theater.

5.3 Temperature Evolution During Conventional Machining

Current section reviews works based on various machining operations. Effects of important machining parameters on evolution of temperature are explored. Especially, efforts related to lowering the bone temperature during the machining process are discussed.

5.3.1 Temperature Rise in Drilling

Drilling operation has been extensively investigated from the temperature point of view [1, 2, 21–23]. Important drill parameters largely dealt with include drill force, rotation speed, feed rate, and drill geometry. The related research has been discussed

Table 5.1 Peak temperatures reached during drilling of bone using various drill bits at 0.5 mm from drill age

Type of drill bit	Time to peak temperature (s)	Peak temperature (°C)
New orthopedic	~10	~43
Used orthopaedic	~12	~49
Orthopaedic with blocked flutes	~9	~55
New bullet drill	~4	~40
New twist drill	~7	~41

extensively. Conventional orthopedic drills were compared with other drill bit designs commercially available for engineering applications [24]. All the experiments were performed in controlled temperature environment and rise in temperature was monitored via three thermocouples situated at 0.5, 1, and 1.5 mm from the circumference of 2.5 mm diameter drilled hole. A standard orthopedic drill bit in used condition resulted in generating temperatures in the range of 48–54 °C at 0.5 mm away from the circumference of the hole. Additionally, regions at the distance of 1.5 mm from circumference of the hole remained above 42 °C, facing a possibility of necrosis. This temperature rise was attributed to the blunt edges of the used drill coupled with point angle of 90° leading to requirement of higher drill force, thus generating more heat. Same drill bit in new condition resulted in 42 °C temperature at 0.5 mm from the circumference of hole. Temperatures were safe within the length of 1.5 mm distance from the circumference of hole. Commercial drill bits having point angle of 118° on the other hand resulted in temperatures below 40° at the distance of 0.5 mm from circumference of the hole making the drilling operation safer with regards to the thermal damage. Table 5.1 represents the peak temperatures reached using various drill bits at 0.5 mm distance from the circumference of hole [24]. In another similar effort [25], a two phase drill was compared with regular surgical drill (Fig. 5.4). The geometrical factor such as lower feed rate and lower tip angle resulted in generating safer temperatures in case of a two phase drill. The peak temperature attained was ~30° in case of two phase drill, much lower compared to 47 °C in case regular surgical drill. One of the latest efforts even compared TiBN coated drills with the uncoated ones and concluded that coated drills were harsher on the bones [26]. These studies pointed towards importance of drill design with regards to the temperature rise.

Drill force applied has been found to have great influence on the temperatures generated during drilling process. Numerous studies have been taken up to explore this dependence. Mathews and Hirsch [2] observed that in case of human cortical bone, higher drilling forces resulted in generating lower temperatures. Similar observations were made by others [27, 28]. Larger drill forces were thought to result in lesser time required for drilling and less heat generation. The time spent above 45 °C also drastically reduced with the increase in the drilling force. This overall effect illustrated in Fig. 5.5 [28] clearly indicates that the drilling forces of the order of 100 N are desirable during drilling of the bones. On the contrary to the results discussed

Fig. 5.4 Photograph of **a** normal surgical drill and **b**, **c** two phase drills

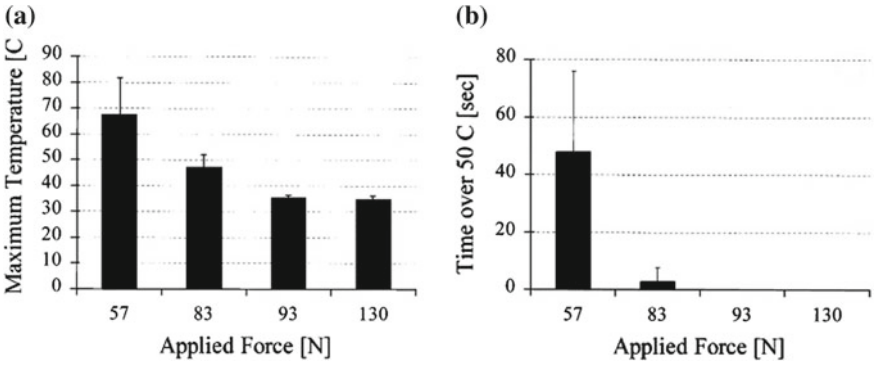

Fig. 5.5 Bar charts illustrating, **a** effect of drill force on temperature and **b** time spent above the necrosis temperature for the various forces during the drilling of human cortical bone (reprinted from Bachus et al. [28] with permission. © Elsevier)

before, some researchers have reported increase in the temperature with the drilling force [29–31]. This opposite effect was attributed to other process parameters such as feed rate and rotation speed [28].

Effect of drill rotation speed has been investigated in various studies [25, 29, 32–34]. It is found that temperature increased for the drill speed range up to 10,000 rpm and decreased for higher speeds [9], indicating that the relationship between temperature and drill speeds is non-linear. The amount of heat produced and heat transfer to the bone are dependent on the rate of heat generation (which is expected to increase with speed and force), and the duration of the drilling or cutting process (which decreases with speed and force) [34]. The overall increase in drill force and speeds resulted in reduced times of drilling, and temperatures were lower for higher values of speeds and force (Fig. 5.6). In addition, drill bits of larger diameter gave rise to relatively less temperature [32].

Wiggins and Malkin [35] ingeniously correlated specific energy (energy required to remove unique volume of material) with feed rates. The specific energy turned out to be less for higher feed rates leading to relatively lesser rise in the temperature. Krause et al. [36] noted that higher feed-rates and lesser depth of cuts would be

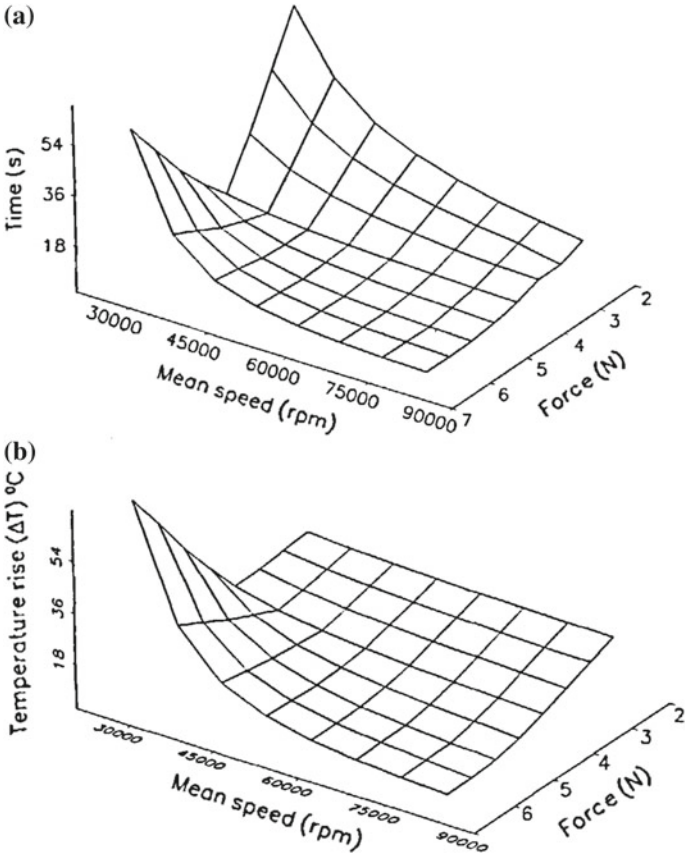

Fig. 5.6 Surface plots showing, **a** duration of drilling as a function of drilling force and speeds and **b** combined effect of drilling force and speed on temperature rise during drilling of cortical bones (reprinted from Abouzgia and Symington [34] with permission. © Elsevier)

beneficial to reduce the bone machining temperature. The limitation was that Krause et al. performed orthogonal cutting and not drilling. In their work, increasing feed rate as well as axial force as noted above, the drilling time went down dramatically, so did the heat generated and subsequently, the maximum temperature attained during drilling. The same has been corroborated by the likes of Udiljak et al. [27], Reingewirtz et al. [21], and Kalidindi [20]. The effect of feed rate on temperature is presented in Table 5.2 [20].

To view overall picture, there are various factors ranging from drill bit design to drill operating parameters which greatly influence the drill temperature. The process needs careful optimization in order to achieve effective drilling which induces least possible damage. The summary of various drilling parameters and their influence on lowering the temperature has been presented in Table 5.3.

Table 5.2 Peak temperature values for various feed rates

Feed rate (mm/s)	Temperature (°C)
0.005	45
0.010	38
0.015	33

Table 5.3 Effect of drilling parameters on temperature rise in drilling

Parameter	Effect on temperature
Drill tip angle	Lower the tip angle, lower the temperature
Drill diameter	Larger the diameter, lower the temperature
Drill force	Higher the force, lower the temperature
Feed rate	Higher the feed rate, lower the temperature
Drill speed	Lower temperatures for low (0–1000 rpm) or very high speed (<40000 rpm)

5.3.2 Temperature Rise in Milling

Milling has been considered as very similar to drilling with regards to the process parameters and the temperature rise. Sugita et al. [13] carried out experiments to determine the temperature distribution during end-milling on cortical bones during orthopedic surgeries. Their analysis stated that the temperature at a depth of 0.15 mm below the surface reached 35 °C and consequently, that on the surface it was 50 °C. Same group in another study investigated new tool design and temperature rise during milling of cortical bone [37]. The new tool design (Fig. 5.7) aimed at having advantage of straight edge to have better surface finish combined with serrated edge to have optimum cutting force. Most desirable milling conditions were achieved. In addition, a double groove further lowered the temperature during milling (Fig. 5.8). In another effort, the same group explored effect of force controlled method and usual method of milling on urethane bone model [38]. They concluded that even though temperatures reached were around 36 °C in both the cases, the time required for milling was much shorter in force control method. The same group went ahead and investigated effect of up and down milling and indicated that the former had temperature levels lower than 20 °C compared to the later (Fig. 5.9 [3]).

Effect of feed rate and milling depth on temperature evaluation was investigated by Shin et al. [3]. They observed that higher feed rates were beneficial where as lower cutting depths in each milling cycle helped to have a control over temperature rise (Fig. 5.9). Malvisi et al. compared milling with sawing [39]. All the main parameters including temperature, amount of chips, and post surgery patient satisfaction were better in case of milling except that the resection times were longer than sawing. This brings the discussion to the temperature rise during cutting.

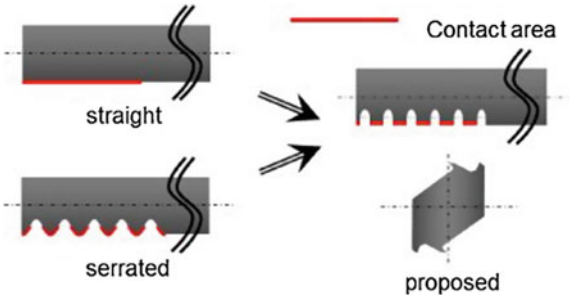

Fig. 5.7 Proposed tool design by Sugita et al. showing combined effect of straight and serrated cutting edges (reprinted from Sugita et al. [37] with permission. © Elsevier)

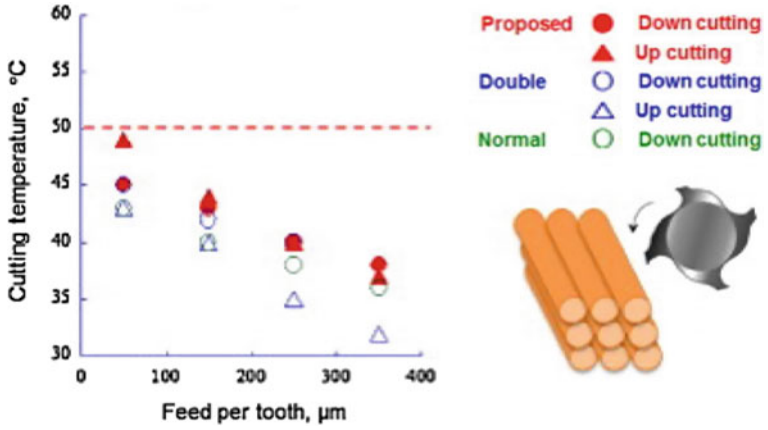

Fig. 5.8 Temperature evaluation during milling (reprinted from Sugita et al. [37] with permission. © Elsevier)

5.3.3 Temperature Rise in Cutting

The work of Krause et al. [36] compared cutting action on bone using burrs and saws. In case of burrs, similar to drilling, the increase in feed rates reduced the temperature rise and bigger diameter was beneficial compared to smaller one by obtaining lower temperatures. In addition, notably the tool rotation speed within the range of 20,000–100,000 rpm did not have a marked difference with regards to the temperature rise (Fig. 5.10 [36]). Temperature increased with the depth of cut as expected. In addition, the feed rate dominated the process and temperatures remained in the safer zone (less than required for necrosis) for any other parameters. Same group further noted that exposure above 50 °C could trigger death of osteocytes and that above 70 °C could cause irreparable damage due to the certain biochemical changes co-occurring subsequently [40]. Furthermore, critical role of coolant was pointed out without which the temperatures reached were as high as 250 °C. Saw

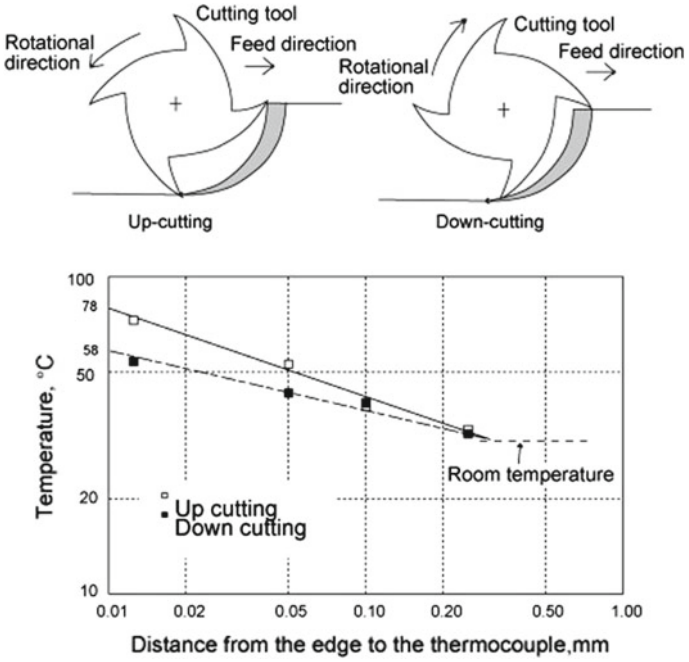

Fig. 5.9 Schematic of up and down milling along with the temperature profiles (reprinted from Shin and Yoon [3] with permission. © Elsevier)

blades were much harsher compared to the burrs in terms of temperature rise to the order of 100 °C. The saw temperatures were much higher than the bone (>150 °C). Similar observations were made in case of saws by others [41, 42]. The temperatures at the surface (Zone 1) were above 80 °C for considerable amount of time, however, even though temperatures were lower in subsurface regions (Zone 2 and 3), they were still above necrosis threshold temperature of 40 °C (Table 5.4 [41]). The reason that could be thought behind this increase is a large area of contact of bone with the saw teeth. In addition, many cuts required to be performed in order to complete the cutting operation. In view of this, the following considerations were suggested for manual sawing [42].

- Use of lower speeds.
- Avoid excessive pressure.
- Start superficially followed by gradual increase in the depth.

For shorter depth of cuts, the preferred tool is a cutting burr where as for through cutting, a saw blade is strongly recommended. This fact emphasizes need for cooling via irrigation.

In a relatively latest study a robotic setup was employed to perform cutting [17]. A square endmill of high speed steel with two flutes was used as a cutting tool and the side edge performed the cutting action using robotic arm. It is to be noted

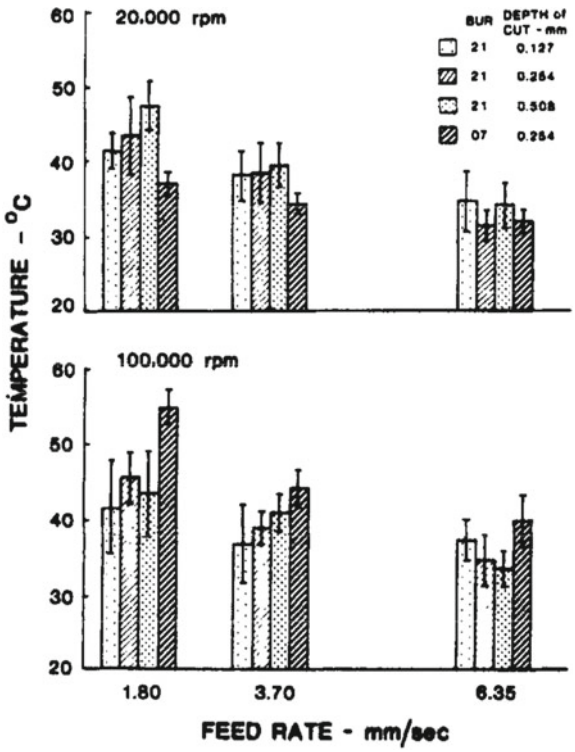

Fig. 5.10 Effect of tool rotation speed, depth of cut, and bur type on temperature rise during cutting of bovine cortical bone (reprinted from Krause et al. [36] with permission. © Elsevier)

Table 5.4 Peak temperatures during saw cutting of the bone

Location	Approximate time to peak temperature (s)	Peak temperature range (°C)
Zone I (Surface)	220	95–105
Zone II (Sub surface)	300	70–75
Zone III (Matrix)	350	58–60

here that as a separate chapter has been devoted to automation and robotics, the sole focus of this chapter is temperature. This study reported a rise in temperature with an increase in cutting speed. In addition, the increase in feed per tooth also increased the temperature. Two methods of cutting, namely up and down cutting were compared. The later resulted in comparatively lower temperatures (Fig. 5.11 [17]). The higher temperature in up cutting is due to a large accumulated heat effects in front of the cutting edge because of the lower thermal conductivity of bone. This is further assisted by the friction of cutting edge and slipping at the beginning point of cutting on the specimen surface. In case of down cutting however, the thickness of cutting chip dwindles with the rotational movement of the cutting edge within one revolution of the tool. Also, in this case it is easy for the cutting chip to leave

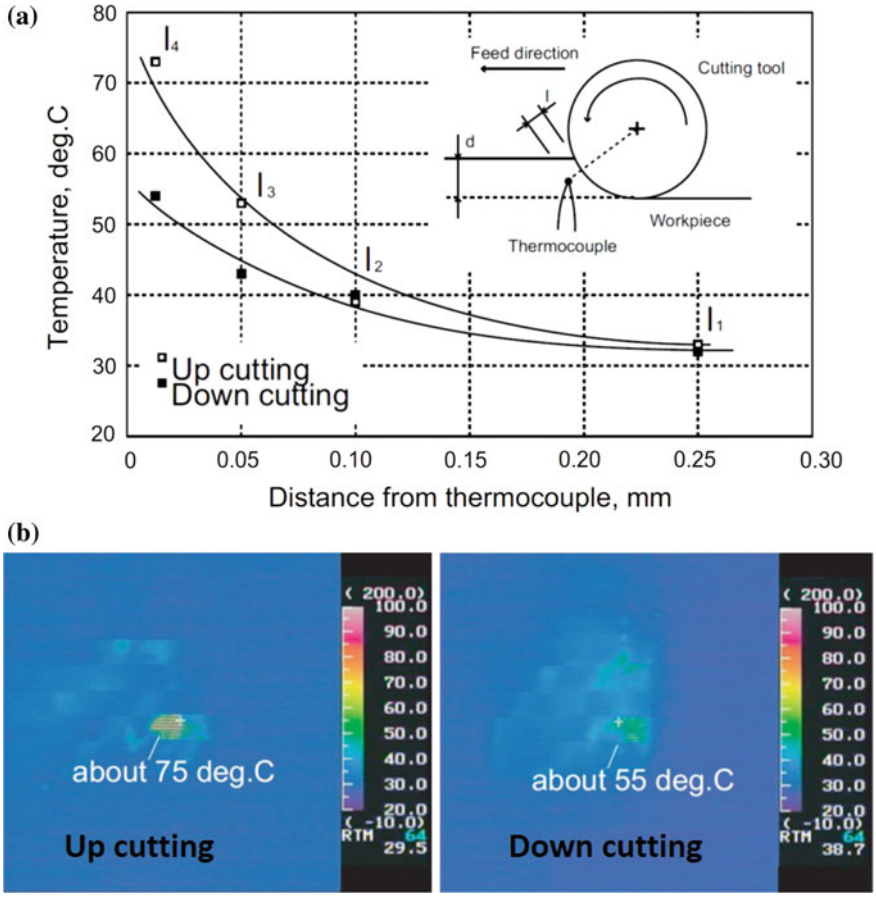

Fig. 5.11 Effect of up and down cutting of bone on temperature rise **a** at a distance from thermocouple and **b** using infrared thermography (reprinted from Sugita et al. [17] with permission. © ASPE)

from the cutting edge. This facilitates reduction in heat and development of lower temperatures.

In case of cutting, it is clear that the temperature rise can be much higher and hence caution has to be taken to choose proper tool for cutting depending on the requirement. In addition, a careful operational practice needs to be opted for safer cutting.

5.3.4 Temperature Rise in Grinding

Compared to other conventional operations, grinding has been studied to a limited extent from the point of view of temperature rise [4, 43–45]. These are some of the latest efforts and are involved other aspects such as thermal modeling and effect of cooling. The former has been dealt in a separate chapter whereas the later has been dealt in a separate section in the current chapter. Usually the temperatures reached during grinding are higher than cutting. The ways to get an idea about spindle power in machining processes are to assess machine performance, tool condition, and process stability. The control of tool motor via pulse width modulation (PWM) alters the current input and provides adequate torque to overcome the motor loading. Thus any change in PWM signal is related to the machining process and thus heat generation. The difference in duty cycle (time for which the tool motor remains on) for the motor running without any load and when performing machining is shown on a voltage vs time plot (Fig. 5.12 [14]). The heat generated leads to temperature rise. In one such study the thermocouples gathered information of temperature rise whereas the PWM signals formed a base of computer simulation (Fig. 5.13 [14]). The angle of contact had minimal influence on temperature. In addition, the temperatures were within safe limits at 2 mm distance from the grinding track. In another effort, effect of coating and cooling was explored [45]. In all the cases, the rotation speed was kept

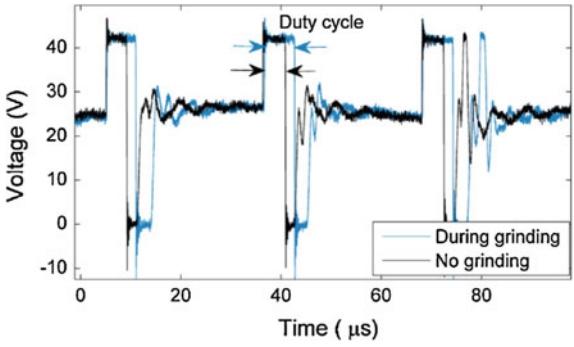

Fig. 5.12 PWM duty cycle during grinding (reprinted from Tai et al. [14] with permission. © Elsevier)

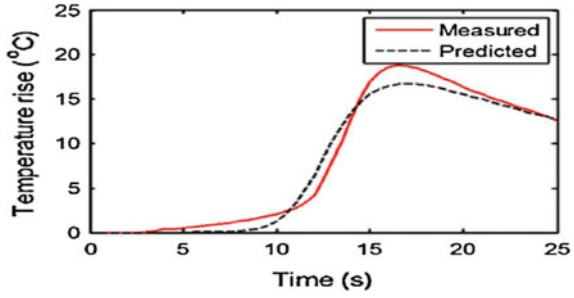

Fig. 5.13 Temperature rise during grinding of a bovine femur bone with tool rotation speed of 60,000 rpm, contact angle 0f 30 °C, feed rate of 30 mm/min and depth of cut 0.1 mm (reprinted from Tai et al. [14] with permission. © Elsevier)

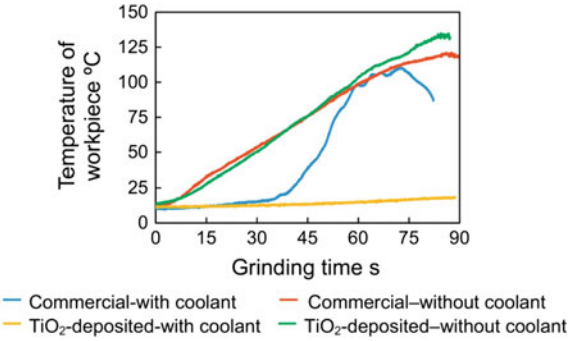

Fig. 5.14 Effect of coating and mist cooling on temperature rise during grinding of bovine femoral cortical bone (reprinted from Enomoto et al. [45] with permission. © Elsevier)

Fig. 5.15 Contact angle measurement of TiO_2 surface showing excellent wetability (reprinted from Enomoto et al. [45] with permission. © Elsevier)

constant at 5000 rpm whereas feed rate was 1 mm/min. The coatings investigated were SiO_2 and TiO_2. SiO_2 was only marginally effective with or without mist cooling and performed very similar to bare commercial grinding wheel after 75 s of grinding time. TiO_2 did not have any effect when coolant was not used and temperature rose rapidly. On the contrary, with the coolant, the grinding tool coated with TiO_2 resulted in experiencing very low temperatures even for the grinding times of the order of 100 s (Fig. 5.14 [45]). This incredible effect was attributed to hydrophilic nature of TiO_2 (Fig. 5.15 [45]) which helped in retaining the coolant and removed the heat in very effective manner. This study clearly pointed towards need for proper choice of coating materials to obtain a desired structure property relationship leading to a significant improvement of commercial bone machining tools.

So far the discussion concerning temperature rise has been focused on conventional methods. It was pointed out that many factors ranging from tool design to operational parameters and potential surface modification have a marked impact on temperature rise. Having built this understanding, the discussion will take a different course with temperature rise during non-conventional bone machining techniques in the following section.

5.4 Temperature Evolution During Non-conventional Machining

Methods such as laser use heat as the primary means of machining rather than having it as only a secondary undue outcome of the machining process. As extensively discussed in the section on laser in Chap. 4, the thermal damage does occur during

laser machining, hence a careful choice of combination of laser system and processing parameters becomes necessary. There are limited number of studies involving temperature measurement employing thermocouples or infrared cameras. Considering extremely short duration of the laser-bone interaction (fs-ms) the resolution of these techniques comes under question. Keeping this fact in consideration, a brief review about the temperature rise in laser machining of bone is presented. In one such study, temperature rise during laser cutting and drilling of the bone was investigated employing a infrared camera [46]. A TEA CO_2 laser (λ = 10.6 μm, pulse duration 1 μs and focus diameter 230 μm) was employed. The temperature rise with the trephine drilling was similar to that of laser drilling with an air jet and the peak temperature reached to the order of 120 °C. The same laser drilling without air jet resulted in temperature rise peaking to 400 °C. During drilling, when a water spray was employed instead of air jet, temperatures were in much safer range with average value of 25 °C. Even though, these attempts indicated temperature rise, it is worth mentioning here that actual measurement of temperature in such a dynamic process is difficult and accuracy of temperature measurement may not be very high. In view of this, temperature prediction with reasonably high accuracy may be possible by computational modeling which is discussed in a separate chapter.

5.5 Temperature Control

It is clear from the previous discussions about thermal necrosis in Chap. 1 and temperature rise in the current one that control on temperature evolution is very necessary. It is noteworthy here that in real life surgical procedures, there are some natural ways in which heat removal can take place. Firstly, the chips can carry out substantial quantity of heat owing to the high surface energy to volume ratio they possess. However, Moses et al. evaluated the thermal conductivity of bone and demonstrated a new inverse technique for conductivity measurements [47]. The average thermal conductivity of dry samples was measured as b 0.70 W/(mK) whereas for wet samples it was 0.80 W/(mK). These results indicated that thermal conductivity of the bone was poor owing to which the heat generated at the surface couldn't be dissipated easily through the chipped bone material. Secondly, natural coolants in the form of blood and fluids from tissues can bring down the temperature. Thus, it is clear that chip formation and cooling via body fluids may not be effective in heat removal and attention has to be given to overall machining process with regards to temperature rise. Some of the important aspects in limiting the heat generation are improved tool design, choosing optimized set of process parameters, and developing careful operational practices. Even though these aspects do reduce the heat generation to some extent, the temperature levels reached are many times above the safer limits. This necessitates deployment of external cooling system during bone machining operations. There are many studies focusing on such means and will be reviewed in the current section.

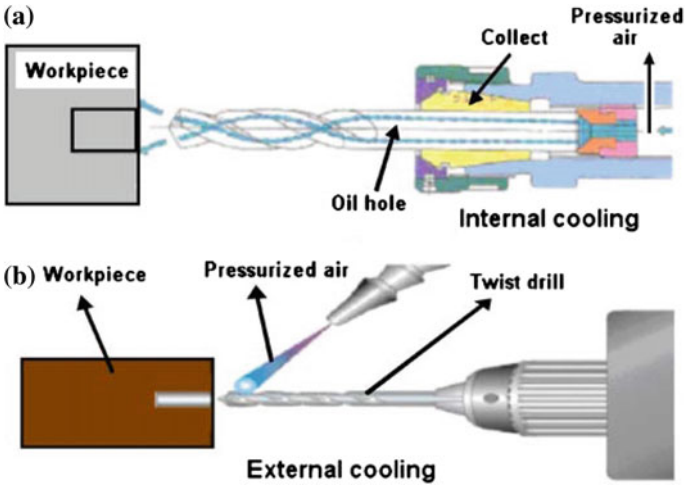

Fig. 5.16 Types of cooling systems adopted in case of drilling operation, **a** internal cooling and **b** external cooling (reprinted from Bagci and Ozcelik [48] with permission. © Springer)

In case of conventional machining methods involving physical tools, the cooling systems can be classified into two types as listed below [9, 48] and schematically shown in Fig. 5.16.

1. Internal cooling systems
    i. Closed type
    ii. Open type
2. External cooling systems

Internal cooling systems are those in which the cooling fluid is circulated inside the tool. The closed type consists of cooling fluid circulated in a closed circuit and does not come directly in contact with the bone undergoing machining. This helps to cool the tool but there are chances of bone being heated up. Open type on the other hand has the cooling fluid coming out of the tool tip and thus directly contacts the bone. External cooling system is not attached to the tool and directly supplies the coolant to the tool-workpiece system. It can be an automated or manual variety. The cooling fluid is usually saline solution (sterile NaCl). The following discussion will be focused on efforts related to various machining operations.

Cooling systems have been investigated for drilling operation in an extensive manner [12, 23, 30, 32, 49–51]. The irrigation clearly helps to bring down the temperature to safe level during drilling for same set of parameters and same drill bits used (Fig. 5.17). The coolant temperature itself markedly influences the efficiency of cooling with relatively cooler saline (10 vs. 25 °C) performing better as expected [10]. Both internal and external cooling methods have been found effective on surface level. On the other hand, as the depth of hole increases, the internal cooling naturally

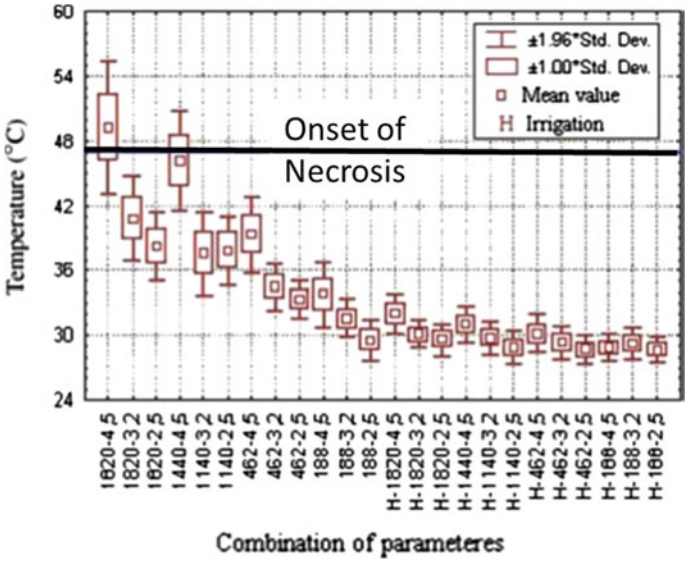

Fig. 5.17 Effect of irrigation on temperature of bone during drilling. Necrosis onset temperature is also indicated. The first number on the x-axis represents the drill speed (rpm) and the second one, drill diameter (mm) (reprinted from Augustin et al. [32] with permission. © Springer)

performs better [9, 52]. Another facet from which the cooling systems for drilling operation have been investigated is sterilization. There is always a possibility of having infections on the tools after actual usage in surgery and then the danger of transmission of these infections. Therefore, cleaning the tools and cooling systems becomes vitally important. In one study it was observed that the cooling channels in case of internally cooled drill bit were contaminated [53]. It was concluded that careful autoclaving and disinfecting practices removed the infection from the drill bits. These effects can also arise in case of externally cooled drill bits where a danger of sprinkling of bio fluids during surgery to the surroundings and thus proper sterilization and careful operational practices become essential.

Irrigation has a more critical role in processes such as cutting and milling where the temperature levels expected are much higher. For cutting process done via burs the internally cooled burs containing central channel are found to be effective [52]. Even the surface temperatures obtained were in safe level with the external saline irrigation as observed by infrared thermography [37] (Fig. 5.18).

In case of saw blades, it was reported that external cooling did not result in noticeable effect [54]. Internally cooled lab designed double saw (Fig. 5.19) however was found to be most effective as reported in successive studies by Toksvig-Larsen and coworkers [55, 56]. Effect of flow rate of the saline through this saw indicated that such arrangement can maintain reasonably high cooling rates (Table 5.5) during lab trials. Even though, the flow rates higher than 80 ml/min reduced the bone temperature, the quantity of saline required was unreasonable (cutting of the tibia during

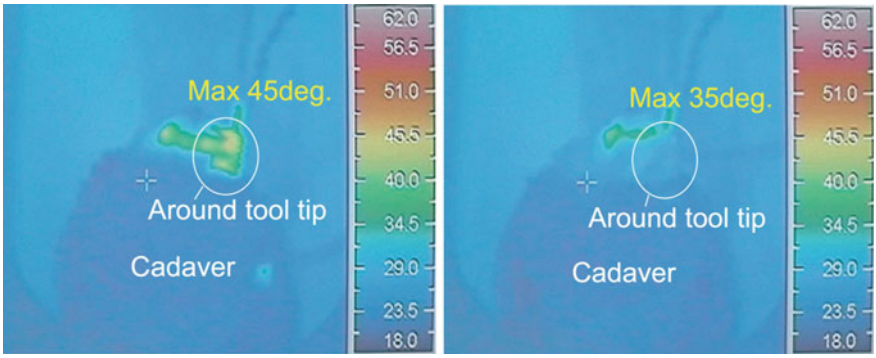

Fig. 5.18 Effect of external water cooling on bone temperature during burr cutting (reprinted from Sugita et al. [17] with permission. © ASPE)

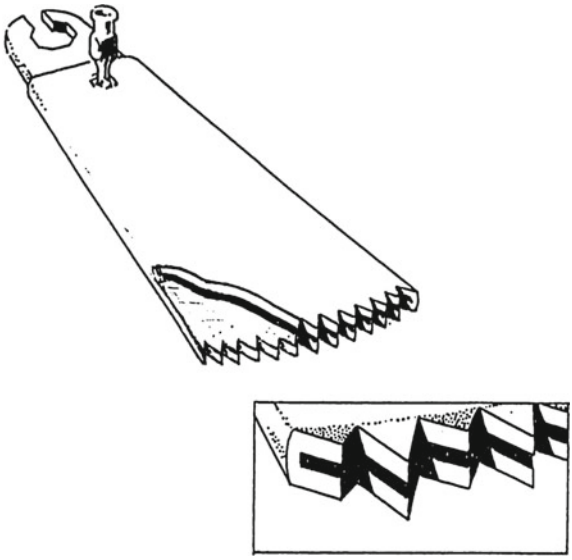

Fig. 5.19 Custom designed internally cooled saw blade (reprinted from Toksvig-Larsen et al. [56] with permission. © 1990 Informa UK Ltd)

knee arthroplasty required 1200 ml of saline for 600 ml/min flow rate). The same saw was taken to the next level and tried in vivo [56]. The measurements were done during 30 knee arthroplasties. The effectiveness of double saw was evident. The observation also indicated the sharp spike in temperature when the saline supply was turned off (Fig. 5.20). Same research group went ahead to isolate effectiveness of the design aspects of the blade and concluded that internal irrigation was the only effective parameter and mere saw design changes failed to control heat generation [57].

Cooling was explored in case of grinding in a similar manner to that of burr cutting. Zhang et al. [44] explored the effect of cryogenic saline cooling and compared the traditional flood irrigation mode with the mist mode (Fig. 5.21). The idea of mist

Table 5.5 Temperature as function of flow rate of saline coolant during cutting

Flow rate (ml/min)	10	20	30	40	50	60	70	80
Temperature (°C)	60 ± 15	40 ± 5	35 ± 5	32 ± 2	30 ± 2	28 ± 6	26 ± 2	25 ± 2

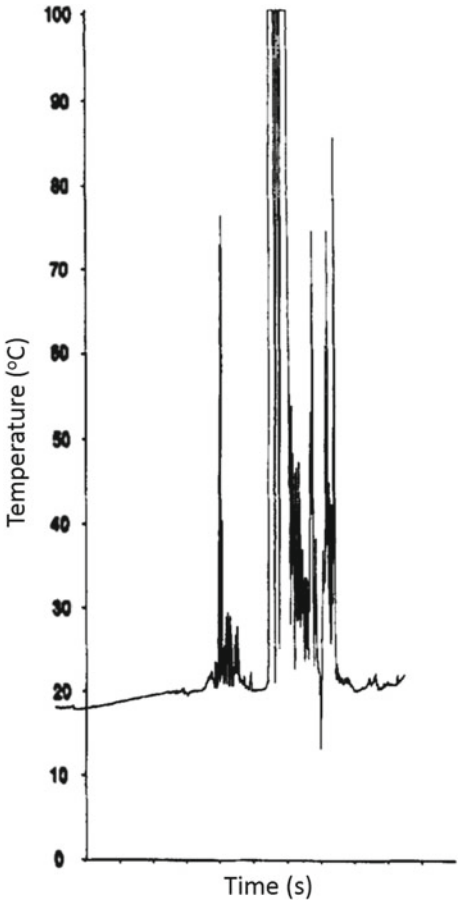

Fig. 5.20 Spikes in temperature when saline supply was turned off (reprinted from Toksvig-Larsen et al. [56] with permission. © 1990 Informa UK Ltd)

cooling was derived from the concept of minimum quantity lubrication (MQL). This essentially means usage of minimum lubricating fluid rather than large quantities. The former has the added advantage of enhancing the visibility of the area undergoing surgery, assisting the endoscopic operations. As stated earlier, the backward grinding method was relatively better in any case compared to forward grinding. The peak temperatures in each grinding cycle were much lower with mist cooled backward grinding method (Fig. 5.22). The authors also recommended using saline at 0 °C for effective cooling. It was also pointed out in another work that unsafe temperature

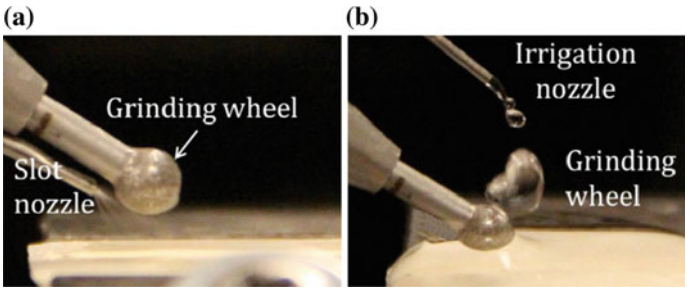

Fig. 5.21 Comparison between **a** mist and **b** flood irrigation cooling set ups during grinding (reprinted from Zhang et al. [44] with permission. © Elsevier)

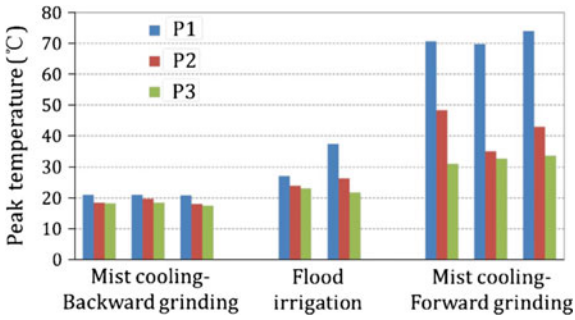

Fig. 5.22 Peak temperatures at depth of 0.5 (P1), 1 (P2) and 1.5 (P3) mm obtained during combinations of cooling systems and grinding modes (reprinted from Zhang et al. [44] with permission. © Elsevier)

level were reached during continuous grinding of bone with a diamond wheel even with a high flood irrigation flow rate of 720 ml/h [58]. It was also pointed out that the flood saline irrigation often obscured the operated area, particularly under the minimally invasive endoscopic operations [59]. These facts pointed out superiority of the mist cooling motivating further research in that direction.

It can be concluded that in case of temperature control, in general the following factors are very important irrespective of the machining process.

- Tool design.
- Proper operational practices.
- Optimum design for coolant dispenser system.
- Sufficiently high flow rate for coolant irrigation.
- Cryogenic coolant temperatures if the operation permits.

So far machining operations, conventional and non conventional methods, important physical aspects including critical factor of temperature rise during bone machining have been discussed. With advent of finite element (FE) based advanced computational capabilities, prediction of important process outcomes like temperature and stress evolution within the bone during machining has become possible. This ability especially becomes critical in case of non conventional techniques such

as laser processing where temperature variation occurs on time frames of the order of few seconds. In view of this, the following section explores the state of the art in computational modeling of the bone machining process.

References

1. W. Allan, E. Williams, C. Kerawala, Br. J. Oral Maxillofac. Surg. **43**(4), 314 (2005)
2. L.S. Matthews, C. Hirsch, J. Bone Joint Surg. **54**(2), 297 (1972)
3. H. Shin, Y. Yoon, J. Biomech. **39**(1), 33 (2006)
4. L. Zhang, B.L. Tai, G. Wang, K. Zhang, S. Sullivan, A.J. Shih, Med. Eng. Phys. **35**(10), 1391 (2013)
5. A. Brendemühl, M. Werner, M. Ivanenko, P. Hering, T.M. Buzug, in *Advances in Medical Engineering* (Springer, Berlin, 2007), pp. 419–424
6. S. Karmani, Curr. Orthop. **20**(1), 52 (2006). http://dx.doi.org/10.1016/j.cuor.2005.09.011. http://www.sciencedirect.com/science/article/pii/S0268089005001672
7. M. Kronenberg, N. Zlatin, *Mach. Sci. Appl*. (ASME, New York, 1967)
8. H. Gillies, Brit. Dent. J **71**, 351 (1941)
9. G. Augustin, T. Zigman, S. Davila, T. Udilljak, T. Staroveski, D. Brezak, S. Babic, Clin. Biomech. **27**(4), 313 (2012)
10. B.C. Sener, G. Dergin, B. Gursoy, E. Kelesoglu, I. Slih, Clin. Oral Implants Res. **20**(3), 294 (2009)
11. M. Hillery, I. Shuaib, J. Mater. Process. Technol. **92**, 302 (1999)
12. A.R. Eriksson, T. Albrektsson, B. Albrektsson, Acta Orthopaedica **55**(6), 629 (1984)
13. N. Sugita, T. Osa, M. Mitsuishi, Med. Eng. Phys. **31**(1), 101 (2009)
14. B.L. Tai, L. Zhang, A.C. Wang, S. Sullivan, G. Wang, A.J. Shih, Med. Eng. Phys. **35**(10), 1545 (2013)
15. G. Augustin, S. Davila, T. Udiljak, D.S. Vedrina, D. Bagatin, Arch. Orthop. Trauma Surg. **129**(5), 703 (2009)
16. O. Nam, W. Yu, M.Y. Choi, H.M. Kyung, in *Key Engineering Materials*, vol. 321 (Trans Tech Publications, 2006), pp. 1044–1047
17. N. Sugita, S. Warisawa, M. Mitsuishi, A cutting temperature study of bone machining for orthopaedic robotic surgery, in *Proceedings of the 20th Annual Meeting of the ASPE* (2005), pp. 142–145
18. C.D. Gerardi. Investigation of the Pool Boiling Heat Transfer Enhancement of Nano-engineered Fluids by Means of High-Speed Infrared Thermography, PhD Thesis, Massachusetts Institute of Technology, USA (2009)
19. C. Meola, G.M. Carlomagno, Meas. Sci. Technol. **15**(9), R27 (2004)
20. V. Kalidindi, Optimization of Drill Design and Coolant Systems During Dental Implant Surgery, PhD Thesis, University of Kentucky, USA (2004)
21. Y. Reingewirtz, S. Szmukler-moncler, B. Senger, Clin. Oral Implants Res. **8**(3), 189 (1997)
22. S.R. Davidson, D.F. James, J. Biomech. Eng. **125**(3), 305 (2003)
23. R.K. Pandey, S. Panda, J. Clin. Orthop. Trauma **4**(1), 15 (2013). http://dx.doi.org/10.1016/j.jcot.2013.01.002. http://www.sciencedirect.com/science/article/pii/S0976566213000039
24. C. Natali, P. Ingle, J. Dowell, Br. J. Bone Joint Surg. **78**(3), 357 (1996)
25. T. Udiljak, D. Ciglar, S. Skoric, Adv. Prod. Eng. Manag. **3**, 103 (2007)
26. F. Karaca, B. Aksakal, Acta Bioeng. Biomech. **15**(4) (2013)
27. T. Udiljak, D. Ciglar, K. Mihoci, in *9th International Scientific Conference on Production Engineering CIM2003* (Hrvatska znanstvena bibliografija i MZOS-Svibor, 2003)
28. K.N. Bachus, M.T. Rondina, D.T. Hutchinson, Med. Eng. Phys. **22**(10), 685 (2000)
29. M.B. Abouzgia, D.F. James, J. Oral Maxillof. Surg. **53**(11), 1308 (1995)

30. D.L. Brisman, Int. J. Oral Maxillof. Implants **11**(1), 35 (1995)
31. J. Eichler, R. Berg, Z Orthop **110**, 909 (1972)
32. G. Augustin, S. Davila, K. Mihoci, T. Udiljak, D.S. Vedrina, A. Antabak, Arch. Orthop. Trauma Surg. **128**(1), 71 (2008)
33. M. Hillery, I. Shuaib, J. Mater. Process. Technol. **92**, 302 (1999)
34. M.B. Abouzgia, J. Symington, Int. J. Oral Maxillof. Surg. **25**(5), 394 (1996)
35. K. Wiggins, S. Malkin, J. Biomech. Eng. **100**(3), 122 (1978)
36. W.R. Krause, D.W. Bradbury, J.E. Kelly, E.M. Lunceford, J. Biomech. **15**(4), 267 (1982)
37. N. Sugita, K. Ishii, J. Sui, M. Terashima, CIRP Ann.-Manuf. Technol. **63**(1), 101 (2014)
38. N. Sugita, T. Nakano, Y. Nakajima, K. Fujiwara, N. Abe, T. Ozaki, M. Suzuki, M. Mitsuishi, J. Mater. Process. Technol. **209**(17), 5777 (2009)
39. A. Malvisi, P. Vendruscolo, F. Morici, S. Martelli, M. Marcacci, in *Medical Image Computing and Computer-Assisted Intervention–MICCAI 2000* (Springer, 2000), pp. 1238–1244
40. W. Krause, J. Biomech. Eng. **109**(3), 263 (1987)
41. H.K. Parsa, An Investigation Into the Temperature Distribution Resulting from Cutting of Compact Bone Using a Reciprocating Bone Saw, Master's Thesis, Institute of Technology, Sligo, Ireland (2006)
42. P. Tetsch, J. Maxillof. Surg. **2**, 141 (1974)
43. B.L. Tai, L. Zhang, A. Wang, S. Sullivan, A.J. Shih, Procedia CIRP **5**, 226 (2013)
44. L. Zhang, B.L. Tai, A.C. Wang, A.J. Shih, CIRP Ann.-Manuf. Technol. **62**(1), 367 (2013)
45. T. Enomoto, H. Shigeta, T. Sugihara, U. Satake, CIRP Ann.-Manuf. Technol. **63**(1), 305 (2014)
46. A. Brendemühl, M. Werner, M. Ivanenko, P. Hering, T.M. Buzug, Biomedizinische Technik **50**(1), 1264 (2005)
47. W. Moses, F. Witthaus, H. Hogan, W. Laster, Exp.Therm. Fluid Sci. **11**(1), 34 (1995)
48. E. Bagci, B. Ozcelik, Int. J. Adv. Manuf. Technol. **34**(9–10), 867 (2007)
49. J. Lundskog, Scand. J. Plast. Reconstr. Surg. **9**, 1 (1971)
50. M. Esposito, J.M. Hirsch, U. Lekholm, P. Thomsen, Eur. J. Oral Sci. **106**(3), 721 (1998)
51. G. Augustin, S. Davila, T. Udilljak, T. Staroveski, D. Brezak, S. Babic, Int. Orthop. **36**(7), 1449 (2012)
52. C. Lavelle, D. Wedgwood, J. Oral Surg. (American Dental Association: 1965) **38**(7), 499 (1980)
53. P. Proff, T. Bayerlein, A. Kramer, S. Allegrini Jr., S. Dietze, J. Fanghänel, T. Gedrange, Folia Morphologica **65**(1), 34 (2006)
54. S.T. Larsen, L. Ryd, Acta Orthop. **60**(4), 439 (1989)
55. S. Toksvig-Larsen, L. Ryd, A. Lindstrand, Br. J. Bone Joint Surg. **73**(1), 13 (1991)
56. S. Toksvig-Larsen, L. Ryd, A. Lindstrand, An internally cooled saw blade for bone cuts: Lower temperatures in 30 knee arthroplasties. Acta Orthop. **61**(4), 321 (1990)
57. S. Toksvig-Larsen, L. Ryd, A. Lindstrand, J. Arthroplasty **7**(1), 21 (1992)
58. S. Kondo, Y. Okada, H. Iseki, T. Hori, K. Takakura, A. Kobayashi, H. Nagata, Neurosurgery **46**(5), 1162 (2000)
59. M. Sasaki, S. Morris, T. Goto, K. Iwatsuki, T. Yoshimine, Neurol. Med.-Chir. **50**(10), 900 (2010)

Chapter 6
Computational Modeling in Bone Machining

In general machining of materials is a complex process involving several process and material parameters. During machining, multiple physical phenomena are associated with combination of these process and material parameters. These physical phenomenon may occur simultaneously or in sequence rendering the process of machining very complex. The complexity of machining further depends upon the type of machining process and the nature of material being machined. Especially, in case of bone, as described in Chap. 1, which is a multicomponent, multi-composition, and hierarchical material that in turn makes its interaction with a machining tool (mechanical or heat based) very complicated. To understand such interaction and involved physical phenomena during bone machining is very important to control the machining process for desired outcome. However, inherently complex nature of bone machining renders it to inability for in-situ probing of the physical phenomena employing any experimental techniques. In view of this, either numerical or analytical computational modeling appears to be a suitable approach in designing a bone machining process for desired outcome. Nonetheless, due to the complex nature of bone machining, the search of open literature revealed paucity of efforts on computational modeling. Only limited efforts were focused on heat transfer and stress based computational modeling. Furthermore, some of the efforts have also tried to model micro scaled mechanics in bone. Hence, the current chapter is divided in to three sections; heat transfer model, stress based models, and micro scaled models. Key equations and process parameters in each case have been elaborated. Important studies concerning all these aspects have been discussed.

6.1 Heat Transfer Models

Prediction of heat transfer during bone machining process aids in optimization of the operation intended to minimize the damage by thermal necrosis. Basic equation governing the heat transfer (Eq. 6.1) within the bone forms the foundation of thermal finite element model (FEMs).

N.B. Dahotre and S.S. Joshi, *Machining of Bone and Hard Tissues*,
DOI 10.1007/978-3-319-39158-8_6

$$\rho C_P \left(\frac{\partial T}{\partial t}\right)_{(x,y,z)} = k' \left[\left(\frac{\partial T}{\partial x}\right)_{(y,z.t)} + \left(\frac{\partial T}{\partial y}\right)_{(x,z.t)} + \left(\frac{\partial T}{\partial z}\right)_{(x,y.t)}\right] \tag{6.1}$$

where ρ is the density, C_P is the specific heat capacity and k' is the thermal conductivity of the material, T is the temperature, t is the time and x,y,z are the Cartesian coordinates of the position. If $Q_{x,y,z}$ is the heat generated by the heat source then the net heat balance because of heat losses happening as a result of convections and radiation is expressed according to Eq. 6.2.

$$-k'\left[\frac{\partial T}{\partial x} + \frac{\partial T}{\partial y} + \frac{\partial T}{\partial z}\right] = Q_{x,y,z} - h[T - T_0] - \epsilon' S'[T^4 - T_0^4] \tag{6.2}$$

where ϵ' is the emissivity, h is the convective heat transfer coefficient, S' is the Stephen Boltzman's constant and T_0 is the ambient temperature. Appropriate boundary conditions are to be applied based on the geometry of the machining setup being modeled to get the solution of temperature distribution.

Heat transfer model was designed for grinding process [1]. The spherical tool was considered to be composed of number of elemental grinding wheels (EGW) of radius r and width b_w (Fig. 6.1a). The number of EGWs in contact with bone surface were calculated using depth of cut, a and tilt angle, α. The heat flux was divided into each EGWs (Fig. 6.1b, c), and expressed according to Eq. 6.3.

$$Q_{x,y,z} = P' \frac{F_t V_s}{b_w l} \tag{6.3}$$

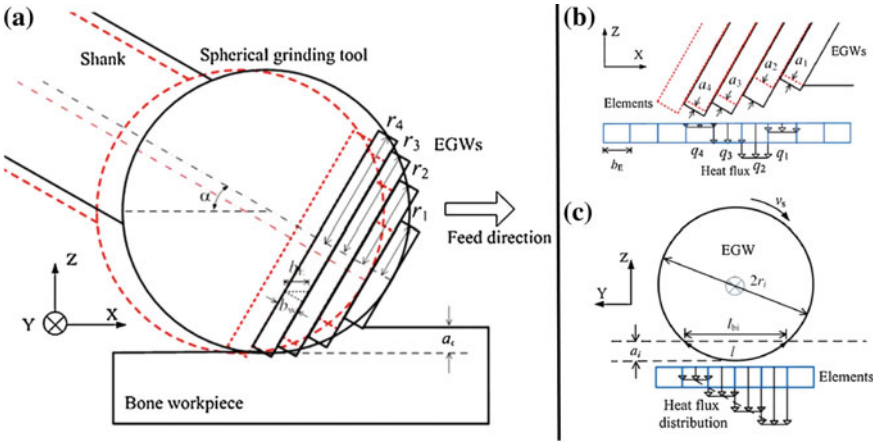

Fig. 6.1 Schematic of geometry of grinding wheel. **a** Elemental grinding wheels (EGWs), configuration of EGWs with heat flux distribution in **b** XZ plane and **c** YZ plane (reprinted from Zhang et al. [1] with permission. © Elsevier)

where F_t is the tangential force, V_s is the tangential speed, l is the contact length between EGW and bone surface in the YZ-plane, and P' is the partition ratio defined as the percentage of power consumption that is transferred to the bone as thermal energy. F_t has been related to cutting depth (Eq. 6.4) and V_s has been related to rotational speed ω of the tool and radius r of the EGW (Eq. 6.5).

$$F_t = ka \tag{6.4}$$

$$V_s = \omega r \tag{6.5}$$

where k is a constant. The model was verified using experimental setup consisting of four thermocouples situated around the grinding tool and temperature predictions were remarkably close to the thermocouple readings (Fig. 6.2). Same group also investigated prediction of grinding temperatures by coupling the pulse width modulation (PWM) factor of high speed grinding motor and FEM [2]. The prediction was again very close to the experimental results with an error of less than 20 %.

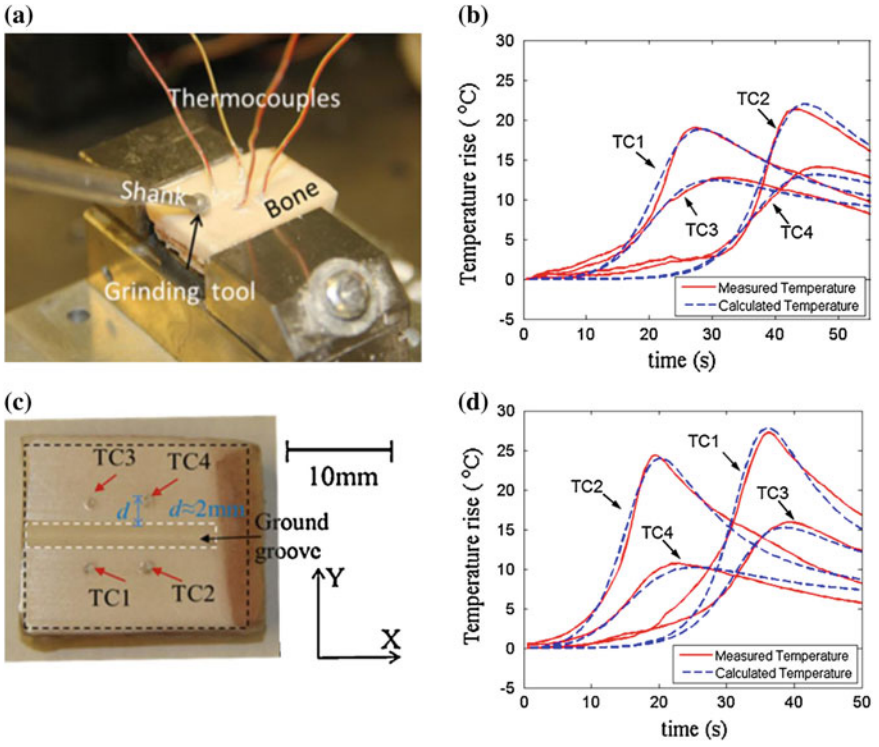

Fig. 6.2 Photographs illustrating **a** the thermocouples and the grinding tool, **b** location of thermocouples, and validation plots for **c** forward feed and **d** backward feed (reprinted from Zhang et al. [1] with permission. © Elsevier)

Heat transfer model was also applied to drilling process [3, 4]. Similar to the case of grinding, the input energy for each cutting lip was calculated in terms of shear force and shear velocity (Eq. 6.3). Summation of heat generated by each lip gave total heat generated. Extensive details about evolution of the model and specific boundary conditions have been given in the literature refereed here [3, 4]. The present discussion has been confined to key equations and predictions. This heat can be further expressed in terms of shear rate, shear force, and velocity as per the Eq. 6.6 [4].

$$Q_{x,y,z} = \eta A_s \tau_s \dot{\gamma_{AB}} V_s \tag{6.6}$$

where η is the axial coordinate of the cylindrical system, A_s is the shear plane area, τ_s is the shear stress, and $\dot{\gamma_{AB}}$ is the shear strain rate. Polar coordinate system can be employed to incorporate the effect of drill bit radius. The progress of drilling predicted by the model by Lee et al. [3] is shown in Fig. 6.3. Rise in temperature with increasing drilling depth is clearly seen. Cooling was incorporated in a simplistic manner by assigning the lower initial temperature to the drill bit and predictions were made (Fig. 6.4). In another modeling study, influence of drill parameters on bone temperature and necrosis was investigated [5]. The effects of various parameters on bone temperature during drilling were very similar to actual experimental results as discussed in Chap. 5. In addition, the effect of gender on bone temperature rise was also explored (Fig. 6.5) [5]. The variation in bone mineral density (BMD) was thought to give such trend of temperature with drill rotation speeds. Alam et al. [6] predicted an increase in the necrosis penetration depth as function of drilling speed based on a thermo-mechanically coupled FEM for various cooling conditions. Increase in feed rate was also reported to increase the bone temperature. In a similar effort [7], a damage function was defined as the natural logarithm of the ratio of

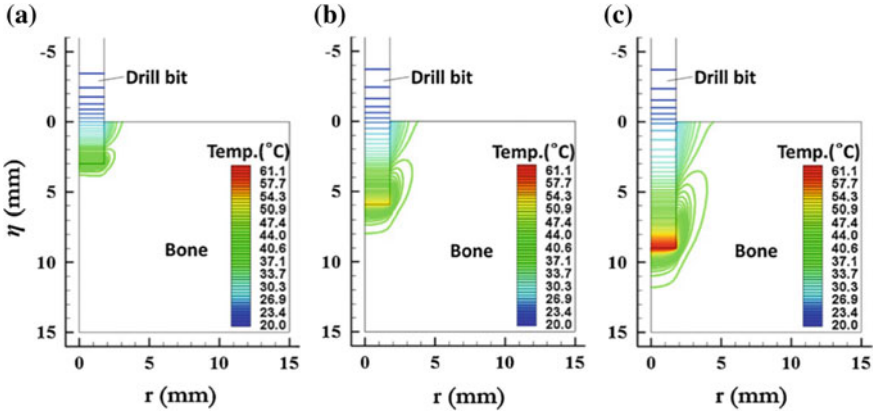

Fig. 6.3 Predicted temperature distribution during bone drilling at the depth of **a** 3 mm, **b** 6 mm, and **c** 9 mm (initial drill temperature 20 °C and bone 37 °C, drill diameter of 3.5 mm, point angle of 90° and helix angle of 23° (reprinted from Lee et al. [3] with permission. © Elsevier))

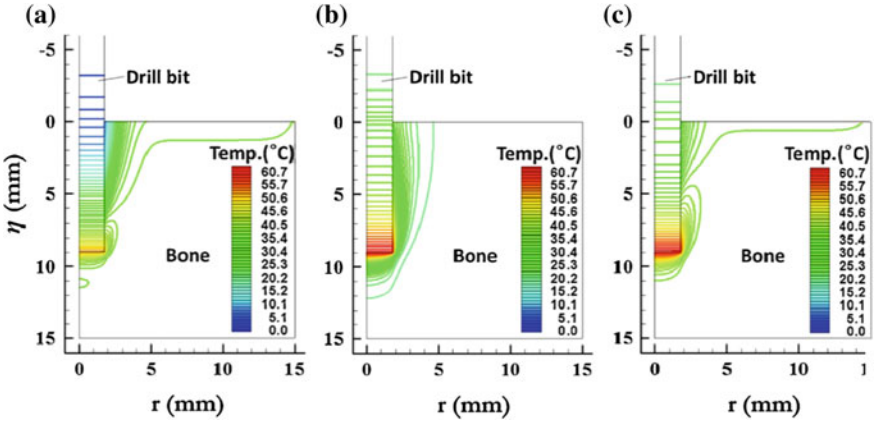

Fig. 6.4 Effect of cooling with initial temperature of drill bit and bone as **a** 0° for drill bit and 37° for bone, **b** both at 20° and **c** 20° for drill bit and 37° for bone (reprinted from Lee et al. [3] with permission. © Elsevier)

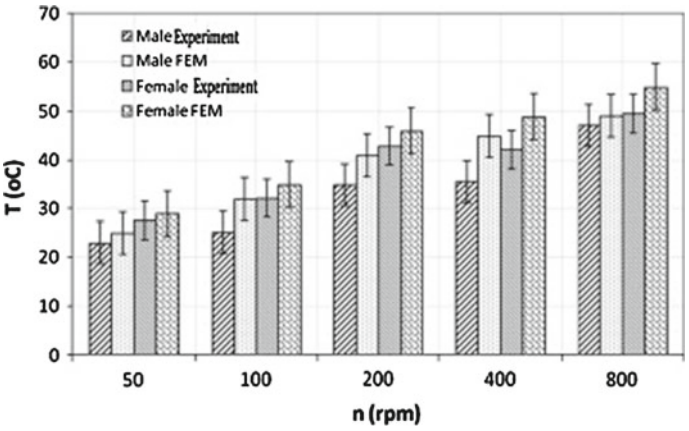

Fig. 6.5 Predicted and experimental values of temperatures during drilling of male and female bones for various drill rotation speeds (reprinted from Sezek et al. [5] with permission. © Elsevier)

original concentration of undamaged bone cells to the concentration of remaining undamaged bone cells at time t. It was expressed according to Eq. 6.7 and coupling it with heat transfer model indicated the regions on the bone surface undergoing thermal necrosis.

$$D(t,x) = \int_0^t \alpha e^{\left(\frac{-\beta}{RT(t,x)}\right)} dt \tag{6.7}$$

where R is the universal gas constant, α and β are tissue parameters determined experimentally. Thermal modeling in case of drilling has been extensively advanced. Here only some of the selected works have been reviewed to provide an idea about approaches of the model. In addition, there are number of other modeling studies one

might refer to, exploring the effect of drilling parameters on temperature evolution in the bone [8–13].

Temperature in most of the cases is a side effect of machining forces applied by the tools. Only exceptions are heat based machining methods such as laser processing. In view of this, it becomes an integral part of the modeling community. A review of mechanical force (stress) based modeling has been presented in the next subsection.

In case of laser processing, the heat from the beam is expressed according to Eq. 6.8 [14, 15]. This gives the Gaussian distribution of the energy. The incoming heat is then distributed according to Eq. 6.2. In this case, the material removal takes place by means of heat rather than by mechanical tools as in case of the conventional methods.

$$Q_{x,y,z} = \frac{P_0}{A} * exp\left[-\frac{(x - Vt)^2 - y^2}{2S_D^2}\right] \tag{6.8}$$

where x, y, and z are the coordinates of beam on sample surface, P_0 is the laser power, A is the beam cross sectional area, V is the beam velocity, t is the time and S_D is the standard deviation of the beam. A typical example of beam profile and model geometry along with the boundary conditions are shown in Fig. 6.6 [15] and corresponding mathematical equations are listed in Table 6.1. The corresponding depth profiles of the temperatures developed during Nd-YAG laser base machining of a bovine bone are shown (Fig. 6.7a) [15] along with the calculated machining

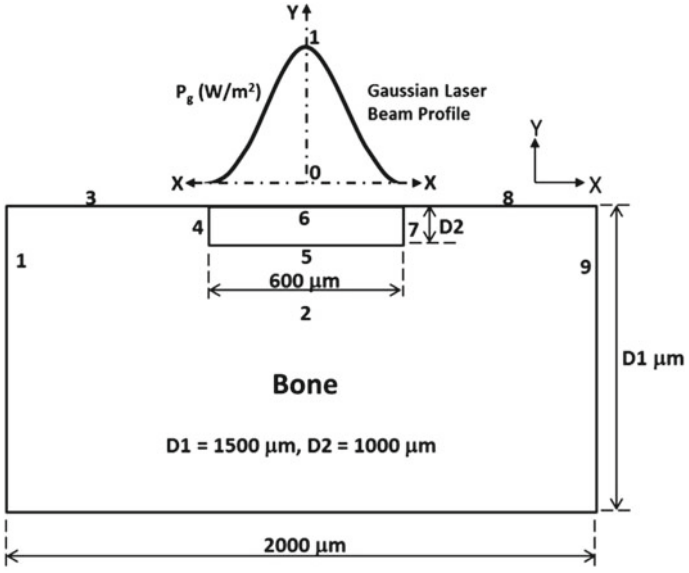

Fig. 6.6 Schematic of bone geometry used in the modeling as well as the boundary conditions applied [15]

Table 6.1 Boundary conditions associated with Fig. 6.6 [15]

Boundary no.	Boundary conditions	Equation
Whole geometry	Governing equation	$\rho c_p \left[\frac{\partial T}{\partial t}\right] = k\left[\left(\frac{\partial^2 T}{\partial x^2}\right) + \left(\frac{\partial^2 T}{\partial y^2}\right)\right]$
6	Heat flux, natural convection cooling and radiation	$-k\frac{\partial T}{\partial y} = \varphi P_g - h[T - T_i] - \varepsilon\sigma\left[T^4 - T_i^4\right]$ where, $\varphi = 1$ for $0 \leq t \leq t_r$, and $\varphi = 0$ for $t \geq t_r$
	Average laser power density in Gaussian distribution	$P_g = A\left[\frac{P}{\left(\frac{\pi}{4}D^2\right)}\right] \cdot \exp\left[-\left(\frac{(x-x_r)^2}{2\emptyset^2}\right)\right]$
1, 9	Natural convection cooling and radiation	$-k\frac{\partial T}{\partial x} = h[T - T_i] - \varepsilon\sigma\left[T^4 - T_i^4\right]$
3, 8	Natural convection cooling and radiation	$-k\frac{\partial T}{\partial y} = h[T - T_i] - \varepsilon\sigma\left[T^4 - T_i^4\right]$
2	Insulation	$\frac{\partial T}{\partial y} = 0$

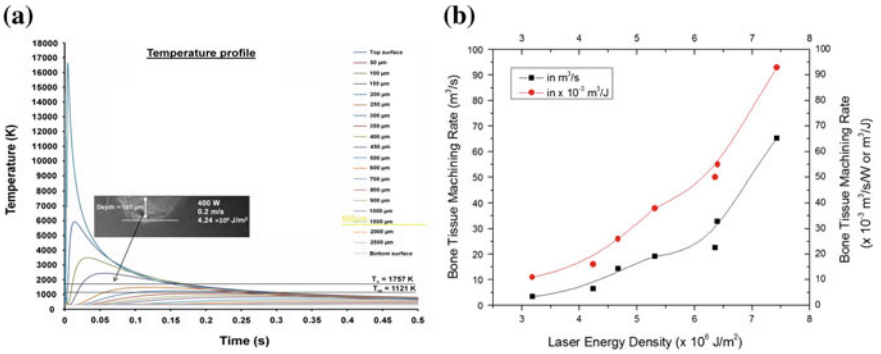

Fig. 6.7 Output of laser based machining of bovine bone. **a** Temperature evolution as function of time, and **b** machining rate as function of laser energy density [15]

rates (Fig. 6.7b) [15]. These results clearly illustrate the short time frames and ease of material removal by means of a laser.

Thermal FEMs are thus a good tool in predicting the temperature evolution in surface sub-surface regions of the bone during various conventional and non-conventional machining methods. Table 6.2 summarizes equations for the heat fluxes input by these various processes. Apart form temperature, mechanical loading also determines the machining characteristics as well as induces effects such as surface damage and roughness as discussed in Chap. 1. Computational efforts related to mechanical force (stress) based FEMs have been reviewed in the following section.

Table 6.2 Heat flux equations for various bone machining processes

Machining process	Input heat flux (Please see the text for parameters)
Grinding	$Q_{x,y,z} = \epsilon \frac{F_t V_s}{b_w l} Q_{x,y,z} = \eta A_s \tau_s \dot{\gamma_{AB}} V_s$
Drilling	$Q = -(k_d A_d + k_c A_c) \frac{\partial T}{\partial Z}\|_{z=0} k_b (A_d + A_c) \frac{\partial T}{\partial \eta}\|_{\eta=\eta_D}$
Laser (Gaussian beam)	$Q_{x,y,z} = \frac{P_0}{A} * exp\left[-\frac{(x-Vt)^2-y^2}{2S_D^2}\right]$

6.2 Stress Based Models

During any bone machining involving mechanical operation with tools, shearing takes place. When shear force exceeds the fracture strength of the material, chip formation takes place resulting in material removal. Along with shear, these forces can be divided/resolved into various components such as gravity, normal, and shear components.

A 3D FEM was developed for thrust force experienced during drilling of the bone. An elastic-plastic material model was used to predict the fracture of cortical bone [16]. Thus the total strain ϵ was expressed according to Eq. 6.9.

$$\epsilon = \epsilon^{el} + \epsilon^{pl} \tag{6.9}$$

where ϵ^{el} is the elastic and ϵ^{pl} is the plastic component of ϵ. Hill's potential for anisotropic materials was used to explain elastic regime. Strain rate dependent behavior of the bone was considered as expressed in Eq. 6.10.

$$\epsilon^{pl} = d\left(\frac{\sigma}{\sigma_0} - 1\right)^n \tag{6.10}$$

where σ is the yield stress under different strain rates, σ_0 is the static yield stress, and d and n are material constants. Element removal scheme was applied in order to depict chip formation and plastic strain at the onset of damage was defined according to Eq. 6.11.

$$\epsilon_D^{pl} = f(\eta, \dot{\bar{\epsilon}}^{pl}) \tag{6.11}$$

where η= p/q is the stress triaxiality (p is the pressure stress and q is the Mises equivalent stress) and $\dot{\bar{\epsilon}}^{pl}$ is the strain rate. A state variable, ω_D was defined to increase monotonically with plastic deformation. The damage was initiated when condition in Eq. 6.12 was met by ω_D. Finally, the fracture energy G_f was expressed according to Eq. 6.13. The geometry of simulation has been shown in Fig. 6.8a, while the boundary conditions are shown in Fig. 6.8b. The results predicting thrust force and torque for simulations with 73 N force were quite matching with the experimental trials performed with 70 and 75 N (Fig. 6.8c, d). Similar matching was observed in case of feed rates.

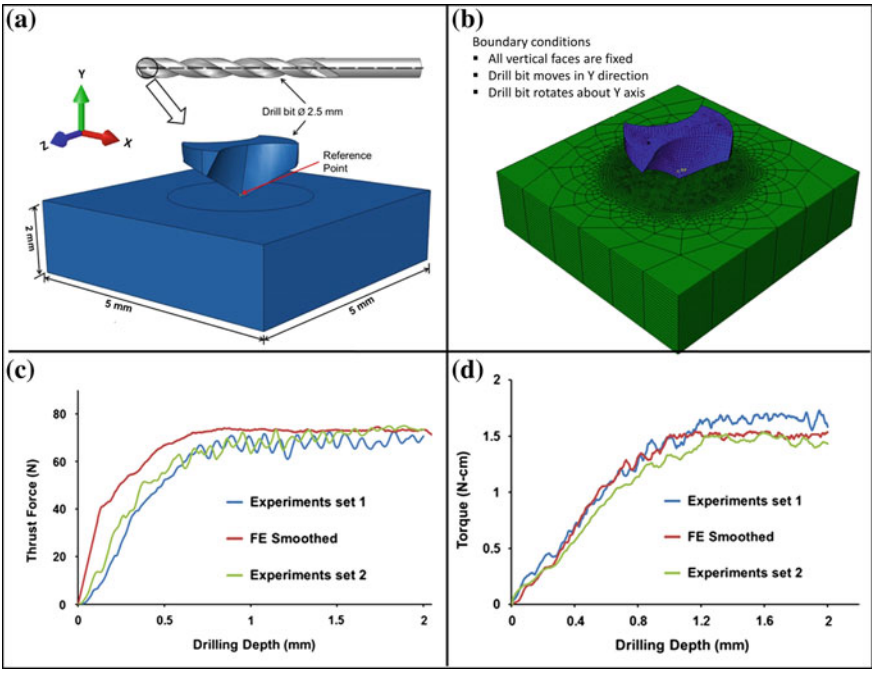

Fig. 6.8 Set of figures showing **a** over all geometry, **b** boundary conditions, and **c**, **d** match between thrust force and torque (reprinted from Lughmani et al. [16] with permission. © Elsevier)

$$\omega_D = \int \left(\frac{1}{\epsilon_D^{pl}(\eta, \dot{\bar{\epsilon}}^{pl})} \right) d(\bar{\epsilon}^{pl}) = 1 \tag{6.12}$$

$$G_f = \int_{\bar{\epsilon}^{pl}}^{\bar{\epsilon}^f} \sigma_y d\bar{\epsilon}^{pl} \tag{6.13}$$

where $(\bar{\epsilon}^{pl})$ is strain hardening term and $\bar{\epsilon}^f$ is the strain at failure.

Force based modeling approach has been applied extensively in case of orthogonal cutting [11, 17–21]. The basic issue in this process is related to the bone structure consisting of osteons (Fig. 6.9a). The orientation of osteons also has a great influence on overall orthogonal cutting process (Fig. 6.9b). This arises because of anisotropy within the properties of the osteons depending on their orientation with respect to the loading direction (Fig. 6.10 and Table 6.3 [22]) as well as rate dependence (Fig. 6.11) [23]. The influence of anisotropy in numerical modeling of orthogonal cutting of cortical bone was taken in to account by Santiuste et. al. [17]. The stress during cutting was defined as the function of strain hardening term $(\bar{\epsilon}^{pl})$, strain rate $(\dot{\bar{\epsilon}}^{pl})$, and temperature influence term (Φ) as expressed in Eq. 6.14. The temperature effect in

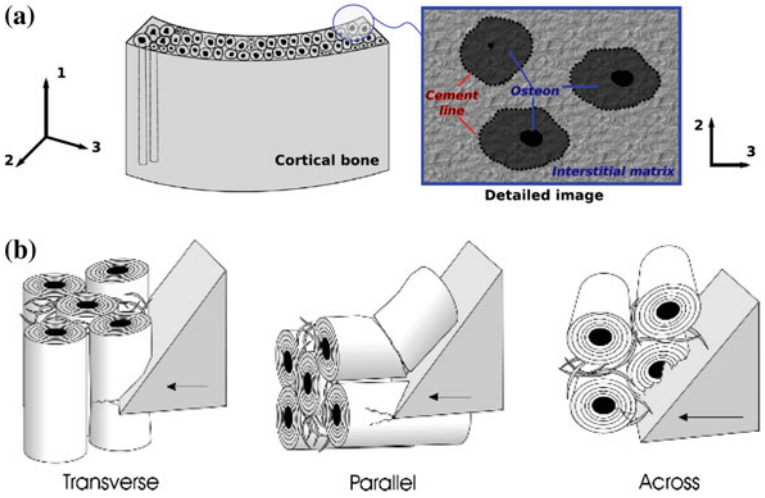

Fig. 6.9 Schematics showing **a** a general structure of bone consisting of osteons (reprinted from Santiuste et al. [17] with permission. © Elsevier) and **b** various cutting modes based on the orientation of osteons with respect to cutting tool (reprinted from Plaskos et al. [19] with permission. © Springer)

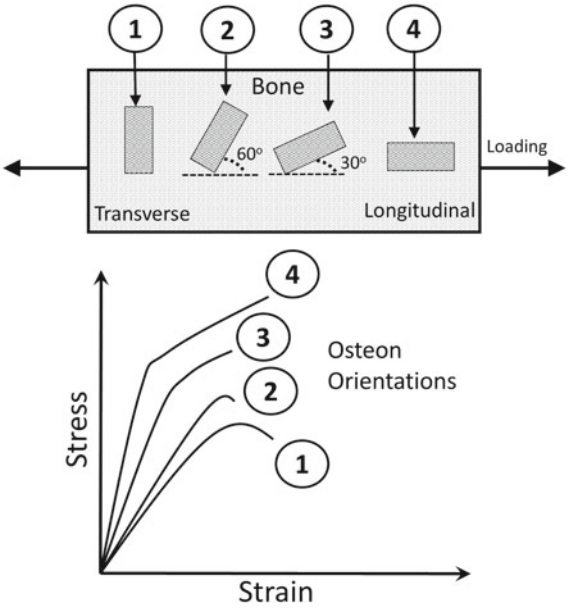

Fig. 6.10 Schematic of effect of orientation of osteons on stress strain behavior of cortical bone [23]

terms of Φ was expressed according to Eq. 6.15. Temperature influence on the other hand was neglected by some researchers [18]. In addition, the frictional stresses, σ_{fr}, arising because of tool-material interaction haven been expressed according to Eq. 6.16 [11].

Table 6.3 Approximate stress strain values of cortical bone for various osteon orientations

Osteon orientation	Yield strain (%)	Yield stress (MPa)	Strain to failure (%)	Ultimate tensile strength (MPa)
Transverse	0.50	80	0.65	90
30°	0.45	100	0.55	110
60°	0.55	150	0.90	170
Longitudinal	0.40	170	1.6	210

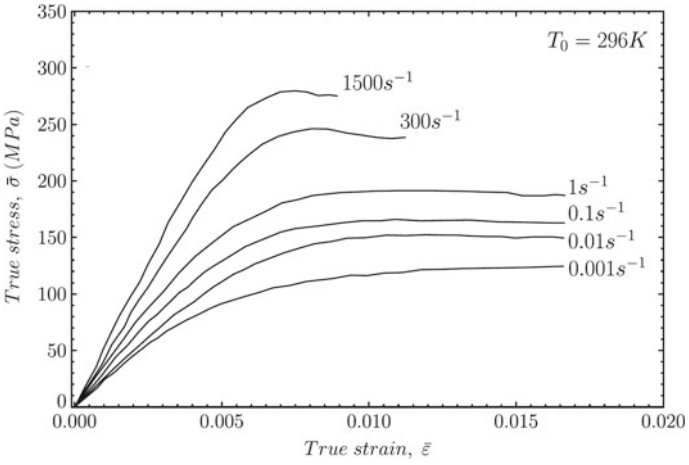

Fig. 6.11 Strain rate sensitivity of cortical bone (reprinted from Keaveny et al. [23] with permission. © McGraw-Hill)

$$\sigma(\bar{\epsilon}^{pl}, \dot{\bar{\epsilon}}^{pl}, T) = [A + B(\bar{\epsilon}^{pl})^n]\left[1 + Cln\left(\frac{\dot{\bar{\epsilon}}^{pl}}{\dot{\bar{\epsilon}}_0}\right)\right][1 - \Phi^m] \tag{6.14}$$

$$\Phi = \frac{T - T_0}{T_M - T_0} \tag{6.15}$$

where A and B are material constants, n is the strain hardening exponent, m is the temperature sensitivity, C is the constant with its value being 0.03 for bone, T_0 is the initial temperature, and T_m is the melting temperature and $\dot{\bar{\epsilon}}_0$ is the strain in osteon.

$$\sigma_{fr} \leq -\mu\frac{\bar{\sigma}}{\sqrt{3}}\frac{2}{\pi}arctan\left(\frac{V_r}{V_{cr}}\right) \tag{6.16}$$

where $\bar{\sigma}$ is the equivalent stress, V_r is a relative sliding velocity, V_{cr} is a critical sliding velocity below which sticking occurs, and μ is a friction coefficient.

Further progress of simulation of orthogonal cutting with consideration to temperature effects and comparison between isotropic and anisotropic approaches (incorporating orientation influences) is shown in Fig. 6.12 [11, 17, 18]. The realistic

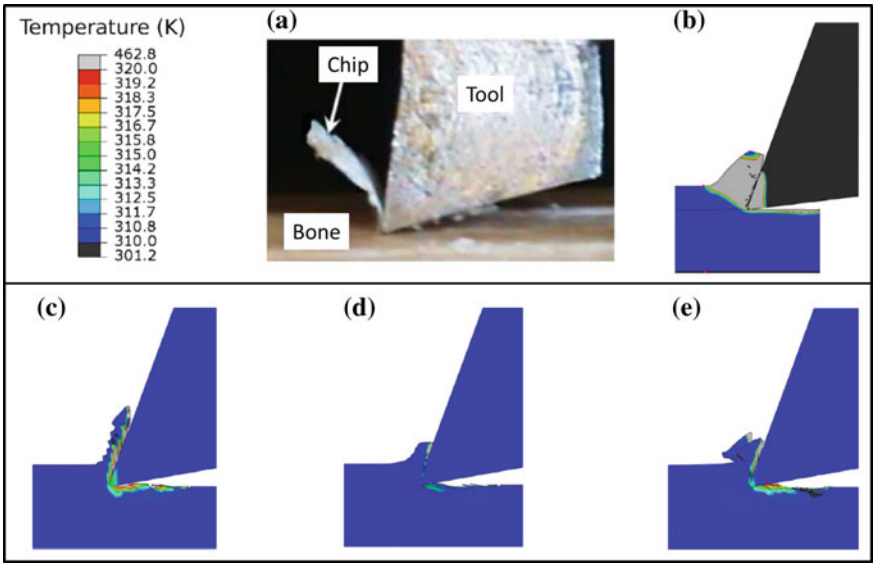

Fig. 6.12 Set of figures showing, **a** actual orthogonal cutting of bone; **b** modeling of the process with isotropic approach; and three modes of cutting using anisotropic approach showing **c** longitudinal, **d** across and **e** transverse cutting (reprinted from Santiuste et al. [17] with permission. © Elsevier)

nature of anisotropic model in chip formation and temperature distribution can be clearly seen. Formation of continuous chip is predicted for longitudinal orientation (Fig. 6.12a) whereas small chips due to the erosion for the across orientation (Fig. 6.12b). Triangular shaped chip is predicted for the transversal orientation, corresponding to the rupture of the interstitial matrix (Fig. 6.12c). The force generation in isotropic and anisotropic models is manifested in stabilization of the phase in both the cases (Fig. 6.13a). The force predicted increases as the orientation of bone changes from longitudinal to across to transverse (Fig. 6.13b). The experimental measurement matches with overall average of these three orientations.

In another study, saw cutting based process was modeled to predict mechanical response of the bone [24]. The geometry of the model consisted of particle elements in the cross section which was in direct contact with the saw surface so as to mimic the bone structure. The rest of the geometry was treated as a continuum. The cutting tool was first scanned by a 3D scanning optical microscope and then was modeled as the rigid body (Fig. 6.14). The coefficient of friction was assumed to be 0.3 between the blade surface and the bone. The penetration of blade into the bone was modeled based on depth of cut, stress and strain distribution, and fracture mechanics. Furthermore, in order to have a realistic approach, progressive damage of the bone was considered. It was based on decrease in yield strength and stiffness of the bone and was governed by energy dissipation rate. The onset of failure was assumed at 2 % failure strain. The difference between model considering progressive damage and

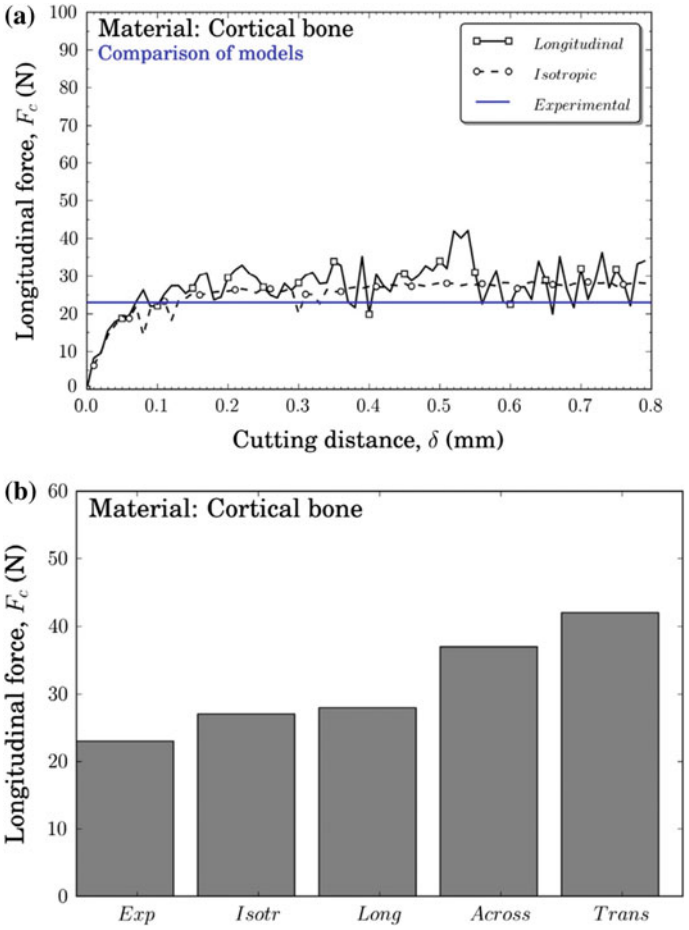

Fig. 6.13 Comparison of isotropic and anisotropic models showing, **a** force profile and **b** orientation effects on predicted force (reprinted from Santiuste et al. [17] with permission. © Elsevier)

the one which does not take it into account is shown in Fig. 6.15. The stress distribution indicated a higher stresses at the tool tip. It also indicated that as the depth of cut increased, higher fraction of bone cross section was stressed. Furthermore, the model predicted that mechanically failed regions remained in the vicinity of the tool in spite of having much larger stressed zones (Fig. 6.16). The damage induced as result of crack propagation was predicted using the model in two different bone axis orientations and was confirmed using high speed camera and optical images of actual cutting process (Fig. 6.16). The predictions of model closely matched that of actual process with parallel orientation experiencing maximum damage.

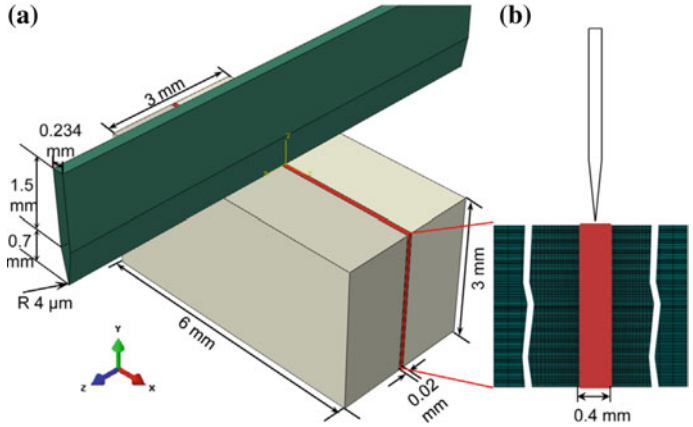

Fig. 6.14 **a** Schematic of geometry of sharp-cutting tool model and the bone (*gray* color presents the shape of experimental specimens, *red* is used for the FE model); and **b** x–y plane of FE model showing cross section containing particle elements [24]

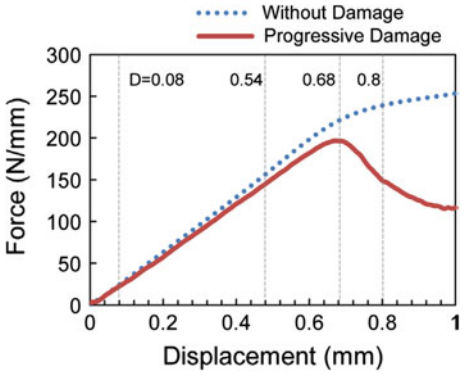

Fig. 6.15 Evolution of cutting force (per unit width) with penetration depth calculated employing models with and without account for damage [24]

The understanding developed in case of conventional cutting was also carried forward for ultrasonic cutting [11]. In this case, the tool and work piece remain in intermittent contact. The tool has a vibrating frequency, f; angular frequency, ω; amplitude, a, and time period, $t_p r$. The cutting occurs during the interaction time periods t_a and t_b (Fig. 6.17). The maximum cutting force is generated and applied during this period. The displacement, x and tool vibration, speed V_{vib} are expressed by Eqs. 6.17 and 6.18 [11]. The vibrational condition gets satisfied if the tool speed (2πaf) becomes higher than work velocity (V_c). The ratio r of time of cutting to time period expressed as $(t_b - t_a)/t_{pr}$. The cutting relation based on this frame work is then expressed according to Eq. 6.19 [25].

$$x = asinn\omega t = asin(2\pi ft) \tag{6.17}$$

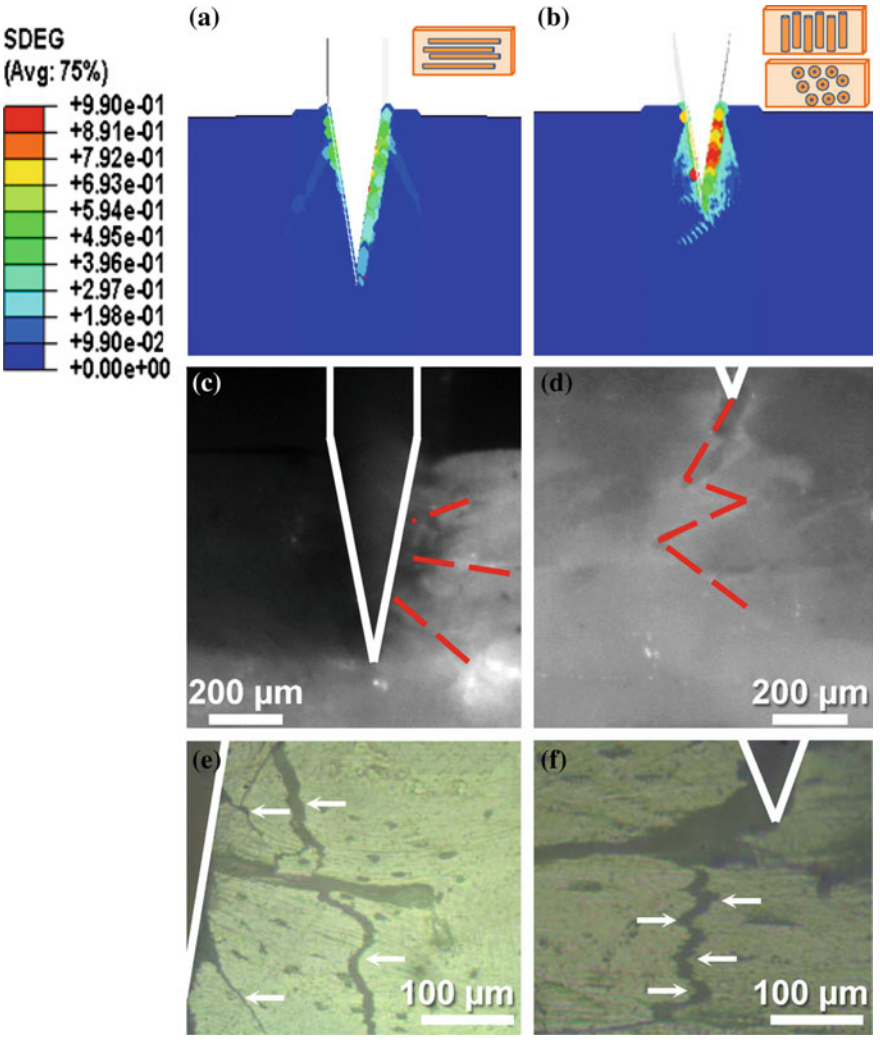

Fig. 6.16 Comparison of simulation results (**a**, **b**) with images taken with high-speed camera (**c**, **d**) and optical microscopy (**e**, **f**) of damage induced by cutting along different directions: **a**, **c** and **e** perpendicular to bone axis, lateral damage propagation was observed; **b**, **d** and **f** parallel to bone axis, damage was in front of cutting tip. *White lines* designate the profile of razor blade and *red dotted lines* indicate crack lines and *arrows* point at the crack path [24]

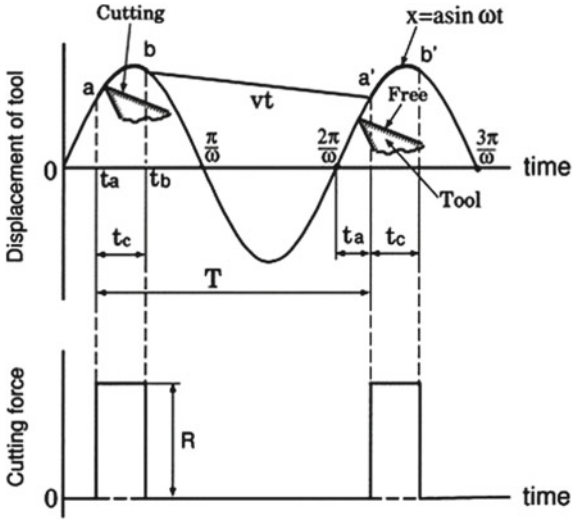

Fig. 6.17 Mechanism of pulsating cutting force in ultrasonically-assisted cutting (reprinted from Xiao et al. [25] with permission. © Elsevier)

where n is the angular velocity.

$$V_{vib} = a\omega cos\omega t \tag{6.18}$$

$$\frac{af}{v_c} = \frac{1-r}{2sin\pi r cos\left[cos^{-1}(\frac{v_c}{2\pi af}) - \pi r\right]} \tag{6.19}$$

So far the models which are primarily based on continuum approach have been discussed from thermal and mechanics point of view. It was clear from the discussion that thermophysical properties of bone play a critical role in determining its response to machining. The distribution of bone constituents on micro scale forms the basis of overall thermophysical properties of bones and hard tissues. The following section reviews some of the efforts which have attempted to model the micro mechanics of the bone in a micro structure based geometry.

6.3 Micro-scaled Modeling

As discussed in Chap. 4, micro-cracks play a critical role during bone fracture process and may also act as toughening agents. In order to capture the physical phenomena occurring on micro scale during bone machining, the bone microstructure was modeled using XFEM model [26, 27]. Three types of composite structures were considered and designated as Model A (homogeneous), Model B (a composite structure

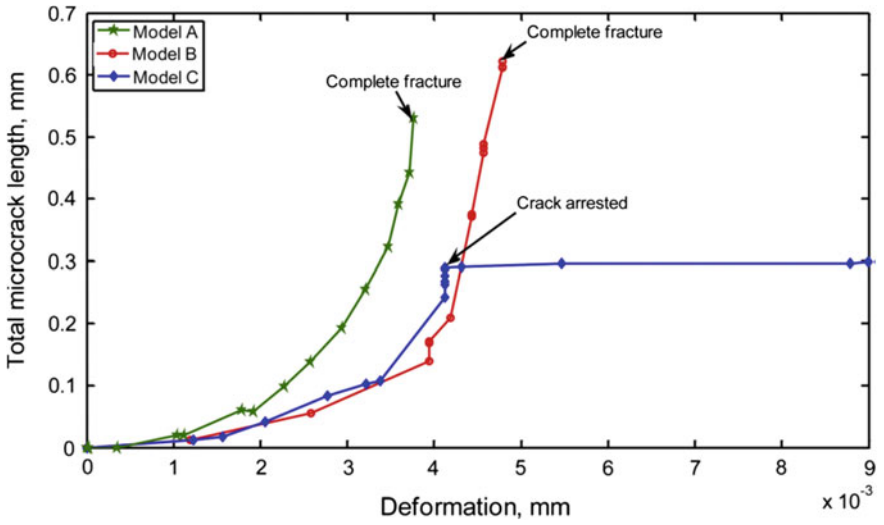

Fig. 6.18 Evolution of total crack length with deformation under tension in three studied models (reprinted from Xiao et al. [25] with permission. © Elsevier)

without cement lines), and Model C (composite with cement lines). The geometry was constructed after acquiring actual bone micrograph and osteon were constructed as circular elements (Fig. 4.1 [26]). The model assumed linear elastic behavior followed by damage initiation and progression. The Models A and B indicated crack growth leading to failure where as presence of cement lines in Model C predicted a crack arrest (Fig. 6.18). The results were realistic and presence of cement lines was considered very critical so as to sustain presence of micro cracks and further arresting their growth (Fig. 6.19).

Similar approach was involved in another investigation where a geometry of fracture toughness specimen of the bone was modeled using using cohesive finite elements [28]. A continuum based model was constructed and at the crack trip the micro scaled geometry was constructed (Fig. 6.20). The study concluded with the similar finding that the bone response to macro level loading is critically influenced by micro scale features especially cement lines and cohesive model approach is one of the feasible tools for micro scale modeling of the bone. Same set of authors employed the cohesive finite element based modeling and predicted the loss of toughness of human bone as a function of age by introducing changes in material proportions [29]. Another study employed artificial intelligence (AI) to construct the microscaled bone geometry [30]. It has summarized important steps in micro scale modeling. Even though these steps are suggested for the AI approach, they are also applicable in other modeling approaches. For example, instead of analyzing images using AI approach one cane use some other tools. The suggested steps are summarized below.

- Acquire micrographs of the bone.
- Segregate micro features into separate images using MATLAB® AI module.

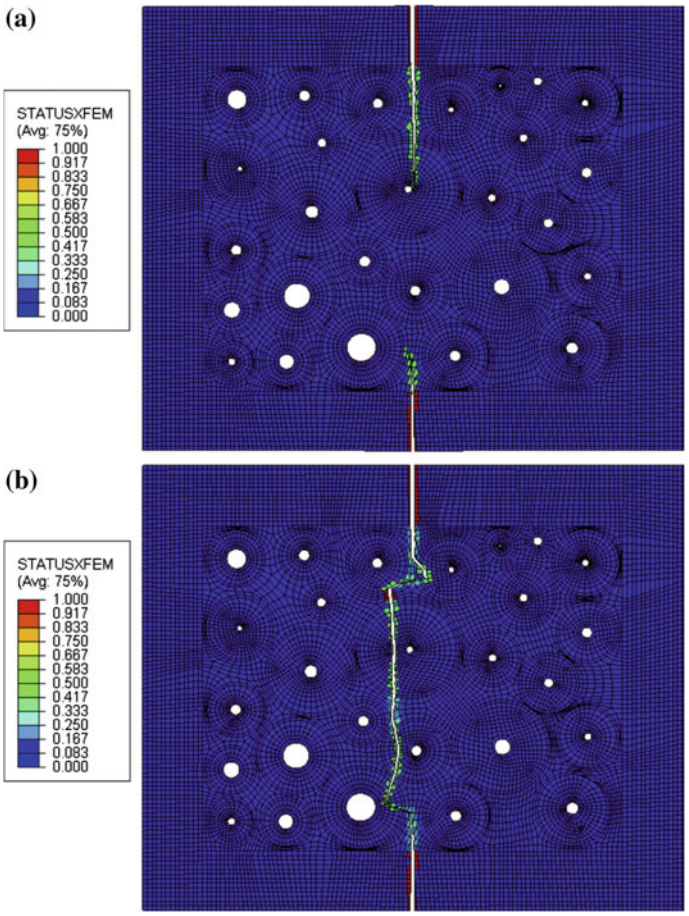

Fig. 6.19 Final crack propagation paths for **a** Model C and **b** Model B of osteonal cortical bone tissue (reprinted from Xiao et al. [25] with permission. © Elsevier)

- Tag the individual elements with the corresponding mechanical properties.
- Reassemble the micro geometric features into one master image and feed it as FEM geometry.

Thus, it is clear that computational modeling is a good tool in order to predict the behavior of bone machining operation and method. It can help to decide the suitable machining parameters so as to perform the machining operation in most efficient and least damaging way. In order to design the model accurately, it is necessary for professionals from medical and engineering fields to actively collaborate and exchange the views. This will not only make the predictions more accurate but also facilitate seamless integration of the modeling approach with the surgical procedures. This forms an important step in modernization of the current procedures. Another

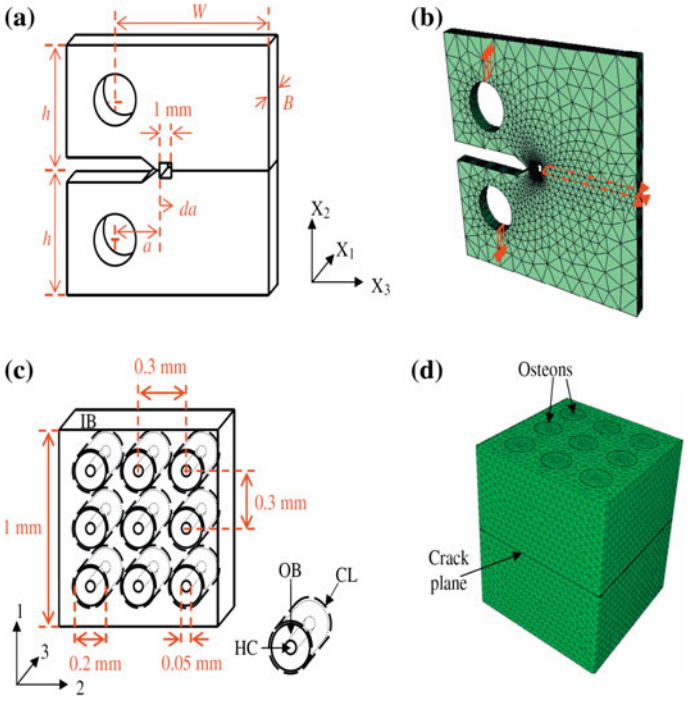

Fig. 6.20 Schematic showing **a** continuum geometry and **b** corresponding meshed structure, **c** a micro model with **d** corresponding meshed structure (reprinted from Ural et al. [28] with permission. © Elsevier)

aspect of modernization is potential automation which also involves robotics apart from the computer aided methods. Progresses done in the field of surgical automation especially in the field of orthopedics have been explored in the following Chap. 7.

References

1. L. Zhang, B.L. Tai, G. Wang, K. Zhang, S. Sullivan, A.J. Shih, Med. Eng. Phys. **35**(10), 1391 (2013)
2. B.L. Tai, L. Zhang, A.C. Wang, S. Sullivan, G. Wang, A.J. Shih, Med. Eng. Phys. **35**(10), 1545 (2013)
3. J. Lee, Y. Rabin, O.B. Ozdoganlar, Med. Eng. Phys. **33**(10), 1234 (2011)
4. S.R. Davidson, Heat transfer in bone during drilling, PhD Thesis, University of Toronto (1999)
5. S. Sezek, B. Aksakal, F. Karaca, Comput. Mater. Sci. **60**, 13 (2012)
6. K. Alam, M. Khan, V.V. Silberschmidt, J. Med. Biol. Eng. **34**(6), 618 (2014)
7. S. Li, Y.P. Chui, P.A. Heng, in *4th IEEE International Conference on Information Science and Technology (ICIST)*, 2014 (IEEE, 2014), pp. 569–573
8. A.S. Inamdar, Drilling in bone: modeling heat generation and temperature distribution by using HBIM, BTech Thesis, Indian Institute of Technology, Roorkee, India (2009)

9. M. Stańczyk, J. Telega, Acta Bioeng. Biomech. **4**(2), 3 (2002)
10. M. Basiaga, Z. Paszenda, J. Szewczenko, M. Kaczmarek, Acta Bioeng. Biomech. **13**(4), 29 (2011)
11. K. Alam, Experimental and numerical analysis of conventional and ultrasonically-assisted cutting of bone, PhD Thesis, Loughborough University, UK (2009)
12. Y. Wang, M. Cao, X. Zhao, G. Zhu, C. McClean, Y. Zhao, Y. Fan, Med. Eng. Phys. **36**(11), 1408 (2014)
13. R. kumar Pandey, S. Panda, Procedia Eng. **51**, 676 (2013). doi:10.1016/j.proeng.2013.01.096. http://www.sciencedirect.com/science/article/pii/S1877705813000970. Chemical, Civil and Mechanical Engineering Tracks of 3rd Nirma University International Conference on Engineering (NUiCONE2012)
14. S.S. Joshi, A.V. Gkriniari, S. Katakam, N.B. Dahotre, J. Phys. D: Appl. Phys. **48**(49), 495501 (2015)
15. N.B. Dahotre, S. Santhanakrishnan, Laser-assisted machining (LAM) of hard tissues and bones (2014). US Patent App. 14/216,966
16. W.A. Lughmani, K. Bouazza-Marouf, I. Ashcroft, J. Mech. Behav. Biomed. Mater. **42**, 32 (2015)
17. C. Santiuste, M. Rodríguez-Millán, E. Giner, H. Miguélez, Compos. Struct. **116**, 423 (2014)
18. K. Alam, A. Mitrofanov, V.V. Silberschmidt, Comput. Mater. Sci. **46**(3), 738 (2009)
19. C. Plaskos, A.J. Hodgson, P. Cinquin, in *Medical Image Computing and Computer-Assisted Intervention-MICCAI 2003* (Springer, Berlin, 2003), pp. 254–261
20. K. Alam, A. Mitrofanov, V.V. Silberschmidt, Int. J. Exp. Comput. Biomech. **1**(3), 236 (2010)
21. M. Marco, M. Rodríguez-Millán, C. Santiuste, E. Giner, M.H. Miguélez, J. Mech. Behav. Biomed. Mater. **44**, 179 (2015)
22. M. Kutz, *Standard Handbook of Biomedical Engineering and Design* (McGraw-Hill, New York, 2003)
23. T.M. Keaveny, E.F. Morgan, O.C. Yeh, *Standard Handbook of Biomedical Engineering and Design* (McGraw-Hill, New York, 2004)
24. S. Li, A. Abdel-Wahab, E. Demirci, V.V. Silberschmidt, J. Biomech. **47**(5), 1117 (2014)
25. M. Xiao, S. Karube, T. Soutome, K. Sato, Int. J. Mach. Tools Manuf. **42**(15), 1677 (2002)
26. A.A. Abdel-Wahab, A.R. Maligno, V.V. Silberschmidt, Comput. Mater. Sci. **52**(1), 128 (2012)
27. L. Vergani, C. Colombo, F. Libonati, Procedia Mater. Sci. **3**, 1524 (2014)
28. A. Ural, S. Mischinski, Eng. Fract. Mech. **103**, 141 (2013)
29. A. Ural, D. Vashishth, J. Biomech. **39**(16), 2974 (2006)
30. I.S. Hage, R.F. Hamade, Procedia CIRP **8**, 385 (2013)

Chapter 7
Potential Automation of Bone Machining

The ultimate aim of research related to surgery is to reduce human dependency during operational procedures. The current chapter focuses on such automation efforts undertaken in the field of bone machining. State of the art in the field has been presented. The need for such efforts arises from the fact that involvement of human being in the surgery as an operator requires a lot of experience to develop the precise skills and it always involves a risk of human error. Another important aspect is the constraint on geometry which can be machined in manual operation. With this background, the efforts related to automation and robotics in the field of bone machining are described.

7.1 Computer Aided Planning

There have been many in vitro efforts in case of conventional machining and explorations have begun for non-conventional techniques as well. Some of the efforts help plan the surgery by automated generation of details about bone to be operated on [1–14]. The collected information is then fed to an algorithm which in turn helps to plan the surgery. Extensive information about computer aided planning of orthopedic surgery can be found in a book by Haaker and Werner [15], here only a brief discussion is presented. The main tasks to be executed during planning are listed below [14].

1. **Image data acquisition and processing**—This consists of gathering the data based on various methods and process this data to generate tomographic information about the bone for tool guidance.
2. **Matching**—It involves registration of patient's anatomy with the medical image. The features on actual bone are matched with the image. External feature markers can be introduced before gathering the image data.
3. **Referencing**—The features identified during matching also serve as reference markers during surgery. Dynamic actions keep the bones constantly under vibrations and the reference points help in tracing exact location of interest.

N.B. Dahotre and S.S. Joshi, *Machining of Bone and Hard Tissues*,
DOI 10.1007/978-3-319-39158-8_7

4. **Tool tracking**—In order to visualize the real time operation within the medical images, it is necessary to track the location and orientation of the tools. Tracking can be done with the help of infrared LED and with the help of tool features such as tip in case of a drill or a cutting edge in case of saw and chisel.
5. **Tool visualization**—It is the static or dynamic image formed with the help of gathered data from bone and instrument trackers. Examples for this kind of presentation are sections through interesting regions of the data volume, maximal intensity projections (X-ray simulations), or rendered 3D scenes.

As explained above, the data gathering system and successive planning are required. Normally there are three methods of planning as listed below.

- **Computer tomography (CT) scan based imaging**—Even though this method is commonly used in neuro and spinal surgeries, it has also been employed in case of orthopedic surgeries [16]. CT scans conducted on the human body are processed to obtain a 3 D image. Matching is done with the patient's anatomy by fixing the tracking markers visible to the computer. This data is then utilized to operate a pointing device visible to the computer. The surgeon has access to 3D template with the markers during the operation and determines the precise locations on the bone where the tool should be at. An example of CT scan aided planing is shown in Fig. 7.1.
- **Intraoperative fluoroscopy based imaging**—This method is commonly employed in the trauma surgery. Modified fluoroscopy with the help of computer software helps to create an anatomical map. Basic principle behind this technique is based on X-ray imaging of the bones. Some of the X-rays are pass through where as some are scattered. The directly passed rays form an image whereas the scattered X-rays with charged direction and relatively low energy are traditionally considered for radiation exposures. The multiple fluoroscopic images can be acquired and processed by computer software to provide real time multi-planar images without the need for extensive fluoroscopy exposure. The software superimposes the position of surgical instruments and the path of an implant onto real

Fig. 7.1 Example of CT scan aided surgery planning: The femoral tunnel is positioned so that the cutting miller or drill emerges at the desired point and forms the correct angle of inclination with the condyle (reprinted from Petermann et al. [16] with permission. © Elsevier)

time imaging, allowing the surgeon to modify implant trajectory without the need for further fluoroscopy. 3-D fluoroscopy is an evolution of this technique and consists of a mobile C-arm unit, modified to incorporate a motorized rotational movement that is linked to a computer to provide multi-planar 3-D images of bony structures. An example of intraoperative fluoroscopy is shown in Fig. 7.2 where the bone and tool are seen in two different views [17].

- **Image free** Computer software has an anatomical model, built up from a database of stored CT scans, for the procedure to be performed. The computer model is then augmented by 'surface registration' whereby a pointing device held by the surgeon, and visible to the computer, marks out predetermined areas of the patient's anatomy (Fig. 7.3). This system avoids radiation exposure to the patient and surgical team. The technique is refereed to as bone morphing [18]. The data is collected as surgeon makes a movement. Data is gathered from predetermined number of random points. The bone morphing algorithm then utilizes this data to construct a image based on the radius of the bone. Finally, following three steps are required to obtain this 3D statistical shape similar to the one shown in Fig. 7.3:

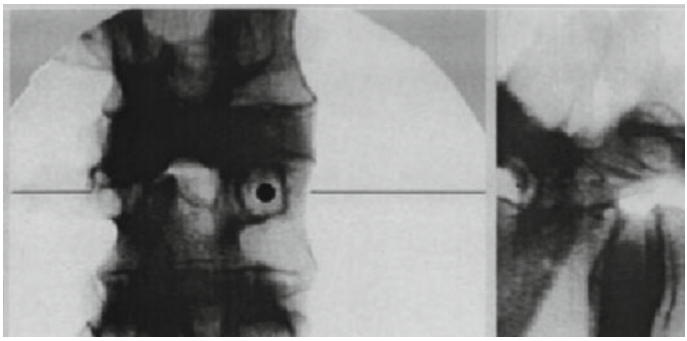

Fig. 7.2 In vitro image-interactive navigation. In two previously acquired C-arm images, the current location of one pedicle instrument is displayed. *Left* right oblique view with the tool's axis shown as a *black circle* in the center of a cross-hair. *Right* lateral view. The instrument is represented as a *black line* with a cross-hair identifying the tool's tip. A *dotted line* indicates the trajectory that the instrument is about to follow (reprinted from Nolte et al. [17] with permission. © Springer)

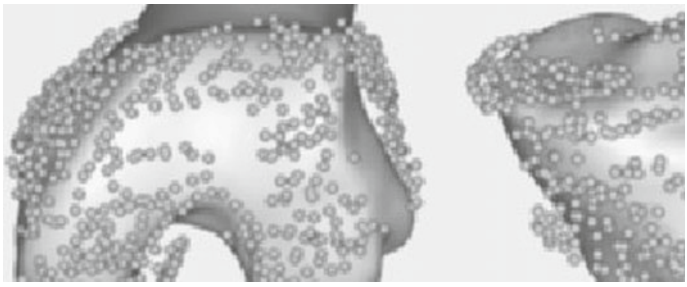

Fig. 7.3 Digitization of a cloud of random points on the bone surfaces of the patient (reprinted from Stindel et al. [18] with permission. © 2002 Informa UK ltd)

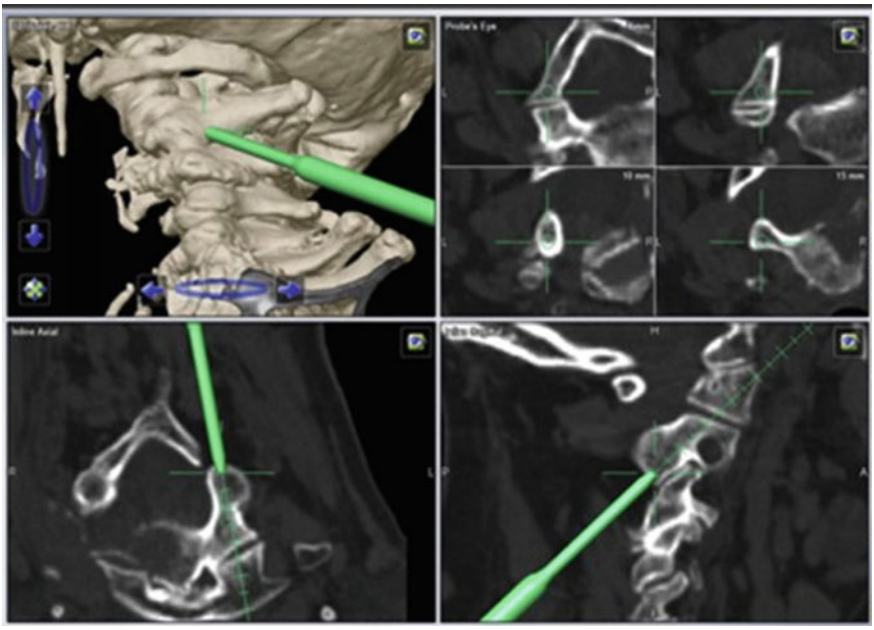

Fig. 7.4 Three-dimensional view of pedicle screw fixation-using navigation (reprinted from Rambani and Varghese[12] with permission. © Elsevier)

(a) acquisition of training shapes
(b) definition of a point-to-point correspondence between training shapes
(c) statistical analysis.

Thus it is clear that, more the number of times the algorithm analyses the data, more will be the accuracy. This data is then used for planning of the surgery assisting in navigation of the tools and alignment of the bone (Fig. 7.4 [12]).

It can be concluded that the technology of surgery planning can result in accurate positioning and better alignment assessment of the deformity, improved gap balancing, and a decreased incidence of fat embolism due to the avoidance of intramedullary instrumentation [12, 19–21]. On the other hand, it has some demerits at this point of time such as the learning curve associated with embracing a new technology, prolonged surgical time, setup, and maintenance costs and the lack of long-term evidence on clinical outcome [22]. The key characteristics of computer aided surgery planning that are currently adopted in the clinical environment are summarized in Table 7.1. This points towards more advancements in the field of surgery planning in order to make this process efficient and timely.

Table 7.1 Key features of various methods of computer aided surgery planning

Method	Characteristics
Computer tomography	• CT scans are employed produce 3D image
	• Tracking markers are used for navigating pointing device
	• 3D template guides surgeon for accurate placement of tools
Intraoperative fluoroscopy	• X-ray imaging of the bones with the aid of computer
	• Quick capture of multiple images help produce 3D reconstruction
Image free	• A pointing device is manually traced on patients anotomy
	• Data collection at random points to generate 3D images
	• Virtual construction of images
	• Algorithm gets better with usage

7.2 Robot Assisted Surgery

Another aspect of automation is employment of robots for actual surgical operations [23–37]. This becomes feasible as a result of bone not undergoing large amount of deformation during machining. On a broader scale, the robotic systems are classified as passive, active, positioning, and cutting/milling aids. In passive systems, the robot remains under the control of a surgeon. Active systems on the other hand have much autonomy to perform the operations. The reference points are tracked and machining can be done by robot independently. Positioning systems are similar to methods described in previous section. The positioning of tools is done via robots based on algorithms which are then operated by surgeons. Last type that is cutting/milling aids combine capability of navigation and passive systems. The initial efforts of robotic surgery date back to 1987. Since then the technique is constantly evolving. A brief chronological summary of evolution of surgical robotics are schematically shown in Fig. 7.5 [38] which gives the extent of rapid progress in this field. The general steps followed during robot assisted surgery are summarized (Fig. 7.6 [39]). The first step consists of image acquisition from which the data is extracted for the purpose of feeding it to the planning algorithm . After these steps, the actual execution of surgical step by a robotic unit takes place followed by post surgery monitoring and evaluation.

There are certain advantages of robot assisted surgery over conventional surgery as pointed by Adili and listed below [37].

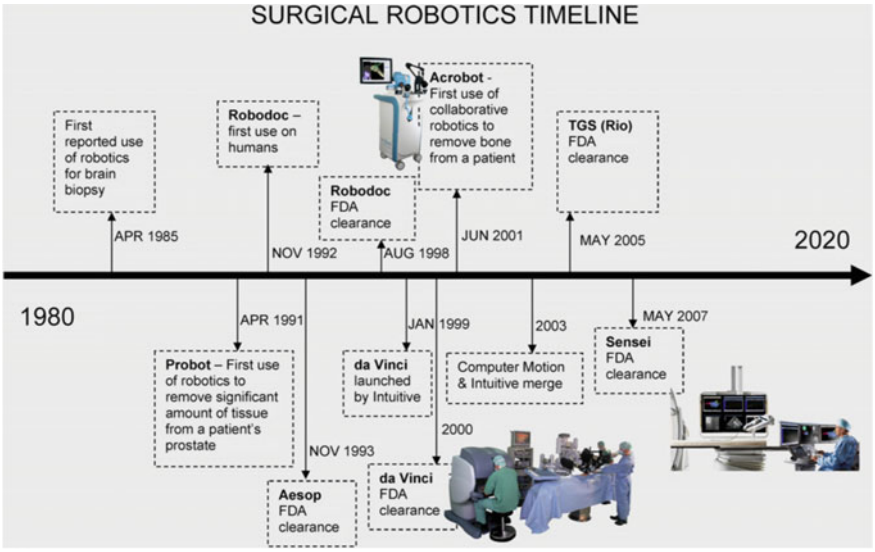

Fig. 7.5 Evolution of surgical robotics (reprinted from Gomes [38] with permission. © Elsevier)

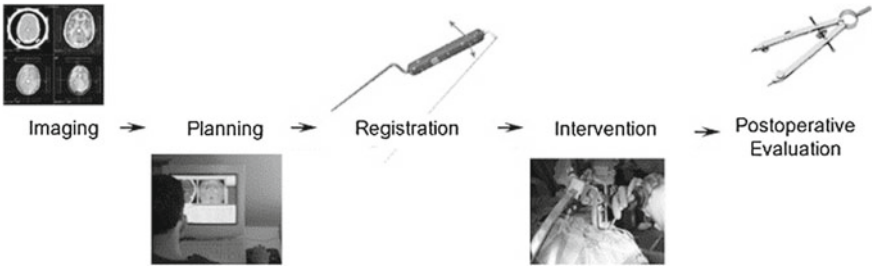

Fig. 7.6 Steps during robot assisted surgery (reprinted from Korb et al. [39] with permission. © Elsevier)

- Improved accuracy and precision in the preparation of bone surfaces.
- More reliable and reproducible outcomes
- Greater spatial accuracy.
- Ability to make repetitive motions tirelessly.
- Ability to accurately and predictably position and orientate equipment to a re-programmable point.
- Ability to move to a location and then hold tools there for long periods accurately, rigidly, and without tremor.
- Ability to actively constrain tools to a particular path or location to achieve accurate cuts and positioning of equipment.
- Ability to make precise micromotion adjustments.

Because of these advantages, robotic techniques have been employed in many surgical fields such as neurology, maxifocal, cardiac, opthalmo, and orthopedic. How-

ever, current discussion will be focused on robotics employed in orthopedic surgery and few case studies related to conventional and non conventional methods will be covered.

Robots render suitable for orthopedic surgery because of the structure of the bone. The rigidity of bone allows the robotic devices to secure on them. Being radio opaque, the skeletal structures can be easily imaged and can feed data to planning algorithms used in robot navigation. Easily definable reference points or the implantation of dynamic reference bodies (fiducials) greatly facilitate the registration process in case of bones that all robotic systems require. Bones can be relatively easily manipulated and fixed in known positions and then robotic devices can generate high forces needed to create accurate cuts. As the robot system can be constrained and bounce off hard surfaces; the possibility of avoiding/minimizing cutting of the vulnerable surrounding soft tissues is very high.

One of the earliest studied system for orthopedic application was ROBODOC^{TM} which consists of a planning station, a robot for machining, and a controlling station [38, 40]. The robotic arm can be carefully designed so as to have flexible and controllable movement (Fig. 7.7 [40]). Various tools can be attached to the arm to perform precise machining. Locating pins need to be mounted on the bone in order to provide navigational guide for the robotic system. The CT scans obtained here after are transfered to the planning station. The surgeon can then plan the machining parameters, for example by checking different positions, and assess the impact on anteversion, neck length, and stress loading in case of hip replacement with an implant [32]. The cutting times in case of hip replacement are 25–30 min during which the surgeon monitors the process from the control station. The process can be stopped in case of unusual events. After completion of milling, the remaining operations are done in conventional manner. The schematic of ROBODOC^{TM} system is shown in Fig. 7.8. It has also been reported that, even though the cuts are made in reproducible and tireless manner, the inserted navigational pins play a critical role [32]. It has been reported that, after clinical trials, a severe pain may occur in the area where the navigational pins were inserted [41]. Careful choice of location on the other hand has been reported to reduce the pain to much lower level [42]. ROBODOC^{TM} has been successfully employed in clinical trials, for example it was used in 1000 surgeries in Frankfurt, Germany [43]. Apart from ROBODOC^{TM}, the other systems employed are PAKY/RCM^{TM} [44], kawasaki^{TM}, BRIGIT^{TM}, and Acrobot^{TM} [32] and have been reported to work on similar principle.

Even though robot assisted surgery wields a great potential, the following few key issues still remain associated with it.

- Significant forces are required to cut/penetrate the rigid bone which might compromise accuracy.
- Increased operative exposure and disruption of soft tissue structures to allow access for current robotic end effector designs and bone motion sensors can compromise clinical outcomes.
- Significant capital cost.
- Steep learning curve for operating personnel.

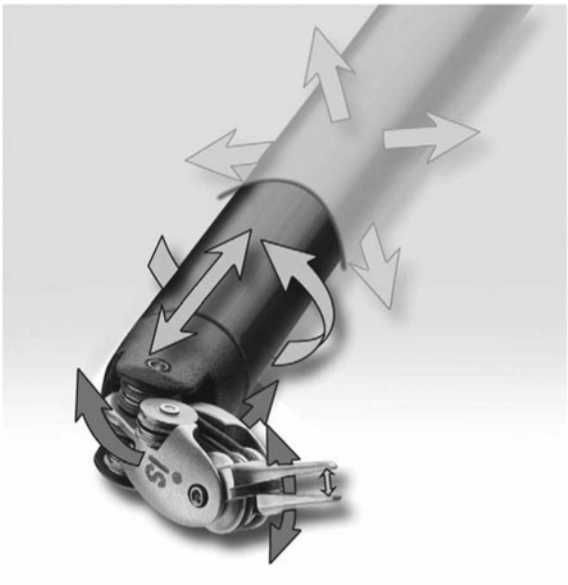

Fig. 7.7 Design of robotic arm illustrating degrees of freedom with the *arrows* (reprinted from Camarillo et al. [40] with permission. © Elsevier)

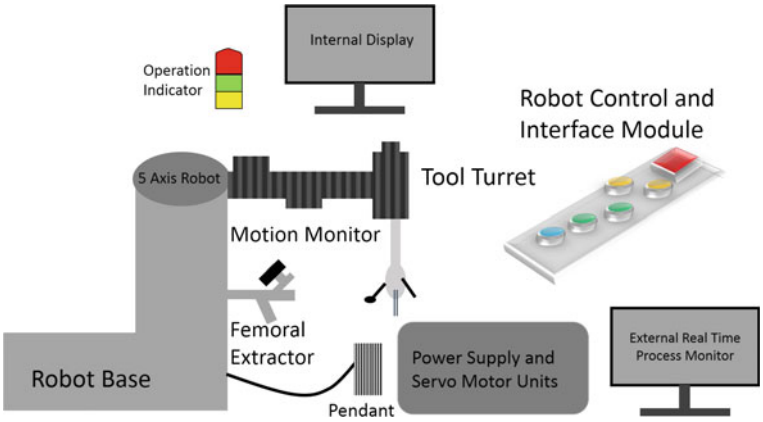

Fig. 7.8 Schmatic of ROBODOC^{TM} with various subsystems

- Additional technicians are required in the operating room.
- Most importantly, additional invasive procedures are required to implant the dynamic reference bodies (fiducials), leading to increased operating time for the procedure.

Considering these issues, it is clear that surgical robotics has a long way to go to become feasible in routine surgeries at grass root level hospitals. A collective

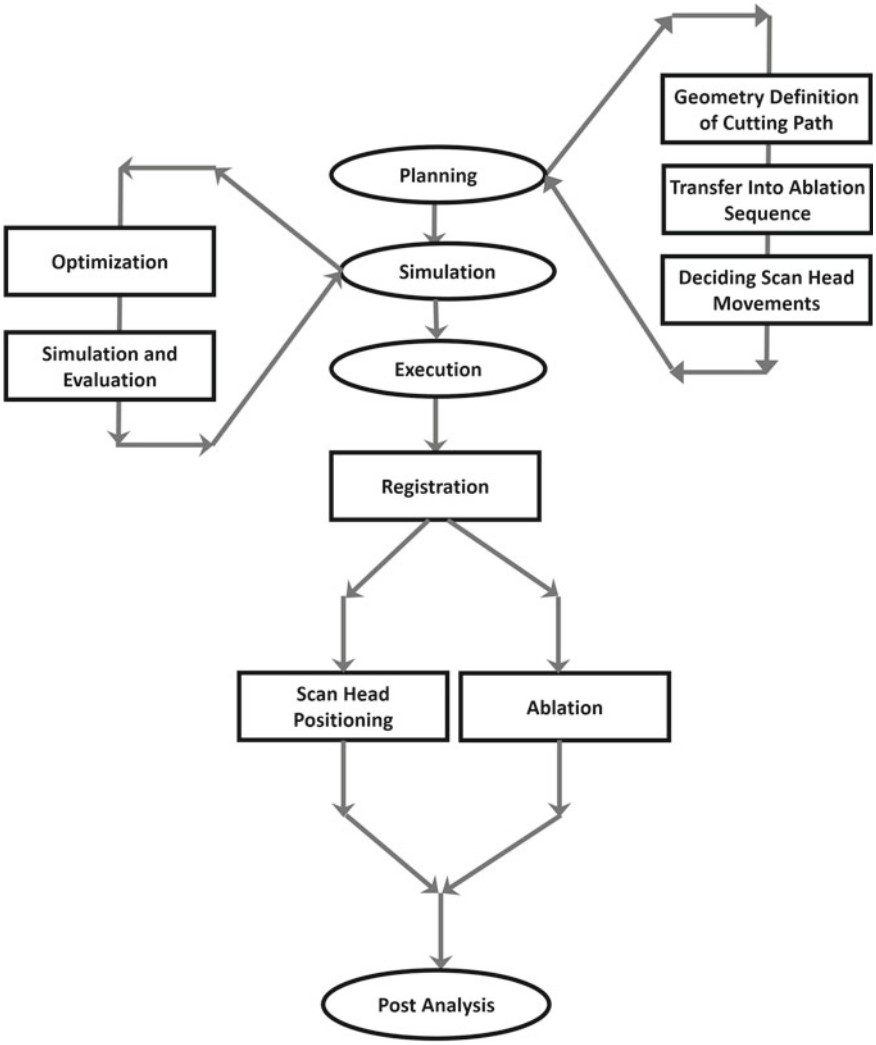

Fig. 7.9 Work flow of laser robotic surgery

effort of medical professionals and engineers is needed to design the system with least issues. Nonetheless, the robots are being explored in surgeries, especially for non-conventional bone machining techniques such as laser machining [45].

Lasers due to their inherent monochromatic and inherent nature posses inherent precession machining characteristics as discussed in previous chapters. It has been proposed that if the lasers are combined with surgical robotics, the control and precession would be further better [24, 28, 46]. Another advantage of laser is some types can easily be transmitted through glass fibers allowing main laser unit to be located remotely away from the surgery theater to improve radiation safety of patients

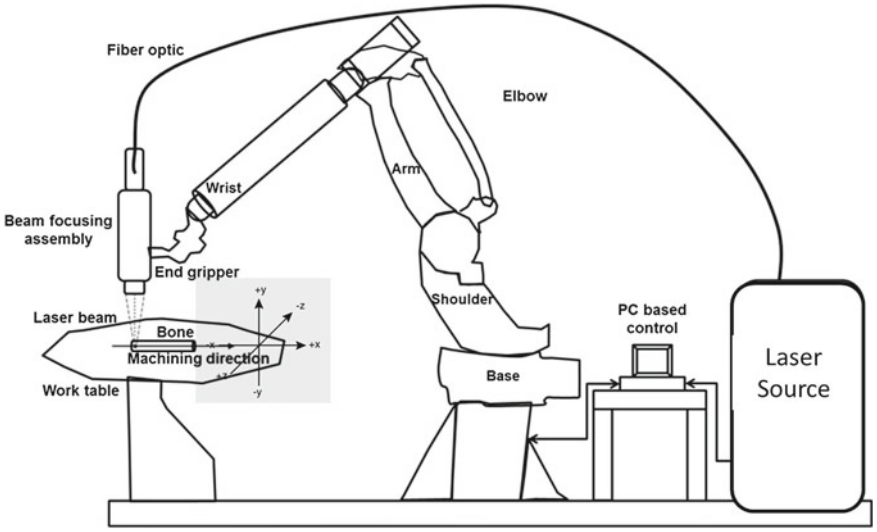

Fig. 7.10 Setup for robot assisted laser machining of bones [45]

and operators alike. The basic work flow adopted for laser based surgery is similar to one opted for conventional methods (Fig. 7.9). The process starts with collection of data about the bone geometry in order to choose the ablation pattern and figure out execution of the chosen pattern [47]. Simulation follows the collection of data, which can virtually determine the ablation characteristics of various input parameters and determine the most optimum condition on a computer. These optimum parameters are then fed to the laser robot setup (Fig. 7.10 [45]), and the most optimum ablation region is figured out based on lens characteristics. The head movement is decided by the algorithm and the ablation operation is thus performed by the laser held in robotic arm/head to machine the desired portion of the bone.

Thus robot based orthopedic surgery, irrespective of what machining technique (mechanical or heat based) is used, involves several major components as depicted in Fig. 7.9. These major components are first level of essential gradients of a semi or fully automated robotic surgery. However, each of these components also comprise of many subcomponents to execute their role in synchronized manner during an integrated robotic surgery. Due to need of integration of these components in synchronized manner at multiple levels for desired outcome, design and fabrication of a complete robotic orthopedic surgery system is a complex and long term endeavor. Such enduring efforts would require multidisciplinary collaborative efforts among all engineers (design, mechanical, computer, electrical, and biomedical), material scientists, physicists, and orthopedic surgeons. As iterated in Chap. 1, the orthopedic field is growing in leaps and bounds around the globe. Hence, this is likely to drive the development of integrated robotic orthopedic surgery system for several reasons including a need for accurate and faster surgery, cost effective surgery and rapid post surgery recovery in the near future.

References

1. N.M. Krause, L.E. Weiss, K. Shimada, T. Kanade, Computer-aided orthopedic surgery. US Patent 6,711,432 (2004)
2. S. Raab, Computer-aided surgery apparatus. US Patent 5,251,127 (1993)
3. P. Keppler, F. Gebhard, P.A. Grützner, G. Wang, G. Zheng, T. Hüfner, S. Hankemeier, L.P. Nolte, Injury **35**(1), 68 (2004)
4. J. Chapuis, A. Schramm, I. Pappas, W. Hallermann, K. Schwenzer-Zimmerer, F. Langlotz, M. Caversaccio, IEEE Trans. Inf. Technol. Biomed. **11**(3), 274 (2007)
5. S.L. Delp, J.P. Loan, C.B. Robinson, A.Y. Wong, S.D. Stulberg, Computer-assisted surgical system. US Patent 5,682,886 (1997)
6. M. Hafez, K. Chelule, B. Seedhom, K. Sherman, Clin. Orthop. Relat. Res. **444**, 184 (2006)
7. J. Xia, N. Samman, R.W. Yeung, D. Wang, S.G. Shen, H.H. Ip, H. Tideman, Int. J. Oral Maxillofac. Surg. **29**(4), 250 (2000)
8. W. Hallermann, S. Olsen, T. Bardyn, F. Taghizadeh, A. Banic, T. Iizuka, Plast. Reconstr. Surg. **117**(7), 2431 (2006)
9. S. Zachow, E. Gladilin, R. Sader, H.F. Zeilhofer, in *International Congress Series*, vol. 1256 (Elsevier, 2003), pp. 362–369
10. D.E. Altobelli, R. Kikinis, J.B. Mulliken, H. Cline, W. Lorensen, F. Jolesz et al., Plast. Reconstr. Surg. **92**(4), 576 (1993)
11. K. Radermacher, F. Portheine, M. Anton, A. Zimolong, G. Kaspers, G. Rau, H.W. Staudte, Clin. Orthop. Relat. Res. **354**, 28 (1998)
12. R. Rambani, M. Varghese, Orthop. Trauma **28**(1), 50 (2014)
13. M. Fadda, D. Bertelli, S. Martelli, M. Marcacci, P. Dario, C. Paggetti, D. Caramella, D. Trippi, in *CVRMed-MRCAS'97* (Springer, 1997), pp. 617–628
14. F. Langlotz, M. Stucki, R. Bächler, C. Scheer, R. Ganz, U. Berlemann, L.P. Nolte, Comput. Aided Surg. **2**(6), 317 (1997)
15. R. Haaker, W. Konermann (eds.), *Computer and Template Assisted Orthopedic Surgery* (Springer, Berlin, 2013)
16. J. Petermann, R. Kober, R. Heinze, J.J. Frölich, P.F. Heeckt, L. Gotzen, Op. Techn. Orthop. **10**(1), 50 (2000)
17. L.P. Nolte, M. Slomczykowski, U. Berlemann, M.J. Strauss, R. Hofstetter, D. Schlenzka, T. Laine, T. Lund, Eur. Spine J. **9**(1), S078 (2000)
18. E. Stindel, J. Briard, P. Merloz, S. Plaweski, F. Dubrana, C. Lefevre, J. Troccaz, Comput. Aided Surg. **7**(3), 156 (2002)
19. W.G. Blakeney, R.J. Khan, S.J. Wall, J. Bone Joint Surg. **93**(15), 1377 (2011)
20. J. Mahaluxmivala, M. Bankes, P. Nicolai, C. Aldam, P. Allen, J. Arthroplast. **16**(5), 635 (2001)
21. W.M. Mihalko, J. Boyle, L.D. Clark, K.A. Krackow, J. Arthroplast. **20**(1), 25 (2005)
22. D.K. Bae, S.J. Song, Clin. Orthop. Surg. **3**(4), 259 (2011)
23. P.J. Swaney, R. Lathrop, J. Burgner, K. Weaver, H.B. Gilbert, R.J. Webster, D.B. Comber, System, method, and apparatus for configuration, design, and operation of an active cannula robot. US Patent App. 14/177,864 (2014)
24. J. Burgner-Kahrs, in *Soft Robotics* (Springer, Berlin, 2015), pp. 222–230
25. K. Weaver, R. Webster, P. Swaney, J. Burgner, P. Russell, H. Gilbert, J. Bekeny, R. Hendrick, J. Neurol. Surg. Part B: Skull Base **74**(S 01), A123
26. J.S. Schneider, J. Burgner, R.J. Webster III, P.T. Russell III, Curr. Opin. Otolaryngol. Head Neck Surg. **21**(1), 11 (2013)
27. J. Burgner, P.J. Swaney, R. Lathrop, K.D. Weaver, R.J. Webster et al., IEEE Trans. Biomed. Eng. **60**(9), 2567 (2013)
28. J. Burgner, M. Müller, J. Raczkowsky, H. Wörn, Int. J. Med. Robot. Comput. Assist. Surg. **6**(4), 489 (2010)
29. J. Burgner, *Robot Assisted Laser Osteotomy* (KIT Scientific Publishing, Karlsruhe, 2010)
30. J. Burgner, F. Knapp, L. Kahrs, J. Raczkowsky, H. Wörn, J. Schipper, T. Klenzner, in *Proceedings of the 23rd International Congress and Exhibition CARS* (2009)

31. R. Phillips, M.A. Hafez, A. Mohsen, K.P. Sherman, J.R. Hewitt, I. Browbank, K. Bouazza-Marouf, Stud. Health Technol. Inf. **70**, 265 (1999)
32. K. Cleary, C. Nguyen, Comput. Aided Surg. **6**(6), 312 (2001)
33. P. Maillet, B. Nahum, L. Blondel, P. Poignet, E. Dombre, in *Proceedings of the 2005 IEEE International Conference on Robotics and Automation, 2005. ICRA 2005* (IEEE, 2005), pp. 211–216
34. W.W. Choi, B.A. Green, A.D. Levi, Neurosurgery **47**(4), 872 (2000)
35. P. Vendruscolo, S. Martelli, Inf. Softw. Technol. **43**(2), 87 (2001)
36. H. Paul, B. Mittlestadt, W.L. Bargar, B. Musits, R.H. Taylor, P. Kazanzides, J. Zuhars, B. Williamson, W. Hanson, et al., in *1992 IEEE International Conference on Robotics and Automation, 1992. Proceedings.* (IEEE, 1992), pp. 606–611
37. A. Adili, Surg. Innov. **11**(2), 89 (2004)
38. P. Gomes, Robot. Comput.-Integr. Manuf. **27**(2), 261 (2011)
39. W. Korb, R. Marmulla, J. Raczkowsky, J. Mühling, S. Hassfeld, Int. J. Oral Maxillofac. Surg. **33**(8), 721 (2004)
40. D.B. Camarillo, T.M. Krummel, J.K. Salisbury, Am. J. Surg. **188**(4), 2 (2004)
41. A.P. Schulz, K. Seide, C. Queitsch, A. von Haugwitz, J. Meiners, B. Kienast, M. Tarabolsi, M. Kammal, C. Jürgens, Int. J. Med. Robot. Comput. Assist. Surg. **3**(4), 301 (2007)
42. S. Nishihara, N. Sugano, T. Nishii, H. Tanaka, N. Nakamura, H. Yoshikawa, T. Ochi, J. Orthop. Sci. **9**(5), 452 (2004)
43. M. Börner, A. Lahmer, A. Bauer, U. Stier, in *Proceedings of the CARS*, pp. 689–693 (1998)
44. R.H. Taylor, B.D. Mittelstadt, H. Paul, W. Hanson, P. Kazanzides, J.F. Zuhars, B. Williamson, B.L. Musits, E. Glassman, W.L. Bargar et al., IEEE Trans. Robot. Autom. **10**(3), 261 (1994)
45. N.B. Dahotre, S. Santhanakrishnan, Laser-assisted machining (LAM) of hard tissues and bones. US Patent App. 14/216,966 (2014)
46. J. Burgner, M. Mueller, J. Raczkowsky, H. Woern, in *International Conference on Advanced Robotics, 2009. ICAR 2009* (IEEE, 2009), pp. 1–6
47. M. Müller, Transferring cutting trajectories into pulse sequences and optimized robot locations for laser osteotomy, Diploma thesis, Universität Karlsruhe (TH) (2009)

Index

N.B. Dahotre and S.S. Joshi, *Machining of Bone and Hard Tissues*,
DOI 10.1007/978-3-319-39158-8

M

N

O